PARAMETRIC IMPACT CHARACTERISATION OF A SOLID SPORTS BALL, WITH A VIEW TO DEVELOPING A STANDARD CORE FOR THE GAA SLIOTAR

by

FIACHRA CIARÁN COLLINS
B.E.

A thesis submitted for the degree of
Doctor of Philosophy

School of Mechanical and Manufacturing Engineering
Faculty of Engineering and Computing
Dublin City University

January 2011

Supervisors

Dr. Dermot Brabazon, School of Mechanical and Manufacturing Engineering

Dr. Kieran Moran, School of Health and Human Performance

PhD 2011

Declaration

I hereby certify that this material, which I now submit for assessment on the programme of study leading to the award of Doctor of Philosophy is entirely my own work, that I have exercised reasonable care to ensure that the work is original, and does not to the best of my knowledge breach any law of copyright, and has not been taken from the work of others save and to the extent that such work has been cited and acknowledged within the text of my work.

.....

FIACHRA COLLINS

ID No.:

57123837

January 2011

Publications

This work has been disseminated through the following publications:

Print publications:

- Collins, F., Brabazon, D., Moran, K. Mathematical modeling of the impact behaviour of the solid sports balls used in the Irish sport of Hurling. Modeling and Simulation in Materials Science and Engineering, submitted December 2010
- Collins, F., Brabazon, D., Moran, K. Viscoelastic impact characterisation of solid sports balls used in the Irish sport of Hurling. Sports Engineering, submitted December 2010
- Collins, F., Brabazon, D., Moran, K. The dynamic viscoelastic characterisation of the impact behaviour of the GAA sliotar, The Engineering of Sport 8, Volume 2, Issue 2, pp 2991-2997, June 2010
- Collins, F., Brabazon, D., Moran, K. Dynamic characterisation of high velocity ball impacts with NI LabVIEW, NI IMAQ Software and NI PCIe Hardware, Proceedings of NIDays Professional Development Conference for Engineers and Scientists, pp 14-15, November 2009
- Collins, F., Brabazon, D., Moran, K. Development of a single standardised core for the GAA sliotar, Proceedings of the 25th International Manufacturing Conference, pp 583-590, Dublin Institute of Technology, September 2008

Industrial publications:

- Collins, F., Brabazon, D., Moran, K. Performing measurement and analysis of a ball's impact characteristics using LabVIEW and NI Vision hardware and software, National Instruments Online Case Studies, 2009, *http://sine.ni.com/cs/app/doc/p/id/cs-12479*

- Collins, F., Brabazon, D., Moran, K. Giving it a hurl, The Engineer, pp 34-36, April 2010

- Collins, F., Brabazon, D., Moran, K. Impact testing, Industrial Plant and Equipment Ireland, p12, Spring Edition 2010

Seminars and presentations:

- Collins, F., Brabazon, D., Moran, K., The dynamic viscoelastic characterisation of the impact behaviour of the GAA sliotar, Presentation [First prize in mechanical engineering], Faculty of Engineering and Computing Research Day, DCU – Ireland, 12th May 2010

- Collins, F., Brabazon, D., Moran, K., Using NI hardware and software for the control and analysis of impact characterisation, Seminar, National Instruments Technical Symposium, Dublin – Ireland, 18th Feb 2010

- Collins, F., Brabazon, D., Moran, K., Use of M-series multifunction DAQ cards for control and analysis of impact characterisation, Seminar, National Instruments Worldwide Graphical System Design Conference, Savoy Place, London – UK, 17th Nov 2009.

- Collins, F., Brabazon, D., Moran, K., Development of an impact characterisation methodology for evaluating the behaviour of the GAA sliotar, Presentation, Symposium for Mechanical Engineering Research and Practice, DCU – Ireland, 28th May 2009.

- Collins, F., Brabazon, D., Moran, K., Development of a single standardised core for the GAA sliotar, Presentation contest [shared second prize], IMechE Speak Out For Engineering Competition, Engineers Ireland Headquarters, Dublin – Ireland, 20th Feb 2009.

Dedication

To Mom & Dad

For keeping my feet on the ground and my head in the stars

Acknowledgements

I am deeply grateful to my supervisors, Dr. Dermot Brabazon and Dr. Kieran Moran. Having two such expansive sources of knowledge from separate disciplines was hugely beneficial to me. Dermot and Kieran, thank you for the excellent balance of encouragement and critique, for the keen interest that you took in my work, for the generous amounts of time that you allocated to me, for your attention to detail and for your exhaustive efforts to get the best out of me. I could not have asked for two better mentors.

I would like to thank Mr. Pat Daly and members of the Hurling Development Committee of the Gaelic Athletic Association. I am very proud to have been involved with one of our national sports and I am grateful for the opportunity and financial support that they provided for this work.

This work was assisted by the contribution of numerous members of DCU staff: Michael May and Liam Domican for system design and part ordering; Cian Merne, Jim Barry and Martin Johnson for test system fabrication; Michael Tyrell and Stephen Beirne for pneumatics set-up; Eoin Tuohy for prototyping advice and mould fabrication; Chris Crouch for quasi-static testing; Phil Kelly for image processing; and Dr. Fiona Regan for FTIR analysis. In addition, I am grateful for the help provided from industrial experts: Seamus Casserly and Graham Green from National Instruments; Patrick Kearney and Alan Downes from Key Plastics; and Ronan Kennedy from Total Polymer Solutions Ltd.

My time spent in DCU has been greatly enhanced by my fellow postgrads. Aymen, the three Damiens, Evelyn, Arthur, Vittoria, Houman, Katha and Lorna – to name but a few – thank you for your moral support and lunchtime chats.

Finally, I am especially indebted to six people: Mom and Dad, thank you for your unending support; my brothers Aonghus and Cillian for their wisdom and encouragement; my sister Clíona for her cheer-me-up abilities; and Lisa, I could not have done this without her. Go raibh míle maith agaibh.

Abstract

The main aim of this research was to characterise the dynamic impact behaviour of the sliotar core. Viscoelastic characterisation of the balls was conducted for a range of impact speeds. Modern polymer balls exhibited strain and strain-rate sensitivity while traditional multi-compositional balls exhibited strain dependency. The non-linear viscoelastic response was defined by two values of stiffness, initial and bulk stiffness. Traditional balls were up to 2.5 times stiffer than the modern types, with this magnitude being rate-dependent. The greater rate of increase of traditional ball stiffness produced a more non-linear COR velocity-dependence compared to modern balls. The dynamic stiffness results demonstrated limited applicability of quasi-static testing and spring-theory equations. Analysis of ball deformation behaviour demonstrated that centre-of-mass displacement and diameter compression values were not consistently equivalent for all ball types.

The contribution of manufacturing conditions to ball performance was investigated by conducting extensive prototyping experiments. Manufacturing parameters of temperature, pressure and material composition were varied to produce a range of balls. Polymer hardness affected stiffness but not energy dissipation, with increased hardness increasing ball stiffness. The nucleating additive influenced ball COR, with increased additive tending to reduce ball COR, but this effect was sensitive to polymer grade.

The impact response of the ball was simulated using three mathematical models. The first model was shown to replicate ball behaviour to only a limited degree, despite being used previously with reported success for other ball types. The second model exhibited a reasonable representation of ball impact response that was universally applicable to all tested ball types; however, the accuracy in terms of predicting force-displacement response was not as high as required for broad range implementation. The third model exhibited significantly better accuracy in simulating ball response. The force values generated from this model exhibited up to 95% agreement with experimental data.

Contents

List of Tables

List of Figures

Chapter 1: Introduction

1.1 Hurling and the sliotar

Hurling is one of the national Irish sports governed by the Gaelic Athletic Association (GAA). This outdoor sport involves two teams of 15 hurlers in each, playing with a solid, leather-bound ball called a sliotar and a wooden stick called a hurley. A match takes place on a pitch approximately 145 m long by 90 m wide, with scoring achieved by striking the sliotar between the goalposts, either above the bar (one point) or below the bar (goal, worth three points). Scenes of hurling are displayed in Figure 1.1 [1].

Figure 1.1: Scenes from the GAA Hurling Championship

The earliest sliotars were made from horse or cattle hair, rolled between the palms of the hand until it became matted and consolidated, and then wrapped in horse hair cord [2]. Wooden balls, with and without leather covers, were also present in the 19th century.

The balls were larger than the current size, having a diameter of 19 to 23 cm, and a mass of 180 – 200 g [2]. The origin for the word *sliotar* derives either from the words *sliabh* and *thar*, meaning "mountain" and "across" respectively in Irish or from the now obsolete Irish word *liotar*, meaning "hair" [3].

The present-day sliotar consists of a leather skin and solid core. The two-piece white leather skin is stitched to form the distinctive black rims. The material of the core, which is not specified under current GAA regulations, can be categorised into two types of compositions: the more traditional cork wrapped in a yarn winding and the more modern polymer foam core.

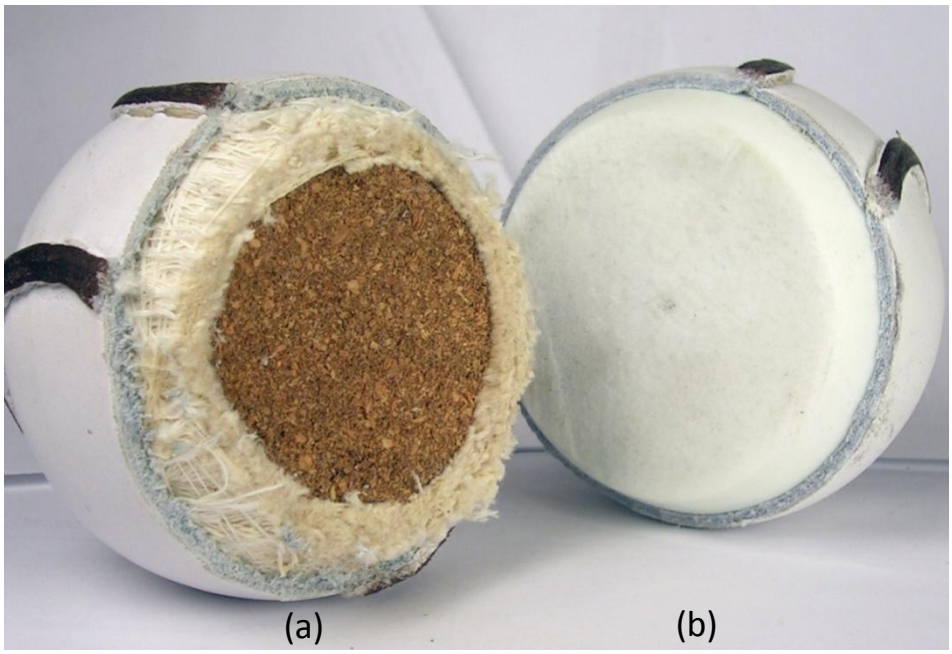

Figure 1.2: Picture of sliotar core construction types: (a) cork with yarn winding, (b) polymer foam

1.2 Project motivation

Current regulations for the sliotar have proved to be inadequate to sufficiently control the behaviour of the sliotar. This has been evident from the controversial statements in

the Irish national media following championship matches in recent years, some of which are abbreviated below:

"…behaved like a ping-pong ball…" – Sunday Times, 20/07/2003

"*…ball is travelling too far…*" – Sunday Times, 03/08/2003

"*Croke Park suspects that Cork introduced their own balls into the All-Ireland final*" – Sunday Times, 22/02/2004

"*…going too far… crazy to see puck-outs nearly reach the full-forward lines…*" – Sunday Times, 18/09/2005

"*…bounced wildly…*" – Sunday Times, 02/07/2006

"*…too light… travelled too fast… almost impossible to control…*" – Irish Times, 20/04/2007

"*...spends most of its time in the air... hardly any midfield play anymore... making a mockery of the game...*" – Irish Independent, 01/07/2010

The regulations for the sliotar are outlined in section 4.3 of the official playing rules of the GAA. Up to 2007, the rules stated [4]:

4.3 (i) The circumference of the hurling ball (sliotar) shall be between 23 cm and 25 cm. The ball weight (mass) shall be between 110 and 120 grams. The rib shall not exceed 2.4 mm and shall not be less than 2.2 mm. The thickness of the leather cover shall not be less than 1.8 mm. The leather cover shall conform with the designated Irish standard. The use of laminated splits, laminated corrected grain, or laminated full grain leathers shall be excluded.

These regulations did not mention materials or constructions for the sliotar core, nor did they specify the desirable performance of the ball. With the aim of developing a standard test method to regulate performance of the sliotar, work was carried out by two Masters projects in National University of Ireland, Galway (NUIG). The first project in 1998 proposed a number of test procedures following preliminary research of sliotar

characteristics [5]. Thirteen tests were recommended to comprehensively describe the balls' properties, including tests for water absorption; rib width and height; circumference and diameter; stiffness; shock loading; coefficient of restitution; and endurance. Following this work, a draft standard specification was issued by the Standards Committee formed by GAA [6]. This committee indicated that standard should contain a smaller amount of tests, with four tests proposed to monitor the performance characteristics of the ball. A second Masters project in 1999 was tasked with developing and validating these tests [7]. The first two tests were concerned with the dimensions and mass of the balls under dry and wet (repeated water immersion) conditions. The third test involved measuring high-speed ball coefficient of restitution (measure of energy dissipation from impact) and the final test related to ball aerodynamics. It was claimed that all four tests were found to produce 'excellent and consistent results', although the author did acknowledge that the latter two tests were time consuming. Despite the endorsement, the standard was not incorporated into GAA regulations due to the complexity and time-consuming operation of the equipment.

The behaviour of the sliotar was particularly unpredictable in years 2002 and 2003, partly due to the resurfacing of Croke Park and partly due to the unexpected liveliness of the ball. The sliotar again made headlines in 2006, when balls were illegally switched by players in some major championship matches. This led to the introduction of a fine of €500 if non-approved brands were used in a championship match [4]. However switching between different approved brands within the same match still caused upset as some teams were more familiar with some brands. The regulation of the sliotar performance recommenced in 2006, with testing conducted at DCU School of Health and Human Performance[1] to regulate the low-speed ball coefficient of restitution. This testing introduced a restriction in bounce height as determined from a 1.8 m drop test.

Irregularities of the sliotars' performance were still observed after the introduction of this tighter regulation. The core of the sliotar was identified as being the dominant factor in the variation in playing performance [8]. Inconsistencies in ball performance were attributed to the varying quantities of cork, yarn and/or polymer in the core construction.

[1] One of the project supervisors (Dr Kieran Moran) is director of an independent testing laboratory charged by the GAA with testing all of sliotars for adherence to their rules and regulations.

It was also believed that changes may have been made to the core's construction by the outsourced manufacturer without the consent of the Irish supplier [8]. The continuing variation in sliotar performance and the subsequent negative publicity was an undesirable distraction from the sport, and so in 2008 the GAA regulations were amended to include the following text [9]:

Sliotars will only be approved for use on the basis of compliance with standards and tests as set out by Central Council. Approved Sliotars shall carry the G.A.A. mark of approval. Annual testing will be carried out, at an independent and approved test centre, to ensure that Sliotars continue to comply with the standards set out only by the Central Council. The Central Council may adopt a single core that shall be used by any manufacturer/supplier who is approved to provide Sliotars for use in official games.

Despite these provisions, the saga arising from the performance variation of the sliotar has been on-going with disputes tending to be with regard to the excessive distance travelled by sliotar. In the Galway-Offaly match in the summer of 2010, a puck-out of the goalie landed at the opposing team's goal. In the 2010 All-Ireland final, the Tipperary goalie scored a point from a penalty at a distance of 80 metres, an unheard-of prospect prior to the recent years of controversy.

It is evident from the on-going variation in sliotar performance that the current regulations are insufficient in governing ball performance. Many of the regulatory standards regarding impact testing employ low speeds that are not representative of those that occur in the sport [10-12]. Such test methods do not subject the ball to conditions relevant to the sport, thus not providing an appropriate characterisation of the ball behaviour. There is a need to develop a more comprehensive test methodology to characterise the sliotar behaviour, allowing more stringent regulation of performance. This entails an analytical investigation of the ball behaviour during impact. Ball impact is a complex process, typically involving high strains, high strain rates, asymmetrical ball deformation and short contact times. A test methodology to define ball behaviour would allow the measurement of the viscoelastic characteristics of dynamic stiffness and energy dissipation. This extent of characterisation has not been conducted for the sliotar before now.

Similar advancement in performance regulation has been evident in comparable ball sports. However, many official regulatory standards for other ball sports involve multiple independent methodologies to characterise ball performance. For example, baseball and softball regulation involves three regulatory standards [13-15], the official characterisation of tennis balls[2] involves up to six machines [11] and cricket balls are characterised by four methodologies [10]. The characteristics resulting from these independent procedures cannot be directly compared given that they represent different test conditions. The collective measurement of impact characteristics from a single impact can yield information about the interaction of different impact characteristics.

The lack of inclusive characterisation of different aspects of ball behaviour is also evident in the literature, with an example being the ambiguous use of different considerations for ball deformation. The centre-of-mass (COM) displacement, derived numerically from force data, has been the predominant measurement of ball deformation despite the inability to track the ball's actual centre-of-mass due to its internal location. The difference between COM displacement and visual measurements of ball deformation has not been adequately explained, with publications conflictingly reporting either equality or disparity between the different deformation measurements [16-20].

None of the official regulatory standards involve the measurement of viscoelastic characteristics directly from ball impact data [10-15, 21-23]. The standards that do specify stiffness use either quasi-static measures or theoretical equations based on ideal assumptions [10, 11, 13, 15]. The measurements arising from such methods are disputable, given that quasi-static conditions differ significantly from dynamic impact conditions [17, 24] and the ideal assumptions of the numerical predictions are violated by non-linear material response [20, 25]. The validity of these methods has not been satisfactorily defined with respect to its relevance to impact. This avoidance of viscoelastic impact characterisation is also reflected in the literature, where numerous non-impact methodologies have been employed with limited success [25-28]. None of the non-impact methodologies could fully measure the short-duration material response for conditions representative of impact. The few studies that conducted viscoelastic

[2] Given their hollow construction, tennis balls differ significantly in behaviour to a solid ball such as a sliotar. However, the methodologies used and the characteristic measured for tennis-based data are relevant to any sports ball and so are of interest in this research.

impact characterisation have involved a single specific ball construction [16, 18, 27], thus providing only a limited insight into the contribution of the different materials and constructions to ball performance. An understanding of the contribution of different ball compositions to performance is particularly important for hurling given the pronounced difference between various sliotar constructions relative to those encountered in other sports.

The contribution of ball construction on performance is of fundamental importance to manufacturers and governing bodies. Ball manufacturers, particular those dealing with high-end products such as golf balls, can manipulate ball construction to produce a precise performance [29]. On the other hand, poor quality control of ball manufacturing can lead to inconsistencies in performance, as has been found for hurling, cricket [30] and golf [31]. In considering the adoption of a single standardised core for the sliotar, it will be necessary to establish a manufacturing procedure with consistent production of a ball with requisite impact characteristics. This is a non-trivial undertaking, requiring knowledge of the contribution of different material constituents to ball performance. Understandably, established ball manufacturers tend to withhold their proprietary knowledge to protect their product. An understanding of the relationship between ball manufacturing conditions and the resulting performance could permit fine tuning of the ball's behaviour without resorting to drastic changes in ball material or geometry that might adversely affect other aspects of the sport.

The determination of the relationship between material properties and ball performance could be aided by modelling the ball impact. Ideally the model input parameters would be based on intrinsic measures of the ball material properties, although such a model has not yet been reported in the literature [26, 30, 32]. An alternative approach is to develop a phenomenological model, where the model parameters are determined such that the model agrees with experimental data. Such models can be useful in understanding ball impact behaviour [16, 33, 34]. Phenomenological mathematical models have been employed in the literature with reported success [16, 18, 35, 36], although they tended to be based on limited experimental data. In addition, these models tend to be derived for single specific ball constructions, thus not indicating the applicability of the model parameters to intrinsic material properties.

1.3 Project aims

There have been three principal objectives of this present work.

The first objective was to design a methodology that enabled the first comprehensive characterisation of the dynamic impact behaviour of a sliotar core. Specifically, this involved the characterisation of ball stiffness and energy dissipation arising from impact. Such characterisation required the development of a test system that subjected the ball to impacts at sports-representative speeds while measuring the appropriate characteristics to describe ball performance. This test system would serve in future years to enforce the official regulatory standard for sliotars. The test system was designed as an advancement of equivalent methods used in comparable sports regulation, with the advantage of enabling the acquisition of multiple characteristics for a wide range of speeds. Analysis of these characteristics and their interaction would facilitate the progression of research in the area of solid sports balls. This would allow the clarification of deformation quantification methods to address conflicting reports in the literature [16-20]. The derivation of viscoelastic characteristics directly from impact would present a number of advantages. Firstly, this approach would overcome the limitations of non-impact methodologies that were frequently employed in the literature [25-28]. Secondly, the evaluation of viscoelastic impact characteristics would allow the investigation of the validity of quasi-static compression and theoretical stiffness equations, as used in other regulatory standards [10, 11, 13, 15]. Finally, the viscoelastic characterisation of the categorically different sliotar cores would yield an understanding of the contribution of ball materials and construction on performance.

The second objective was to develop an understanding of the relationship between manufacturing and ball performance. This involved an industrial collaboration with a plastic processing company. Cores were produced by using controlled material composition and manufacturing conditions, and testing them in the developed test system. This work would allow the determination of manufacturing conditions to produce a specific ball performance, a task that has not been undertaken previously on an official capacity for hurling.

The third objective of this work has been to develop mathematical models of the sliotar core impact behaviour, in order to simulate the viscoelastic characteristics established from the first objective. This involved a parametric study of mathematical models that have been used with reported success in the literature [16, 35]. The applicability of such models to dynamic impact conditions was investigated further in this work, as enabled by the extensive experimental data and categorically different sliotar core constructions. The phenomenological basis of such models was also explored with regard to the relevance of the model parameters to actual ball impact properties.

Chapter 2: Literature Review

2.1 Performance characterisation

2.1.1 Ball impact mechanism

All ball sports involve the impact of the ball against another object, such as a foot, a club or the ground. These impacts typically have a very short duration, ranging from 0.6 milliseconds for a golf ball-club impact to 5 milliseconds for a tennis ball-racket impact [37]. The small duration of the impact has several implications. Besides making the sport challenging for the players and exciting for the spectators, it signifies the limited control that the striker may have on the impact to judging the initial conditions such as aim, striking force or spin generation. Generally contact time is too short for the player to significantly adjust or correct the strike during the impact, as the ball would have long since flown by the time the striker could react. The physical reaction of a strike is therefore dominated by the dynamic behaviour of the ball during impact.

During impact, a ball will deform against the colliding surface to an extent dictated by its stiffness properties. The time duration between initial contact and maximum deformation is called the compression phase. During this time, deformation is induced from the impact force propagating from the contact region. In the restitution phase, the ball regains its shape and rebounds at a lesser speed due to kinetic energy dissipation. The magnitude of energy dissipation is dependent upon the ball's viscous properties. This material response is labelled as *viscoelastic*, where the material exhibits properties of both an elastic solid (deformed and recovered according to stiffness properties) and a viscous liquid (energy dissipated during deformation according to damping properties) [38]. The energy dissipation can occur during the impact process as a result of surface curvature flattening in the vicinity of the contact region [39] and internal friction in the ball, or after the impact process in internal modes of oscillation due to the remaining wave effects or the slow recovery of the ball to its original shape [17].

A sports player describes a ball's performance in subjective terms, such as **liveliness**, **feel** and **hardness** [40, 41]. It is the duty of a sports engineer to interpret these subjective measures and fit scientific measures to these performance perceptions. The **liveliness** of a ball is a relatively easy concept that relates to the amount of energy lost in

an impact. This is typically quantified by a measure called the *coefficient of restitution*, as will be discussed further in Section 2.1.2. Other measures are more abstract and thus more difficult to quantify. Player perception of **feel** is an abstruse quality and one which is the subject of numerous studies [29, 30, 40]. **Hardness** may relate to the tactile grip or the shock felt when catching and striking a ball. The perceptions of feel and hardness are problematic to characterise in isolation, with the closest evaluations possibly being derived from force-time data (peak force, impulse and contact time) described in Section 2.1.3, deformation histories (contact area and ball compression) outlined in Section 2.1.4, and a combination of force and deformation data (stiffness) described in Section 2.1.5.

Impact methodology

For controlled impact testing, methods of projection have ranged from simple drop tests to custom-built devices for higher speeds. Low speed impacts have been achieved easily from drop tests, using gravity to accelerate the ball from a height. This method has been used extensively due to its simplicity and quick set-up [5, 16, 17, 30, 36, 42]. Drop tests are usually limited to less than 7 m/s, corresponding to a drop height of 2 m. Given the high speeds typical of ball sports, this test method has been regarded as insufficiently representative of sport conditions.

High speed impact testing has tended to be in the region of 10 – 40 m/s (36 – 144 km/h or 22 – 90 mph), with some studies extending to 60 m/s (216 km/h or 135 mph). Speeds have been often chosen to reflect the sport conditions, such as using 20 and 35 m/s to represent forehand and service shots in tennis [40]. Other speed selections are based on round numbers, such as using 26.8 and 40.2 m/s (60 and 90 mph) for baseball characterisation. In some cases, the selection of projection speed tends to be dictated by the capacity of the projection method and the durability of the impact plate [16, 17]. Projection methods include pitching machines and pneumatic cannons. The pitching machine, which originates from sport training grounds, has been used frequently in the literature [20, 36, 43-45]. The machine has two or three rotating wheels, between which the ball is squeezed and propelled through. This method has the advantage of producing

a defined spin by adjusting the rotation of the individual wheels. However, the machine has to be carefully adjusted to avoid excessive wear on the ball surface due to friction against the wheels. In addition, the aiming accuracy of this machine has been disputed [46], with pitching machine manufacturers of these machines typically supplying their own make of ball for best results [47].

The pneumatic cannon has been utilised frequently due to its simplicity of design [5, 35, 42, 48-52]. This method works by propelling the ball on the high pressure discharge of air. Similar diameters of the ball and barrel are required for an effective use of the air discharge. This method is cheap and effective, although the ball size is restricted to barrel internal diameter and spin is an issue if the ball rolls within barrel. A variation of this method is to fit the cannon with a sabot, a cup device that travels within the barrel. In this way, a range of ball sizes can be propelled along the barrel without imparting spin, which has been used successfully in a number of studies [7, 24]. The sabot has been either restrained at the end of the barrel or exits the barrel behind the ball. This could result in undesired complications in the form of sabot breakage or multiple projectiles, respectively [7]. This process tends to be non-automated, requiring the sabot to be replaced manually into its firing position.

Performance regulatory standards

The current regulatory standard for the sliotar specifies mass, geometry (diameter, rib height/width) and low-speed rebound properties. A more detailed standard was drafted in 1999 [6], following the work of the two Masters research projects referred to in Section 1.2 [5, 7]. The draft standard included four tests for balls under dry and wet conditions, high-speed COR, and flight trajectory for specific launch conditions. The first two tests were concerned with the dimensions and mass of the balls under dry and wet conditions. In an attempt to make the wet conditioning of the ball more realistic, the ball was impacted 20 times, soaked for 7 minutes, impacted another 20 times, soaked for another 7 minutes, impacted 10 times and soaked for 15 minutes before being tested. The diameter of the ball was regulated using two U-callipers of high dimensional tolerance of the minimum and maximum diameters of 73.2 mm and 79.6 mm

respectively. The mass was required to be in the range of 110 to 120 g when dry, and less than 145 g when wet. The third test was to measure the coefficient of restitution, using a methodology adapted from golf ball testing. The test apparatus consisted of an air cannon that fired a projectile of 350 g (the effective mass of a hurley head) at a stationary sliotar at 29.2 m/s, with light gates used to measure the velocity of the projectile before the impact, and the projectile and sliotar after impact. The acceptable speeds of the ball were required to be less than 31.5 m/s when dry and greater than 29.5 m/s when wet. The final test, concerning the aerodynamics of the ball, used an air cannon to fire the ball at 45° at 27.7 m/s, with the overall flight distance limited to 55 ± 3.3 m. These tests were not incorporated into official GAA regulations due to the time-intensity and complexity of implementation.

All balls from major sports have published regulations, either conforming to a national standard agency or to guidelines laid down by the governing sporting organisation. The cricket ball is governed by a British Standard, BS 5993 *Specificiation for cricket balls* [10]. This standard specifies four separate test procedures for characterising coefficient of restitution (COR), hardness, impact resistance and durability. Baseballs and softballs are regulated according to three standards specified by American Society for Testing and Materials (ASTM). The COR testing and compression stiffness methodologies are independently stipulated in ASTM F1887 and F1888 respectively [13, 14]. A new specification, ASTM F2845, has been introduced in 2010 with testing that is more appropriate to a ball-bat impact [15]. Lacrosse balls are also specified according to the two ASTM standards F1887 (COR) and F1888 (stiffness) [23]. The golf ball is specified by Appendix III of the United States Golf Association (USGA) Rules of Golf. Regulations include specifications for mass, diameter, COR and flight distance [21, 22, 53]. Hockey balls are regulated by the International Hockey Federation (FIH), with tests specifying mass, geometry, coefficient of restitution and stiffness [12]. Tennis balls are regulated by the International Tennis Federation in their Technical Centre in London [11]. In this laboratory, tennis balls are regulated using up to six machines for measuring coefficient of restitution, stiffness, durability, high-speed dynamic testing, spin and court surface impact behaviour. The use of multiple test methods to measure specific individual characteristics of ball performance does not allow direct comparison of these

characteristics, given the different conditions present in the independent test procedures. The principal measures of regulating ball performance can be seen to be energy dissipation and stiffness, as summarised in Table 2.1. Further details of the methodologies of the above regulatory standards, where applicable, will be discussed in the following sections.

Table 2.1: Summary of COR and stiffness regulatory standards for common ball types

Ball type	COR regulation	Stiffness regulation
Baseball/ softball/ lacrosse	Rebound from 26.82 ± 0.3 m/s impact against rigid surface	Peak force from 6.35 mm quasi-static compression
Baseball/ softball	Rebound from 26.8 and 40.2 m/s impacts against rigid half cylinder	Dynamic stiffness theoretical calculation
Cricket/ hockey	Rebound from 6.26 m/s impact against steel plate	Peak deceleration from impact of 5 kg mass at 4.66 m/s
Tennis	Rebound from 7 m/s impact against granite surface	Compression at 8.165 kg for forward and reverse directions
Golf	Launch speed after strike at 43.8 m/s	Compression at specified loads – various test methods

2.1.2 Coefficient of restitution characterisation

A frequently used measure to reflect the energy lost in an inelastic collision is the coefficient of restitution (COR). This measure is determined from ratio of speeds after and before the impact for a rigid-body impact [37].

$$COR = \frac{rebou\,nd\ \ velocity}{incident\ \ \ velocity} = \frac{v}{u} \tag{2.1}$$

For methods involving observation of rebound heights, Equation 2.1 can be reconfigured in terms of height distances:

$$COR = \sqrt{\frac{rebound\ \ height}{initial\ \ height}} = \sqrt{\frac{h_2}{h_1}} \qquad (2.2)$$

Inelastic deformation occurs in most impacts due to material friction [17, 54], wave propagation [55-57] or viscoelastic effects [30, 58] resulting in a COR value of less than 1. COR values for some common sports balls are displayed in Table 2.2.

Table 2.2: Regulatory coefficient of restitution values for some major sports balls

Ball type	COR	Methodology	Ref
Hurling sliotar (size 5)	0.522 – 0.576	1.8 m drop test	
Tennis	0.73 – 0.76	2.54 m drop test	[11]
Cricket	0.53 – 0.62	2 m drop test	[10]
Hockey	0.5 – 0.61	2 m drop test	[12]
Croquet	0.76 – 0.86	2 m drop test	[16]
Baseball	0.543 – 0.549	26.8 m/s impact	[14]
Lacrosse	0.6 – 0.7	26.8 m/s impact	[23]

The proportion of kinetic energy loss during impact can be expressed in terms of the COR:

$$K.E._{loss} = \frac{\frac{1}{2}m\,u^2 - \frac{1}{2}m\,v^2}{\frac{1}{2}m\,u^2} = 1 - \frac{v^2}{u^2} = 1 - COR^2 \qquad (2.3)$$

The coefficient of restitution cannot be considered as an inherent property of the ball for all impact situations. It is dependent upon a number of factors including incident speed, oblique angle and spin, ambient conditions and impact surface properties [59].

Incident speed dependence

The coefficient of restitution tends to decrease at higher speeds. The increased initial kinetic energy results in a greater volume of the ball engaged in inelastic deformation, thus increasing the magnitude of energy loss. Traditionally, official ball regulatory standards have conducted impact tests at a single specified speed, see Table 2.1. The BS 5993 standard, included in cricket and hockey balls regulations, involves an incident speed of 6.26 m/s [10]. Regulations for tennis balls stipulate a 7 m/s impact speed [11]. The ASTM standard for baseball and softball prescribes a speed of 26.82 ±0.3 m/s [14]. The launch test of golf balls uses a striker impact speed of 43.8 m/s [21].

Given the speed dependence of COR, the use of a single speed cannot fully represent the speed relationship of ball energy dissipation. This has been recognised in the new ASTM F2845 standard for baseballs and softballs, with testing conducted at 26.8 m/s and 40.2 m/s [15]. The variation of COR with respect to speed has been observed as linear for some ball types [51, 58, 60]. However, this cannot be assumed for all cases, with ball construction and material properties contributing to non-linear behaviour. The spherical geometry of the ball implies a non-linear variation in contact area throughout the impact duration, with the balls' elastic properties dictating the volumetric deformation and thus energy dissipation. For balls of multi-compositional construction, non-linearity could be manifested due to an increased span of interaction across dissimilar material layers. The effect of construction will be described further in Section 2.2. In addition, some materials exhibit strain-rate dependent properties. Strain and strain-rate dependent phenomena will be discussed in greater detail in Section 2.1.5.

Oblique impact and spin dependence

The spin of the ball has a large effect on the measured coefficient of restitution, as shown in Figure 2.1 [37, 61]. For an oblique impact, spin can be induced in a ball due to the moment of frictional force [62]. Considering the two-dimensional motion of a ball, it can possess either forward spin (clockwise if the ball was moving left to right) or back spin (anticlockwise if the ball was moving from left to right).

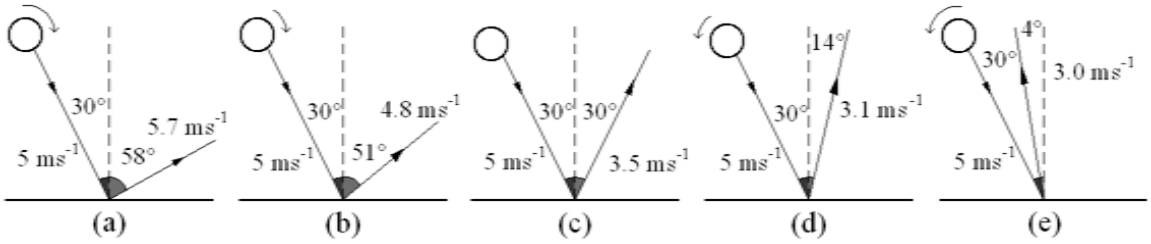

Figure 2.1: Effect of spin upon ball rebound (a) large forward spin, (b) small forward spin, (c) no spin, (d) small back spin, (e) large back spin

Forward spin results in the ball rebounding at a shallower angle to the impact surface than the approach angle. The rebound speed can exceed the approach speed due to the rotational motion being converted to translational motion [37]. Back spin would cause the ball to rebound at a steeper angle, even possibly rebounding to the same side of the perpendicular from which it approached. The study of the spin of a bouncing ball involves splitting of the coefficient of restitution into two components: the normal coefficient of restitution, as defined by Equation 2.1, and the tangential coefficient of restitution, which includes angular speed terms [63, 64]. The contribution of the angular terms to rebound behaviour is dictated by frictional forces, surface compliance and surface geometry [65-68]. High surface hardness or low friction would cause the ball to slip throughout impact, having little effect on spin. Once the ball started to roll, friction increased from its dynamic to static value, increasing back spin and in turn causing the ball to rebound at a steeper angle with lower speed [69, 70]. Variations in factors such as friction and impact surface finish poses an issue for experimental characterisation, where one study reported a tangential COR with three times the experimental scatter relative to that of normal COR [54]. This is a conservative finding as their experimentation involved a relatively precise impact surface compared to a realistic sports surface. Because of the complexities of friction, surface geometry and angular components introduced by oblique impact and spin, all ball regulatory standards specify perpendicular impacts without initial spin to allow unbiased comparison between ball types.

Ambient conditions dependence

The ambient temperature can have an effect on the ball's viscoelastic properties or internal pressure (if hollow). Higher temperatures have been found to increase the COR of tennis balls due to the increased internal pressure [11]. Conversely, the COR of croquet balls was observed to decrease with increasing temperatures due to a change in morphology of the cross-linking agents in the rubber compound used in its construction [71]. The COR of modern real tennis balls was reported to be relatively insensitive to temperatures ranging from 3 to 40 °C [72]. This finding has been reported to contrast with the behaviour of older real tennis balls (from the 1960s and 1970s) that exhibited significant temperature dependence due to their polymer core viscous properties [72, 73]. Baseballs have been reported to have a marginal 2 % increase of COR with temperature from – 4 °C from 20 °C [74].

On a related note, repetitive impacts can result in an increase in core temperature of the ball due to internal friction arising from deformation. An internal temperature rise of 0.5 °C has been recorded for a typical golf ball impact [37]. An increase of 10 °C has been reported for a softball impacted 100 times within 120 minutes [60]. This increase in core temperature of the softball results in a decline of ball COR, in contrast to the previously reported increased COR of a squash ball [37].

Ambient humidity can affect the ball's weight due to moisture absorption. Real tennis balls, immersed in water for 20 seconds to simulate the effect of humidity, have exhibited a 10% increase in ball weight [72]. Using a controlled humidity atmosphere, softballs have been observed to take 14 days to reach steady state mass from humidity moisture intake [24, 75]. A weight increase of 9 % has been reported for softballs from the range of 40 to 90% relative humidity (RH) [76]. Similarly for baseballs, the average ball weight has been reported to increase by 8% at 100% relative humidity (RH) and decrease by 1.3% at 0% RH [77]. The effect of the mass increase on COR depends on the ball material and construction: real tennis balls exhibit a 4 to 10 % decrease in COR [72]; baseballs' COR decreases by 9% [77]; softballs exhibit a COR decrease of 3.3% in one study [76] and a COR increase of about 1% in another study [60]. While these studies disagreed on softball COR variation, they both reported the dominating effect of

mass increase on quasi-static stiffness characteristics. Stiffness characteristics will be discussed further in Section 2.1.5.

Previous studies on hurling have looked at the water absorption capacity of sliotar [5, 7]. These investigations have not focused on humidity, but rather have been motivated by Ireland's wet climate and the balls' porous leather covering and seams. A repetitive procedure of water immersion and impacts was proposed for the draft specification for the sliotar in 1999 [6], although ultimately this draft standard has not been implemented.

In recognition of the effect of ambient conditions on performance, the regulatory standards mentioned in Section 2.1.1 include specifications for temperature and humidity. The control of ambient conditions is particularly important when considering international standard regulations, where typical laboratory temperature and humidity can differ due to a country's climate. This was observed for croquet balls, where a particular brand of ball passed the specification in the UK but was outside specification when tested in South Africa [71]. The specified ambient conditions of the regulatory standards are summarised in Table 2.3.

Table 2.3: Ambient conditions for regulatory standards

Ball types	Pre-testing	During testing
Baseball/ softball/ lacrosse	24 hours at 22 ± 1°C and 50 ± 5% RH	22 ± 1°C and 40 ± 20% RH within 20 minutes of removal
Cricket/ hockey	24 hours at 20 ± 2°C and 65 ± 5% RH	20 ± 3°C and 60 ± 15% RH
Tennis	24 hours at 20 ± 1°C and 60 ± 5% RH	Not stated
Golf	3 hours at 23.9 ± 2 °C	23.9 ± 2 °C

The dependence of COR on the frequency of testing is circumvented by allowing the ball to recover between impacts to avoid internal temperature rise within the core of the ball. One study has recommended that softball impacts be limited to a frequency of 10 impacts per hour [60]. Other studies have used a less conservative minimum rest period

of 2 minutes between impacts [24, 58], while ASTM F1887 standard specifies a minimum of 30 seconds between impacts [14]. The disparity between the different recommendations regarding impact recovery periods reflects the contribution of different ball materials to internal temperature rise and consequent variation in impact COR. Water absorption characteristics have not been incorporated into official regulatory standards, which is understandable given the irrelevance to some sports. Moreover, the presence of water adds significant complication to an experimental apparatus, threatening electronics and visually obscuring high-speed footage. The experimental analysis is further complicated by elastohydrodynamic theory, where the impact can be affected due to fluid adhesion and viscosity [78].

Impact surface dependence

In the observation of a controlled collision between two bodies, the impact characteristics are dependent on the dynamic behaviour of both bodies [79]: i.e. the dynamic response of one body cannot be analysed in isolation of the response of the other body. This has been demonstrated in a study of so-called "happy" and "unhappy" balls, these being novelty ball types with coefficients of restitution of nearly 1 (almost fully elastic) and 0 (almost fully inelastic), respectively [19]. This study finds that the collision of the happy ball and unhappy ball is neither perfectly elastic nor perfectly inelastic, as might have been expected given the balls' respective COR values. This finding has been applied to a tennis ball impact against racket strings. The happy/unhappy ball analogy is transferred by hypothetically considering the tennis ball COR as 0 and the racket stings being perfectly elastic. Based on the analytical analysis derived of the happy/unhappy ball collision, it has been found that the absolute nullification of the tennis ball's COR results in a serve speed reduction of only 19%. In a separate study, croquet balls have been subjected to impacts against rigidly-clamped surfaces of steel, wood and plastic [80]. In comparison to the steel impacts, it has been found that the ball rebounded slightly quicker off the wooden surface and slower off the plastic surface. While both the wooden and compliant surfaces induced similar deformation in the ball, less than that induced by the steel plate, the plastic surface

dissipates a greater proportional of the impact energy. These studies conclude that the relative stiffness of the two colliding bodies, as well as the bodies' individual COR, contribute on the impact behaviour.

Intrinsic characterisation of a ball's impact behaviour is attained by the use of a rigidly-mounted non-compliant impact surface. In such impact, all energy loss is associated exclusively to the deformation of the ball during impact. The coefficient of restitution measured from this method has been referred to as *rigid-body COR*. This characteristic enables the comparison of impact properties of different ball types. The rigid impact plate has two additional advantages. Firstly, being significantly harder than the ball and hence unlikely to suffer permanent deformation, it provides repeatable results over the course of impact testing. Secondly, being producible to a defined specification, it allows inter-comparison between separate studies. The incorporation of a load-cell into the rigid surface enables the measurement of force-time data, which will be discussed further in Section 2.1.3. The load-cell compliance, which threatens the 'rigid' definition of impact surface, has been found to be small enough to have a negligible effect on COR measurement [46]. In a separate investigation, only surfaces of relatively large compliance affected COR measurements [81]. This has been verified for softball impacts, where the 0.7% COR discrepancy between load-cell impact and rigid wall impact was within experimental error [60]. All regulatory standards mentioned in Section 2.1.1 use a rigid impact surface to allow objective comparison of ball types. The ASTM F1887standard for baseball and softball specifies a rigid metal plate: 5 cm thick, 60 cm^2 area, bolted to a 20 cm thick concrete block. The BS 5993 standard specifies a smooth concrete surface, where the concrete block is at least 1000 kg and 0.9 m thick [10]. The International Tennis Federation uses a smooth granite block of unspecified dimensions [11].

The inclusion of sport surfaces, seemingly to increase the resemblance of the testing to the sport conditions, adds substantial complexity and variability to the ball impact characterisation. The regulatory ASTM F1887 standard for baseball and softball specifies in one of the impact test methods to use an impact surface of *"10.2 cm thick northern white ash wood with moisture content between 10 and 15% with a flat smooth surface"*. While this method mimics the material of the baseball bat, the standard does

not specify further details on this wooden surface concerning its durability or surface preparation. In an observation of tennis and golf impacts, it has been noted that the hardness of the more compliant surface contributed the most to impact behaviour: where hardness of turf is an important parameter for golf ball impacts, and the hardness of the ball is a more important parameter for tennis ball impacts [69]. Turf surfaces include variations such as bulk density and moisture content [43], as well as the need to account for indentations due to surface compliance [82]. The friction force between the ball and court surface has been identified to be the dominant factor in categorising slow clay courts and fast grass courts in tennis [83]. The variability of the friction and surface finish is shown in a separate study [84], where the scatter in the experimental data for court surface impacts has made it impossible to distinguish between the two tennis ball types of distinctly different COR values. The relative compliance of the impacting bodies and difficult-to-control variables in sport surfaces signifies that such characterisation is exclusively relevant for the experimental apparatus in question, inhibiting comparison with other experimental data. The degradation of sport surfaces, such as permanent deformation in turf, ground or wooden surfaces, or loss of tension in tennis racket strings, poses difficulties for consistent and accurate characterisation of a ball.

A number of variations of coefficient of restitution have been proposed in characterising ball impact against sport-representative surfaces. The *apparent coefficient of restitution* (ACOR) has been reported as the ratio of ball speed before and after impact with the suspended tennis racket [18]. The ACOR differs from rigid-body COR due to the compliance and deflection of the tennis racket. For such impacts, the racket is suspended freely from a pin at the top of the racket head in an attempt to simulate the support of a player's grip. One study finds the differences between ball types are more apparent with respect to ACOR rather than rigid-body COR, although this has been found to be highly dependent on string tension [35]. The analysis of a separate study claims a 50 % increase in string-bed stiffness results in an 11.1 % reduction in ACOR but only a 3.3% decrease in the launch speed of the ball [18]. The conclusions of these papers have indicated that the ACOR is not particularly insightful in characterising ball energy dissipation due to its dependence on factors such as string tension, racket head size and

string type. Several studies on baseball and softball have focused on the interaction between ball and bat [85-88]. In these studies, this approach has been presented as being useful due to the ball-bat strike being the prevailing action in the sport. A solid steel half-cylinder with 57 mm diameter has been frequently used to represent the barrel of a bat [24, 45, 75]. The COR measure from this set-up is labelled the *cylindrical coefficient of restitution* (CCOR). A geometry-dependent relationship like CCOR is not specifically applicable to hurling given the planar surface of the hurley head. The CCOR of a softball has been reported to be 6.5% less than the flat-surface COR [60]. The extra energy dissipation is attributed to the more concentrated local deformation caused by the impact surface curvature. The curvature of the impact surface necessitates a ball propulsion method with precise aim for correct alignment of the ball, where difficulties have been reported for using a standard pitching machine [60]. Despite this, the CCOR measure of ball energy dissipation has been deemed appropriate for the official characterisation of baseballs and softballs, as evident from its inclusion in the newly developed regulatory standard ASTM F2845 [15]. The effect of bat compliance has been examined by impacting a bat that could pivot about a fixed point [24, 75, 89]. Such ball-bat impact behaviour has been characterised by the *bat-ball coefficient of restitution* (BBCOR). The BBCOR is measured from the sum of ball and bat rebound speeds, divided by the ball incident speed. BBCOR differs from ACOR due to the inclusion of bat speed terms. The relationship between BBCOR and ball rigid-body COR depends upon the bat behaviour. Hollow bats exhibit a so-called *trampoline effect*, where the bat deformation was nearly perfectly elastic. The minimal energy dissipation of the trampoline effect has been found to result in a ball's BBCOR exceeding its rigid-body COR [24]. The trampoline effect is negligible in stiff-barrelled bats, such as thick walled or solid wooden bats [90]. In these cases, the BBCOR is dependent on the relative stiffnesses of the ball and bat. For solid wood bats impacted near the 'sweet spot', the lower compliance of the bat relative to the ball results in a BBCOR similar in magnitude to the ball's rigid-body COR [24]. The effect of bat compliance is characterised by the Bat Performance Factor (BPF), which was the ratio of BBCOR to rigid-body COR [87]. This characteristic has been reported to be limited due to its assumption of a linear relationship between BBCOR and COR [75]. It has been found to be adequate for low performing bats but it overestimates performance for higher performing bats [75].

COR measurement methodology

The predominant method for measuring coefficient of restitution is to propel a ball at a stationary rigid impact surface. Propulsion of the ball is achieved by the use of a pendulum; a drop under gravity from a height; or projection from a device as described in Section 2.1.1. It is measured typically by either of two ways: measuring the rebound height from a drop from known original height (Equation 2.2), a method used by the International Tennis Federation for regulatory testing [11]; or by measuring the ratio of incident and rebound speeds (Equation 2.1). Equipment for measuring speeds includes light-gates, stroboscopic photography and high-speed photography.

Light-gates are a relatively simple device, consisting of two sets of optoelectronic sensors separated by a known distance. Such devices have been used due to their simplicity and low cost [7, 17, 35, 48, 51]. Their accuracy for instantaneous speed measurement can be compromised if the separation distance is too great, such as in one case where the light sensors were separated by 490 mm resulting in an error of up to 12% [7]. In general, light-gates require exact positioning to ensure that the ball passes both beams, which can be problematic when dealing with oblique impacts. This can be circumvented by the use of more complex light-curtains, which consist of a series of light sensors that cover an area through which the ball would pass.

Stroboscopic photography involves the use of a stroboscopic light source in conjunction with one or more still-frame cameras with a long exposure time, with the result that high-speed motion of the object is recorded in a single image frame [91]. While this method is relatively inexpensive, the sample rate (i.e. the frequency of the light source) is limited to avoid overlapping of the ball images. For example, one study on oblique impacts of a cricket ball was limited to a sample rate of 335 Hz, resulting in an time measurement error of 3 milliseconds [43].

The most versatile device for ball motion measurement is a high-speed camera, with the capability of measuring ball motion such as speed, angles, spin and deformation. These cameras have a pixel array with a specific data output rate, signifying that higher frame-rates are achieved by reducing the pixel resolution [92]. Hence, it is a compromise between sample rate and dimensional accuracy. High-speed cameras are classified

according to the frame-rate corresponding to an acceptable resolution. Entry-level cameras have frame-rates below 1000 frames per second (fps); mid-range cameras have 2000 – 10000 fps; and specialist cameras have 10000+ fps.

The images from both stroboscopic photography and high-speed photography require post-analysis to extract speed information. Typically, speeds and angles are derived from the measurement of distance between points that were manually placed on the images using photographic software. In some studies, spin has been measured using markings on the ball surface, such as self-adhesive reflective strips used [43] or ink dots [48]. Care has to be taken that such markings did not interfere with the ball impact process.

A lesser used method has involved the stationary ball being struck by a moving impact surface, although it is difficult to derive a COR value directly from this technique. This method is used in the golf regulatory standard, where the stationary ball is struck by a striker attached to a rotating wheel [21]. A similar method has been considered in the development of a draft specification for the sliotar in 1999, where a stationary sliotar is struck by a projectile fired from a pneumatic cannon at 29.2 m/s [7]. The projectile has a mass of 350 g to represent the effective mass of a hurley head. The complication of measuring the speeds of multiple projectiles is probably one of the reasons that this test was not incorporated into official GAA regulations.

2.1.3 Force-time characterisation

The measurement of force during impact facilitates the evaluation of several impact characteristics. These characteristics are derived from force-time data and include peak force, acceleration, impulse and contact time. Figure 2.2 shows typical force-time profiles for a softball and a tennis ball impact.

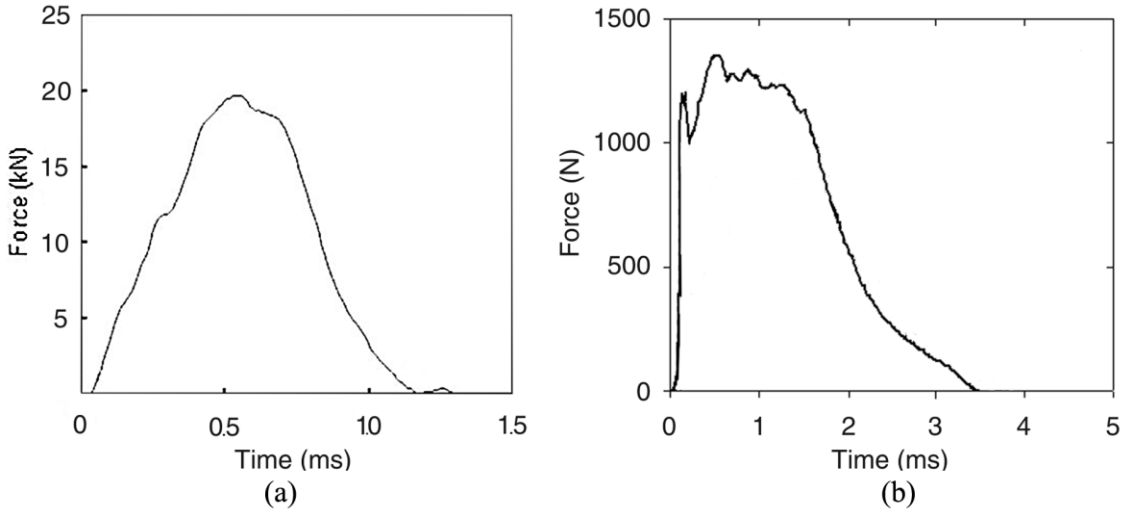

Figure 2.2: Typical force-time profiles of (a) softball and (b) tennis ball

For a ball of homogeneous construction, such as the softball, the peak force tends to be near the middle of the impact duration. This corresponds to the time near to maximum compression, as seen in Figure 2.2 (a) [24]. The profile for a ball of heterogeneous construction can be quite different, as shown by that of a tennis ball in Figure 2.2(b) [50]. A rapid initial rate of force produced the first peak, with the force declining due to a change in stiffness as each material layer becomes progressively engaged (the buckling of tennis ball shell into the hollow centre in this case). The force then continues increasing as the ball continued to deform, reaching a second peak that corresponded approximately in time with maximum deformation. Upon restitution, a third peak may exist as the ball's outer layer unbuckles. This form of force-time profile is present in both hollow balls and solid balls with distinct layers of materials of dissimilar stiffness, with similar steep shoulders with multiple peaks being observed in solid three-piece golf balls [93].

Assuming ball mass can be attributed to a single point, that being the centre-of-mass (COM), the ball COM acceleration can be calculated by dividing the force by the mass. This is valid for a rigid-body impact, where all impact forces exerted are associated exclusively with the ball deformation. The impulse, the change of momentum during impact, is evaluated by integration of the force data with respect to time. Graphically,

this corresponds to the area underneath the force-time curve. For a rigid-body impact, the value of impulse is directly related to COR, as shown in Equation 2.4.

$$\text{Impulse} = \int F(t)\ \mathrm{d}t\ =\ mu - m(-v) =\ m\,(u+v)\ =\ m\,u\,(1+\text{COR}) \qquad (2.4)$$

Contact time, the duration that the ball is in contact with the impact surface, is measured from the width of the force-time profile. The force transducer is a useful method of measuring contact time due to its typically high sampling frequency. Contact time has been reported to decrease with increasing speed due to non-linear ball stiffness [19]. Ball stiffness and its relationship with speed will be discussed in greater detail in Section 2.1.5.

As described in Section 2.1.1, force-time characteristics are relevant to player perception of feel and hardness. In player trials with tennis balls, a reasonably consistent correlation (no R-value included) has been reported between peak force and a player's perception of hardness [40]. A report in 2008 has described new Bridgestone golf balls being developed with the aim of reducing peak accelerations in the ball, thus feeling softer and more comfortable to the player [29]. A report on traditional and modified baseballs finds that traditional ball types have steep, short force-time curve (high peak force, short duration) while modified ball types have a shallow, long force-time curve (lower peak force, extended duration) [51]. The areas underneath the force-time curves for each ball type have been found to be similar in magnitude, implying comparable impulses and hence similar rigid-body COR values. The study [51] has recommended the use of modified baseballs for games at youth level due to the additional safety of lower peak accelerations and the extra degree of controllability associated with longer contact time.

Force-time measurement methodology

A load-cell can be used to measure force. There are two primary types of load-cell: piezoelectric and strain-gauge. Both of these devices output a voltage proportional to the applied force. Piezoelectric load-cells contain a material that generates a specific voltage when subjected to compression, while strain-gauge load-cells are comprised of strain-

sensitive variable resistors. Piezoelectric load-cells tend to have a smaller deflection at maximum load [46], implying a closer representation of a rigid-plate. However, piezoelectric load-cells have been reported to have a lower force capacity than strain-gauge load-cells [46], limiting the speed range of impact characterisation. As mentioned in Section 2.1.2, the compliance of a strain-gauge is found to produce a negligible effect when compared to impacts against a rigid wall [60]. A custom designed apparatus used in one study consisted of a steel bar, 3 cm diameter impact surface and 1.8 m long, with the impact force obtained using the 1D theory of wave propagation from a strain gauge fixed to the steel bar [52].

Given that impulse can be derived from force data and momentum can be measured from an independent device, the equation of rigid-body impulse and differential momentum (Equation 2.4) can be used to calibrate the experimental apparatus [16, 17, 24]. In one study, the momentum measurement device was identified as being more accurate [24]. By scaling the force data in accordance with Equation 2.4, the experimental scatter was reported to have decreased from 3% to 1.5%.

Of the regulatory standards introduced in Section 2.1.1, the impact force, impulse nor contact time are regulated per se. The regulatory standards attempt to relate the impact force to a specified deformation or deformation rate. These measures are more applicable to stiffness, and so will be discussed in Section 2.1.5.

2.1.4 Deformation characterisation

Ball deformation results from the abrupt deceleration associated with its impact against another body. Densification occurs when the ball material(s) in the contact region compresses during impact. This is evident from a reduction in the ball's diameter perpendicular to the impact surface. Depending on the ball material and construction properties, the volumetric deformation may lead to expansion of the ball's diameter parallel to the impact surface, particularly for materials of higher Poisson's ratio. The asymmetrical and complex nature of ball deformation poses an issue in selecting which

physical dimensions to measure. The ambiguity of this measurement has been reflected by the abundance of descriptive terms for ball deformation in the literature, some of which have been used interchangeably within individual papers. These terms include *ball deformation* [18, 94], *ball compression* [17, 19, 95, 96], *dynamic compression* [17, 20], *longitudinal/lateral deformation* [97], *ball outer diameter histories* [52], *ball span* [48], *surface-normal/parallel diameter* [98] and *deflection* [16, 36, 99, 100]. This diversity has been further complicated by some studies using the term *dynamic compression* to describe the peak force [60, 81]. The term *deflection* has been carried over from quasi-static testing, where the term applies to the movement of the machine platens and is not particularly relevant to ball impact. In this present work, the term *deformation* is used to describe qualitatively the change in shape of the ball. This change in shape may be two-dimensional, as demonstrated in Figure 2.3, and thus it would not be appropriate to assign a single numerical value to the term *deformation*.

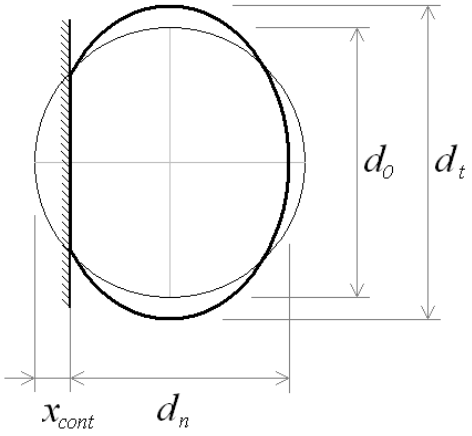

Figure 2.3: Schematic of ball deformation during impact

The quantitative measurement of deformation poses a challenge in terms of deciding the selection of the dimensions to measure and the technological difficulties in determining such dimensions. A number of measures have recurred in the literature: **contact approach**, **diameter compression**, **lateral expansion**, **compression ratios** and **centre-of-mass (COM) displacement**. The **contact approach** has been defined as the

difference between the ball's undeformed radius and the distance between the impact surface and the centre of the circle centred on the deformed ball (x_{cont} in Fig 2.3(b)) [97]. Using simple geometrical methods, the contact approach and ball radius have been used to calculate the contact area. However, the contact approach parameter is an abstract dimension, and so is difficult to physically measure. The complex nature of deformation can be simplified by considering the orthogonal changes in ball shape. **Diameter compression** is the physical measurement of the reduction of the ball diameter perpendicular to the impact surface ($d_0 - d_n$ in Figure 2.3). **Lateral expansion** describes the increase in ball diameter parallel to the impact surface that can occur in some ball types ($d_t - d_0$ in Figure 2.3). These two physical measures have been described in terms of compression ratios [48, 49]. The **normal** (η_n) and **tangential** (η_t) **compression ratios** expresses the ball's diameter compression and lateral expansion respectively in percentage form.

Normal compression ratio: $$\eta_n = 100\ \frac{d_0 - d_n}{d_n} \tag{2.5}$$

Tangential compression ratio: $$\eta_t = 100\ \frac{d_t - d_0}{d_t} \tag{2.6}$$

where d_0 is the original ball diameter, d_n is the maximum diameter compression and d_t is the maximum lateral expansion. For a study of golf balls tested over a range of speeds, a nearly linear relationship was found between the lateral expansion and diameter compression, where the tangential compression ratio was observed to be 25 – 35% of the normal compression ratio [48, 49]. The percentage form of the compression ratios are useful for characterising ball performance; however these measures are not applicable where absolute deformation values are required. The predominant method for quantifying ball deformation appears to be **COM displacement** [16-20, 24, 30, 35, 36, 50, 101]. This measure is evaluated from the double time integral of the acceleration, as derived from force data for a rigid-body impact. This measure has been found to agree with the estimated motion of the ball's centre-of-mass, as observed from tracking markings on the surface of a golf ball [23].

The relationship between COM displacement and other physical deformation measures has been the subject of conflicting reports. The relationship between diameter compression and COM displacement has been described as “not easily determined” due to the asymmetrical deformation of the ball [17]. A separate study theorised, without experimental verification, that the diameter compression was up to 70% greater than the COM displacement for tennis balls [20]. Another paper approximates that the diameter compression equals the COM displacement if the diameter compression is significantly less than the ball diameter [19]. In spite of the two aforementioned assertions, a subsequent publication assumed explicitly that COM displacement was analogous to diameter compression for a tennis ball for a range of impact speeds [18]. In another paper by the same author, the COM displacement and ball diameter have been to geometrically calculate the contact area [50]. The analogous calculation of contact area in independent publications using contact approach [97] and COM displacement [50] would suggest equivalence between contact approach and COM displacement, although this does not appear to have not been verified in any publication to date. In a study of cricket balls, it has been claimed that COM displacement equals diameter compression since the impact surface is rigid [16]. Other studies employing the COM displacement method do not refer to diameter compression [24, 35, 36, 50, 100, 101], inferring that COM displacement is the exclusive measurement of a balls’ physical deformation. These studies do not seem to consider lateral expansion and the possible effect it has on the relationship between COM displacement and diameter compression. The studies that have evaluated both diameter compression and lateral expansion do not contain COM displacements. The relationship between theoretically-derived COM displacement and the physical measures of diameter compression and lateral expansion remains ambiguous in the literature.

The measurement of ball deformation has a number of merits in performance characterisation. Ball deformation is likely to have an influence on players’ perception of ball hardness or softness. Larger deformations result in a greater area of the ball surface in contact with the impact surface. Increased contact area between the ball and striker could affect aim and control of a strike due to the greater influence of the trajectory of the striker on the direction of the ball. For ball constructions with multiple

layers, the extent of deformation dictates the various constituent materials' contribution to the impact, thus having an effect on ball performance. Deformation characterisation is also relevant to evaluating ball durability, where increased wear and material distortion could arise from larger deformations. In addition to charactering ball performance, the quantification of ball deformation is useful for viscoelastic characterisation and model simulation validation. Viscoelastic characterisation involves the compilation of force-displacement graphs, where the appropriate measurement of deformation is required for the X-axis of such graphs. This process will be described further in Sections 2.1.5. Model simulations describe the equations of motion and change of shape of a ball, where the choice of quantitative measurement depends on the aspect of deformation that the model is attempting to represent. Impact modelling will be discussed in Section 2.3.

Deformation measurement methodologies

The methods of quantifying deformation outlined in the previous section are distinguished by their measurement methodologies. The COM displacement is derived from the double time integration of COM acceleration as measured by a force transducer. As mentioned in Section 2.1.3, the ball acceleration can be evaluated from the division of force by ball mass in a rigid-body impact. The experimental simplicity of requiring only a force transducer fitted to the impact plate may explain, in part, the popularity of the COM displacement method.

The other methods of deformation quantification have been measured using **laser light gates** [17], **laser vibrometer** [97], and **high-speed footage** [35, 48, 49, 52]. The use of **laser light gates** has been found to involve iterative trial-and-error in positioning the light-gate sensors [17]. A **laser vibrometer** measures deformation by recording the motion of the ball surface by analysis of the Doppler shift of the emitted laser beam. This method is reported to be highly sensitive to the laser beam alignment and may be limited to an upper capacity of 15 m/s [97]. This capacity limit is also reported in another study [81], calling into question the appropriateness of this device for this type of measurement. **High-speed cameras** have been the most versatile measurement method. The limiting compromise between frame-rate and pixel resolution has been an

issue in early studies [17]. A high frame-rate is necessary to acquire data from the typically small impact durations. High pixel resolution provides greater accuracy with each pixel corresponding to a more precise real-world dimension. The image-processing of the high-speed footage is complicated by the curvature of the ball, where the luminance of the two-dimensional ball image has been reported to darken towards the edges, inhibiting isolation of the ball from the background [91].

2.1.5 Viscoelastic characterisation

Viscoelastic characterisation refers to the evaluation of the stiffness and energy dissipation properties. These properties represent the elastic and viscous components of the material viscoelasticity, which can be sensitive to deformation magnitude (strain dependence) and deformation rate (strain-rate dependence). The viscoelastic characteristics are an inclusive consideration of both force and deformation characteristics, as measured from force-displacement graphs. Examples of force-displacement graphs are shown for a softball [24] and tennis ball [50] in Figure 2.4. Ball stiffness is evaluated from the gradient of the compression phase (top left edge) of the force-displacement curve. The finite area between the compression and restitution phases indicates hysteresis energy dissipation. The proportion of area enclosed within the hysteresis loop corresponds to the proportion of energy dissipated in the deformation. With regard to impact, the proportion of energy dissipated equates to the proportion of kinetic energy loss, as calculated from Equation 2.3.

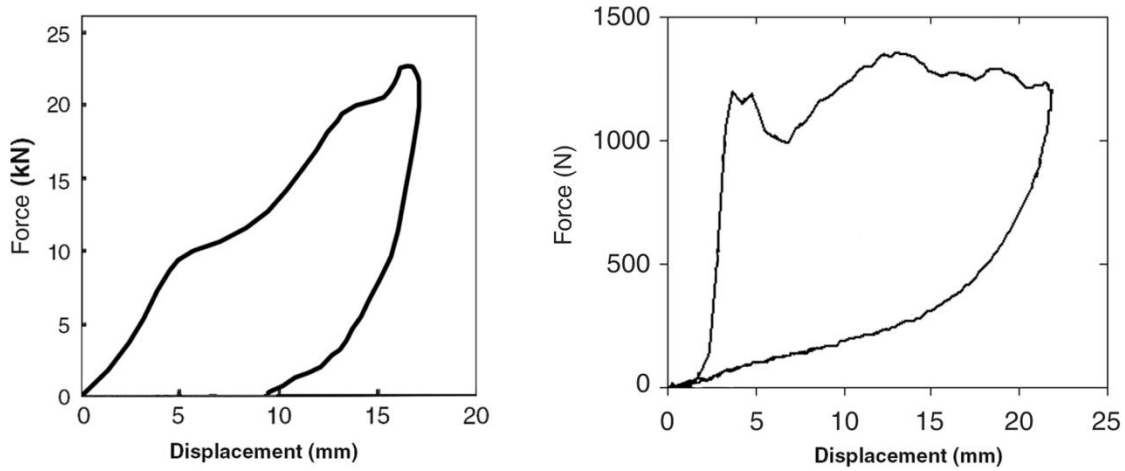

Figure 2.4: Typical force-displacement graphs for (a) softball, (b) tennis ball

The consideration of stiffness is significant to sport for two major reasons: firstly, it is the engineering measurement that is the closest equivalent to player perception of **hardness**; and secondly, for **compliant-body impact**, the relative stiffness of the ball and impact surface determines how incident kinetic energy is partitioned between the two impacting bodies.

Player perception of **hardness**, as mentioned in Section 2.1.1, has been reported as an abstruse quality to define scientifically [35, 40]. In spite of the difficulties in relating engineering measures to user-subjective perceptions, the association of ball stiffness with ball hardness has been evident from regulatory standard testing, as summarized in Table 1. The methods employed in regulating ball stiffness are described in further detail later in this section.

In addition to representing ball hardness, the evaluation of stiffness can allow for the translation from rigid-body impact to sports-representative **compliant-body impact** [19]. This has been the subject of studies on baseball and softball [75, 89, 99], investigating the so-called *trampoline effect* of the bat. As mentioned in Section 2.1.2, the trampoline effect describes the elastic recovery of a thin-walled hollow bat. A stiffer ball induces a greater extent of deformation in the bat and a lesser extent of deformation in the ball. Due to the efficient recovery of energy from the deformed bat, a stiffer ball

would rebound at a greater speed than a more compliant ball. Therefore consideration of ball stiffness as well as coefficient of restitution is important in characterising ball performance.

Strain dependence

The strain dependence of viscoelastic characteristics has been apparent from dynamic stiffness fluctuations throughout impact duration. This variation in stiffness can be due to surface curvature flattening, multi-compositional material contribution and inherent material effects.

Considering the spherical geometry of a ball, the deformation magnitude dictates the extent of flattening of a ball's surface curvature. The Hertz theory for elastic collision, shown in Equation 2.7, has been developed to account for the effect of the flattening of a surface curvature [39]. This theory states that stiffness is a constant, *k*, related to the extent of ball deformation to the power of 1.5

$$F = k\, x^{1.5} \tag{2.7}$$

The 1.5 factor is an advancement of Hooke's law. While Hertz theory has been found to give reasonable agreement for low speed ball impacts [102, 103], its basis on purely elastic collision implies a limited applicability to typical sports ball impact.

The multi-compositional constructions of some sports balls introduce an extra factor in the strain dependence of stiffness. This variation in stiffness is due to the progressive engagement of distinct material layers of different stiffness properties with increasing impact deformation. This results in a difference in performance for multi-compositional constructions, such as in tennis balls [20, 50], multi-piece golf balls [58, 93] and hockey balls [94]. The fluctuation of stiffness during a tennis ball impact has been attributed to cloth cover compression and buckling of the ball shell at a certain magnitude of deformation [20]. Such stiffness fluctuations have been observed to become more pronounced for higher speed impacts [50]. In solid balls with dissimilar material layers,

the stiffness has been observed to vary depending on the contribution of each layer engaged in the impact deformation [58, 93, 94]. The dependence of stiffness on the deformation magnitude can have a significant effect on ball performance. For example, two- and three-piece golf balls have been observed to have a similar performance at normal or low angle impacts but a divergence in behaviour at higher angle impacts [93]. The dissimilarity in outer layers of the different ball types has not been manifested in normal impacts, where deformation extends within the outer layers. As higher angle impacts induce less deformation, the outer layers become the dominant contributor to behaviour thus producing a deviation in performance between the two different ball types.

In addition to the interaction of distinct material layers, some materials exhibit strain dependence due to inherent material effects. This has been reported for polymer foam materials, where the cellular structure has a stress-strain characteristics comprising of three regions typically labelled linearly elasticity, plateau and densification [104-106]. The first region involved initial strains up to 5 % strain, where an initially stiff response has been reported that corresponds to foam cell wall bending. This stiffness has been reported as linearly elastic, with the stress-strain slope equalling Young's Modulus [104-106]. The subsequent region involved an abrupt reduction in stiffness due to foam cell collapse [107-109]. This plateau response typically extends up to 30% strain. This material response has been referred to in softball studies as non-linear material softening [27, 110], and has been reported to dominate other strain dependent properties such as surface curvature and geometrical effects [110]. The final region of stress-strain behavior consists of a rapid increase in stiffness, where the opposing cell walls meet and touch, consolidating such the stiffness response is that of the matrix material other than the foam [104-106].

Strain-rate dependence

Early work on impact characterisation has assumed that the stiffness remains independent of impact speed [111]. A constant stiffness had been reported for cricket ball impacts, although it involved only a small range of low speeds (2.7 to 6 m/s) [16].

No indiscernible difference in quasi-static stiffness had been observed for baseballs for a range of compression rates (0.01 to 1.0 mm/s) [45]. However this study acknowledged that this might not be the case for deformation rates approaching that of actual impact. Subsequent studies have observed an increase in ball stiffness with increasing speed [19, 35], an unsurprising finding given the stiffness strain dependence at larger deformations associated with increased speeds. However, in addition to viscoelastic strain dependence, some materials exhibit strain-rate dependence. This has been observed for cricket balls [30, 100] and golf balls [112], where higher stiffnesses have been recorded for faster quasi-static compression rates (0.08 to 83.3 mm/s). Polymer foam materials, in particular, have been observed to exhibit sensitivity to strain-rate, where the stiffness modulus was observed to increase by 41% for strain-rates ranging from 0.001 to 460 s^{-1} for polystyrene foam [105, 107, 109, 113]. The high strain-rate dependence of polymeric foams is due to both the matrix material properties and the presence of air inside the foam [105, 114]. When the foam deforms, the air is compressed or forced outside depending on the foam cellular structure (closed or open cells, respectively). This air flow is strongly influenced by the deformation rate, hence resulting in strain-rate sensitivity [105]. The strain-rate dependence of some polymers has been found to be more pronounced at strain-rates above 1000 s^{-1} [109, 113]. Such strain-rates are representative of impact conditions. High-density polyethylene and expanded polystyrene foam was found to be have a 28% and 32% increase in stiffness, respectively, from 0.01 to 1000 s^{-1}, with a subsequent 52% and 45% increase in stiffness, respectively, from 1000 to 4000 s^{-1} [113]. In a study on polymer softballs, the strain-rate dependence was evident from a 33% increase in stiffness over the strain-rate range from 0.3 to 2780 s^{-1} (no values for intermediate strain-rates were reported [25].

Viscoelasticity measurement methodologies

In the evaluation of material viscoelastic properties, a number of methodologies have been employed as an alternative to actual impact testing. These methods include **stress relaxation**; **Dynamic Mechanical Analysis**; **split Hopkinson pressure bar** apparatus; and **quasi-static compression**. All of these methods have limitations in replicating ball impact conditions.

Stress relaxation, featured in numerous studies [26, 30, 32, 99, 112, 115], involves the placing of the ball under an applied load (typically 1 to 6 kN) and measuring the force response over an extended period of time (1 hour). However, a study on hockey balls concluded that stress relaxation is not sufficient for predicting rapid material response, thus having limited applicability to dynamic impact conditions [26].

Dynamic Mechanical Analysis (DMA) is a well-established method for determining material viscoelastic properties [27, 116]. This method involves subjecting the material sample to cyclic vibrations (0.1 to 100 Hz) and measuring material response [117]. Issues have been reported in using DMA to characterise softball material, where the small strains induced during DMA (typically 20 μm) did not account for the strain dependent non-linear softening that occurred to the polymer material at large strains [27].

The **split Hopkinson pressure bar** (SHPB) apparatus is another well-established material characterisation methodology [115, 118, 119]. It involves the analysis of a force signal that is transmitted and partially reflected through the material sample. A number of issues have been observed in the application of this method to testing softball polymer materials [28, 46]. Firstly, the SHPB does not describe the unloading response, thus not permitting material hysteresis to be quantified. Secondly, the small thickness of the sample limits the deformation magnitudes (up to 0.5 mm) and range of strain rates (not less than 2780 s^{-1}) achievable by the apparatus. A sample of thickness 2 mm has been used to achieve an acceptable signal-to-noise ratio and to attain uniform stress distribution, both of which are requisites for the validity of this technique. Such small strains do not replicate the strain-dependent response exhibited by polymer materials.

Quasi-static compression has questionable applicability to impact behaviour due to the difference in deformation (bilateral symmetrical compression in quasi-static compression compared to unilateral asymmetrical deformation in impact) and in deformation rate. The International Tennis Federation use a quasi-static compression method, recording two measures of ball compression corresponding to specific force reading in the compression and recovery phases to account for hysteresis [11]. This method was called into question in one study, where the quasi-static stiffness of 10.9 to

14.3 kN/m of a Wilson ball has no apparent link to the dynamic stiffnesses of 87.5 kN/m and 34.1 kN/m at t = 0.2 ms and maximum compression, respectively [20]. The ASTM F1888 standard regulates the so-called *compression value* (quasi-static peak force) for baseballs, softballs and lacrosse balls [13, 23]. The method specifies 6.35 mm quasi-static compression of the ball between two steel plates at a rate of 0.42 mm/s. The appropriateness of this standard has been disputed, with claims that the deformation magnitude and rate are 5 and 10,000 times lower respectively than play conditions [110]. One study has compressed baseballs to 50% of the original diameter [120], although such compressions could present a risk of permanent damage to the ball. In a separate study of baseballs, no relationship has been found between the quasi-static hysteresis dissipation and the impact kinetic energy dissipation ($1 - COR^2$) [51]. The quasi-static hysteresis loss for golf balls has been reported to agree with general trends for coefficient of restitution, but proportional differences between the COR values for individual ball types have not been replicated [58]. In a study of various softball materials, balls of similar dynamic stiffness exhibit a greater variation in quasi-static compression than anticipated by the authors [25]. At low deformation rates, the strain-rate sensitivity of polymer foams is not particularly evident [109, 113]. It has been reasoned that air cannot escape from foam cells at high strain-rates, imposing a strong 'spring back' to the material [108]. The strain-rate sensitivity of polymer foams has been reported to be dependent on material density [106] and foam cell structure [121]. Polymer materials can also be affected by the *Mullins effect*, where the material exhibits an increasingly compliant response for a sequence of compression cycles [122]. The change in response arises from the unrecovered strain in the material, where repeatable response has been observed beyond the first compression cycle [107]. Studies conducting quasi-static testing have neglected the first few compression cycles to account for this effect [32, 58]. In addition to material effects, quasi-static compression has been found to be highly sensitive to humidity. Elevated humidity has been reported to result in a 21 % reduction in quasi-statically measured peak force [60, 76]. By comparison, the same degree of humidity increase has produced less than 1% increase in impact peak force [60]. Therefore quasi-static compression differs drastically from impact conditions in terms of load application, strain-rate, material response and

humidity sensitivity, factors that hinder correlation between quasi-static and dynamic conditions.

The methods outlined so far have been conducted as alternatives to actual impact testing. Few studies appear to measure viscoelastic characteristics directly from actual impact data, perhaps due to the complexities involved with high speeds and tiny durations of typical ball impacts. The BS 5993 standard includes a form of impact testing, where a static ball is stuck by a projectile at a specified speed [10]. Cricket and hockey balls are regulated by this method by measuring the peak deceleration of a projectile [10, 12]. A variation of this method was adopted in previous work on the sliotar, where the ball compression is recorded for a static ball struck impacted by a free-falling specified weight [5]. In conducting actual impact testing, the selection of deformation values poses an issue in the compilation of force-displacement graphs. As discussed in Section 2.1.4, deformation values are evaluated either from measuring the diameter of the ball normal to the impact plate (diameter compression) or from the double time integral of the centre-of-mass acceleration (COM displacement). The choice of deformation values is deemed correct if these values represent the distance through which the measured force acts during the impact. The equality between the proportion of area enclosed within the hysteresis loop and the proportion of kinetic energy loss is useful for validating the force-displacement graph. The publications that constructed dynamic force-displacement curves have used COM displacement values, although these studies do not seem to consider physical measurement of diameter compression [16, 18, 27, 35].

Given the complexities involved with the compilation of dynamic force-displacement graphs, a number of expressions have been derived to allow the simple evaluation of dynamic stiffness from impact data. These expressions produce a singular value of stiffness, a questionable purpose given the observed fluctuation of dynamic stiffness throughout impact. Derived from mathematical model theory, Equation 2.8 has been used in modelling tennis ball impacts [18].

$$k = m\,\frac{\pi^2}{{T_c}^2} \tag{2.8}$$

where k is dynamic stiffness, m is ball mass and T_c is contact time. The application of Equation 2.8 to ball modelling is discussed further in Section 2.3.1 and derivation of this equation is included in Appendix E.

Another expression for dynamic stiffness has become prevalent in recent years, particularly in softball studies [24, 25, 110]. This expression is based on assumptions that the ball acts as a non-linear spring according to non-linearity exponent n and that the ball's kinetic energy before impact equals its stored potential energy at maximum deformation. The non-linear spring equation for peak force is substituted into the energy balance equation as follows:

$$F_p = k\,x^n$$

$$\frac{1}{2}\,m\,u^2 = \left(\frac{1}{n+1}\right) k\,x^{n+1}$$

$$\Rightarrow k = \left[\frac{2}{m\,(n+1)}\right]^n \frac{{F_p}^{n+1}}{u^{2n}} \tag{2.9}$$

where k is dynamic stiffness, F_p is peak force, x is maximum displacement, m is ball mass, n is the spring non-linearity exponent and u is the incident speed. Equation 2.9 has been used to determine the effects of the strain dependence of softballs [110]. In this study, it was reasoned that surface curvature flattening and the geometric effects of large deformation caused a hardening response (increasing the exponent n) while polymer material softening reduced the exponent n. An exponent value of $n = 1.25$ was seen to produce dynamic stiffness values that were relatively constant with increasing speed. Given that this exponent value was less than Hertz theory of $n = 1.5$, the authors suggested that the effect of material softening dominates the other geometrical non-linearities in a ball's viscoelastic strain dependence [110].

Equation 2.9 has been simplified by setting the exponent *n = 1* to produce the following expression for dynamic stiffness:

$$k = \frac{1}{m}\left(\frac{F_p}{u}\right)^2 \tag{2.10}$$

The assumption that the ball behaves as a linear spring is significant given the known non-linearities associated with dynamic stiffness. The decision of setting *n = 1* has been justified by claiming firstly, that it allows for simple calculation (Equation 2.10 compared to Equation 2.9) for use in a regulatory standard, and secondly, it provides a stiffness value *k* with convenient SI units of force/distance [110]. The usefulness of this expression has been reported in a separate study [24], where a better correlation (R-values not reported) has been found between BBCOR and dynamic stiffness (evaluated from Equation 2.10) than between BBCOR and quasi-static stiffness (measured according to ASTM F1888 [13]). This indicates that the equation provides a better representation than quasi-static stiffness of actual dynamic stiffness. However, the agreement between the computed stiffness value and the actual dynamic stiffness has not been reported. Despite this, the stiffness value calculated according to Equation 2.10 has been incorporated in official regulations for baseball and softball in the recently published ASTM F2845 standard [15].

The studies that successfully compiled dynamic force-displacement have involved a single type of ball, those being a cricket ball [16], a softball [27] and a tennis ball [35]. The cricket ball has been observed to have a constant stiffness with respect to speed, although this was a low speed range (2.7 to 6 m/s) [16]. Such limited testing does not induce the deformations or speeds to exhibit the materials' strain and strain-rate sensitivities. The stiffness of the softball has not been measured quantitatively from the dynamic force-displacement curves. While significant strain and strain-rate sensitivities are apparent from the fluctuating force displacement curve, DMA has been used to measure the polymer material's viscoelastic characteristics with limited success [27]. The study on tennis balls considers other types of tennis balls, reporting a 35% lower stiffness for a punctured ball relative to a new pressurised ball. However, the stiffness values were based on a theoretical calculation, as stated in Equation 2.8. The singular

value of this computed stiffness does not indicate the variation of stiffness throughout impact, thus not revealing the strain sensitivity of tennis balls. The relevance of this computed single stiffness is disputable given the significant non-linearity of the dynamic force-displacement curve, thus calling into question whether it can represent the actual ball materials' strain-rate sensitivity. In all of the above cases, the tendency of focusing on a single ball construction does not provide much insight in the dependent of stiffness on different materials' inherent strain and strain-rate effects.

2.2 Performance modification and manufacturing

2.2.1 Ball performance modification

As described in Section 2.1, ball impact behaviour can be described in terms of coefficient of restitution (energy dissipated in an impact) and stiffness (force and deformation of a ball during impact). Official regulatory standards tend not to stipulate the material or construction for use in the ball, instead specifying the required range of COR and stiffness characteristics. The International Tennis Federation have reported that of the 272 brands submitted in 2006, 5.5% had failed. Similar figures have been reported from 2005 (240 submitted: 7% failed). The most common failures have been from rebound and deformation testing, with size and mass tests having the highest pass rates [11]. The regulatory testing aims to ensure a consistent ball performance to provide a fair, safe and enjoyable game. However aspects such as increasing athleticism and technological advancements in equipment can require modification of the ball to maintain performance consistency over time.

Coefficient of restitution modification

An increase in COR, evident from faster ball speeds and longer travel distances, has been observed for many sports including baseball, golf and tennis [84, 123]. This change

in performance has had a negative effect for some sports. The introduction of hollow aluminium bats has led to a 60 % increase in home run rates due to the *trampoline effect* [124]. The 'sweet spot' has become enlarged for golf club heads, where the hollow metal driver heads provide a larger volume than the traditional wooden heads of the same mass [123]. In addition to this, titanium-based alloy golf drivers exhibit a trampoline effect, leading to a further leap in performance since their introduction [123]. The increased travel distance of golf balls require longer courses, which has implications for expense and enjoyment [37]. In tennis, the increased speed of the serve has been linked with an increasing trend of tie-break matches [84, 125]. The increase in tennis ball speed has been attributed to the expansion of the sweet spot, where the evolution of racket frames from wood to aluminium to fibre reinforced composites resulted in a larger racket head [126].

The introduction of a larger tennis ball is an example of work to modify COR in response to increasing ball speeds. An increasing trend of tie-breaks has become evident, highlighting the dominant effect of the serve on winning. The oversize ball has a 6.5 % larger diameter and is 3 % heavier than the standard tennis ball. The performance characteristics of the oversize ball have been investigated on behalf of the ITF [84]. Compared to the standard ball, the oversize ball is reported to have a slightly larger COR for an impact against a fixed racket. This has been attributed to the thinner wall section (easier to deform) and the larger radius (shallower radius through which it deformed). The oversize and standard balls have been reported with similar aerodynamic drag coefficients in wind tunnel testing. Impact testing, involving the projection of the balls at 33 to 44 m/s at acrylic and clay court surfaces, could not discern the difference in COR of either ball type due to the experimental scatter. With the performance characteristics of either ball size being indistinguishable from experimental testing, a computer program was developed to compute the trajectory time of the ball. This program incorporates the rebound from the racket, flight time through the air, impact on the court surface and flight time to the receiving player. The program simulations indicated that the oversize ball increased the travel time for the first serve by 10 ms and for the second serve by 16 ms for acrylic court surface. Subsequent studies on player perceptions have found players tending to describe the oversize ball as slower

than the standard [40, 127, 128]. The theoretical study, along with the affirmed player perceptions, has indicated that the 6.5% increase in diameter serves to slow the game. However, the theoretical travel time increment is marginal: 1.5 % and 1.8% increases for the first and second serve, respectively. Comparing this to the court surface variations, a standard ball has been reported to be 4% slower for clay than acrylic. This suggests that the impacting material properties are more dominant than ball geometry for the rebound behaviour. The authors propose that an 11% larger ball with stiffness adjusted to give the same COR as a standard ball would be up 6.1 % slower [84]. Other than to suggest adjusting the internal pressure, the achievement of a ball stiffness to produce a specific COR has not been explored.

Stiffness modification

A report in 1997 has commented that baseball manufacturers have progressively increased ball hardness to improve durability [129]. This unregulated increase in ball stiffness has repercussions for safety in the sport. Ball-player impact has been reported to account for approximately 55% of emergency room-treated injuries to children in 1995 [130]. Unsurprisingly, many of the numerous studies on sports injuries recommend the use of protective equipment such as helmets [131-134]. An alternative approach is to modify the ball to exhibit less stiffness. A study on baseballs recommended the use of a modified category of ball types for games at youth level, where the modified ball types exhibited similar COR but less stiffness compared to traditional ball types [51]. Soccer balls of lesser stiffness has also been observed to decrease the risk of head and neck injuries, where a 50% reduction in ball pressure results in a 31% reduction in severity of head response [135].

In addition to improving safety, lower ball stiffness provides more comfort to players [129]. This has motivated manufacturers to produce such ball types for market appeal. Development of modern golf balls have focused on the modification of the core stiffness [29]. The manufacturing process, which will be discussed further in Section 2.2.2, has been controlled to attain a stiffness profile decreasing towards the interior of the core. The gradation of stiffness allows the new ball to feel more compliant at higher speeds,

while matching the conventional balls' stiffness at lower speed impacts. This enables a longer drive and greater control in putting, two compromising aspects for homogeneous ball construction. The core with multiple incremental grades of stiffness has been reported to result in less spin in the driver shot, producing an increase in ball launch speed. The lesser core stiffness implies that that the new ball has lower peak acceleration and consequently a softer 'feel', which is more conducive to greater control.

2.2.2 Ball construction

The composition of a sports ball has a significant influence on the imposed regulation of the sport. As discussed in Section 2.1.5, the constituent materials can affect performance due to inherent strain and strain-rate dependencies. The ball construction has implications for the sport with regards to player safety and comfort. In addition, cost-effectiveness and performance consistency are important considerations in developing the manufacturing process for a ball. The constructions of common sports balls are described in the following section with reference to the manufacturing method and influence on performance.

Golf balls have multi-piece constructions, typically comprising of a core surrounded by mantle and cover layers [29]. There have been two distinct categories of constructions: wound balls and solid balls. In the past, solid balls had the advantage of a long travel distance, making these ball types preferable to amateurs [93]. Wound balls were traditionally used by golf professionals due to a more favourable feel and spin generation [136]. However, insufficiently tight manufacturing tolerances in the winding process have been observed to lead to performance variations in wound ball types [31]. With improving production technologies, solid golf balls have offered preferable feel; favourable spin on the green; less temperature dependence; and more consistent properties than wound balls [29]. A dramatic increase in drive distance has been observed in 2000 – 2002 when solid balls became more popular than the wound constructions [123]. The success of ball manufacturing development has been reflected by all tour players favouring solid core balls today [29]. Differences between multi-

piece ball types, such as two- and three-piece balls, can exist due to the strain dependencies of such constructions as described in Section 2.1.5.

Modern cricket balls typically consist of a rolled construction, where yarn, cork and/or rubber layers are wrapped around a dense rubber cylinder and covered in leather with a circumferential seam. The axisymmetrical nature of this construction has been observed to produce an orientation-dependent behaviour of the ball [16, 30], where increased stiffness has been measured perpendicular to the seam. The orientation-dependent variation of ball performance has been accepted as one of the challenging aspects of the sport [137]. Differences in construction of various cricket ball brands have been detailed in one study with reference to the amount and tension of the woollen twine, the lacquer surface finish and the composition and size of the core [30]. Of the five brands tested, four have been reported to have an unacceptable variation in construction with regard to the tension of the woollen twine, the lacquer surface finish and inconsistencies in core material. Variations in construction within individual brands have been observed to include significantly different core diameters, highly irregular core geometry and different cores materials (cork and rubber). With these differences confined within the ball core, they are externally indistinguishable and hence not visually perceptible to players. The authors have acknowledged that a certain degree of variation is inevitable due to the biological origin of the materials and the hand-crafted nature of the production. However, the variation observed in the four brands was considered unacceptable given the consistency evident in the fifth ball.

Baseballs typically comprise of a small cork and rubber core, called a pill, surrounded by layers of wool windings and covered in leather with smoothly stitched seams [45]. Balls for the professional Major League are supplied exclusively from one manufacturer [138]. For the amateur game, various other compositions have been observed to include centre cores of varying sizes and materials (sponge/polymer/cork), the absence or presence of rubber layers, and wool windings of various thicknesses [45]. As mentioned in Section 2.2.1, sponge and polymer constructions exhibit lower stiffness, providing more safety and comfort [51].

Modern softballs are manufactured from a homogenous polymer core surrounded by a leather skin. The polymer core, typically polyurethane foam [24, 125], has replaced the traditional use of cork. This transition was motivated by the International Softball Association to increase ball speed and reduce the sensitivity of ball performance on humidity [139]. Numerous issues, particularly regarding ball durability, have been encountered in the early stages of producing polymer ball types [140]. It has been claimed that the modern manufacturing process is sufficiently advanced to allow control of both energy dissipation and stiffness properties [24]. This process will be described in further detail in Section 2.2.3.

Tennis balls are made from a hollow rubber shell covered in a cloth outer layer. The balls are categorised as 'pressurised' or 'pressureless'. Pressurised balls are filled with gas at approximately 82 kPa during the manufacturing process [98]. These ball types have been reported as preferable by players, but have a short lifespan due to pressure loss with age – as little as nine games at the professional level [41]. A complete loss of internal pressure has been reported to reduce dynamic stiffness and COR by 35% and 20%, respectively [35]. In the attempt to replicate pressurised ball performance, various pressureless balls have been developed by modifications of the shell material composition, the shell thickness and inclusion of internal foam [35, 98]. Interesting, studies have shown that aesthetics can be a significant factor in perception of ball performance by players [40, 41]. A study found that players struggled to distinguish between visually identical new and aged balls [40], despite the reported reduction in stiffness due to pressure loss [35]. This finding suggests that aesthetic and tactile factors can have a dominant effect on player perceptions.

Real tennis, the predecessor of the globally popular sport of lawn tennis, uses solid balls that consist of a cork core surrounded by a cotton winding and a felt cover. These balls have been constructed from an intensive hand-crafting process, taking up to 50 minutes to create a ball from the raw materials [72]. Inconsistencies arising from the hand-crafted nature of this construction method have been reported to result in a variation in the performance of the ball [72]. In this study, alternative materials have been investigated to produce a more consistent and cost-effective ball of appropriate performance. Homogenous polyurethane foam has been found to have acceptable

density and energy dissipation characteristics but was discounted for having inadequate stiffness. The finalised design consisted of a central cork core surrounded by a relatively dense polyurethane foam coating. Preliminary testing concluded that this prototype exhibited desirable performance in terms of COR and stiffness [72].

2.2.3 Polymer ball manufacturing

Polymeric materials have been utilised in a number of sports balls including golf balls [29, 93], hockey balls [94], softballs [24, 46, 125] and modern hurling balls. In addition to ball performance, the impact properties of polymers foams have been researched extensively in the areas of crash-absorption [141, 142] and sports surfaces [143, 144]. The performance characteristics of such polymers arise from the parameters of the controlled manufacturing process. Injection moulding is one of the most common methods of plastics processing, reported to consume approximately 32% by mass of globally produced plastic [145]. Figure 2.5 displays a typical thermoplastic injection moulding machine cross-section [146], where molten plastic extrudes from the barrel to fill the mould cavity and solidify by cooling.

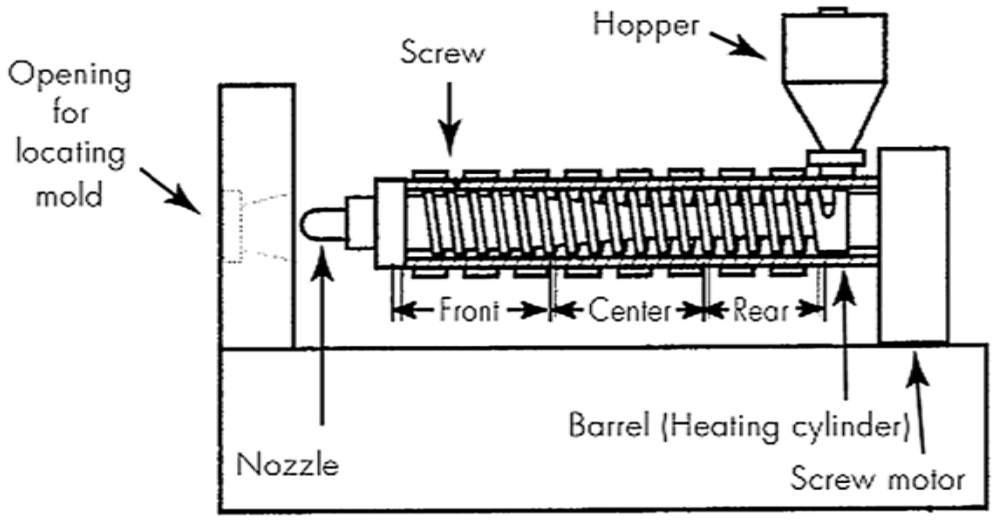

Figure 2.5: Cross-sectional view of injection moulding process

The polymer is melted in the barrel by a combination of heat transferred from the external heaters in the barrel wall and frictional heat generated by screw rotation (plasticising). The optimisation of the injection moulding process involves the adjustment of several variables, including the ratio of external heat to frictional heat, the injection speed and pressure, the holding pressure and time, the cooling time and the mould temperature [147, 148]. These variables are controlled by the machine parameters configuration as summarised below:

- *Barrel temperatures (rear/middle/front zones):* maintains consistent melt temperature, depending on screw geometry, frictional heating, cycle time and material flow length.
- *Nozzle zone temperature:* independent from barrel heating system, typically slightly higher than front barrel zone temperature.
- *Mould temperature:* lower temperature effectively cools thick parts within reasonable cycle time
- *Shot size:* the amount of material in the barrel to be injected into the cavity. Shot size typically 40 to 80% of barrel capacity to avoid material degradation from excessive heat build-up [152].
- *Injection pressure and speed:* attains complete filling of cavity to avoid either under-filling with voids or over-packing with flashing at seams.
- *Hold pressure:* maintains filling of cavity during cooling. Typically 60 to 80% of injection pressure.
- *Injection cushion:* extra material in barrel to allow packing of cavity.
- *Plasticising delay:* time between injection and start of plasticising to allow sprue to freeze off.
- *Back pressure:* pressure applied to plastic during screw operation. Affects plasticising and hence frictional heat and mixing.
- *Screw speed:* typically kept low to allow uniform temperature gradient in barrel.
- *Clamp tonnage:* specifies pressure for keeping mould closed, determined by matching part surface area to the machine capabilities.
- *Cooling time:* set to allow part to become sufficiently solid to be removed from mould.

- *Cycle time:* the total time between mouldings, inclusive of injection, cooling and ejection times. Cycle time is minimised to allow maximum output and cost-effectiveness.

Foam moulding is typically required in injection moulding of a sports ball to attain the correct lower density. A foaming or blowing agent added to the polymer melt causes an expansion in the cavity to produce a porous structure. This expansion can be achieved by the chemical reaction of organic compounds in the blowing agent releasing nitrogen or carbon dioxide at elevated temperatures [149]. Due to the generation of pressure from the blowing agent, foam moulding requires low values of holding pressure and injection cushion.

The performance of a moulded part, in terms of stiffness and energy dissipative properties, can be modified by adjusting machine parameters and constituent materials. The mould temperature can influence the polymer solidified structure, where higher mould temperatures are reported to increase stiffness and reduce creep characteristics for polybutylene terepthalate (PBT) [150]. Polymer foam strain-rate sensitivity has been reported to be influenced by foam cell size and structure [121]. Typical blowing agents produce a coarse foam structure, where a fine and uniform cell structure can be attained by the addition of a nucleating agent. This additive creates nucleating sites in the melt, resulting in a larger number of smaller cells [148]. The constituent materials are regarded to have a more dominant effect than machine conditions in a moulded part's performance [151, 152]. Commercially available polymer batches tend to be categorised by hardness grade expressed in terms of Shore A and D hardness.

Another established method of sports ball manufacturing involves more sophisticated form of injection moulding called reaction injection moulding (RIM). This process involves a chemical reaction requiring specialised equipment beyond the capability of a standard thermoplastic injection moulding machine [145]. The exact manufacturing specifications for most sports balls tend to be proprietary knowledge of the manufacturer [153].

Softballs are manufactured from polyurethane by the RIM method [25]. The constituent materials of polyisocyanates and polyols are mixed and poured into rotating moulds. It

typically takes three minutes to cure, where temperature is continuously monitored due to the exothermic reaction. Different properties of the softball are attained by adjusting the cure time, the reactants proportions and temperature. This process has been claimed to allow independent control of COR and stiffness properties, although this proprietary knowledge is withheld by softball manufacturers [24].

In the manufacturing of golf balls, the curative agent can be varied to produce different ball stiffnesses [96]. The material chemistry of the layers of a golf ball can be quite complex [153], where the exact formulations of high-end multi-piece balls are mostly kept as proprietary secrets. In a report on high-end Bridgestone golf ball production, the composition of polybutadiene rubber, unsaturated carboxylic acid metal salt, peroxide and organic sulphur have been used to improve rebound characteristics [29]. Using a polybutadiene synthesised with a lanthanide catalyst instead of a nickel or cobalt catalyst also improves the core rebound characteristics. In developing their Tour B330 ball, a gradational hardness was attained in the core material by controlling the vulcanisation reaction. The vulcanising process involves a temperature gradient in the moulding spanning 70 to 90 °C between the surface and interior. A new formula and optimised mixture ratio of sulphur compound and organic peroxides in the base polybutadiene has been described to promote or delay the vulcanising process to produce the desired gradational hardness [29].

2.3 Ball impact modelling

For ball impact simulation the model inputs are the parameters that define the material response, and the model outputs are the predictions of the ball's impact characteristics. For an intuitive model, the inputs should be directly related to quantifiable material properties and the outputs should correlate well with experimental data. There are numerous motivations to ball impact modelling. The development of a model representing a ball's dynamic response is useful for predicting and extrapolating ball behaviour. Modelling impact behaviour can lead to an understanding of the contribution

of material properties to performance. Such an understanding would be relevant to ball manufacturing, where a desired performance could be achieved by production of balls with specific material properties. In addition, a model that simulates ball behaviour is useful to developing a model of ball-surface interaction, allowing development of playing equipment, surfaces and protective apparel. In Section 2.3.1, the development of ball models in recent years is outlined. The ball models are categorised according to their methodology: spring-damping mathematical models, logarithmic mathematical models and finite element models. The basis of input parameters of these models can be either phenomenologically-derived or independently-measured. Phenomenological models are developed where the parameters are assigned values such that the model simulations fit to experimental data. Other models have parameters based on independently measured material characteristics. The appropriateness of the parameter basis is discussed in Section 2.3.2.

2.3.1: Ball impact model categories

Spring-damper mathematical models

Mathematical models typically use simple spring and damper components to approximate the ball material response to impact. Equations of motion are expressed in terms of coefficients relating to material stiffness and energy dissipation (damping). A Kelvin-Voigt unit, which has a purely elastic spring in parallel with a purely viscous dashpot damper, has been used to simulate viscoelasticity. The spring simulates the ball stiffness while the dashpot damper simulates the energy dissipation. The earliest attempts to model viscoelastic behaviour have used a mass-spring-damper consisting of a linear spring and linear damper in parallel, as shown in Figure 2.6 [111]. The equation of motion is an expression of the displacement of the ball's centre-of-mass (COM). This system has constant coefficients for stiffness and damping, thus assuming that both are independent of displacement (x) and incident speed (u).

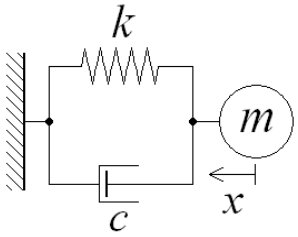

Equation of motion: $m\ddot{x} + c\dot{x} + kx = 0$ (2.11)

Stiffness: $k = const$

Damping: $c = const$

Figure 2.6: Kelvin-Voigt model with linear components and constant coefficients

In this simple model, *m* is ball mass, *c* is the damping coefficient, *k* is the stiffness coefficient and $\ddot{x}$, $\dot{x}$ and *x* are the COM acceleration, COM speed and COM displacement, respectively. With the observed strain and strain-rate dependencies of ball performance, it has been recognised that non-linearity has to be introduced to the model to adequately simulate real impact behaviour [111]. There have been two approaches to introducing this non-linearity: use of linear components with variable functions for stiffness and damping coefficients, or non-linear spring and damper components with exponent and constant coefficients. To clarify, a non-linear spring or damper component has properties that vary as a function of displacement.

In modelling tennis ball impacts, a spring-damper system has been developed based on experimental data [18]. A linear spring and linear damper was used, accounting for non-linear behaviour by use of non-constant functions for stiffness and damping coefficients, as seen in Figure 2.7. The stiffness coefficient was expressed as a function of the impact contact time (T_C) and the damping coefficient was treated as a function of contact time and coefficient of restitution (COR). The stiffness and damping coefficients vary with impact speed but remain constant throughout the impact duration.

Equation of motion: $m\ddot{x} + c\dot{x} + kx = 0$ (2.12)

Stiffness: $k = m\frac{\pi^2}{T_c^2}$ (2.13)

Damping: $c = -\frac{2m}{T_c}\ln(\mathrm{COR})$ (2.14)

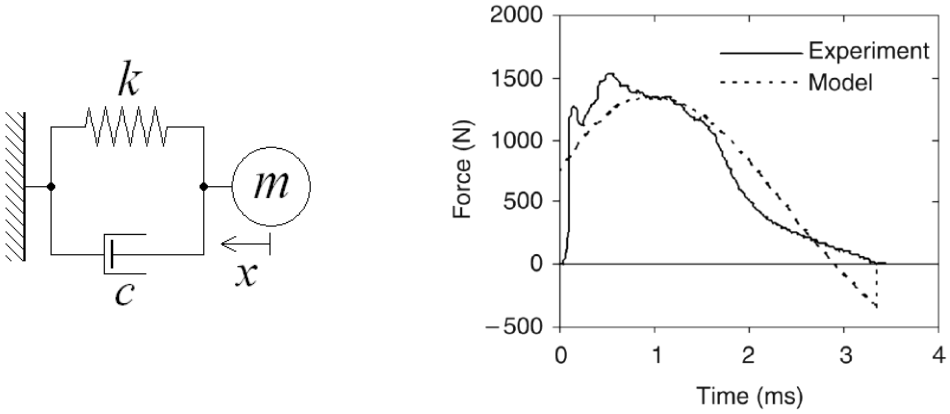

(a) (b)

Figure 2.7: Tennis ball Model One (a) configuration and (b) typical comparison between model force and experimental data [50]

This model showed limited agreement with experimental results [35], as shown in Figure 2.7 (b) [50] (no correlation factors reported). For higher speed impacts, the model was found to predict a high instantaneous initial force. This is due to the large $c\dot{x}$ term, where the high COM speed results in an erroneous prediction of impact force [18, 35]. This discrepancy has been accounted for in a subsequent study by the same authors, where the damping element was a function of contact area rather than directly dependent on COM speed. Additional terms were also incorporated into the model to account for the non-linearity of stiffness and damping within the impact duration, as shown in Equations 2.15 to 2.18 [50].

Equation of motion: $$m\ddot{x} + (c_b + c_m)\dot{x} + kx = 0 \quad (2.15)$$

Stiffness: $$k = k_{(0)} + A_K x^{\alpha} \quad (2.16)$$

Damping: $$c_b = A_C (d_{CONT})^2 \quad (2.17)$$

$$c_m = \frac{m\left\{\rho_{area}\,\pi\left[(d_{CONT\ (t)})^2 - (d_{CONT\ (t-\Delta t)})^2\right]\right\}}{4\,\Delta t\,(M_1)_t} \quad (2.18)$$

where c_b is the material damping coefficient, c_m is the momentum flux, $k_{(0)}$ is defined as the stiffness at zero deflection, A_k and α are model constants, A_C is damping area constant, d_{CONT} is the diameter of the contact area, ρ_{area} is the mass per unit surface area, Δt is a unit time interval and M_1 is the instantaneous mass of uncompressed section of the ball.

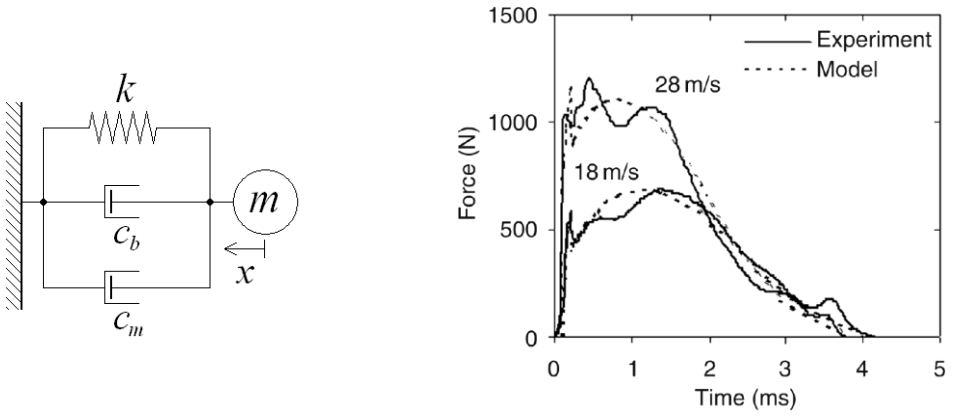

(a) (b)

Figure 2.8: Tennis ball Model Two (a) configuration and (b) typical comparison of model force and experimental data [50]

There are three principal differences between Model Two (Figure 2.8) and the previous Model One (Figure 2.7). Firstly, the stiffness coefficient k is expressed in terms of the stiffness at zero deflection $k_{(o)}$ and constants A_k and α, as seen in Equation 2.20. The dependence of the x term on the index α implies that the stiffness coefficient varies throughout impact. The stiffness at zero deflection $k_{(o)}$ is extrapolated from experimental measurements of stiffness at a range of speeds. The constants A_k and α have been initially assigned arbitrary values, then iteratively refined using a Goal Seek function in a Visual Basic Script Macro to fit to experimental data. The second difference between models removes the erroneously high initial force. The material damping coefficient c_b depends on the volume of material being deformed and has been expressed in terms of a damping area constant A_C and the diameter of the contact area d_{CONT}. The final difference is to simulate momentum flux loading with the addition of another damper in parallel in the model. Momentum flux, an additional force acting in the compression phase, was the term used to describe the instantaneous change of momentum of the

contacting surface of the ball being brought to rest against the impact surface. This force, represented as a damping term c_m, is proportional to the mass flow rate of material into the compressed region of the ball. It is expressed in terms of the mass per unit surface area ρ_{area}, the instantaneous values of diameter of contact area, the unit time interval Δt and the instantaneous mass of uncompressed section M_1. As this force occurs only during the compression phase, c_M is equal to zero for the restitution phase. This model also had two other minor modifications specific to tennis ball impact. The modification sets the force to zero at $x < 2$ mm to account for the initial low load corresponding to the compression of a low stiffness cloth cover. The second modification is to set a high constant stiffness k_{CONST} at $t < 0.2$ ms to represent the rapid increase in force due to the high stiffness of the shell prior to buckling. These modifications have been reported to slightly improve the realism of the model simulation. The model has been reported to have good agreement with reality, as shown in Figure 2.8 (b), with simulation values within 10% of experimental data. It has been concluded that the momentum flux is independent of ball stiffness and is the dominant contributor to the initial force, explaining the similar initial peaks observed in experimental data for all tested ball types [50].

An alternative approach to modelling ball impact has been the use of non-linear stiffness and damping components. This involves the assignment of an exponent to either one or both of the components. A non-linear relationship that represents purely elastic properties of ball collision has been proposed by Hertz theory [39]. This theory states that the force of impact is proportional to the displacement raised to the power of 1.5, as stated in Equation 2.7. The application of Hertzian non-linearity to a mathematical model has been achieved by including an addition factor of $x^{0.5}$ on the stiffness and damping components, as seen in Figure 2.9 [111]. As before, the stiffness and damping coefficients have been assumed to be constant for all displacements and speeds.

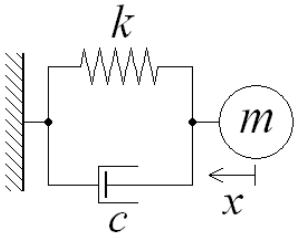

Equation of motion: $m\ddot{x} + c\dot{x}|x|^{0.5} + kx|x|^{0.5} = 0$ (2.19)

Stiffness: $k = const$

Damping: $c = const$

Figure 2.9: Hertzian non-linear ball model with constant coefficients

This model has been claimed to fail to fully represent impact behaviour [42], an unsurprising finding given that Hertz theory has been developed specifically for elastic impact. An advancement of this model consists of non-linear spring and non-linear dampers assigned with phenomenologically-derived exponent values, as displayed in Figure 2.10 [42]. The ball examined in this study was a two-piece golf ball, where the cover and core were represented by two effective masses m_1 and m_2, respectively.

Equation of motion: $m\ddot{x} + c\dot{x}|x|^{b} + kx|x|^{a} = 0$ (2.20)

Stiffness: $k = const$

Damping: $c = const$

Exponent: $a = const \quad b = const$

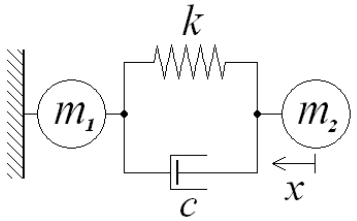

(a)

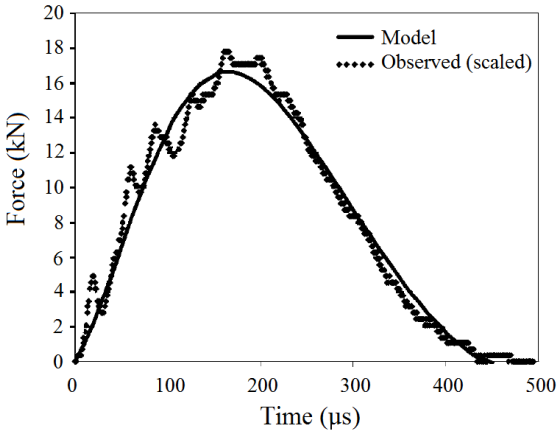

(b)

Figure 2.10: Non-linear two-piece golf ball model (a) configuration and (b) comparison between model force and experimental data (arbitrarily scaled) [42]

The division of the total mass into the cover and core masses has been reported as necessary to explain why the extrapolated value of COR at zero speed was 0.883 rather than 1 [42]. It has been reasoned that the cover mass is inactive within the impact duration, with the spring-damper combination acting only on the core mass. Upon rebound, the core mass must drag back the cover mass. The stiffness and damping coefficients (*k* and *c* respectively) and their respective exponents *a* and *b* are reported with seemingly arbitrary constant values in order to fit the model simulations to experimental data. For example, the following values have been reported: $k = 1.08 \times 10^7$; $c = 6.85 \times 10^6$; $a = 0.32$; and $b = 2.2$. The large magnitudes of the *k* and *c* values have no clear relevance to real-world properties of stiffness and damping, while the non-unity values of *a* and *b* result in non-standard SI units. The relationship of these coefficients and exponents to actual impact characteristics and material properties was not discussed by the authors [42]. Moreover, the accuracy of this model as shown in Figure 2.10 (b) is questionable given that the observed force measurement was arbitrarily converted from volts to kN, thus not providing independent validation.

Work on modelling a cricket ball has used a non-linear spring and a linear damper model, as seen in Figure 2.11 [16]. This model uses a non-constant stiffness coefficient *k* that is a function of the incident speed, and a non-constant damping coefficient *c* depends on both displacement and speed.

Equation of motion:	$m\ddot{x} + c\dot{x} + kx^a = 0$	(2.21)
Stiffness:	*k = exp fn(u)*	
Damping:	$c = \ p\,\pi\,R^2 = q(d - x)x$	(2.22)
Parameter:	*q = exp fn(u)*	
Spring exponent:	$a = const$	

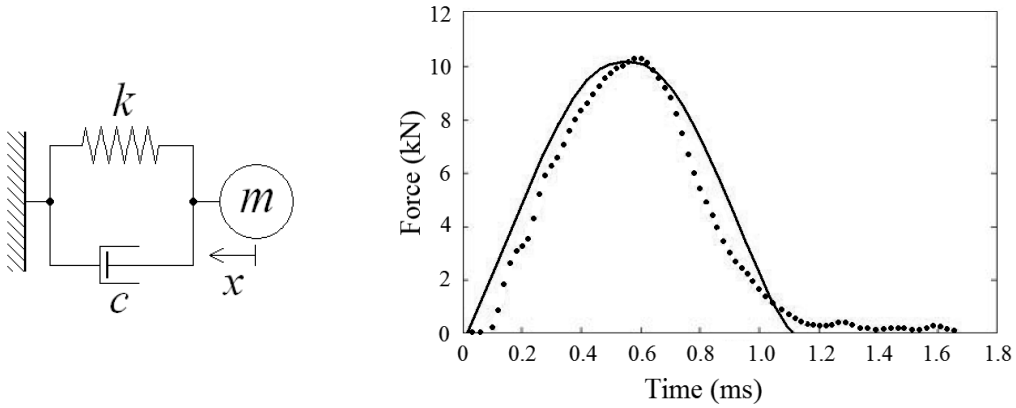

(a) (b)

Figure 2.11: Non-linear cricket ball model (a) equations with non-constant coefficients and (b) comparison between model force and experimental data [36]

where k is the stiffness coefficient, c is the damping coefficient, p is a model parameter, R is the radius of contact area, d is the ball diameter, q is a model parameter and a is a constant. The stiffness component is dependent on both displacement and speed. It is a function of an exponent, a, and stiffness coefficient, k, which in turn is exponentially related to the speed, u. In this study, $a = 3.09$ and $k = (2.58 \times 10^{11})\, e^{-0.319u}$ for impacts on the seam and $a = 2.72$ and $k = (1.32 \times 10^{12})\, e^{-0.357u}$ for impacts perpendicular to the seam. As with the tennis ball Model Two, shown in Figure 2.8, it has been reasoned that the damping coefficient is dependent on the contact area. The COM displacement x is assumed to represent to the proportion of material being compressed and hence is geometrically related to the size of the contact area. In this way, the damping coefficient is expressed in terms of displacement and a model parameter, q, which in turn is exponentially related to the speed. Values of the model parameters have been reported as $q = (5.35 \times 10^{6})\, e^{-0.157u}$ for impacts on the seam and $q = (3.49 \times 10^{6})\, e^{-0.157u}$ for impacts perpendicular to the seam. The model was reported to have good agreement with experimental data, as indicated in Figure 2.11 (b) [36] (no correlation factors reported).

This non-linear model has been developed further by using a configuration consisting of three spring-damper units in parallel [36], as shown in Figure 2.12. The masses m_1, m_2 and m_3 have been allowed to change freely within the constraint that they add up to the

total mass of cricket ball. A genetic algorithm, which originates from biological considerations, has been used to determine the model parameters.

Equation of motion: $(\sum m)\ddot{x} + (\sum c)\dot{x} + k_1 x^{a_1} + k_2 x^{a_2} + k_3 x^{a_3} = 0$ (2.23)

Stiffnesses: $k_1 = fn(u) \quad k_2 = fn(u) \quad k_3 = fn(u)$

Damping: $c_1 = fn(u) \quad c_2 = fn(u) \quad c_3 = fn(u)$

Spring powers: $a_1 = fn(u) \quad a_2 = fn(u) \quad a_3 = fn(u)$

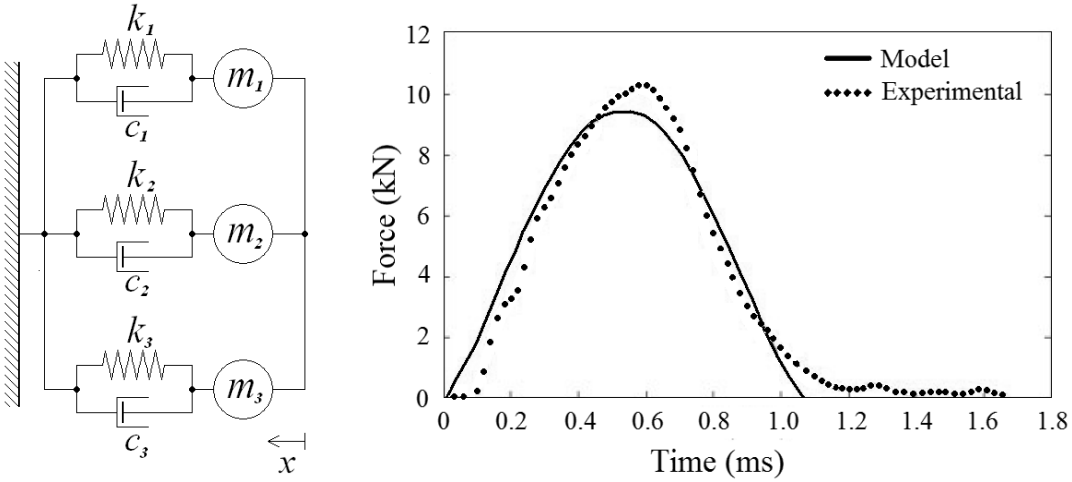

(a) (b)

Figure 2.12: Non-linear cricket ball model (a) multiple parallel configurations and (b) comparison between model force and experimental data [36]

This model has been claimed to be superior to the original model (compare Figure 2.12 (b) to Figure 2.11 (b)) by being quicker solving and more accurate for impact force predictions (actual RMSE values not published) [36]. The splitting of the coefficients into three individual components, presumably to reflect a three-piece material construction, seems intuitive given that varying proportions of each material with distinctive viscoelastic properties deforms to different extents throughout the impact.

The use of the genetic algorithm allows automated calculation of model parameters, but does so in a hidden algorithm that does not provide insight into the role of each parameter in the impact mechanism. This algorithm seems to account for variation of damping and stiffness within the impact duration, thus not requiring modifications such as momentum flux.

Logarithmic mathematical modelling

A number of studies have deviated from the use of spring-damper representation in their mathematical models [30, 99, 100, 112, 154]. These studies have employed a different methodology based on parameters derived from quasi-static compression (loading to 9 kN at speeds of 500, 160, 50, 16 and 5 mm/min) and stress relaxation testing (pre-loaded between 1.6 and 5.9 kN at 500 mm/min, load measured for 3600 seconds). A logarithmic law was found to express the quasi-static ball behaviour in terms of the initial compression x_0, a speed-independent elasticity parameter A (derived from static compression testing) and the viscosity coefficient B (derived from stress relaxation testing).

$$F = x_o \, A \, t^{-B} \tag{2.24}$$

Laplace transform manipulation of Equation 2.24 has been used to evaluate the elasticity parameter A in terms of characteristics derived from quasi-static testing, namely the compression x, the compression rate v and the stiffness k_v corresponding to that compression and compression rate.

$$A = k_v \, x^B \, v^{-B} \tag{2.25}$$

To account for the difference in deformation between the quasi-static compression and impact deformation, a multiplier was applied to elasticity parameter A. The authors [30] investigated data from previous publications [16, 20], interpreting a multiplier of 2 (dynamic stiffness being twice that of quasi-static stiffness) for tennis balls and a multiplier of 1.56 for cricket balls. In the development of this model, a multiplier of 1.33

was calculated from continuum mechanics, although this is later revised to 1.5 to yield agreement with experimental data [30]. The model is based on the equilibrium of forces within the ball during impact, namely the inertial force F_I, the reaction force F_R and the applied force F_A.

$$F_I \quad + \quad F_R \quad = \quad F_A \tag{2.26}$$

$$m\ddot{x} \; + \; x_0 \, A \, t^{-B} = m \, u \, \delta_{(t)} \tag{2.27}$$

where $x_o \, A \, t^{-B}$ is the power law function from Equation 2.24, u is the initial impact speed and $\delta_{(t)}$ is the Dirac delta function signifying a unit impulse acceleration. Taking a Laplace transform of Equation 2.27 yielded:

$$s^2 \hat{x} \, m \; + \; s^B \hat{x} \, A \, \Gamma(-B+1) \; = \; m v_0 \tag{2.28}$$

where s is the Laplace variable, the caret '^' denotes a transformed variable and 'Γ' signifies a gamma function. Equation 2.28 has been solved for transformed displacement, speed and acceleration:

$$\hat{x} = \; v_0 \; \frac{1}{s^2 + s^B \frac{A \, \Gamma(1-B)}{m}} \tag{2.29}$$

$$s \, \hat{x} = \; v_0 \; \frac{s}{s^2 + s^B \frac{A \, \Gamma(1-B)}{m}} \tag{2.30}$$

$$s^2 \, \hat{x} = \; v_0 \; \frac{s^2}{s^2 + s^B \frac{A \, \Gamma(1-B)}{m}} \tag{2.31}$$

Using a previously developed algorithm for inverse Laplace transformation in Matlab, Equations 2.28 and 2.29 have been used to predict the peak force, the deflection at peak force and the time between initial contact and peak force [30, 99, 100]. The model has been reported to predict peak force within 4% (computed from Figure 17 from Fuss [30]), although deviations were observed between the model and experimental force-time profiles [112].

Finite element modelling

Finite element (FE) models are more sophisticated than mathematical modelling, enabling the simulation of impact mechanics such as stress propagation waves and energy transactions. This method involves the discretisation of the ball geometry into individual elements that are assigned with specific material properties. The computation of the FE model considers the interaction of these elements in order to simulate the impact behaviour. The ball's impact characteristics are represented as 'material' properties, such as hyperelastic and viscoelastic material models that are inbuilt in commercial finite element analysis (FEA) software. Hyperelastic models, which have a stress-strain relationship that is independent of strain-rate, are used typically to represent rubber-like materials. FEA packages have a selection of methods for modelling hyperelasticity, with the most common being the Mooney-Rivlin equation [120]:

$$U = C_{10}(\bar{I}_1 - 3) + C_{01}(\bar{I}_2 - 3) + \frac{1}{D_1}(J_{el} - 1)^2 \tag{2.32}$$

where U is the strain energy per unit of reference volume; C_{10}, C_{01} and D_1 are material parameters; $\bar{I}_1$ and $\bar{I}_2$ are the primary and secondary invariants of the Cauchy-Green strain tensor; and J_{el} is the determinant of the deformation tensor. The material parameters C_{10}, C_{01} and D_1 for the Mooney-Rivlin equation have been estimated from the following equations:

Initial shear modulus $$\mu_0 = 2(C_{10} + C_{01}) \tag{2.33}$$

Initial Young's modulus $$E_0 = 6(C_{10} + C_{01}) \tag{2.34}$$

Initial bulk modulus $$K_0 = {}^{2}/_{D_1} \tag{2.35}$$

Poisson's ratio $$\nu = \frac{3K_0/\mu_0 - 2}{6K_0/\mu_0 + 2} \tag{2.36}$$

Viscoelasticity is often modelled by the Prony series [26, 36, 52, 116, 143] which is based on a three-element mathematical model that consisted of a Maxwell unit (spring

in series with a damper) in parallel with a damper [155]. The Prony series is expressed using the following equation:

$$G(\tau) = G_0 \left\{1 - \bar{g}_1^p \left(1 - e^{-t/\tau_1^G}\right)\right\} \quad (2.37)$$

where $G(\tau)$ is the relaxation shear modulus, G_0 is the instantaneous shear modulus and $\bar{g}_1^p$ and τ_1^G are Prony series parameters, where τ_1^G represents the material viscosity.

Analogous to the development of the majority of mathematical model, a number of FE models published in the literature are phenomenologically-derived [36, 52]. These models were developed by adjusting parameters in Equations 2.32 to 2.37 to fit experimental data, i.e. the model parameters were computed based on experimental impact data. In modelling a golf ball impact [52], the ionomer resin cover was represented by 1536 hyperelastic elements, totalling 2403 nodes, and the polybutadiene rubber mantle and core were modelled at hyperelastic/viscoelastic elements with 2403 and 2601 nodes, and 1536 and 2048 elements respectively [52]. ABAQUS/Explicit software was used for the simulation, with hyperelasticity and viscoelasticity modelled using the Mooney-Rivlin and Prony series as shown in Equations 2.32 and 2.37. The model was constructed based on experimental data: the initial Young's modulus of the core was determined from curve-fitting to on peak force; initial Young's modulus of the cover was determined from the rebound angle and spin rate; and viscoelastic parameters were evaluated from focussing on the time to reach peak force, the maximum deformation value and the deformation profile during restitution. The model was reported to perform well in simulating experimental data as shown in Figure 2.13 [52] (correlation factors not reported).

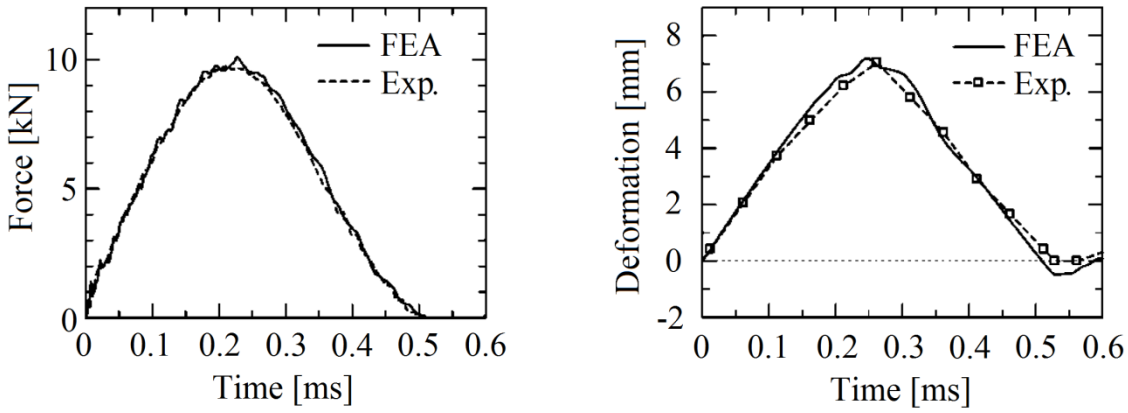

Figure 2.13: Comparison of FEA golf ball model and experimental data for (a) impact force and (b) deformation [52]

In a separate model of a cricket ball [36], the Mooney-Rivlin and Prony series equations parameters are determined from an algorithm called an artificial neural network (ANN). The ANN was used to calibrate the model by computing the material parameters based on 19 input parameters that were derived from experimental data. The 19 input parameters consisted of combinations of contact time, time to various load values, time to maximum load, maximum load value, incident and rebound speeds and accelerations. This model was claimed to exhibit a good alignment for the FEA simulation and experimental data, as seen in Figure 2.14.

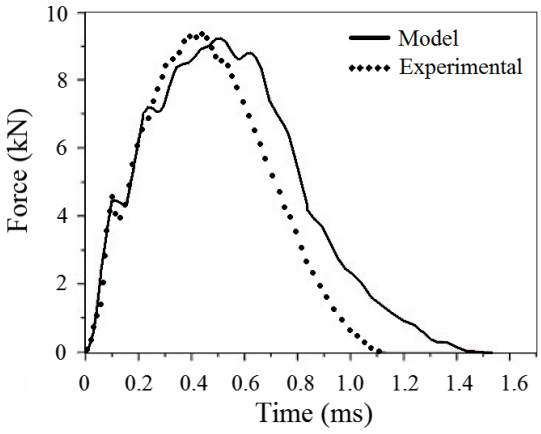

Figure 2.14: Comparison of FEA cricket ball model and experimental force data [36]

2.3.2 Model parameter basis

The basis of a ball impact model can be either phenomenologically derived or independently measured. In the first instance, the model's input parameters are assigned seemingly arbitrary values to enable the model predictions to fit the experimental data; in the second, the parameters are calculated by methods independent of the experimental impact data.

The majority of published ball impact models, both mathematical and FE, were phenomenologically developed. Therefore, it comes as no great surprise that model simulations agree with realistic impact data, given that the model parameters were derived from the same real data. Such models are based exclusively on the impact data from which they have been derived from, and so cannot be universally applied to different ball types or to impact conditions outside of those tested. Despite these limitations, phenomenological models can be useful. An established model that replicates ball impact behaviour is useful for modelling other aspects of ball behaviour. This has been demonstrated by a cricket ball model, originally phenomenologically developed from normal rigid-body impact, being used to model oblique impact [16] and compliant surface impact [33]. Another study uses a simple linear elastic model of a golf ball to satisfactorily model club-head characteristics, despite the authors acknowledging that such a ball model does not correctly represent the ball's viscoelastic nature [34]. In addition to ball-surface modelling, the phenomenologically-derived model parameters values may give insight into the material impact response. This is particularly applicable to the simple spring-damper mathematical models, where the model parameters are intuitively linked to viscoelastic characteristics of stiffness and damping. The departure from such simplicity by the logarithmic mathematical models and FE models serves to obscure any relationship between parameters of these models and realistic material characteristics.

The use of parameters independently measured from standard laboratory equipment would be considered a more robust approach. Once validated, models of this basis are truly representative of actual material properties. However, limited success has been reported from this approach. The limitation of this approach relate to the independent measurement methodologies, as described in Section 2.1.5, where such methodologies

have issues in representing short-term material response and realistic impact conditions. The logarithmic mathematical models reported previously are not wholly based on independent measures, where the authors have proposed a multiplying factor to produce more agreeable model predictions [30]. Attempts at FE modelling based on independently-measured parameters have been reported with mixed results. The development of a golf ball FE model has been reported with positive preliminary results, where parameters have been determined from stress relaxation and quasi-static compression [32]. This work is currently on-going. Stress relaxation has been reported as unsatisfactory in obtaining energy loss parameters for FE models of hockey balls [26]. In this study, the authors suggest that Dynamic Mechanical Analysis (DMA) could provide more accurate parameters assuming the ball material demonstrates linear viscoelasticity. However the assumption of linear viscoelasticity is not trivial, particularly with synthetic ball materials that exhibit significant strain and strain-rate dependencies [25]. This has been demonstrated for FE modelling of softballs, where DMA has been reported as being inadequate in characterising dynamic energy dissipation [27, 46].

2.4 Literature review summary

2.4.1 Performance research summary

- In research studies and official sports regulations, ball impact has been characterised by measuring COR, force and deformation. These measures correspond to the two viscoelastic components of energy dissipaton (COR) and stiffness (force + deformation). However, the regulatory standards typically involve multiple separate methodologies to characterise ball performance, which does not permit the direct comparison of the resulting impact characteristics given their independent measurement methods.
- Impact energy dissipation is typically expressed by the coefficient of restitution (COR), measured from the ratio of speeds after and before impact. Ball COR is found to be dependent on a number of factors, including incident speed, incident angle, ball spin, ambient conditions and impact surface properties. All regulatory

standards have specified conditions for the aforementioned factors to maintain consistent ball characterisation. However, given the dependence of ball COR on speed, many of the regulatory standards are limited in specifying only a single test speed**.**

- The measurement of force-time data allows the evaluation of a number of characteristics, including peak force, centre-of-mass acceleration, impulse and contact time. The equation between impulse and momentum allows the verification of the force-time data.
- A number of different methods and descriptive terms have been used to quantify ball deformation. The two principle measures are diameter compression and centre-of-mass (COM) displacement. The relationship between these measures has been the subject of numerous conflicting reports. The publications that assumed the two measures equal do not appear to account for the effect of lateral expansion, if any, of the ball. The publications that stated a non-equivalence between the measures did so without experimental verification and did not explain the reason for the difference between the two measures. This clearly needs investigating.
- Viscoelastic characterisation is an inclusive consideration of force and deformation properties. As well as being the closest representation of hardness perception, stiffness is significant in determining how the ball rebounds from a sports-representative compliant surface.
- A number of non-impact methodologies have been employed as alternatives to the complexities of deriving viscoelastic characteristics directly from impact data, such as stress relaxation, Dynamic Mechanical Analysis, split Hopkinson pressure bar apparatus and quasi-static compression. The ball materials and constructions can have inherent strain and strain-rate sensitivities that can significantly influence ball stiffness. Such material sensitivities are not considered in non-impact methodologies, significantly limiting their usefulness.
- The ambiguity surrounding deformation quantification poses an issue for the construction of force-displacement curves, from which dynamic stiffness can be experimentally derived. The studies that compiled force-displacement graphs have used COM displacement without consideration of other measures of deformation. Theoretically developed equations have been proposed to evaluate values for

dynamic stiffness. The singular values of these calculated stiffnesses contrast with the observed non-linearities in dynamic stiffness, calling into question how such equations can reflect the strain and strain-rate sensitivities of some ball materials.

- The few studies that have evaluated dynamic force-displacement graphs have appeared to avoid determining stiffness directly from the force-displacement data, instead favouring methods such as the non-impact methodologies or theoretical equations. In addition, these studies have focused on one ball type, thus not providing much insight into the strain and strain-rate sensitivities of various materials and constructions.

2.4.2 Manufacturing research summary

- Ball performance has been modified on various occasions to promote enjoyment of the sport. Ball COR has been modified to counter increased athleticism and evolution of equipment, as evident from work to slow the speed of the tennis ball. Ball stiffness has been modified to produce ball constructions that are safer and more favourable to players.
- The construction of sports balls has a significant effect on ball performance, principally due to the viscoelastic contribution of the various constituent materials. The manufacturing of this construction has implications for cost-effectiveness and performance consistency. A wide range of constructions are evident for common sports balls, where these constructions are an important factor in their respective sports. Numerous ball types exhibit performance variations that have been attributed to inconsistencies in the manufacturing method.
- A form of injection moulding is typically used to produce polymer foam sports balls. Consistent production can be attained by careful control of machine parameters. A variation in stiffness and energy dissipation properties can be achieved by adjusting mould temperature, additives such as blowing agent and nucleating agent, and selection of various polymer grades. Established methods of ball production, such as those producing softballs and golfballs, use sophisticated control of chemical reactions to produce definable ball performance. The exact details of such methods are proprietary knowledge of the manufacturers.

2.4.3 Model research summary

- Different approaches have been employed in the simulating of ball impact behaviour, including spring-damper mathematical modeling, logarithmic mathematical modeling and finite element modeling. The development of a ball model is useful for predicting and extrapolating ball behaviour, for understanding the contribution of material properties to impact response and for investigating ball-surface interaction.
- Mathematical models typically use spring and damper components to represent ball stiffness and energy dissipation. Non-linearity in the form of variable coefficient functions or non-linear components are necessary to adequately describe ball impact behaviour. These models are relatively simple and economical to compute and with sufficient refinement have been found to have good agreement with experimental results.
- Some mathematical models derive logarithmic relations from quasi-static methods to develop their models. While the use of independently measured parameters is a commendable approach, the Laplace transforms used to solve the model conceals the effect of the material parameters on the impact process in mathematical obscurity.
- Finite element models are a more sophisticated advancement of mathematical models. While the increased complexity leads to a greater degree of accuracy, the mechanisms occurring in the process of FE modelling are less intuitive. This makes the parameters of the FE model more difficult to relate to measures of stiffness and energy dissipation.
- The majority of published ball models are phenomenologically developed, where model parameters are adjusted to agree with experimental data. This can be useful for modelling other aspects of ball behaviour, as well as potentially providing insight into a material's response to impact. This is particularly evident for spring-damper mathematical models, where the simple representation of stiffness and damping components intuitively corresponds to impact characteristics. While the departure from simplicity allows FE models to more accurate simulation, the relevance of the model parameters to impact characteristics becomes less apparent.

From a material characterisation point of view, a more robust approach would be to calculate model parameters from independent test methods. Limited success has been reported so far from this approach, principally due to deficiencies in the independent measurement methods.

Chapter 3: Experimental work

3.1 Test system development

An automated test system was designed and developed to evaluate dynamic impact characteristics of the sliotar as described in Sections 2.1.2 to 2.1.5. In this system, a custom-built pneumatic system projected the ball at speeds of 5 to 38 m/s (11 to 86 mph), with precise aim and zero spin, to strike a rigidly-mounted impact plate. The collective measurement of multiple impact characteristics was facilitated by the use of high-speed footage and force-time data acquisition. The entire test system was controlled by a Graphical User Interface (GUI) programmed in LabVIEW. This control program managed the pneumatic system, acquired data from measurement devices and subsequently analysed this data to evaluate the ball's performance characteristics. These performance characteristics were displayed to the user and saved in spreadsheet format for post-test analysis.

3.1.1 Test system design

The test system was designed to be an all-inclusive system, i.e. all equipment and measurement devices were incorporated into a single unit, with room for a user to operate the system. The evolution of design of the test system is described in Appendix A, with a schematic of the final design version shown in Figure 3.1. The system was designed using 3D modelling software (Solidworks 2005, Solidworks Corporation, USA), which allowed a virtual assembly of the individual components for visual inspection of how the parts would fit together prior to final design. Orthogonal draft plans were acquired from the 3D design, with all parts of the system being fabricated in DCU School of Mechanical Engineering workshop. The size of the system was largely dictated by the distance required for ball projection, the size of the pneumatic components and the ergonomic space required for the user.

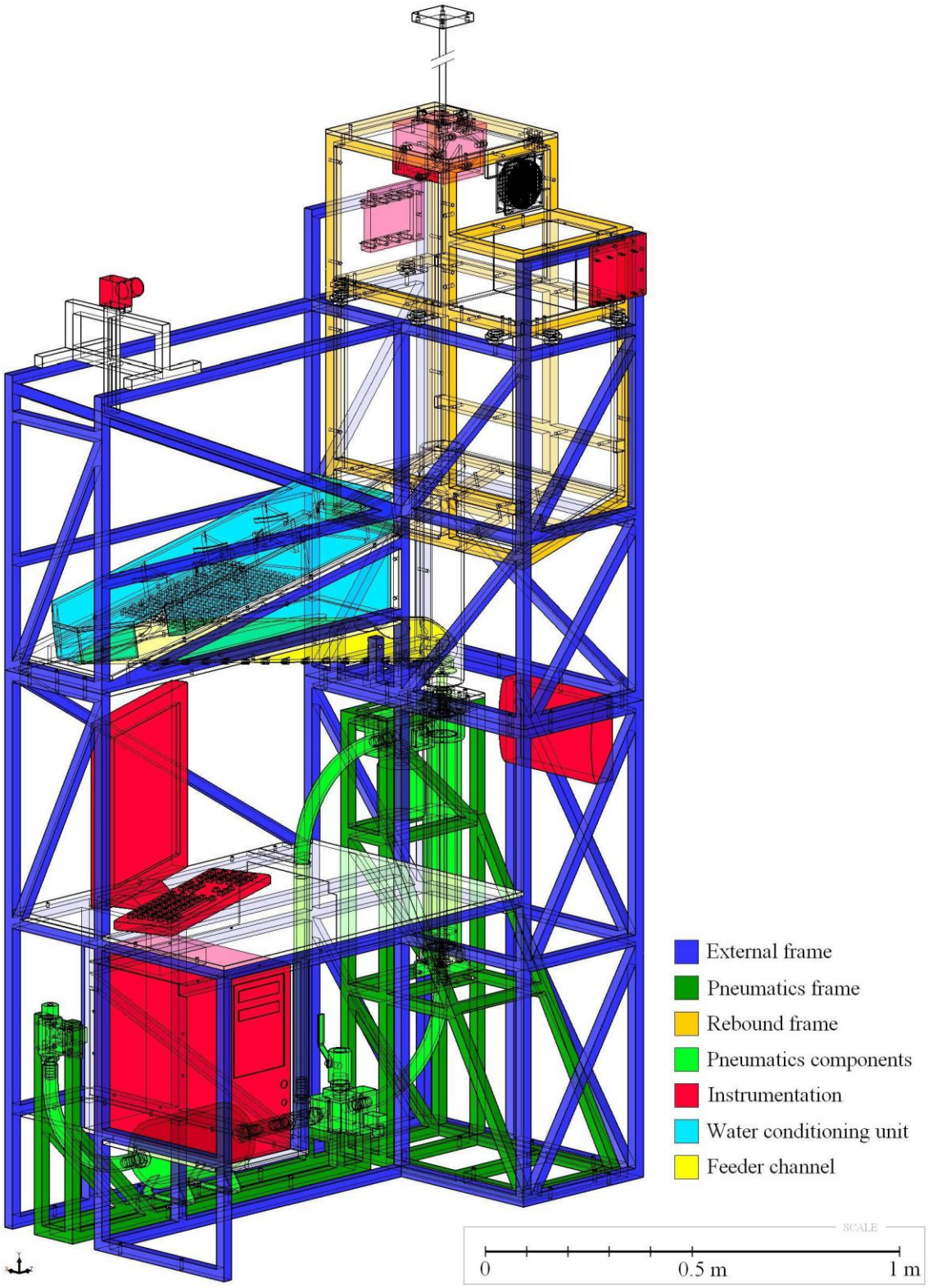

Figure 3.1: Schematic of test system components

Figure 3.2: Developed test system: (a) pneumatic actuator, (b) impact area, (c) high-speed camera, (d) water conditioning unit, (e) feeder channel, (f) user control interface

The pneumatic projection system was designed to fulfil four criteria: speed range capability (up to 38 m/s), zero spin induced, precise aim, and ball size capacity (diameters 40 to 90 mm). As discussed in Section 2.1.2, ball impact behaviour is dependent on incident speed and ball spin. The maximum speed encountered in hurling has been measured previously[3] as 38 m/s. To avoid undesirable variation in rebound angles and speeds, the ball was propelled with zero spin. This was achieved by placing the ball in a conical indent that enabled one-dimensional propulsion through the ball's centre of mass. A precise aim was required due to the small impact area and the detectable region capabilities of the data acquisition devices. The final criterion of the pneumatic system was to accommodate balls with range of diameters. This allowed for the small variation of sliotar cores' diameters (65 to 70 mm), as well as enabling potential testing of other ball types. The four design criteria were satisfied by the use of a pneumatic actuator (C95SDB63-500, SMC Pneumatics Ltd, Dublin) that was modified for this application to achieve higher extension speeds. A bore (internal diameter) of 63 mm and a stroke (actuator travel distance) of 500 mm were specified based on calculations outlined in Appendix A. The first modification was to enlarge the inlet and outlet ports to facilitate a greater air flow: the original G3/8 port (diameter 9.53 mm) was modified to a G1 specification (diameter 25.4 mm), resulting in a 7 times larger cross sectional flow area. The second modification involved the replacement of the original steel and aluminium piston assembly (2.1 kg) with a lighter polymer piston assembly (0.5 kg) for greater acceleration. A slideway lubricant (Ultraglide spray, Rocol) compatible with the piston polymeric material was used to minimise wear, with this verified by the consistent speed and aim accuracy as evident from high-speed footage. Careful programmatic control of the actuator extension was necessary given the lower strength of the polymer piston relative to the original metal piston. This was achieved by the digital control of two 3/2 directional control solenoid valves (VP3165-105DA-Q, SMC Pneumatics Ltd, Dublin), which allowed high pressure air into either end of the actuator to accelerate and decelerate the piston. An air reservoir (CRVZS-5, Festo Ltd, Dublin) acting as a buffer was located immediately before directional control valves to avoid restrictive choked flow developing in the narrow apertures of the pneumatic system. An oil lubricator (AS3, Bosch Rexroth AG, Germany) and filter

[3] Conducted by Dr. K. Moran, Dublin City University, July 2005

(AS3 semi-automatic drain, Bosch Rexroth AG, Germany) were installed in-line before the reservoir for smooth operation of the system. Both the actuator and the air reservoir were fitted with pressure sensors (40PC, Honeywell, USA) for recording the internal pressure. The development of this pneumatic system, shown in Figure 3.3, will be discussed in greater detail in Appendix A.

The pneumatic system was mounted in a rigid frame that allowed adjustment of the actuator to achieve precise alignment to the impact plate. This frame was bolted to the concrete floor, disconnected from the larger external frame to avoid the vibration transmission. Both frames were manufactured from 25 mm steel box-section and had traverse struts for extra rigidity. The external frame was comprised of two halves, bolted one on top of the other, for ease of manufacture and to facilitate transportation. During manufacture, a considerable amount of care was taken to correct for the deformation resulting from the heat of welding. The rebound frame was supported in the external frame by shock-suppression bolts to prevent the transmission of the impact shocks and vibrations into the rest of the system. This frame was clad with Perspex sheeting to allow observation of the impact. A loose nylon wire net was stretched across one of the bottom corners of the chamber to facilitate the dissipation of the balls' bouncing. This net, coupled with 10° incline of the rebound chamber floor, guided the ball to exit the rebound chamber after impact.

The ball sat in a cup-like device attached at the output of the actuator, see (a) in Figure 3.2. A bevelled edge machined into the cup ensured that the ball was centred relative to the piston, permitting the ball to be projected without spin. This was verified from high-speed footage analysis of markings on the surface of a projected ball, which shows a zero spin rate. This bevelled cup also allowed a range of ball sizes to be used. Precise aim was inherent in the actuator due to the axial motion of the piston. This was confirmed from analysis of the ball incident trajectory of high-speed footage, which determined an incident angle dispersion of within 0.7°. The direction of projection was vertical to avoid gravitation deviation of the ball from its incident path, thus maintaining one-dimensional motion. The gravity force (approximately 0.98 N for the sliotar core) had a negligible effect on the ball impact given the magnitudes of the impact forces (typically 0.8 to 5.5 kN depending on incident speed and ball type). It was decided to

launch the ball upwards to facilitate the collection of the projected ball, which rolled back to the projection area under gravity so that testing could be automated.

The impact plate assembly, (b) in Figure 3.2 and also Figure 3.4, was positioned directly above the pneumatic actuator. The impact assembly comprised of a rigidly mounted steel plate that was significantly harder than the ball so that it did not deform under impact. The impact plate was 20 mm thick and braced against the room's concrete ceiling such that it did not deflect under impact loading. This set-up conformed to 'rigid-body' impacts as conducted in previous literature, as described in Section 2.1.2. This signified that the impact plate had a negligible contribution to the energy loss of the impact, thus providing data that was intrinsic to the ball itself.

A high-speed camera was mounted on a linear rail positioned at the level of the impact plate, see (c) in 3.2 and also Figure 3.5. This allowed the camera to be adjusted in two directions: towards and away from the impact plate, and vertically up and down along the ball trajectory. The horizontal motion of the camera was not necessary as it was centred on the impact plate. The tiny exposure time associated with high-speed footage necessitated high illumination for the clarity. This illumination was provided by a 200 W and 150 W halogen floodlights shining from above and below the impact plate respectively. A 50 W halogen spotlight was positioned between the floodlights to remove the shadows between the impact plate and the curved surface of the ball. A cooling fan was installed in the rebound chamber to reduce the temperature rise from the radiant heat of the halogen bulbs.

A water conditioning unit, see (d) in Figure 3.2, was incorporated into the system design to allow testing of balls under wet conditions. The water conditioning unit had a series of variably-angled protruding walls that partially obstructed the passage of the rolling ball. The extent of the wetness of the core was dependent on two control variables: firstly, the volume flow-rate of water into the unit; and secondly the angles of the protruding walls, which increased the time that the ball was in the shower unit by up to 60 %. The protruding walls also altered the rotational axis of the core, allowing a more distributed wetting over the ball surface. The actual testing of balls in wet conditions was not conducted in this work.

The feeder channel, see (e) in Figure 3.2, could accommodate up to 14 balls for automated batch testing. The feeder channel was manufactured from transparent Perspex tube, with two steel rods running along the inside of the tube to ensure the balls were aligned in the middle, rather than piling up along the sides of the tube. A sprung mechanism at the base of the feeder channel was controlled by the retraction of the actuator to allow one ball at a time to enter the firing position.

The system was designed with consideration to user ergonomics and safety. The data acquisition electronics and the pneumatic system components were easily accessible for adjustment and maintenance. Hazardous areas were shielded from the user, while an electrical safety system was installed by a qualified electrician to Irish regulatory standards (I.S. EN 60947-2).

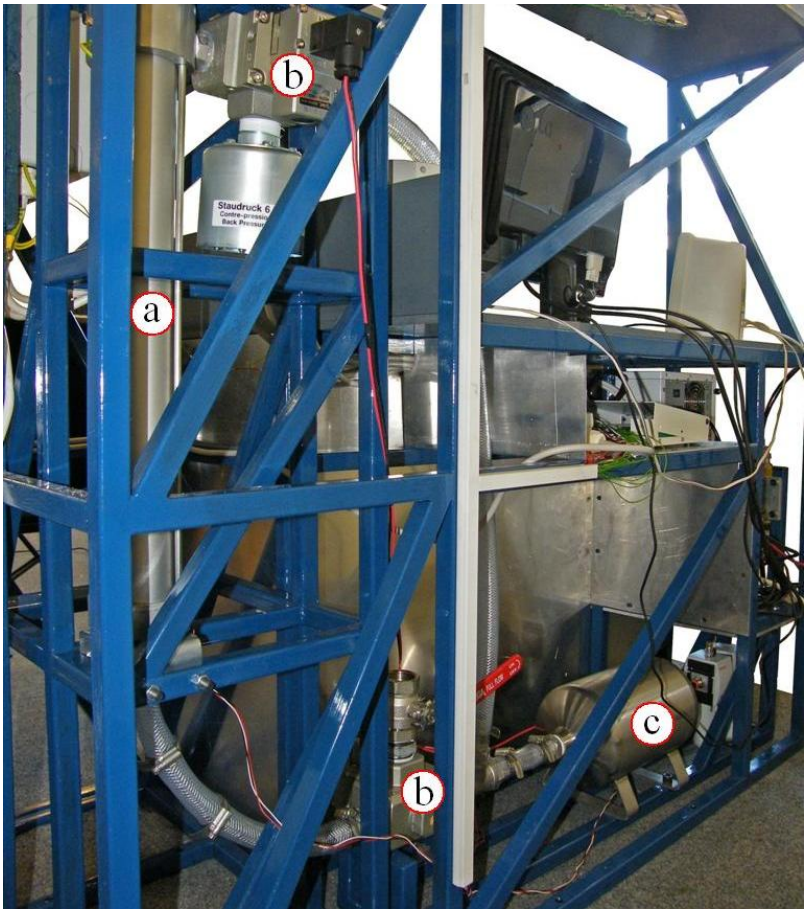

Figure 3.3: Pneumatic system for ball propulsion: (a) customised pneumatic actuator, (b) inlet and exit directional control valves, (c) air reservoir for storing air charge

Figure 3.4: Impact plate assembly directly above pneumatic actuator

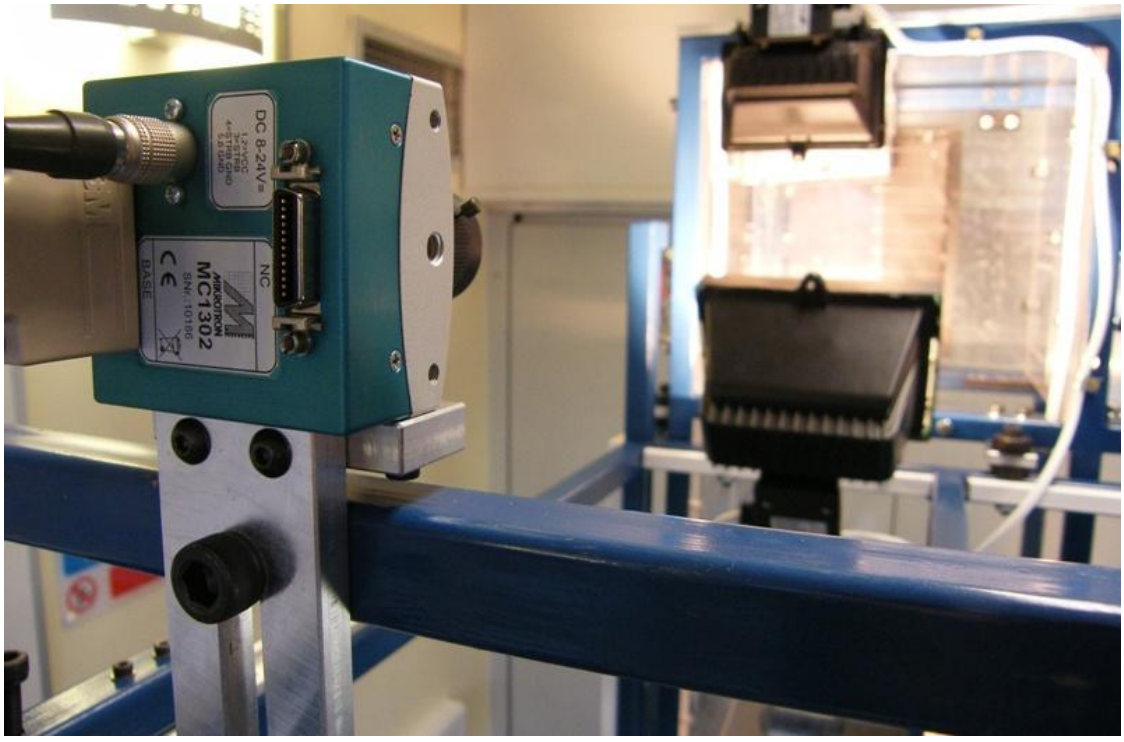

Figure 3.5: High-speed camera and halogen floodlights (50W spotlight not shown)

3.1.2 Test system operation

The test system was controlled from a PC using a graphical software programming language called LabVIEW (Version 8.5, National Instruments, UK). The operation of the system involved the synchronised use of nine LabVIEW Virtual Instrument (VI) programs. A complete description of all the acquisition and control programs for the test system is contained in Appendix C. The top-level VI (the Graphical User Interface shown in Figure 3.6) allowed the input of the ball identification names and the desired projection speed. This program executed the subVIs (sub-programs) in the correct sequence and displayed the impact characteristics following analysis of the acquired data. Communication between the software and data acquisition hardware was achieved using a PCIe multi-function card (PCIe-6251, National Instruments, UK) and break-out box (SCB-68, National Instruments, UK) facilitated the input and output of voltages and timing signals. Figure 3.7 shows the input and output data for the system.

The pneumatics system was operated using digital outputs triggering the solenoid valves via relays, with the air pressure sensor output being read as an analog input. At maximum capacity, the actuator could accelerate from rest to 38 m/s (137 km/h or 86 mph) in 12 milliseconds and decelerate to stop before the end of the 0.5 m stroke. The signal timings of the directional control valves were crucial, to allow the maximum use of the extension stroke to accelerate the ball, yet decelerating the piston before it struck and fractured against the end of the stroke. Programmatic control of the valves allowed a speed capability of 5 to 38 m/s with a precision of ±0.1 m/s.

The impact characteristics were derived from the speed, deformation and force data from the impact. The high-speed camera (MC1302, Mikrotron GmbH, Germany) had a CMOS pixel sensor with a full frame resolution of 1280 x 1024 pixels at 100 frames per second (fps) – higher frame-rates (increased data resolution) were obtained by reducing pixel resolution (reduction in either field-of-view or dimensional precision). A frame-rate of 4000 fps with resolution of 210x127 pixels was used typically. These settings could be adjusted for prioritising either data resolution or dimensional precision. The exposure times for acquisition were in the region of 1/10000 of a second to avoid motion blur at higher incident speeds. High-speed footage of the impact was acquired from the high-speed camera via a base CameraLink connection to the dedicated frame-

grabber card (PCIe-1429, National Instruments, UK) installed in the PC chasis. The frame-rate, resolution and exposure settings of the camera were specified by serial commands specified within LabVIEW. Due to the high rate of image acquisition, the high speed footage had to be saved on the hard-drive before being processed. High-speed image acquisition was achieved by the use of an LL ring buffer algorithm, which created the memory allocation for the frames before the acquisition, allowing the rapid saving of each frame in an uncompressed AVI movie file. The path of this file was automatically passed to the image processing algorithm for subsequent processing. Details of the image processing will be discussed in Section 3.1.3 with regard to speed and deformation measurements respectively. To prevent excessive use of CPU and disk space, and to reduce the time taken for the image processing, the duration of acquisition was set to 90 milliseconds. In order for the small acquisition window to coincide with the impact, a software timer was used to trigger the camera at a precise time after the ball was projected.

An axial compression load-cell (RLU02500, RDP Electronics Ltd, UK) was integrated into the impact assembly to measure force-time data, as shown in Figure 3.4. This load-cell measured the force sensed on its threaded central core. The steel impact plate was bolted directly into the axial compression load-cell using a M12 metric bolt. The load-cell was shielded by a reflective polystyrene cover (not shown in Figure 3.5) to prevent the radiant heat from the halogen lights affecting the calibration of load-cell. The load-cell signal, triggered by the software, was acquired as 50 kHz analog input via the multifunction card. Prior to acquisition, the load-cell's voltage output was amplified to the 0 – 10 volt range by a transducer amplifier (DR7DC, RDP Electronics, UK).

After impact, the ball rebounded within an enclosed rebound chamber until its energy was dissipated. After leaving the water conditioning unit, balls re-entered the firing area via the feeder channel, (e) in Figure 3.2. Microswitch sensors (SPDT IP67, Cherry Corp, USA) positioned along the length of the feeder channel were read by the control program as analog inputs. These signals were used to inform the control program of the number of balls being tested, ensuring that each core returned to the channel before the next one was fired. The communication of these switches with the control program allowed for automated batch testing.

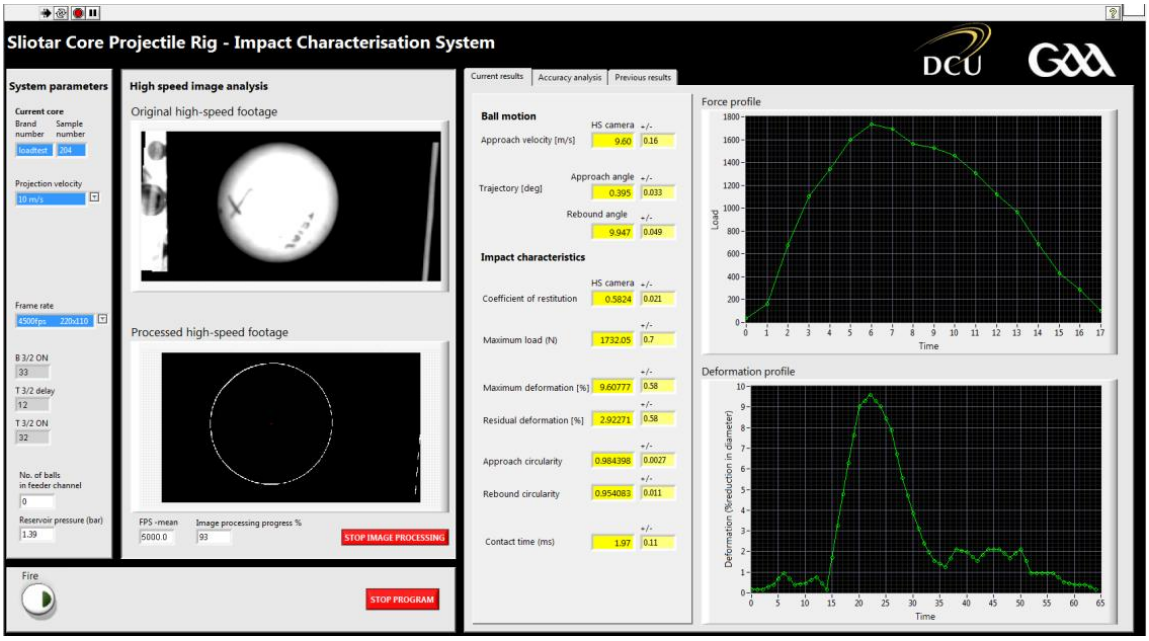

Figure 3.6: Control program graphical user interface

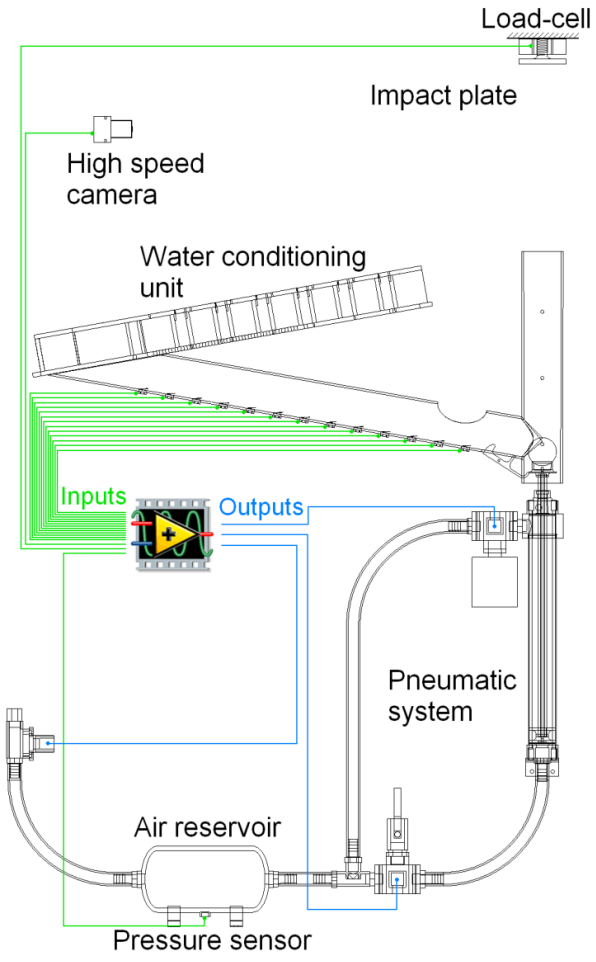

Figure 3.7: System control program inputs and outputs

3.2 Performance characterisation

Impact testing was conducted in the speed range of 5 to 25 m/s in increments of 5 m/s. While the pneumatic system was capable of higher speed, testing was restricted to 25 m/s for operational longevity. The testing procedure followed an order that allowed a period of at least two minutes to elapse between impacts of each ball sample, thus avoiding effects of internal heating. The temperature and humidity of the laboratory were monitored for the duration of testing. Testing was conducted at 22 ± 2 °C at 55 ± 10 % relative humidity.

Sixteen brands of sliotar had passed the current regulatory standard requiring a COR in the range of 0.522 to 0.576. These ball specimens, henceforth labelled as 'approved cores', were comprised of the two main core construction types: polymer and cork as seen in Figure 3.8. The cores' diameters are shown in Figure 3.9. The balls were unbranded and assigned with arbitrary identification numbers so that testing was unbiased towards any brand. Of the 10 samples of sliotars submitted by each approved manufacturer, 4 samples of each approved ball type were characterised in terms of coefficient of restitution, impact force and deformation as described in Sections 3.2.1 to 3.2.3. Such characterisation was conducted with a view of developing a more comprehensive regulatory standard for the sliotar. The resulting performance would also give an indication of the desired performance of prototype balls.

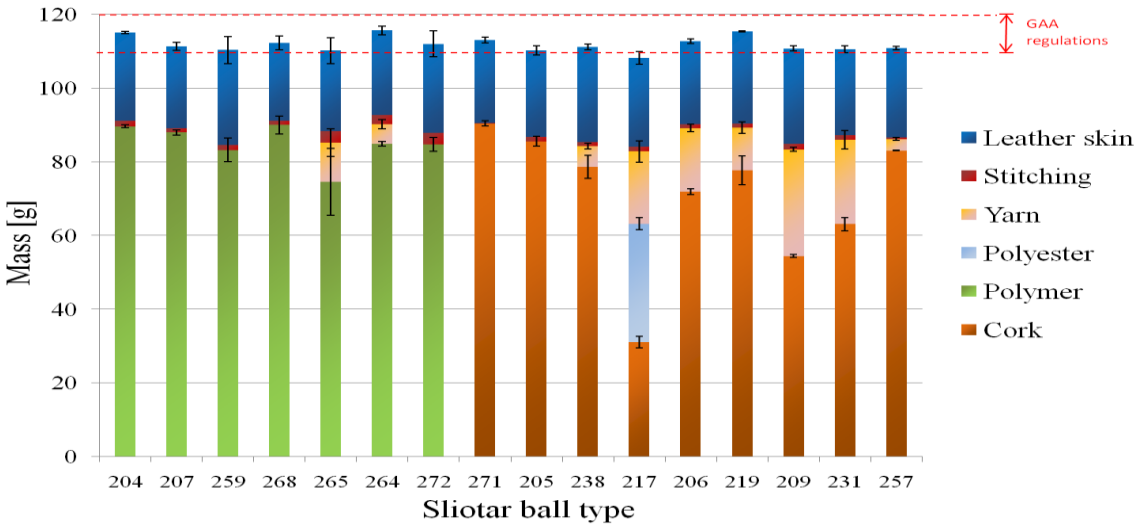

Figure 3.8: Mass compositions of all approved sliotars

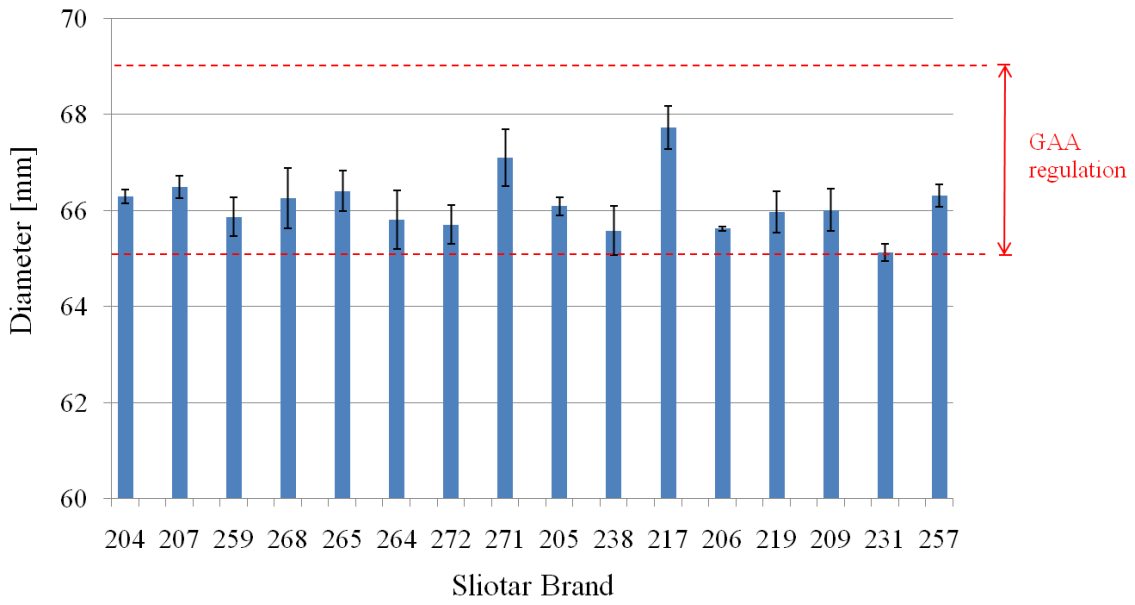

Figure 3.9: Diameters of all approved sliotar cores

Four of the approved cores were selected for more in-depth testing. Three samples of each ball type were subjected to impact testing at speeds between 5 and 25 m/s in 5 m/s increments. The aim of the concentrated analysis of these selected ball types was to advance the research of solid sports ball impact behaviour, particularly with regard to deformation quantification and viscoelastic characterisation. The cross sectional views of these selected ball types are shown in Figure 3.10. Ball type 204 was homogeneous polymer core, selected due to the popularity of this ball type in the sport. Ball type 268 was a different type of homogeneous polymer core, and was selected for being the most compliant (exhibited greatest deformation) of all approved ball types. Ball type 206 had a predominantly cork composition with a thin layer of yarn. This ball type was selected because it exhibited the highest peak forces of all approved ball types. Ball type 217 was a multi-constituent composition of cork, polyester strands and yarn, selected for its distinct construction relative to the other approved sliotar cores. The dimensions of these ball types are displayed in Table 3.1.

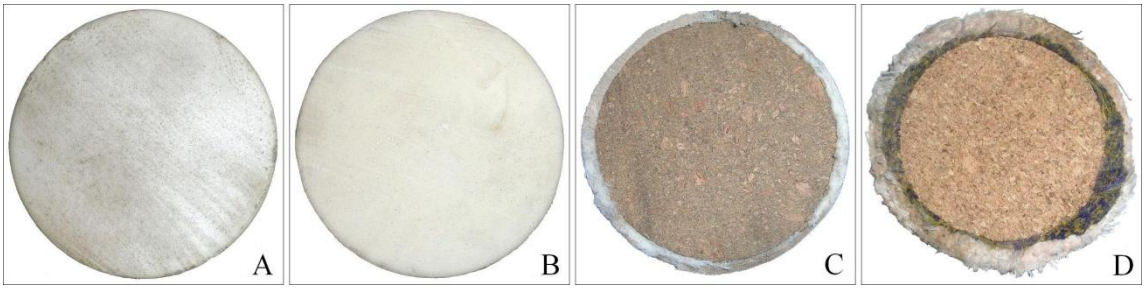

Figure 3.10: Cross sectional pictures of selected sliotar cores (a) 204, (b) 268, (c) 206 and (d) 217

Note: the non-spherical appearance of balls 206 and 217 in Figure 3.10 were due to disfiguration from cutting.

Table 3.1: Properties of selected sliotar cores

Ball type	Diameter [mm]	Mass [g]	Material mass composition
204	66.2 ± 0.1	89.6 ± 0.4	100 % polyurethane-based polymer
268	66.8 ± 0.2	89.9 ± 3.1	100 % polyurethane-based polymer
206	65.6 ± 0.1	89.1 ± 0.9	~20 % yarn, ~80 % cork
217	68.2 ± 0.4	83.1 ± 1.3	~24% yarn, ~38% polyester, ~38 % cork

In addition to four selected sliotar cores, a number of different ball types were tested for comparison purposes. These ball types included a compliant polymer ball labelled ‘180’ (non-approved sliotar core), a cricket ball (GM Clubman 4.75 Oz) and a solid rubber ball labelled ‘PNG’. The dimensions of these ball types are shown in Table 3.2. The inclusion of these different ball types would allow analysis of more diverse impact behaviour. This was particularly motivated by the aim of clarifying ball deformation It also allowed comparison between results of this test system and other publications in the literature that were focused on similar ball types.

Table 3.2: Other ball types tested with regard to deformation characterisation

Ball code	Ball type	Mass [g]	Diameter [mm]
180	Polymer ball	84.89	66.1 ± 0.02
Ckt	GM Clubman cricket ball	135.64	69.7 ± 0.1
PNG	Rubber ball	68.51	61.3 ± 0.05

3.2.1 Coefficient of restitution characterisation

As discussed in Section 2.1.2, the coefficient of restitution (COR) was the most frequently used measure of ball impact energy dissipation. For a rigid-body impact, as was the case with this test system, the coefficient of restitution was calculated from the ratio of ball speeds after and before the impact. During impact, the speed of the ball was measured over a distance of 0.1 m from the impact plate. The effect of gravity on the ball was found to be negligible, within experimental error.

Ball speed was measured using the high-speed camera. The high-speed footage was analysed using an image processing algorithm written in LabVIEW. This program is described in greater detail in Appendix B. The program used a series of functions to clarify, filter and threshold the image. This converted the original 8-bit image (256 shades of grey) to a 1-bit binary image (pure black background and pure white ball shape). Computation of the image pixels allowed the ball centre co-ordinates to be located and tracked from frame to frame. The centre co-ordinates of the ball were recorded between two boundaries, with the left-side boundary excluding the ball when it was in contact with the impact plate, and the right-side boundary excluding the ball when it was not fully visible in the field-of-view. The position of the ball's computed centre co-ordinates were displayed for visual checking by the user to verify that the pixel coordinates represented the centre of mass of the ball during its flight. These pixel measurements were converted to real-world dimensions using a numerical factor derived from a calibration chart. The speed was calculated from these dimensions and the time between frames, that being the reciprocal of the camera frame-rate. Speed measurement

from high-speed footage was found to have an experimental error of ± 0.8%. Details of the camera calibration are described in Appendix B.

3.2.2 Force-time characterisation

A number of performance characteristics were derived from force-time data measurement, as discussed in Section 2.1.3. These characteristics included peak force, acceleration, impulse and contact time. Force-time data was measured using a load-cell incorporated into the rigid impact plate. The load-cell signal was acquired at 50 kHz. A calibration factor yielded from calibration of load-cell was used by the control software to convert the voltage to a force reading. The calibration of the load-cell is described in Appendix B.

Subsequent to impact, the force-time graph was subjected to numerical analysis. The peak force was evaluated from the maximum recorded value. This value was presented as a useful indicator of ball hardness or shock. The balls' centre-of-mass (COM) acceleration was calculated by dividing the force by the ball mass. This was used for evaluation of COM displacement, see Section 3.2.3. The impulse was measured from the area underneath the force-time curve. This measure was compared to the momentum differential as independently measured from high-speed footage for verification of the force-time impact data. The contact time was measured from the width of the force-time signal. The contact time was determined by the load-cell data rather the high-speed footage due to the higher sample rate capacity: 50 kHz for the load-cell as opposed to 4000 fps for the camera.

3.2.3 Deformation characterisation

Physical measurement of diameter compression and lateral expansion were measured from high-speed footage. Ball centre-of-mass (COM) displacement was evaluated from force-time data. There were two aims to evaluating of both considerations of ball deformation. The first aim was to determine the link, if any, between COM displacement and the physical measures of diameter compression and lateral expansion.

The second aim was to verify what quantitative measure of ball deformation was applicable to force-displacement graphs for viscoelastic characterisation.

In the same program that measured ball speed, a separate section of the algorithm focused on the pixels' shape when the ball was in contact with the impact plate. The displacement of the right edge of the pixels shape relative to the left edge (stationary against the impact plate) was recorded to give the diameter compression. The distance between the topmost and bottommost pixels was recorded to evaluate lateral expansion. The diameter compression and lateral expansion were also expressed in terms of normal and tangential compression ratios, respectively, as defined previously in Section 2.1.4. These ratios expressed the maximum diameter compression and lateral expansion values as percentages of the original ball diameter

The COM displacement was measured from the double time integration of the force data divided by the ball mass. For a rigid-body impact, as discussed in Section 2.1.4, the COM acceleration equals the measured force divided by the ball mass. Integrating the acceleration with respect to time, using the incident speed as measured from high-speed footage as the initial condition, produced the COM speed during impact. Integrating this again with respect to time, with an initial condition of zero, resulted in the COM displacement. This method was verified by finding that the ratio of initial and final COM speed tended to be within 2% of the coefficient of restitution as measured from high-speed footage, see Figure B.5 in Appendix B. The relationship between COM displacement and diameter compression was investigated by using various camera settings to prioritise data resolution or dimensional precision. A 6^{th} or 7^{th} order polynomial curve was fitted to the diameter compression data to interpolate between points, with the goodness of fit verified with correlation values.

3.2.4 Viscoelastic characterisation

Ball viscoelastic characteristics were measured from force-displacement curves for quasi-static compression and dynamic impact testing. Ball stiffness was determined from the slope of the force-displacement and hysteresis energy dissipation was

calculated from the area enclosed in the loop. In addition, values for ball stiffness were evaluated from theoretical equations proposed from the literature.

Quasi-static characterisation

For quasi-static compression, the four selected sliotar cores (ball types 204, 268, 206, 217) were tested in a compression testing machine (FB050TM, Zwick/Roell, Germany), shown in Figure 3.11. Each ball was compressed between two parallel steel plates. A frictionless surface, such as PTFE tape, was deemed unnecessary as the curvature of the ball progressively came into contact with the plate surface rather than expanding across it. A maximum compression of 15 mm was used. The basis of this selection was to obtain an extent of deformation representative of impact without inducing permanent damage to the ball. Four compression rates were employed: 0.5, 1, 2 and 3 mm/s, the final value being the maximum deflection rate of the machine. For each compression rate, the ball was subjected to three compression cycles. Each cycle loaded and unloaded at a constant compression rate. There was no delay between loading and unloading at maximum load, while there was a 20 second delay between unloading and a new cycle loading to allow for strain recovery, if any. The selection of 20 seconds was reasoned as a long enough duration to observe the presence of strain recovery, without being impractically long in conducting the test. Each ball was rested for at least 3 hours between each compression test to allow full strain recovery between testing at different strain-rates. Compression testing was conducted at 21 °C at 52 ± 2 % RH, comparable ambient conditions to the impact testing.

Quasi-static stiffness was approximated as linear fit to quasi-static force-displacement curve, neglecting the data curvature at initial 20% of compression that relating to the ball surface flattening against the platens. The quasi-static hysteresis energy dissipation was measured from the proportion of area enclosed within the quasi-static force-displacement loop.

Figure 3.11: Quasi-static compression testing set-up

Dynamic characterisation

The choice of deformation quantification method was investigated for the compilation of dynamic force-displacement curves. Displacement values were derived from deformation measurement, with the choice of using diameter compression values or COM displacement. The diameter compression values were upsampled to the sample rate of the force data by the fitting of a 6^{th} or 7^{th} order polynomial curve. The validity of the choice between diameter compression and COM displacement was determined by measuring the area under the loading portion of the curve. The area should correspond to the accumulated energy involved in the compression phase, that being the ball's incident kinetic energy given the transition from moving ball to stationary ball at maximum compression.

$$\int_{x=0}^{x=max} F \, \mathrm{d}x = {}^{1}/_{2} \, m \, u^2 \qquad (3.1)$$

where F is the force data, x is the deformation value, m is the ball mass and u is the ball's incident speed. An additional verification was that the proportion of area enclosed within the hysteresis loop should equate to the kinetic energy loss, as calculated from Equation 2.3.

The stiffness was derived from the slope of the loading portion of the force-displacement curve. To account for the non-constant gradient of the force-displacement curve, two measures of stiffness were evaluated for each impact. These measures of stiffness were computed by using two linear sections to approximate the compression phase of force-displacement curve. The linear sections were calculated by fitting linear trends to the experimental data using the Least Square method. The extremity points of the linear trends were initially determined visually, with refined adjustment to optimise the R-squared correlation values. The slopes of the two linear trends yielded two stiffness values, where the initial averaged slope was termed *initial stiffness* and the subsequent averaged slope was termed *bulk stiffness*.

Spring theory numerical predictions

Equations for evaluating a single value of dynamic stiffness, as described in Section 2.1.5, have been used frequently in previous literature [18, 24, 25, 110]. The two principal equations, as restated below, were computed to investigate the validity and usefulness of these estimations.

$$k = m\,\frac{\pi^2}{{t_c}^2} \tag{3.2}$$

where k is dynamic stiffness, m is ball mass and t_c is contact time.

$$k = \frac{1}{m}\left(\frac{F_p}{u}\right)^2 \tag{3.3}$$

where k is dynamic stiffness, m is ball mass, F_p is the peak impact force and u is the ball's incident speed.

3.3 Prototyping development

3.3.1 Production method selection

Injection moulding was selected as the method of manufacturing for a number of reasons. Firstly, as discussed in Section 2.2.3, injection moulding is the most common method of processing plastics. This ensured a broad availability of manufacturers and compatible material suppliers. Secondly, it tends to be a fully automated process, providing consistent repeatability and cost-effectiveness for long-term production. Finally, a number of the currently approved polymer cores were identified as products of injection moulding, as evident from the characteristic seam and sprue markings on the ball surface. The other polymer cores appeared to be made by compression moulding, a method that was disregarded due to the inferior surface finish of these ball types. Reaction injection moulding was also considered at the outset, but dismissed due to the technical complexities and expense involved. An industrial collaboration was established with Key Plastics in Bray, Co. Wicklow, to carry out production according to a screening set of experiments.

The materials for prototyping were selected on the basis of characterisation of the approved polymer sliotar cores. Samples of the injection moulded cores were melted to verify that they were thermoplastic. Attenuated total reflectance Fourier-transform infra-red (ATR-FTIR) spectroscopy was conducted[4] on 100 μm thick samples of the sliotar polymers. This method identified polyurethane as the dominant constituent polymer. However, considering the vast amount of polymers types, ATR-FTIR could only verify the general polymers present but could not identify specific polymer grades or other constituent materials.

Since commercially available polymers are graded using Shore hardness, the approved polymer cores were measured using a handheld Shore A durometer, as described Appendix D. The ball types were found to occupy a range of 50 to 80 Shore A. Details on the selected prototyping materials, based upon the aforementioned characterisation results, are shown in Table 3.3.

[4] Dr. Fiona Regan from DCU School of Chemical Sciences conducted the ATR-FTIR analysis

Table 3.3: Prototyping constituent materials for screening set of experiments

Name	Material type	Hardness	Density [g/cm^3]	Recommended addition [%]
OnFlex-U 5355A	TPU	55A	1.02	-
OnFlex-U 5370A	TPU	70A	1.05	-
Pellathane 2103-80AE	TPU	80A	1.13	-
PolyOne 68949 NP	BA	-	-	0.5 – 2
PolyOne 68007 NP	NA	-	-	2 – 10

The materials outlined in Table 3.3 were purchased from Total Polymer Solutions Ltd, Dublin. Three grades of thermoplastic polyurethane (TPU) were selected based on their specified hardnesses being in the range of hardness of existing ball types. As the densities of these material grades were in excess of the required density (approximately 1 g/cm^3 compared to 0.6 g/cm^3), a blowing agent (BA) was used to produce a lighter ball. The final material additive was a nucleating agent (NA) which would affect the cell structure of the foam, adjusting it from coarse to fine. As this influenced the structure properties of the ball, it was envisaged that would affect stiffness and/or energy dissipative properties. In addition, the nucleating agent was used to increase the crystallisation rate, allowing a faster cycle time.

The moulding tool was designed and fabricated in DCU workshop. As it was a prototype tool (<1000 samples required), aluminium was deemed sufficiently resilient for the tool material. As seen in Figure 3.12, the tool had a single cavity with internal diameter of 66 mm, fed by a sprue of length 70 mm and inlet diameter 5 mm. To allow gas to escape upon injection of the plastic, venting slots were machined into the circumference. Venting depth for polyurethane was recommended at 0.02 to 0.05 mm, with the maximum recommended venting depth used for this tool. A venting pin was positioned opposite the sprue with a vacuum pump fitted for extra venting. This vacuum pump operated upon closure of the mould. Cooling channels were machined in a hexagonal pattern surrounding the cavity in both halves of the tool. These channels were

rigged up to a water temperature control unit to control the mould temperature. A shut-off nozzle was fitted between the barrel and sprue opening. This prevented additional material beyond the shot weight entering the cavity.

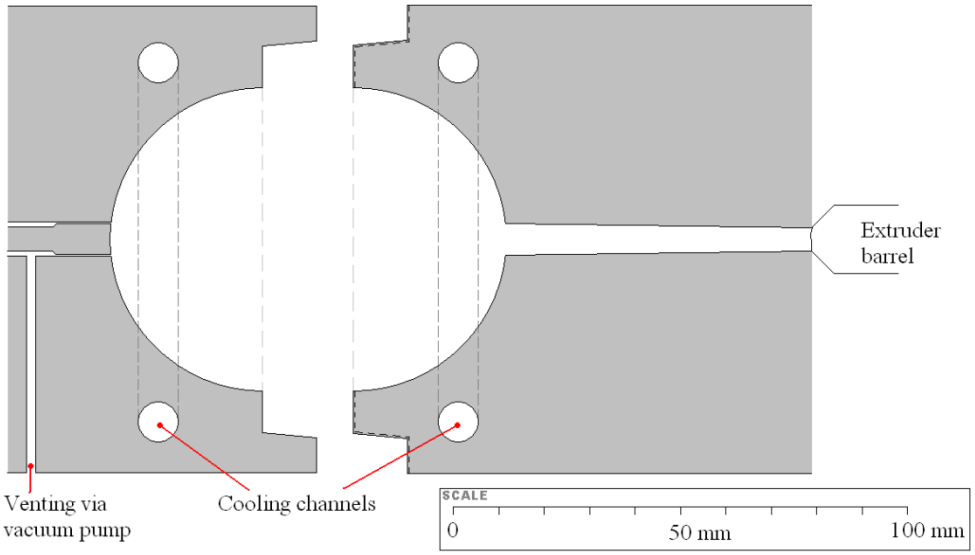

Figure 3.12: Schematic of mould design (open position)

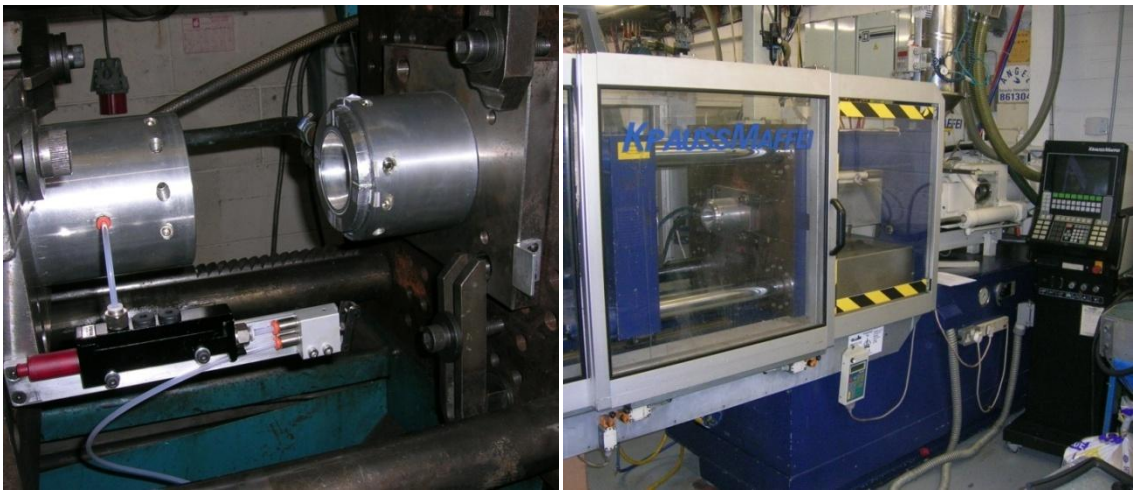

Figure 3.13: Injection moulding production (a) loaded mould tool, (b) injection moulding machine

3.3.2 Screening set of experiments

A screening set of experiments was conducted to establish the consistent production of an acceptable ball type. Due to the hygroscopic nature of the materials, the virgin TPUs and the nucleating agent were dried for 2 to 4 hours at 100 °C. Ideally a drier fitted directly to the injection moulding machine hopper would be used to avoid moisture contamination due to exposure to the atmosphere, but this was not available for the allocated injection moulding machine. Based on research [121, 150] and industry advice [151, 152], three factors were investigated to produce a variation in performance of a sports ball: polymer grade (affecting stiffness), nucleating agent quantity (affecting internal structure and hence stiffness and energy loss) and mould temperature (affecting internal structure due to curing rate). The material composition was mixed manually, a procedure consistent with standard practice for moulding manufacturers.

The criteria for an acceptable ball were a mass of 90 g, a spherical geometry of diameter 66 mm and a uniform mass and material homogeneity throughout the ball. Such criteria were to be fulfilled without manufacturing defects with a continuous and repeatable production. The machine parameters and constituent material preparation techniques were adjusted to produce an acceptable ball. The principle machine parameters were **barrel temperatures**, **mould temperature**, **cooling time**, **plasticising delay time**, **holding pressure**, **back pressure**, and **shot size**. The constituent material preparation techniques applicable to part quality were **blowing agent addition rate**, and **nucleating agent addition rate**.

The **barrel temperatures** specified the temperature gradient along the barrel. To avoid material degradation, barrel temperatures were kept as low as material flow viscosity would allow. The temperature profile was 170/175/180/190 ± 2 °C for the 55A and 70A TPU grades and 170/180/190/210 ± 2 °C for the 80A grade for the rear/middle/front/nozzle temperatures respectively. When the resident time (the time duration that material was in the heated barrel) exceeded 10 minutes, the barrel was purged to remove the degraded material.

The **mould temperature** controlled the cooling rate of the ball. The mould temperature was regulated by a water temperature control unit pumping water through the hexagonal channels. The temperature was varied from 12 to 40 °C.

The **cooling time** was determined by the length of time required for a sufficiently thick skin to form on the ball, such that the shape was maintained when removed from the constraints of the mould. A cooling time of 6 to 7 minutes was used to allow sufficient solidification of the ball surface. On occasion, the balls were immersed in a water bath at room temperature immediately after ejection. The frequency of this occurrence was based on visual and tactile observation of the ball.

The **plasticising delay time** was the time between injection and the commencement of plasticising, where the screw rotated to draw more material from the hopper into the barrel. This was set to 60 seconds to allow the sprue to solidify, thus avoiding cavity over-packing.

The **holding pressure** was the pressure involved in packing the mould. This was set to 10%, a relatively low value to accommodate the pressure induced by the blowing agent activity.

The **back pressure** was the pressure applied to the melt during plasticising. This was set to 30%, a relatively high value compared to the typical 2 to 3% in conventional injection moulding. The high back pressure allowed more thorough mixing of the virgin material and additives.

The **shot size** was adjusted between 70 and 72%, depending on material composition, to achieve the correct ball mass.

The **blowing agent addition rate** of 1% was found to be most stable. The blowing agent pellets with diameters of 2.5 mm were ground down to promote more uniform mixing. Batches of 0.4 kg were removed from the drier, mixed and placed in the sealed hopper. Small batches were advantageous both to visually ensure uniform mixing and to limit the amount of material outside of the drier.

The **nucleating agent addition rate** was varied between 0 and 10%, with these particles sufficiently small to not necessitate further grinding. Excessive quantities of the nucleating agent were found to inhibit the action of the blowing agent, thus preventing full expansion.

3.3.3 Variant production

Six ball variants were produced from the screening set of experiments. These ball types and their material composition are specified in Table 3.4.

Table 3.4: Prototype variants production

Variant #	Polymer grade	Nucleating agent [%]
55_a	55A	0
55_b	55A	2.5
55_c	55A	5
70_a	70A	0
70_b	70A	5
70_c	70A	10

The mould temperature was found to have a more dominant effect on part geometry rather than material properties, thus eliminating it as a factor in ball variant production. Consistent moulding of the 80A polymer grade was not possible due to the persistence of manufacturing defects. The nucleating agent addition rate was limited to 5% for the 55A polymer grade due to a separate manufacturing defect.

The impact characteristics of the produced prototype variants were evaluated in the developed test system. Four samples of each variant were subjected to impacts in the range of 5 to 20 m/s at 5 m/s increments. A period of at least 2 minutes had elapsed between impacts of a sample to avoid the effects of internal heating or slow shape

recovery. Testing was conducted at 20 ± 1°C and 45 ± 5 % RH. As these ambient conditions differed slightly from those when the sliotar cores were tested due to the time of year of testing (February/March/April for approved sliotar cores, June/July for prototypes) a sample sliotar core (ball type 204) was also included in impact testing for comparison purposes.

3.4 Mathematical modelling

Three phenomenological mathematical models were applied to the experimental data of the four selected sliotar cores described in Section 3.2. The models were based on three cases of the Kelvin-Voigt mass-spring-damper configuration, with each progressively accounting for component linearity. The first and third models were utilised with some previous reported success as described in Section 2.3 (see Figures 2.6 and 2.10). The second model used in this present work was an intermediary configuration between the first and third models. Each model was based on the following equation of motion:

$$F = m\ddot{x} = c\dot{x} + kx^{\alpha} \tag{3.4}$$

where F is the impact force, m is ball mass, c is the damping coefficient, k is the stiffness coefficient, α is the spring exponent and $\ddot{x}$, $\dot{x}$ and x are the centre-of-mass (COM) acceleration, speed and displacement. Algorithms were written in LabVIEW to determine these model variables. The COM speed ($\dot{x}$) and COM displacement (x) were determined by the first and second time integration of the impact force divided by ball mass. The parameters c, k and α were calculated according to the individual model methodologies as described in the following sections. Once the parameters were evaluated, the first program calculated the right-hand side of Equation 3.2 to yield the predicted model force. The model force was plotted alongside the experimental force, with the goodness of fit indicating the model validity in terms of R-squared value. Further details of the LabVIEW programs used for the models investigation are outlined in Appendix B.

3.4.1 Model 1

The first mathematical model was the most basic Kelvin-Voigt configuration as used by Goodwill and Haake for tennis ball impacts [18, 35]. Their application of the model was discussed in Section 2.3.1, where the stiffness and damping coefficients were calculated from functions of contact time and coefficient of restitution.

$$k = m\frac{\pi^2}{T_c^2} \tag{2.13}$$

$$c = -\frac{2m}{T_c}\ln(\mathrm{COR}) \tag{2.14}$$

where k is the stiffness coefficient, m is ball mass, T_c is the impact contact time, c is the damping coefficient, and COR is the coefficient of restitution. This model represented the stiffness component as a linear spring, signifying that the spring power $\alpha = 1$. Using experimentally-measured values of contact time and coefficient of restitution, a program was written to compute the model predictions according to Equation 3.2.

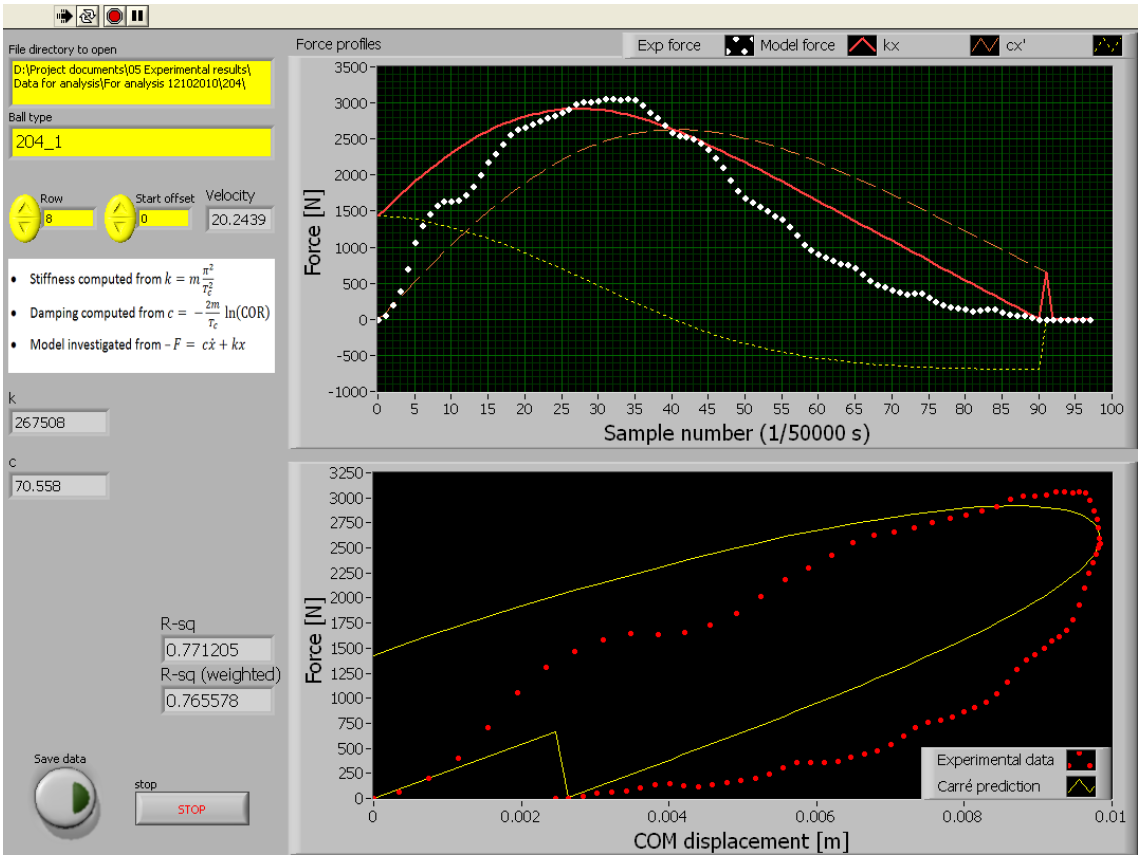

Figure 3.14: Graphical user interface for computing Model 1

3.4.2 Model 2

The second mathematical model had the same equation of motion, but differed in two respects. Firstly, this model was wholly phenomenologically developed: the values of stiffness coefficient *k* and damping coefficient *c* were arbitrarily varied such that the model prediction matched the experimental data. Secondly, a non-linear damper was employed, where the damping coefficient *c* was a function of the contact area and a model parameter *q*. The consideration of damping coefficient as a function of contact area was discussed previously in Section 2.3.1. Given the observed geometrical relationship between COM displacement and contact area, the equation for the damping coefficient was resolved in terms of ball diameter and COM displacement.

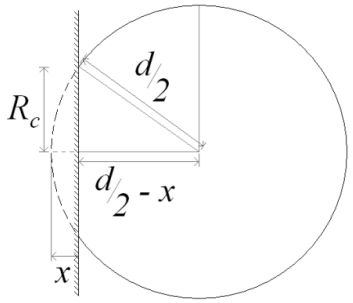

$$c = function\{\pi R_c^2\}$$

$$= function\left\{\pi\left(\left(d/2\right)^2 - \left(d/2 - x\right)^2\right)\right\}$$

$$= q(d - x)x \qquad (2.22)$$

Figure 3.15: COM displacement and contact area geometrical relation

where q is a model damping parameter, d is the ball diameter and x is the COM displacement. The computation of this model involved two steps of programming. The first program used a nested-loop algorithm to determine the values of the parameters k and q for the data from each impact test. This algorithm involved a loop-in-a-loop iterative calculation. The parameters k and q were specified initial values by the user. These values were passed into the loops, where the internal loop iteratively computed the model for a range of the values of q and the first value of k. The nearest curve-fit value of q for the given value of k was determined from the minimum absolute difference between the model predictions and the experimental force. The external loop then incremented the value of k and the internal loop ran again to fit the best fit value of q. This loop-in-loop algorithm continued for until the specified range of k and q were computed. This was a relatively quick process, typically computing 160 thousand iterations in under two seconds. The model predictions for each value of k (with the value of q already fitted) were compared to the experimental force, where the best fit as determined from R-square value was prioritised to the first 80% of the contact time. The focus on fitting to the first 80% of the impact data was to enable the model prediction to match the experiment data for the compressive phase for each respective impact as closely as possible.

The values of k and q for each impact, as individually calculated by nested-loop algorithm, were compiled for the full range of experimental impact data for each ball type. A power trend was fitted to the parameters k and q to express them as functions of

impact speed. Based on the equations of these power trends, a second program was used to calculate the more universal model for each respective ball type.

3.4.3 Model 3

The third mathematical model, consisted of a Kelvin-Voigt configuration with a non-linear spring and a non-linear damper. This model involved the spring power α, which was adjusted to give the best curve-fit to the data. The parameters k and q were determined using a similar nested-loop algorithm as described in Section 3.4.2.

The computation of the model for data from impact test yielded values of k, α and q. A single value of α was selected and power trends were fitted to k and q with respect to impact speed for each ball type. This procedure was consistent with the methods employed by Carré *et al.*, who calculated a universal model of a cricket ball based on a single value of α and trends of k and q with respect to speed [16]. In this work, power trends were found to have a better fit for k and q with respect to speed, while exponential trends had been used by Carré *et al.*

The value of α and the power functions of k and q were used by the second program to calculate the more universal model for each ball type.

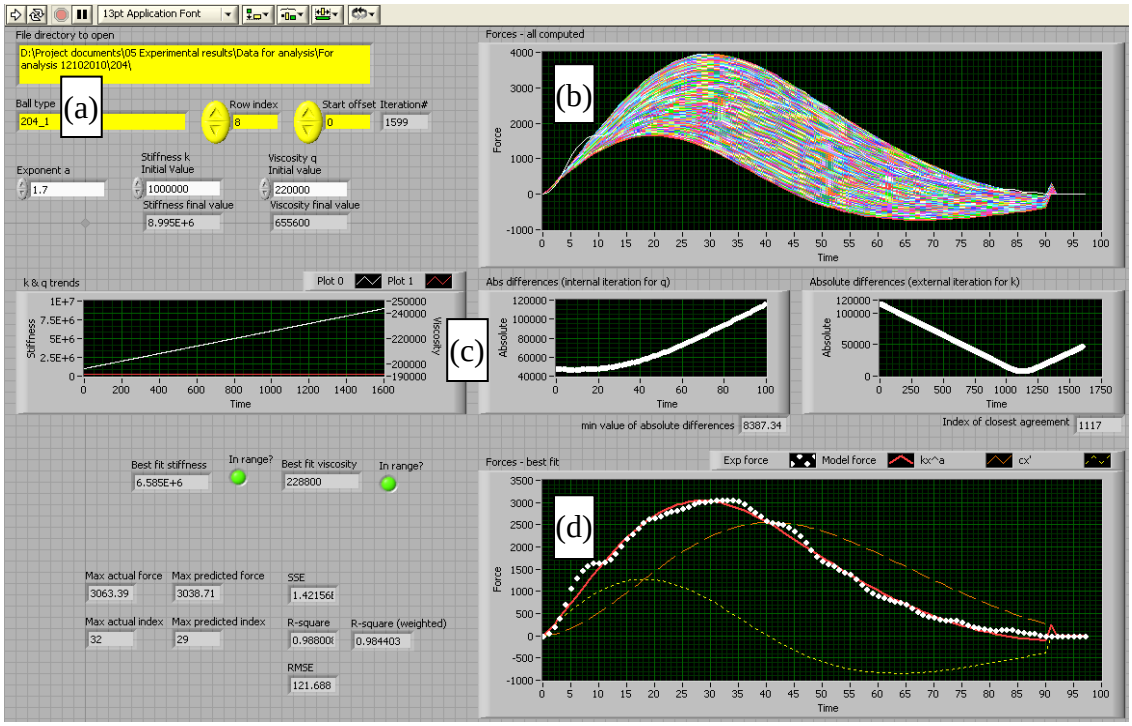

Figure 3.16: Graphical user interface for parametric evaluation of Model 2 and Model 3 (a) experimental data inputs, (b) nested-loop results, (c) model parameters (d) model components contribution

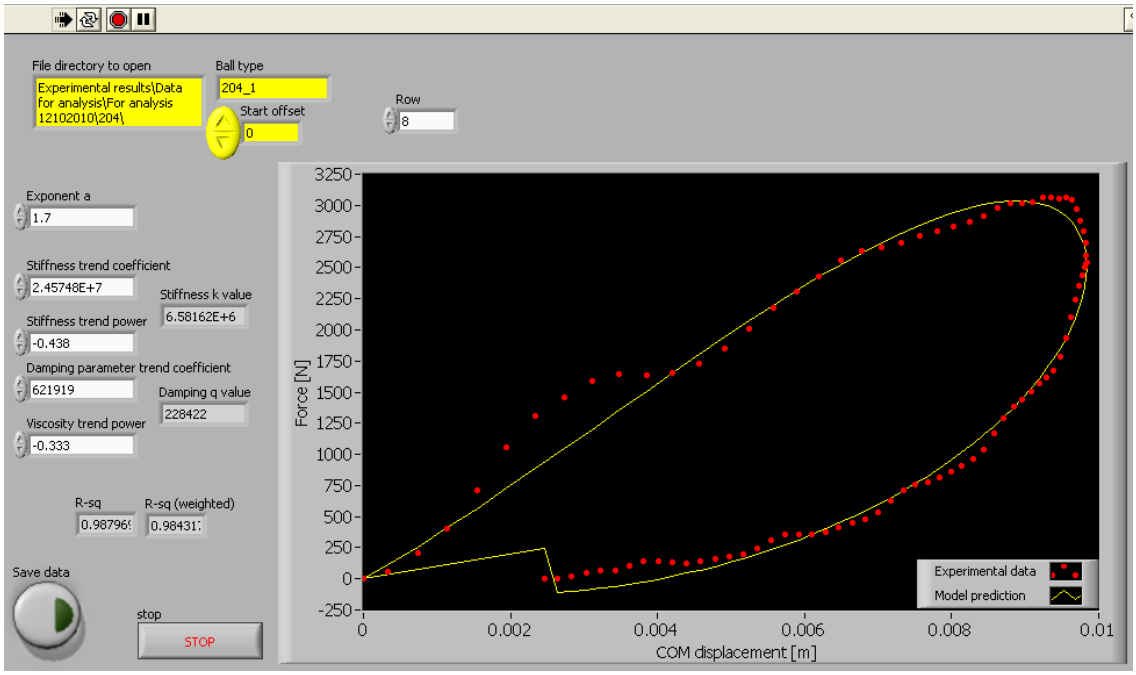

Figure 3.17: Graphical user interface for computing Model 2 and Model 3

Chapter 4: Experimental results

4.1 Performance results

4.1.1 Coefficient of restitution results

The coefficient of restitution (COR) values with respect to impact velocity for the approved sliotar cores are displayed in Figure 4.1. Second-order polynomial trend lines were found to have a reasonably good fit to the data ($R^2 > 0.96$ for majority of balls). Considering each ball category as a whole, the traditional ball types (cork cores) exhibited a greater COR (i.e. less energy dissipation) than the modern ball types (polymer cores). The modern ball types displayed a wider span of COR compared to the traditional ball types.

The intra-ball-type variation, the deviation in COR between samples within a single ball type, was gauged from the R-squared values of the trend lines. Four of the modern ball types, 259, 268, 272 and 257, exhibited a significant intra-ball-type variation as evident from R-square values of 0.9 or less in Figures 4.1. The COR data for each individual sample of these ball types along with ball type 204, is shown in Figure 4.2. To investigate whether the variation between samples shown in Figure 4.2 could be attributed to mass discrepancies, the coefficient of restitution values were mass-normalised as shown in Figure 4.3. Judging by the change of the trend lines' R^2 values (Figure 4.4 relative to Figure 4.1), mass-normalisation was seen to reduce the intra-ball-type variation for ball types 268 and 272, while having an adverse effect on ball types 259 and 257.

The COR of the selected sliotar cores are displayed in Figure 4.4. The traditional cork-based ball types 206 and 217 were seen to exhibit a greater non-linearity with respect to velocity, as evident from the curvature of the trend lines. The modern polymer ball types 204 and 268 exhibited an almost linear trend with respect to velocity.

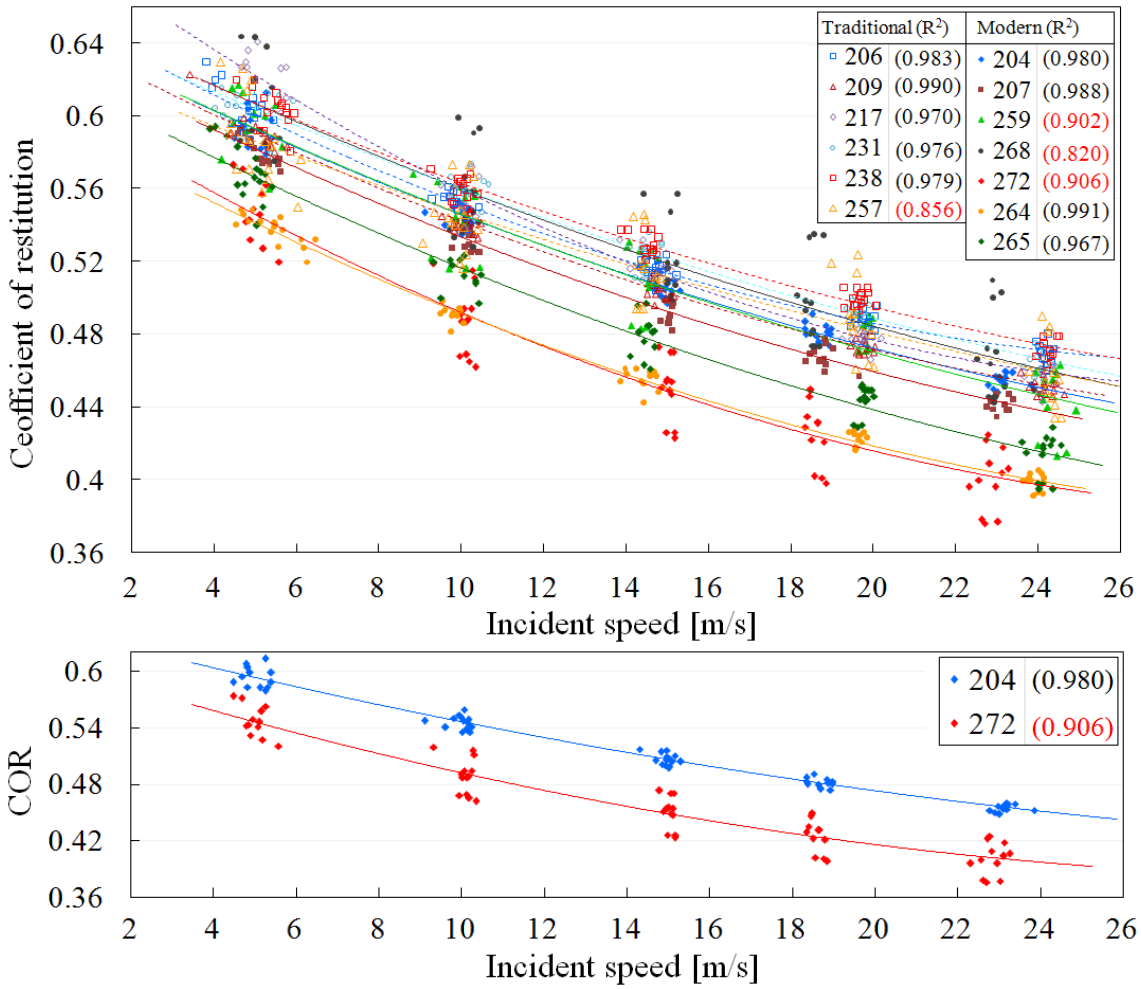

Figure 4.1: Coefficient of restitution values of (a) all approved sliotar cores and (b) detail on sliotar types 204 and 272

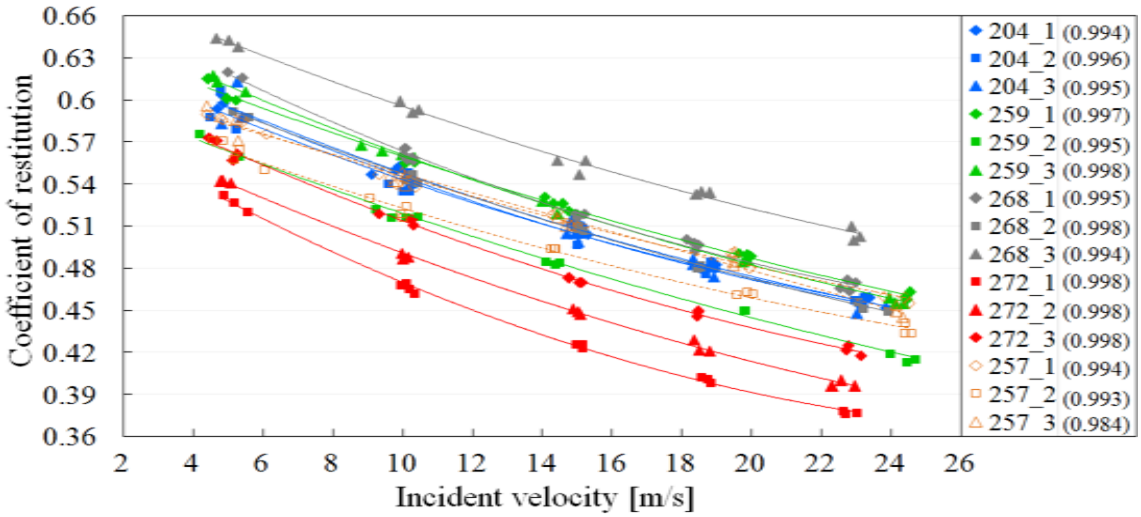

Figure 4.2: COR of individual ball types that exhibited intra-ball-type variation

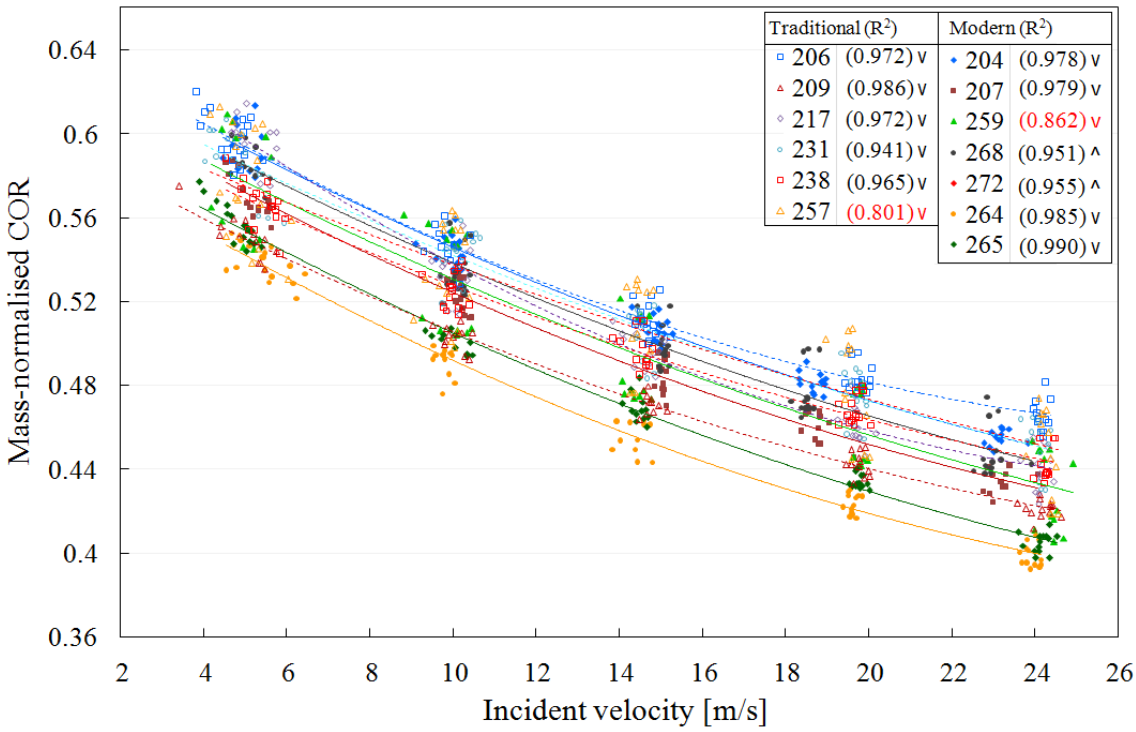

Figure 4.3: Mass-normalised COR of all approved sliotar cores

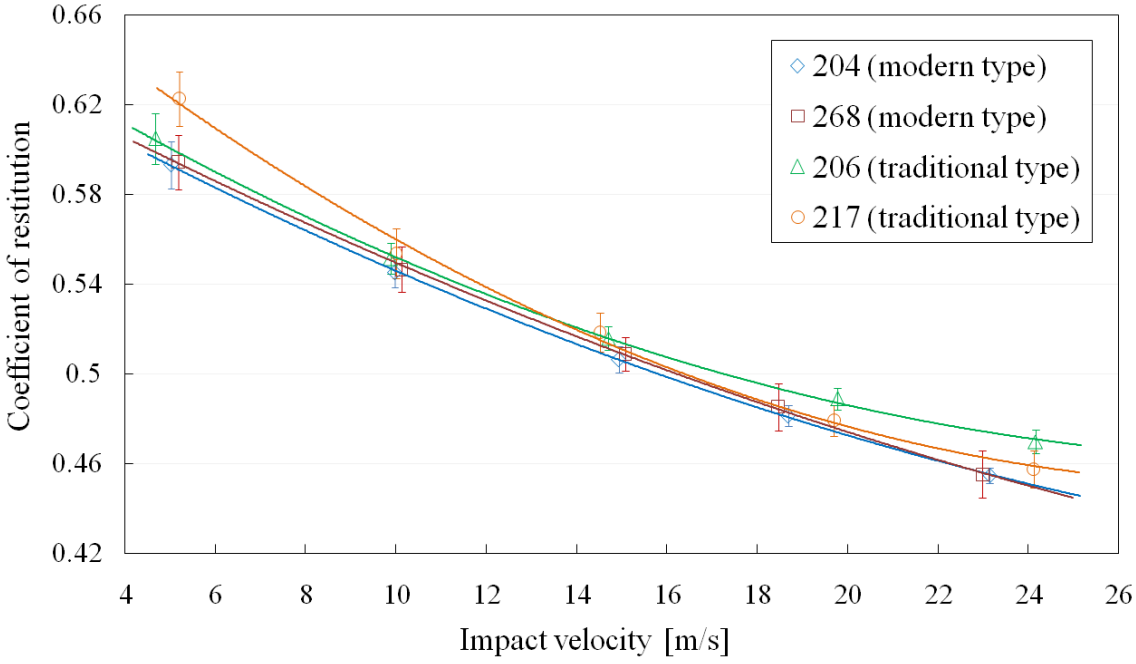

Figure 4.4: Coefficient of restitution of selected four sliotar cores 204, 268, 206 and 217

4.1.2 Force-time results

Force-time data from the impact was verified by comparing the impulse (area under force-time curve) to the differential momentum (measured from high-speed footage) [see Appendix B]. These values agreed within 3% for all impacts, validating the calibration of the force data acquisition.

The peak force for approved sliotar cores is shown in Figure 4.5. The peak force was found to increase linearly for all ball types. The deviation between the ball type categories became more pronounced with increasing velocities, with traditional ball types predominantly exhibiting higher peak forces than the modern ball types.

The four selected sliotar cores exhibited distinct force-time profiles. Examples of these profiles for three impact velocities are shown in Figure 4.6. The fluctuations in ball type 204, seen in Figure 4.6 (a), correspond to surface waves evident in high-speed footage. Ball types 268 and 206 tended to exhibit smoother force profiles. Double peaks with a central trough were evident in ball type 217 in Figure 4.6 (d). This was particularly apparent at higher velocity impacts, where the distinct layers of this ball type's construction engaged in the impact at various extents. The double peak observation was consistent with other studies of multi-compositional ball constructions [50, 93].

The peak forces of the four selected sliotar cores are shown in Figure 4.7. The distinction between the modern and traditional ball types is more apparent here, with the traditional ball types exhibiting higher peak forces for all impact velocities.

The contact times for the four selected sliotar cores were measured from the width of the force profile. These values, based on the force dropping below a threshold of 50N at the end of impact, are shown in Figure 4.8.

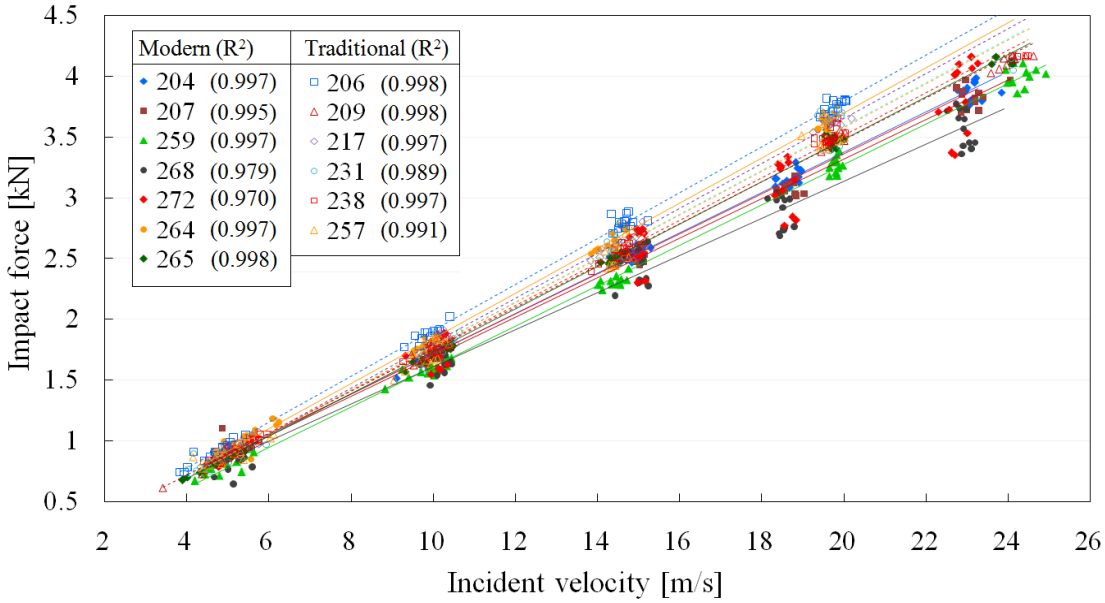

Figure 4.5: Peak forces for all approved sliotar cores

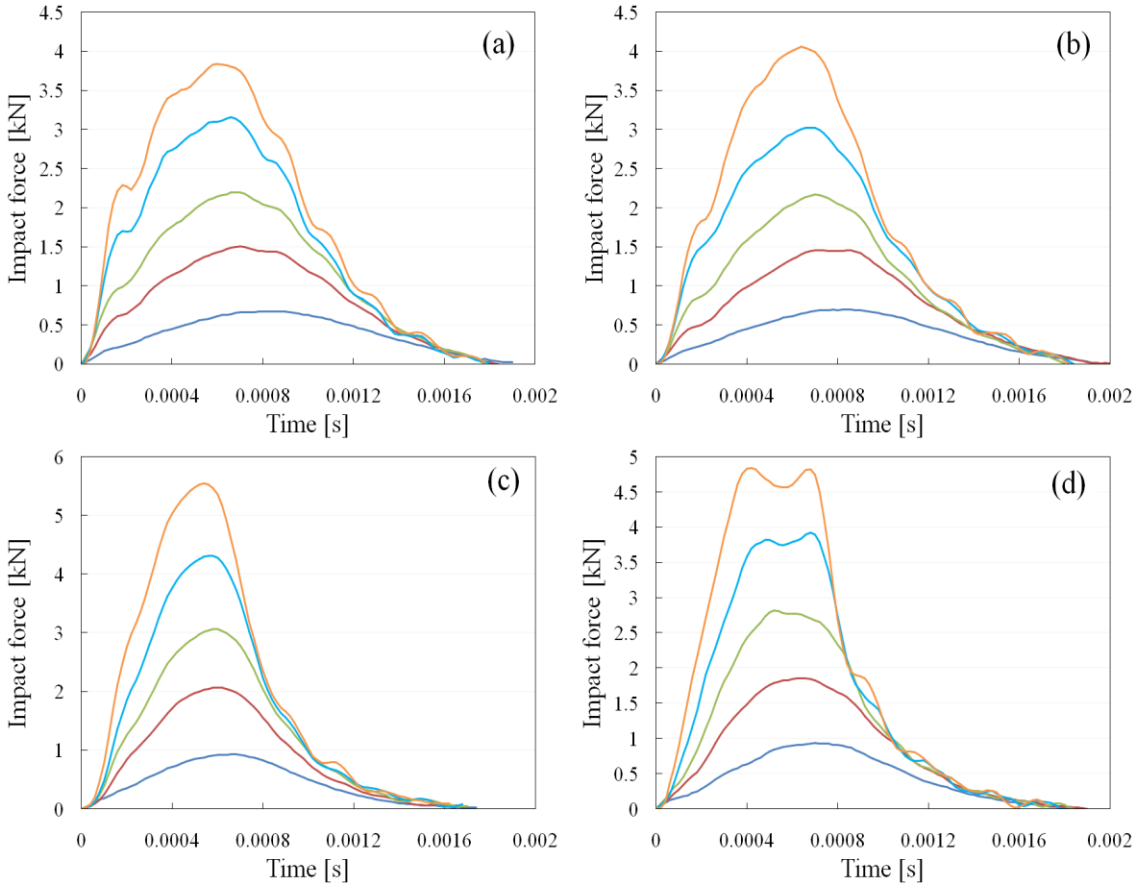

Figure 4.6: Typical force-time profiles for 5, 10, 15, 20 and 25 m/s impacts for sliotar core types (a) 204, (b) 268, (c) 206 and (d) 217

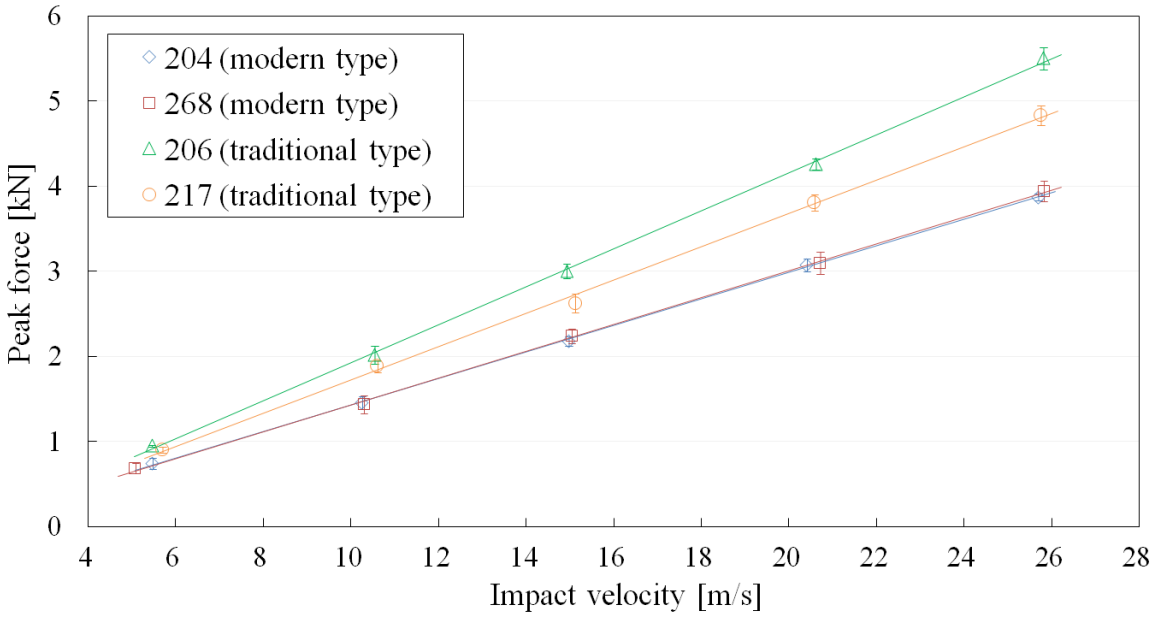

Figure 4.7: Peak forces for the sliotar core types 204, 268, 206 and 217

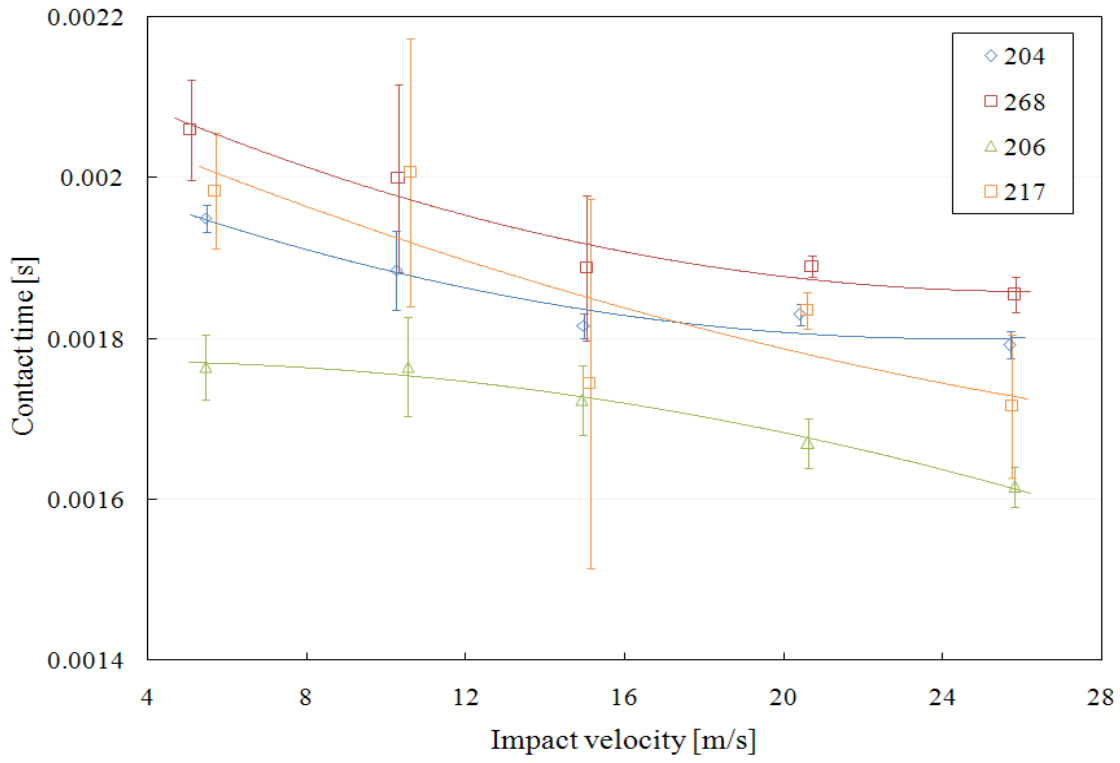

Figure 4.8: Contact times (width of force profile) for the sliotar core types 204, 268, 206 and 217

4.1.3 Deformation results

The deformation of the approved sliotar cores in terms of percentage reduction of diameter compression is displayed in Figure 4.9. The maximum diameter compression appeared to increase almost linearly with respect to velocity, with a 2nd order polynomial trend line having a slightly better agreement. A difference in behaviour between the ball type categories is evident, with modern ball types spanning a wider range of maximum deformations.

A deviation between the diameter compression measurements and COM displacement measurements was observed in some sliotar cores at increased velocities. The disparity between diameter compression and COM displacement is shown for ball type 204 in Figure 4.10. The deviation between the two deformation measures implied that the diameter compression and COM displacement were different for each ball type. The maximum diameter compression, maximum COM displacement and maximum lateral expansion are displayed for approved polymer core 204, approved cork core 206, compliant polymer ball 180 and a cricket ball in Figure 4.11. It can be seen that the extent of deviation between diameter compression and COM displacement is linked to the magnitude of lateral expansion.

The relationship between diameter compression and lateral expansion, in terms of maximum normal and tangential compression ratio values, for the ball types is displayed in Figure 4.12. The relationship between the normal and tangential compression ratio was almost linear, as evident from the linear trends for each ball type. The slope of the linear trend gave an indication of the extent of lateral expansion. Steeper slopes (larger gradient) indicated that diameter compression was more dominant than lateral expansion in the deformation of a given ball type. The slope gradients were 6.4 for ball type 204, 14.5 for ball type 206, 3.43 for ball type 180, and 15.29 for the cricket ball.

The difference between diameter compression and COM displacement was investigated further by visual analysis (Adobe Photoshop CS2) of the high-speed footage, as shown in Figure 4.13. The blue outline indicates the ball's circumference at the instant of first contact, while the yellow outline is offset from this by the experimentally measured COM displacement value for this impact.

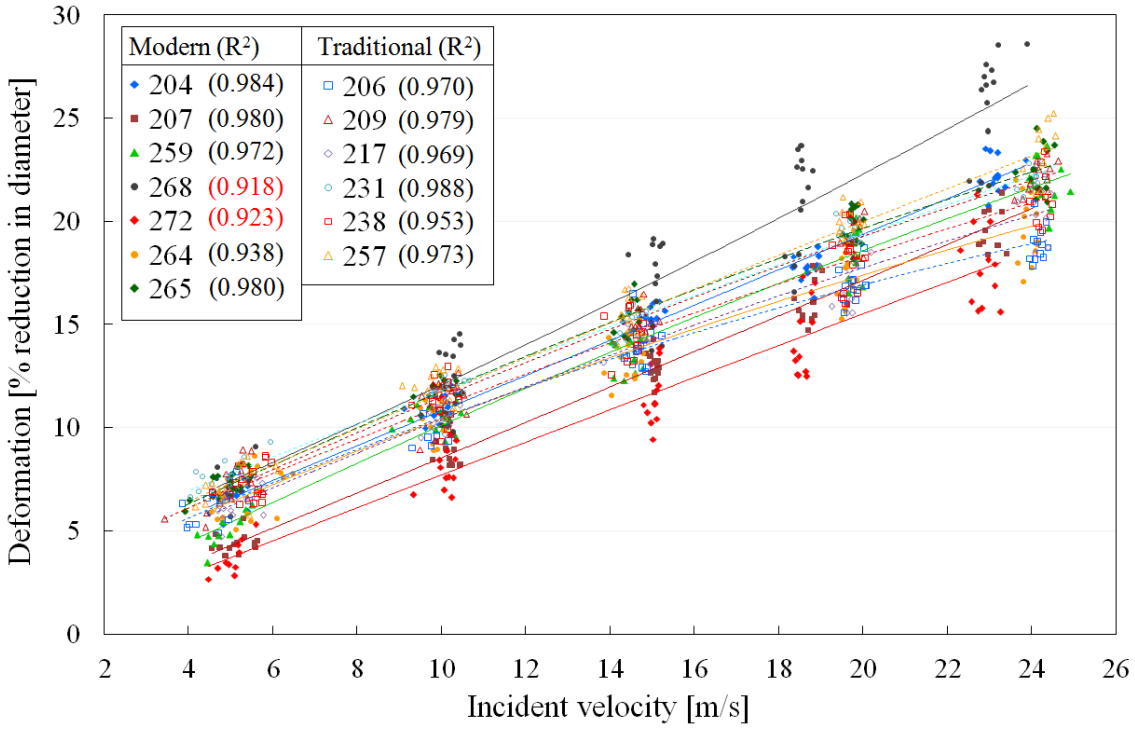

Figure 4.9: Maximum diameter compression of all approved sliotar cores

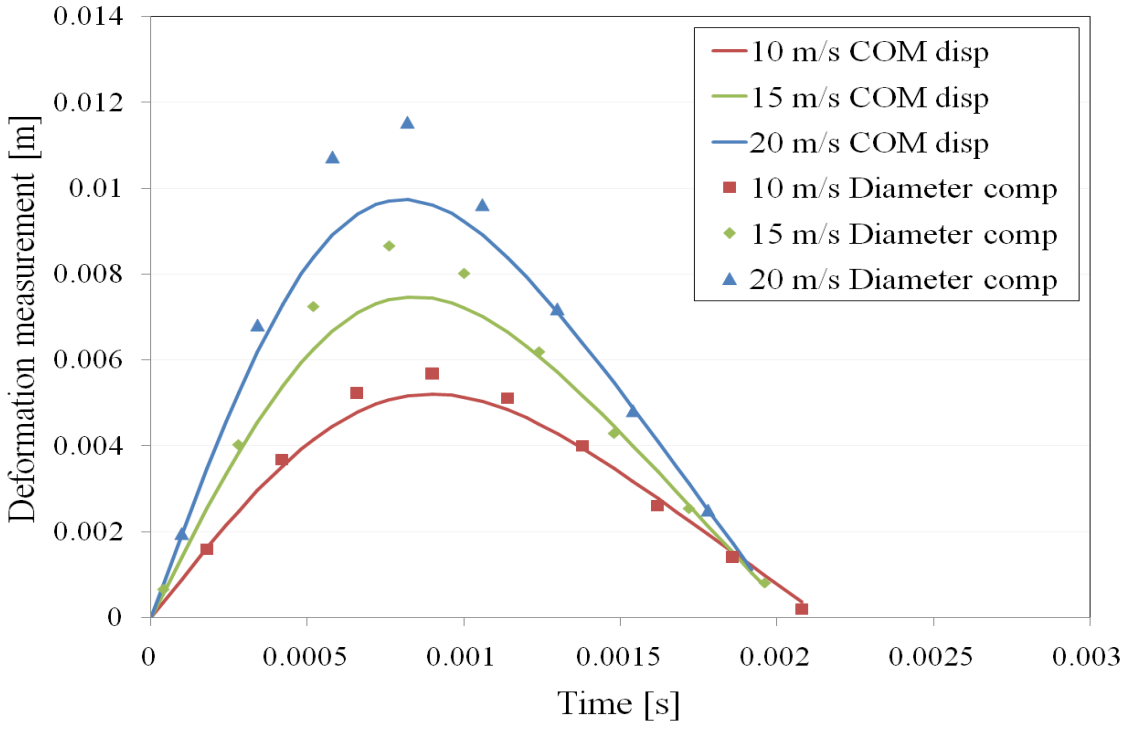

Figure 4.10: COM displacement and diameter compression profiles for ball type 204

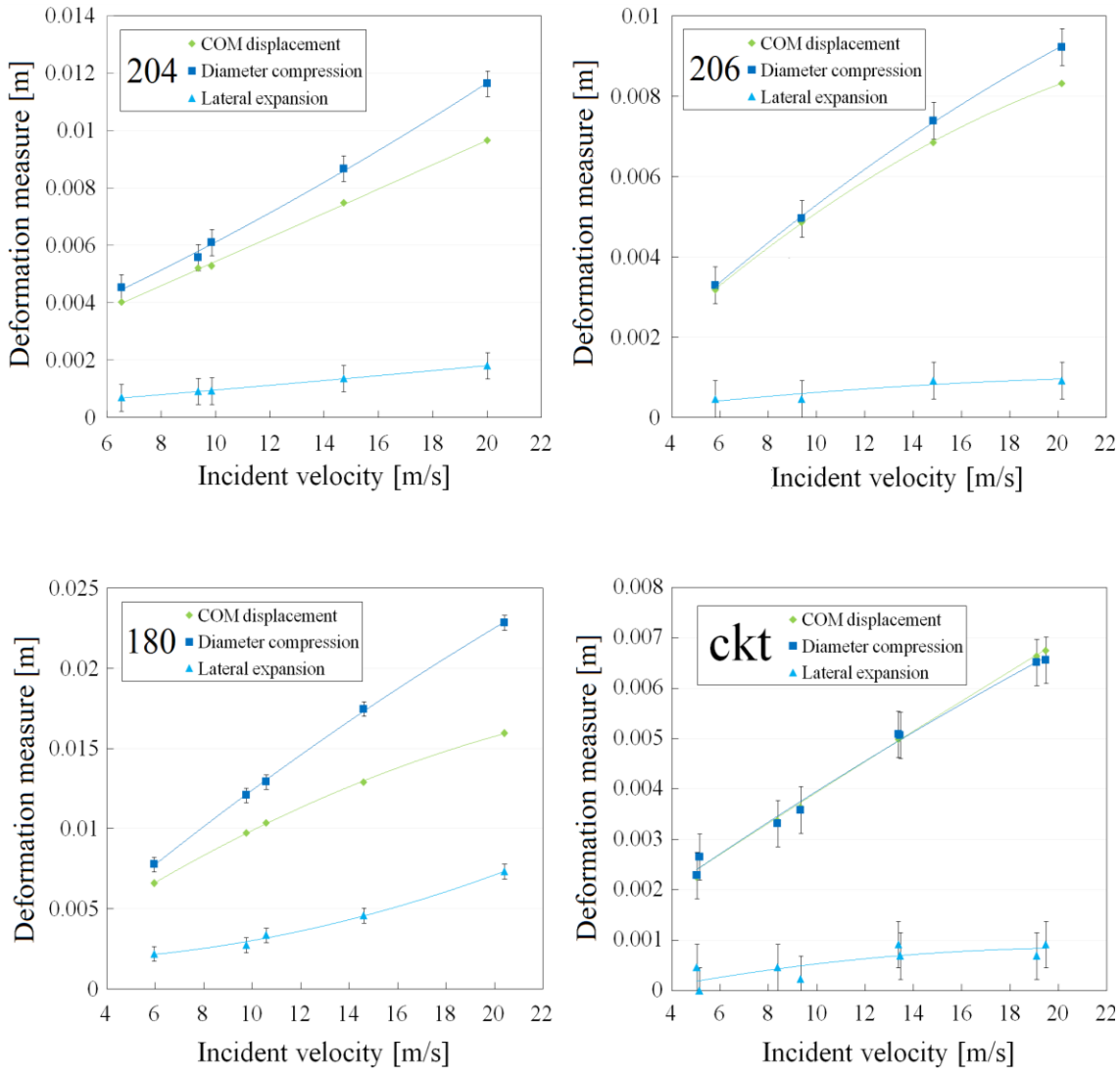

Figure 4.11: Maximum diameter compression, maximum COM displacement and maximum lateral expansion of ball types (a) 204, (b) 206, (c) 180 and (d) cricket ball

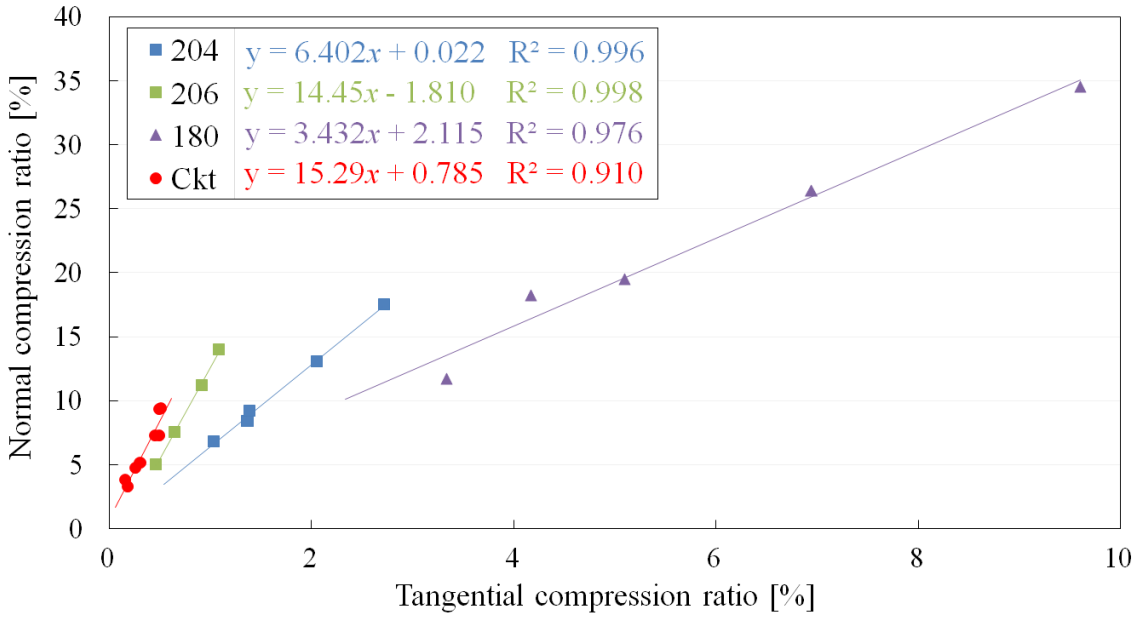

Figure 4.12: Normal and tangential compression ratios for ball types 204, 206, 180, and cricket ball

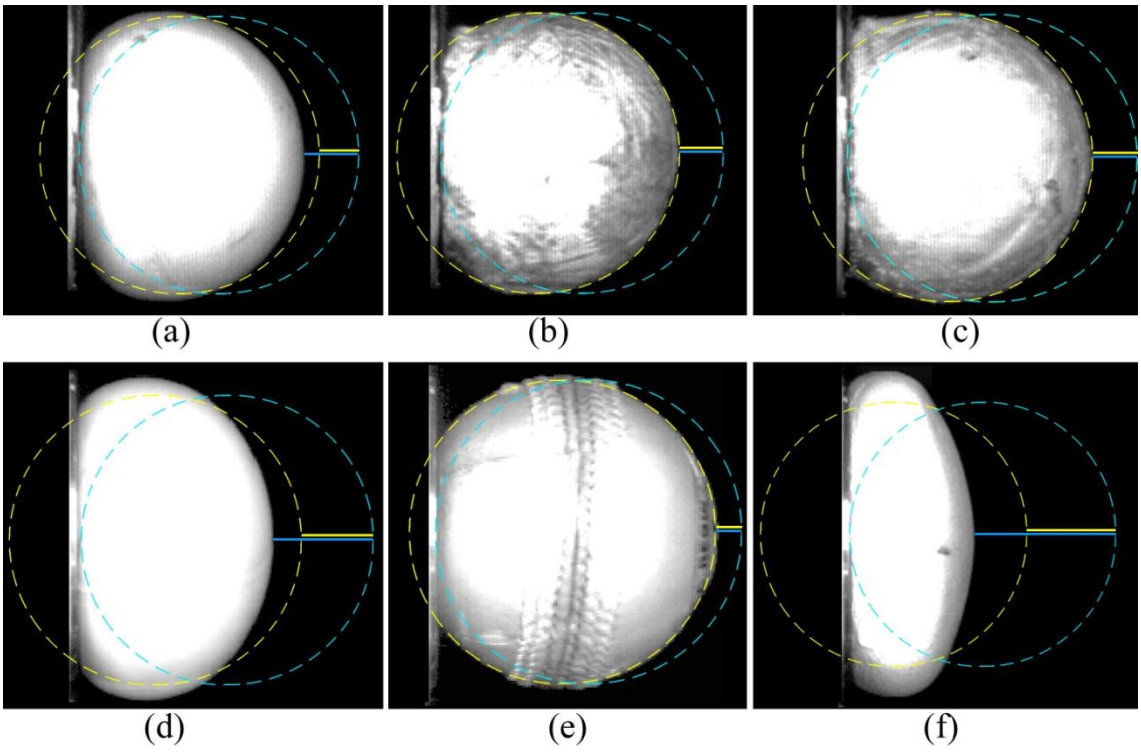

Figure 4.13: High speed images of maximally deformed balls at 25 m/s impact (a) 204, (b) 206, (c) 217, (d) 180, (e) cricket ball and (d) PNG rubber ball. Blue lines indicate diameter compression values, yellow lines indicate COM displacement.

4.1.4 Viscoelastic results

The results from one sample of each of the four selected sliotar cores (polymer types 204 and 268, traditional cork-based types 206 and 217) are presented in the following section. The basis for the selection of one sample of each ball type was to allow the comparison of independent characteristics, such as directly comparing quasi-static to dynamic response, without being misled by averaging across the variations exhibited within individual ball types.

Quasi-static viscoelastic results

The quasi-static three-cycle compression force-displacement curves for ball types 204 and 217 at a compression-rate of 3 mm/s are shown in Figure 4.14. For all compression tests, the subsequent cycles followed a consistent loading (compression) profile that was slightly offset from the first cycle compression profile. This was attributed to the residual strain from the first compression in each test. All three cycles followed a similar unloading profile.

For clear comparison of the effect of compression-rate, the first cycle force-displacement curves for each compression test are shown in Figure 4.15. The polymer ball types 204 and 268 did not exhibit a significant dependence on quasi-static compression-rate. The effect of compression-rate on traditional ball types 206 and 217 was more apparent, though relatively small given the 6x increase in compression-rate.

The averaged stiffness for each compression-rate is shown in Figure 4.16. The small error bars indicate a relatively small difference in stiffness between the three cycles. The stiffness was observed to increase slightly with increasing compression-rate, although this trend was more erratic in the traditional ball types. The averaged hysteresis from the subsequent cycles, as shown in Figure 4.18, was less than the hysteresis measured from the first cycle, as shown in Figure 4.17. The polymer ball types exhibited a marginal increase in hysteresis with increasing compression rate for all cycles. The traditional ball types exhibited a smaller increase in hysteresis for the subsequent cycles, with erratic values obtained from the first cycle hysteresis.

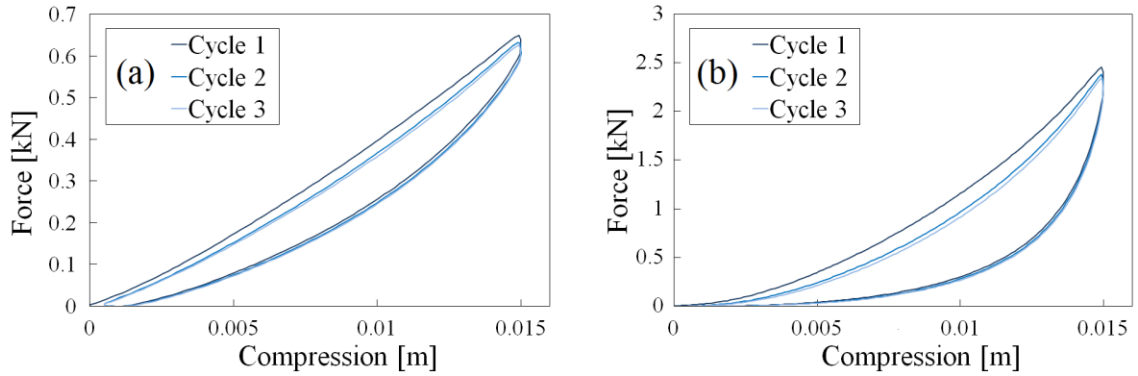

Figure 4.14: Hysteresis loops for three-cycle 3 mm/s compression test for ball types (a) 204 and (b) 217

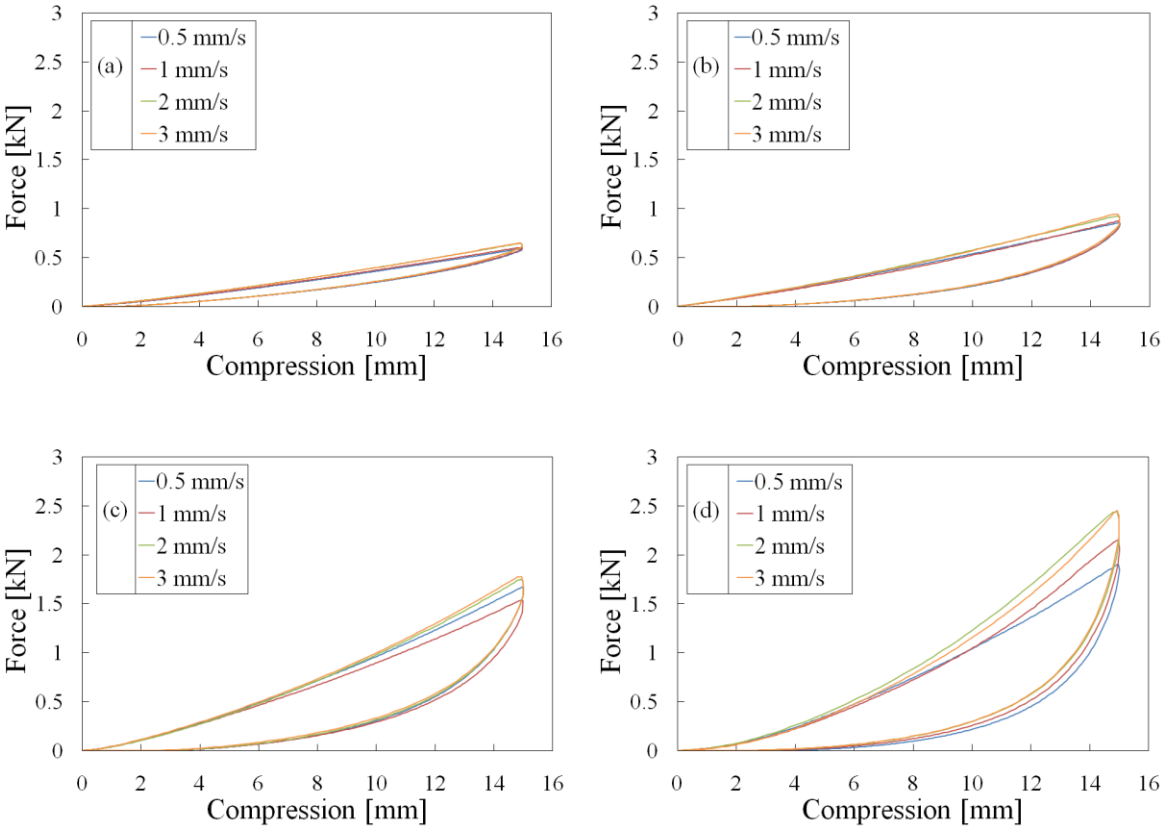

Figure 4.15: Hysteresis loops (showing first cycle only) for ball types (a) 204, (b) 268, (c) 206 and (d) 217

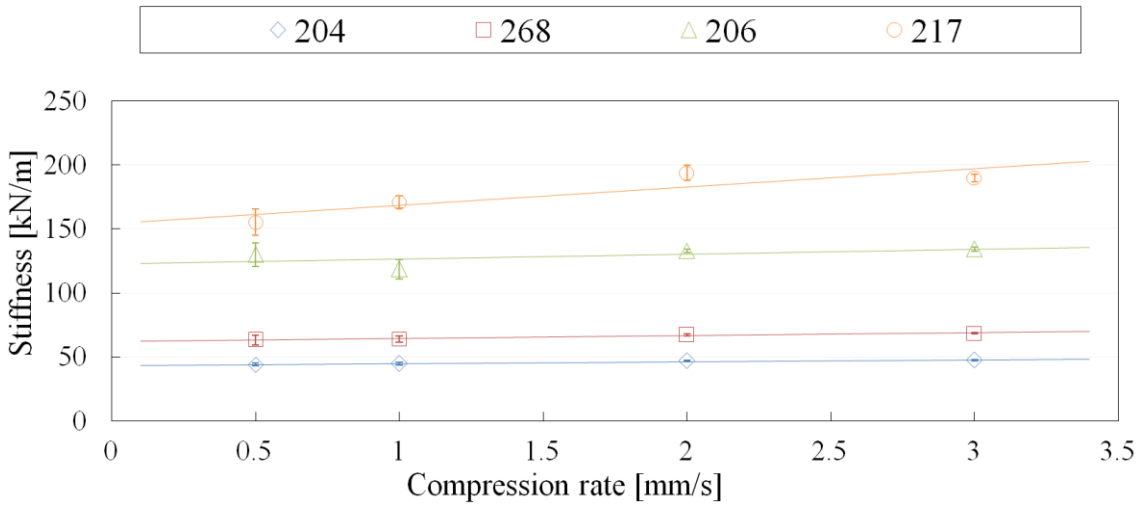

Figure 4.16: Quasi-static stiffness for selected four sliotar core types

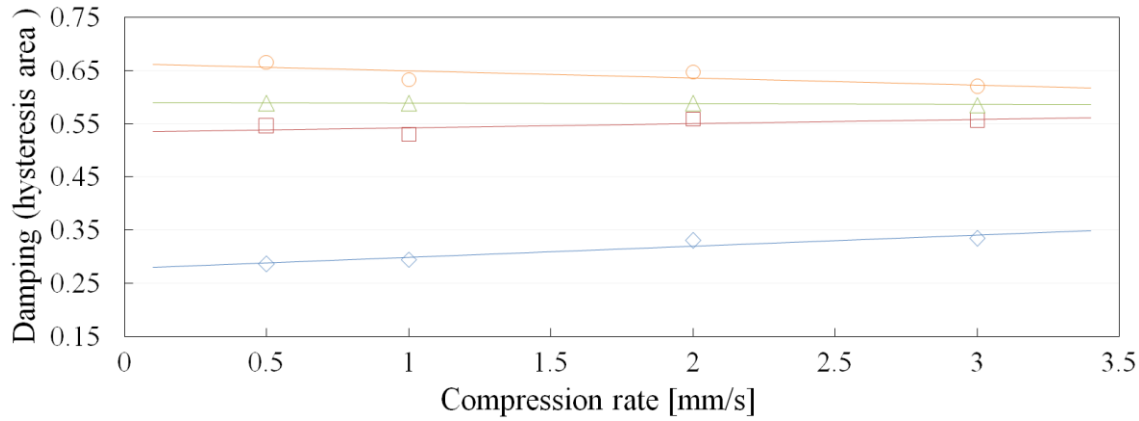

Figure 4.17: Quasi-static hysteresis for first cycle for selected four sliotar core types

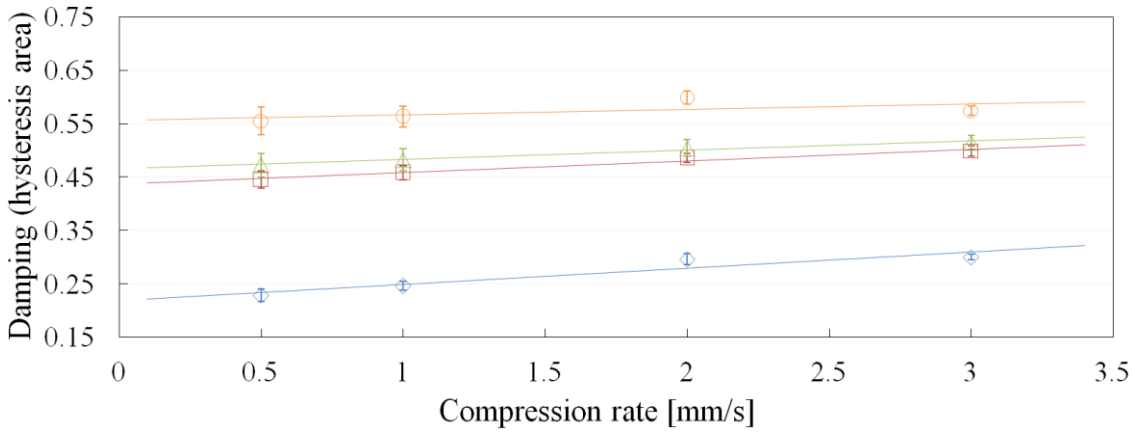

Figure 4.18: Quasi-static averaged hysteresis for subsequent cycles for selected four sliotar core types

Dynamic viscoelastic results

The dynamic force-displacement curves, compiled using both COM displacement and diameter compression, are shown in Figure 4.19. The COM displacement was found to be the most valid for compiling force-displacement graphs due to the graph areas under both the compression and restitution phases agreeing with the incident and rebound kinetic energies, respectively, as shown in Figure 4.20.

Typical force-displacement curves for the four selected sliotar cores are displayed in Figure 4.21. The non-linearity of the compression phase of these curves was approximated by two measures of linear stiffness, namely initial stiffness and bulk stiffness. The evaluation of the initial and bulk stiffness values is illustrated in Figure 4.22, where they accounted for the observed change in gradient of the force-displacement curves that occurred between 20 and 30% of maximum deformation for all ball types. A good R-squared correlation of at least 0.98 was found between the experimental data and the linear trends of both initial stiffness and bulk stiffness. This was seen to reduce to between 0.94 and 0.96 in the presence of wave propagation fluctuations, which were particularly pronounced in ball type 204.

The initial and bulk stiffness values, along with values computed from the two theoretical equations mentioned in Section 3.1.3, were plotted in Figure 4.23. For ball types 204, 268 and to an extent 206, the initial stiffness exceeded the bulk stiffness, with discrepancy diverging with increasing velocities. Conversely for ball type 217, the initial stiffness was less than the bulk stiffness for all impact velocities. Equation 3.2 agreed reasonably well with the bulk stiffness of polymer ball type 204 up to 20 m/s, but underestimated the bulk stiffness for ball types 268, 206 and 217 by 10%, up to 46% and up to 54%, respectively. For the polymer ball types (204 and 268), the results of Equation 3.3 were within the region of the bulk stiffness values, although underestimating the magnitude by approximately 10 %. For ball type 206, the magnitude discrepancy between the equation result and bulk stiffness was less satisfactory at up to 15 %. There was no reasonable association between the equation computation and either experimentally-measured value of stiffness for ball type 217, with significant diverging deviation of 20 to 35 % observed between bulk stiffness and the equation.

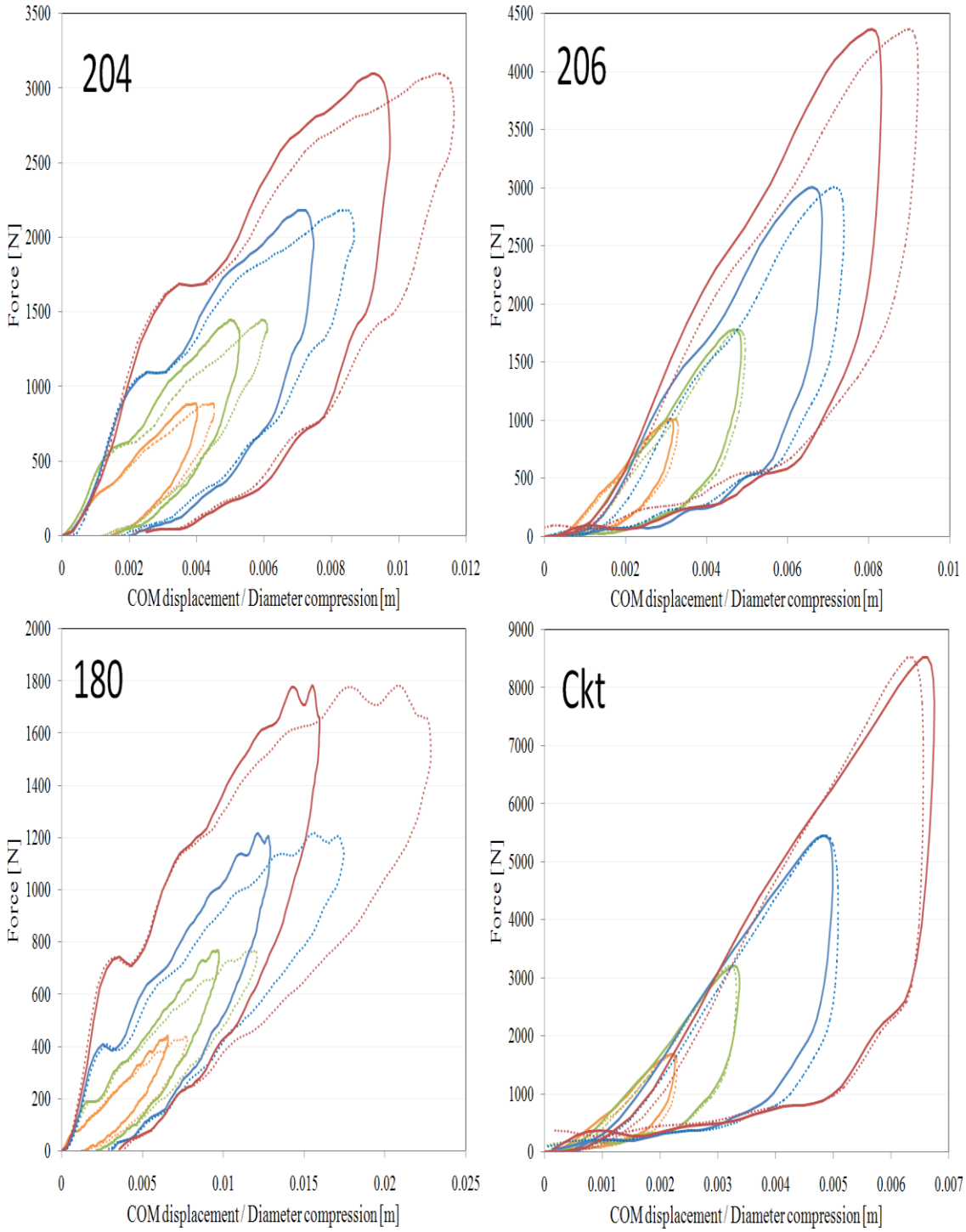

Figure 4.19: Force-displacement curves[5] for ball types (a) 204, (b) 206, (c) 180, (d) CKT

[5] Solid lines represent COM displacement values, dotted lines represent diameter compression values

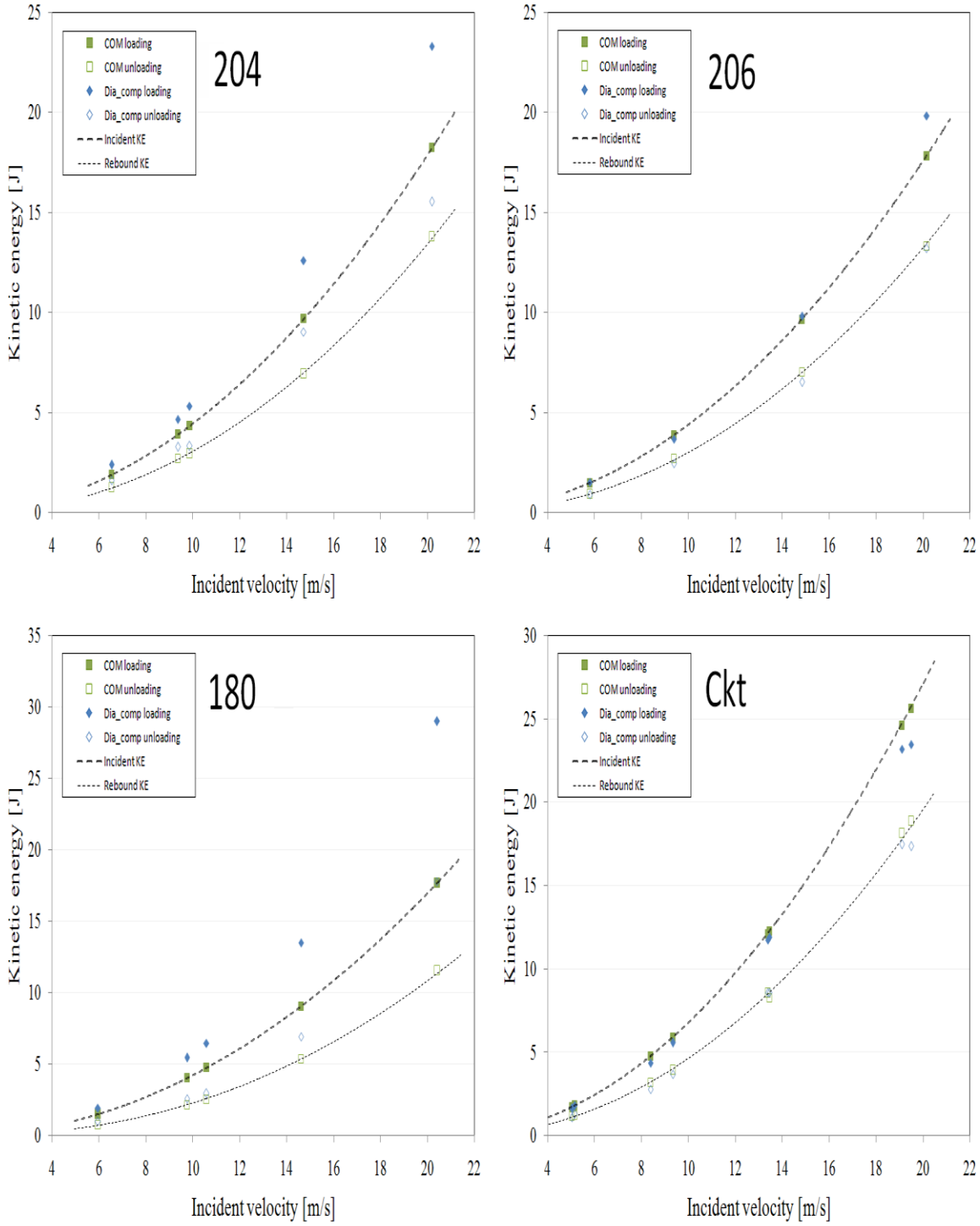

Figure 4.20: Hysteresis loop validity investigation (loading area & initial KE, damping area & dynamic energy loss) for ball types (a) 204, (b) 206, (c) 180, (d) cricket ball

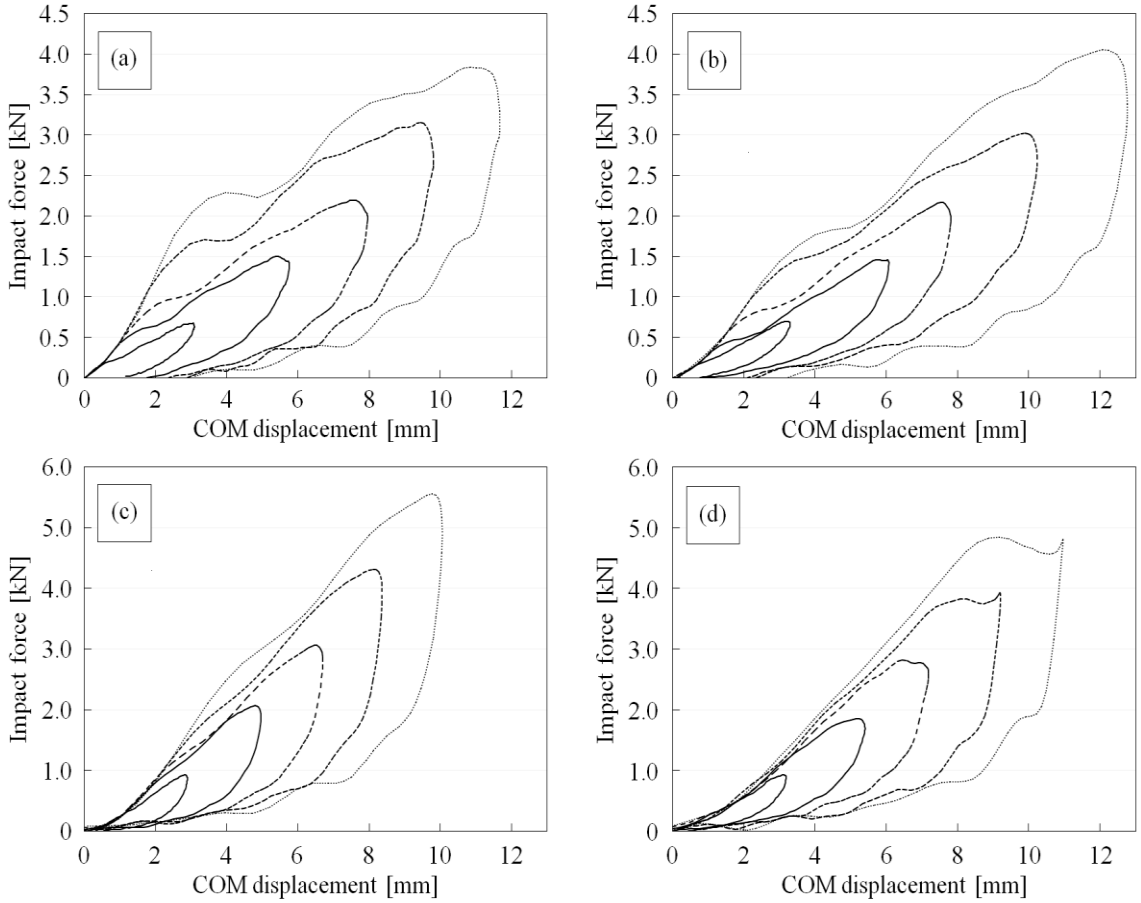

Figure 4.21: Typical force-COM displacement curves for 5, 10, 15, 20 and 25 m/s impacts for ball types (a) 204, (b) 268, (c) 206 and (d) 217

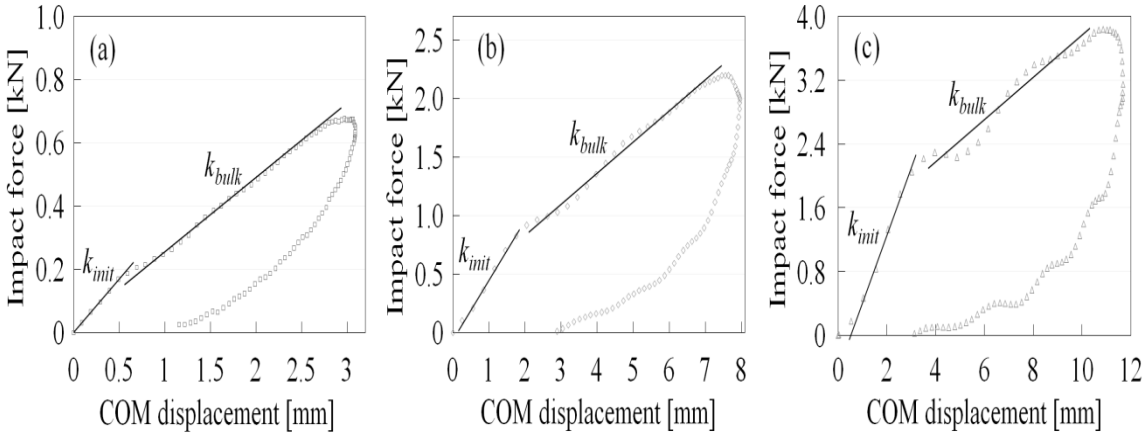

Figure 4.22: Evaluation of initial stiffness and bulk stiffness for ball type 204 for impact velocities of (a) 5 m/s, (b) 15 m/s and (c) 25 m/s

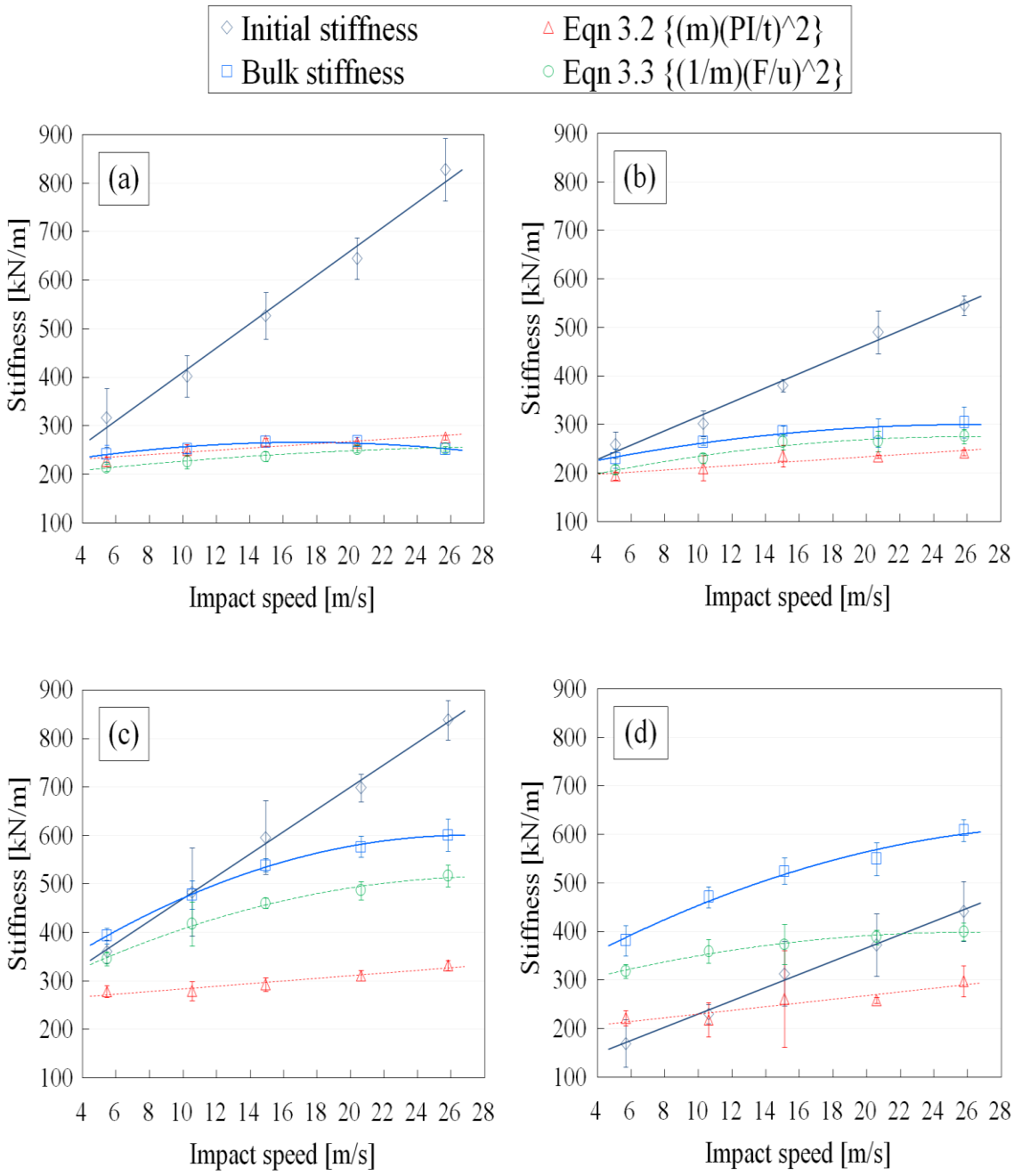

Figure 4.23: Dynamic stiffness values derived from experimentation (initial and bulk) and equations (Eqn 3.2 and Eqn 3.3) for ball types (a) 204, (b) 268, (c) 206, (d) 217

4.2 Prototype production results

4.2.1 Screening experimental results

In trials to produce a ball with acceptable part quality, a number of issues were encountered. Surface eruptions, as seen in Figure 4.24, occurred due to insufficient cooling time, excessive blowing agent activity, excessive barrel temperature or cavity over-packing. Incomplete fills, shown in Figure 4.25, occurred from inadequate shot size or insufficient blowing agent. Low mould temperatures (< 15 °C) produced warpage from shock cooling, while higher mould temperatures (> 20 °C) resulted in balls being more malleable when removed from mould, resulting in loss of shape as they cooled (see Figure 4.26). Material degradation, as shown in Figure 4.27, was a result of long resident times of the material in the heated barrel. Material degradation in the form of moisture contamination was also an issue, resulting in a crumbly moulded part as shown in Figure 4.28. Flow markings, the dark lines evident in Figure 4.26, were present in all moulded balls. These posed an intermittent issue where cracks sometimes developed in a cooling ball along flow lines, as seen in Figure 4.29. Cold slugs, those being discrete solid inclusions in the ball surface shown in Figure 4.30, were eliminated by the fitting of the shut-off nozzle to the barrel. Non-uniform mixing resulted in internal voids and uneven material distribution as shown in Figure 4.31 and 4.32, respectively. Excessive nucleating agent inhibited the action of the blowing agent, resulting in shrunken balls as seen in Figure 4.33. A large void consistently occurred in the moulding of the 80A TPU polymer grade, as shown in Figure 4.34. The amount of blowing agent required to fill this void necessitated in an unfeasibly long cooling time (> 10 min), resulting in material degradation and wastage.

From the screening trial of experiments, it was concluded that mould temperature needed to be kept constant due to its strong influence on ball shape. The 80A polymer grade could not be consistently moulded, indicating that this grade of material was incompatible for this application. The nucleating agent addition rate was limited to 5% and 10% for polymer grades 55A and 70A, respectively, to allow full expansion of the ball geometry. A uniform material distribution was produced by using ground particles of blowing agent, shown in Figure 4.35, to achieve a more diffused mix and increased back pressure for better mixing during plasticising.

Figure 4.24: Surface eruption

Figure 4.25: Incomplete fills

Figure 4.26: Mould temperature distortion

Figure 4.27: Material degradation

Figure 4.28: Moisture contamination

Figure 4.29: Surface cracking

Figure 4.30: Cold slugs

Figure 4.31: Internal voids

Figure 4.32: Non-uniform mixing

Figure 4.33: Nucleating agent shrinkage

Figure 4.34: Settling void in 80A TPU

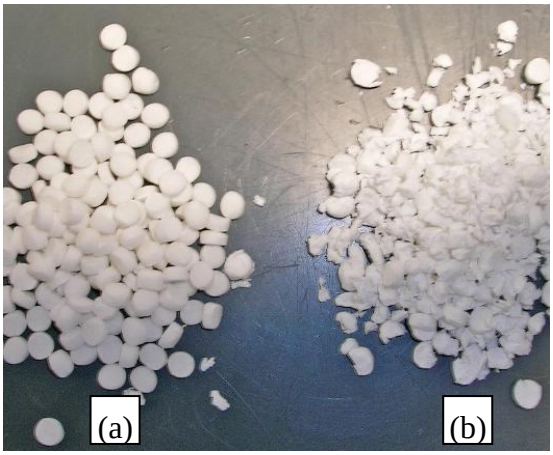

Figure 4.35: Blowing agent (a) as received (b) ground

4.2.2 Variant production

The screening set of experiments yielded six distinct ball type variants, as shown in Figure 4.36. These variants comprised of two TPU polymer grades with three levels of nucleating agent: 70A polymer grade with nucleating agent at 0, 5 and 10 %, and 55A polymer grade with nucleating agent at 0, 2.5 and 5 %.

The masses of the six variants are shown in Figure 4.37. The 70A polymer grades were slightly heavier than the target weight of 90g, where 70_a and 70_b were 2% overweight and 70_c was 4% overweight. The 55A polymer grades were slightly lighter than the target weight. A broader variation in mass between samples was observed in variants with added nucleating agent, with mass tending to increase with increasing nucleating agent quantities.

The coefficient of restitution values for the prototype variants are plotted in Figure 4.38, with approved sliotar core 204 plotted for reference purposes. The two polymer grades exhibited different trends with respect to velocity, with the 70A variants having a slightly more non-linear decrease with velocity. The 55A variants tended to exhibit marginally higher COR values than the 70A variants, though there was little significant difference between the polymer grades compared to the intra-ball-type scatter. The COR decreased with added nucleating agent. The differences between the variants were substantially less than the difference between the prototypes and approved sliotar core 204, where the variants' COR were almost 25% greater than the sliotar core.

The peak impact forces were found to increase linearly with velocity, as seen in Figure 4.39. There was a substantial difference between the 55A and 70A polymer grades with respect to force values. Ball with higher levels of nucleating agent were seen to exert slightly higher forces. The peak forces of the 70A grade occupied the region of forces exerted by approved sliotar ball 204.

The dynamic stiffness of the prototype variants was expressed in terms of initial stiffness and bulk stiffness in Figures 4.40 and 4.41 respectively. The 70A polymer grade was stiffer than the 55A, particularly with regard to the bulk stiffness. The stiffnesses of the 70A polymer grades were of a similar magnitude to the approved sliotar core 204.

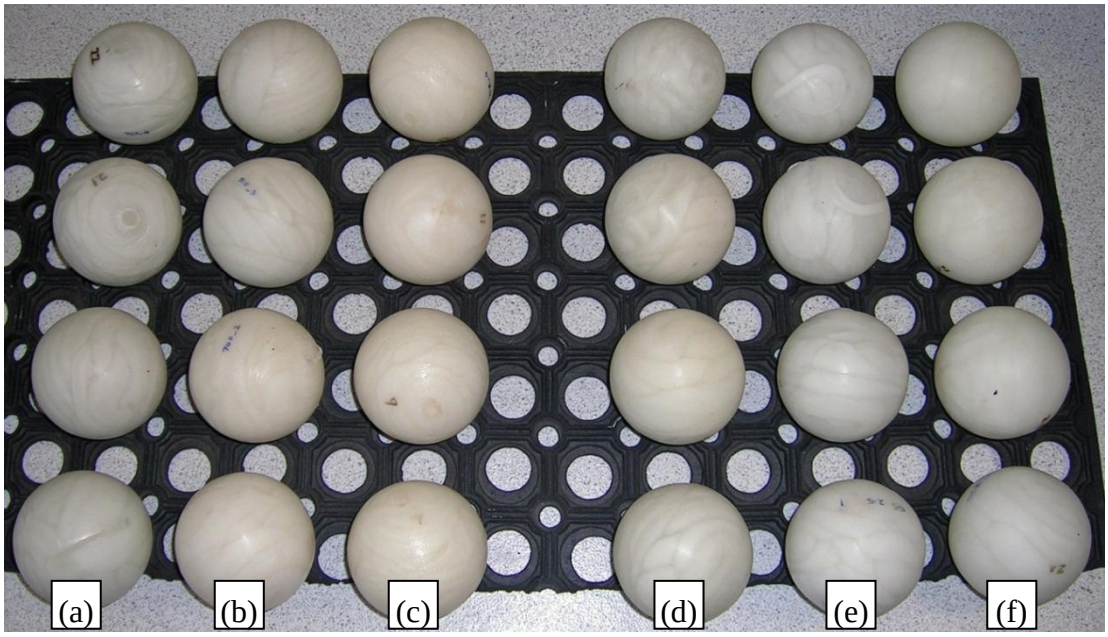

Figure 4.36: Produced prototype variants (a) 55_a, (b) 55_b, (c) 55_c, (d) 70_a, (e) 70_b and (f) 70_c

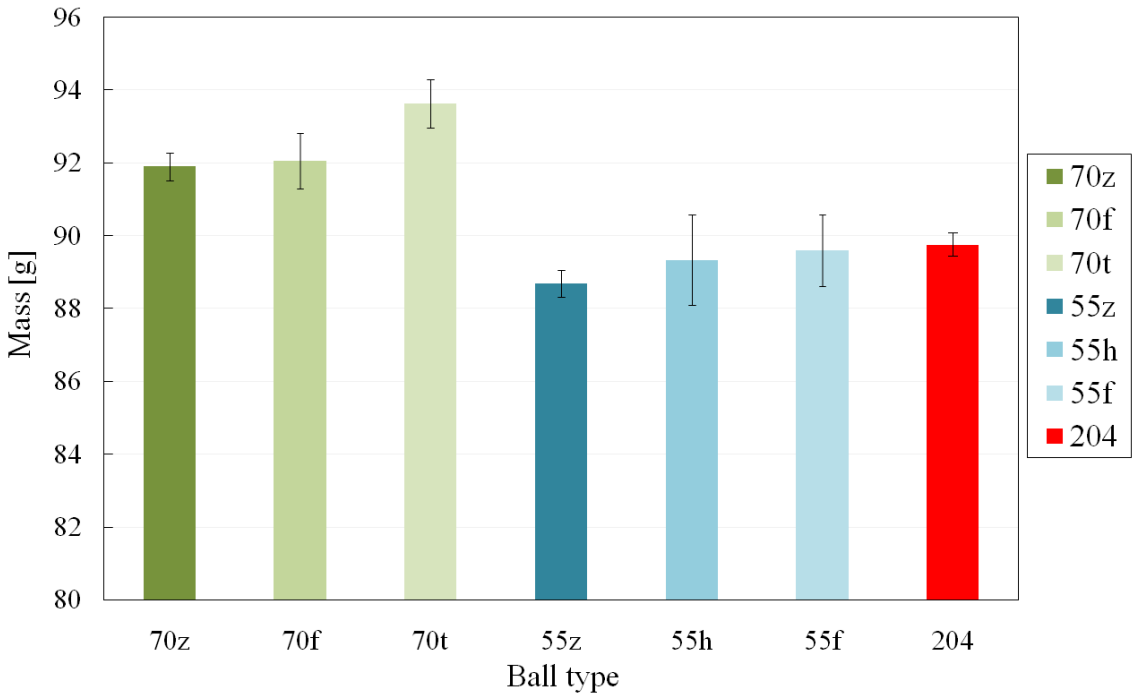

Figure 4.37: Prototype variants' masses

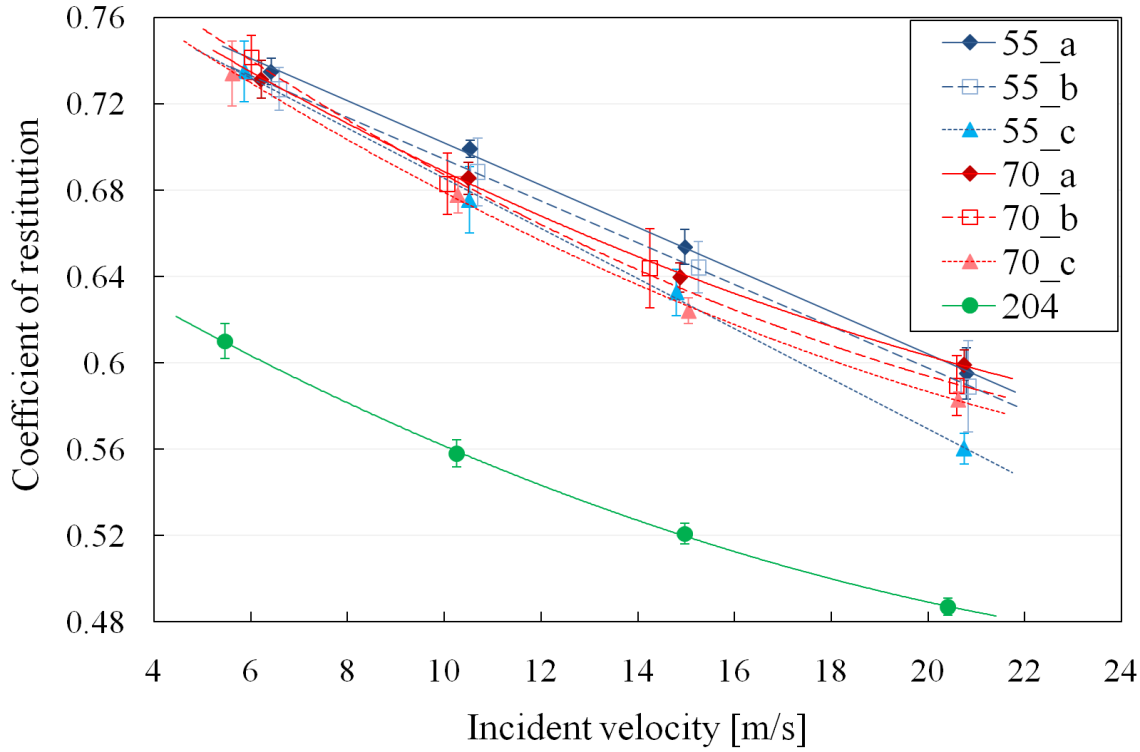

Figure 4.38: Coefficient of restitution values for prototypes variants and sliotar core 204

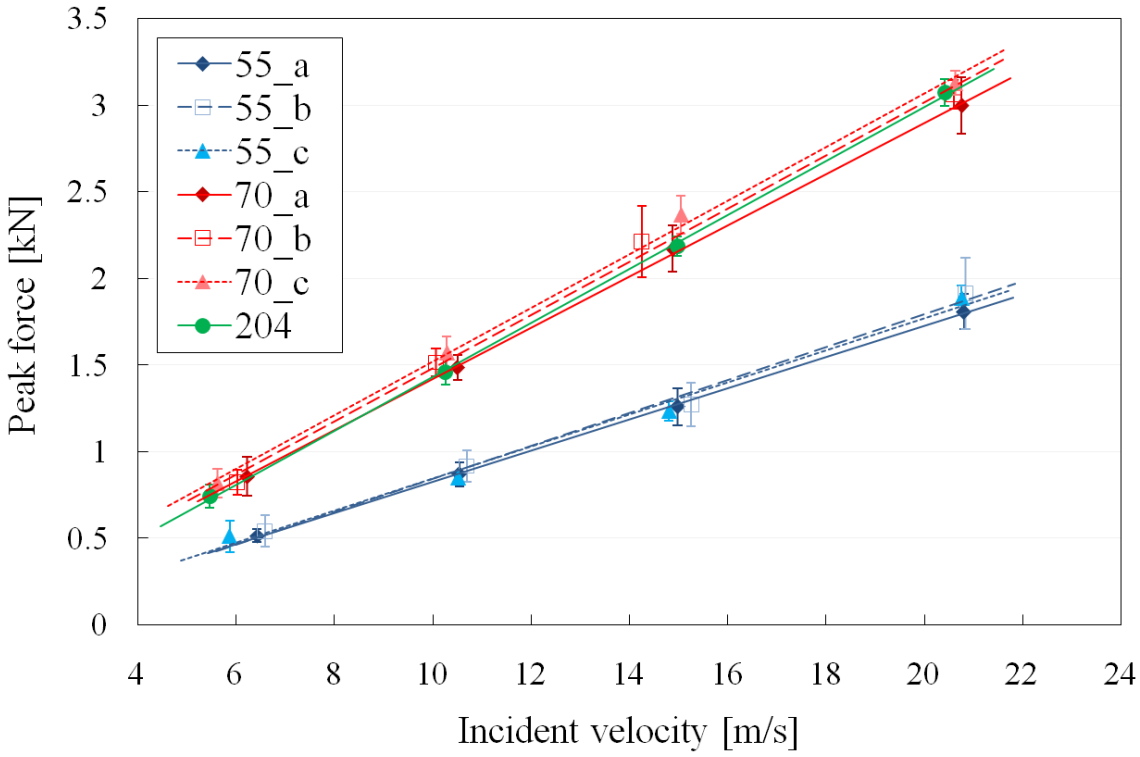

Figure 4.39: Peak impact forces for prototypes variants and sliotar core 204

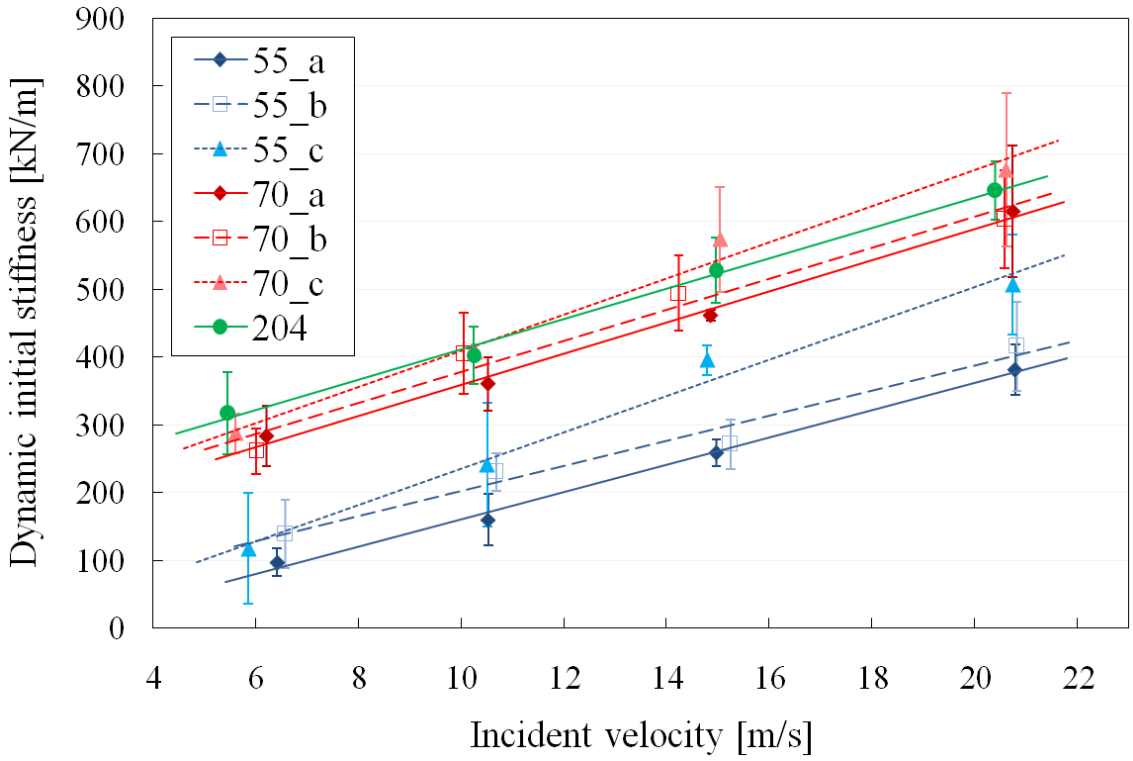

Figure 4.40: Initial stiffness values for prototypes variants and sliotar core 204

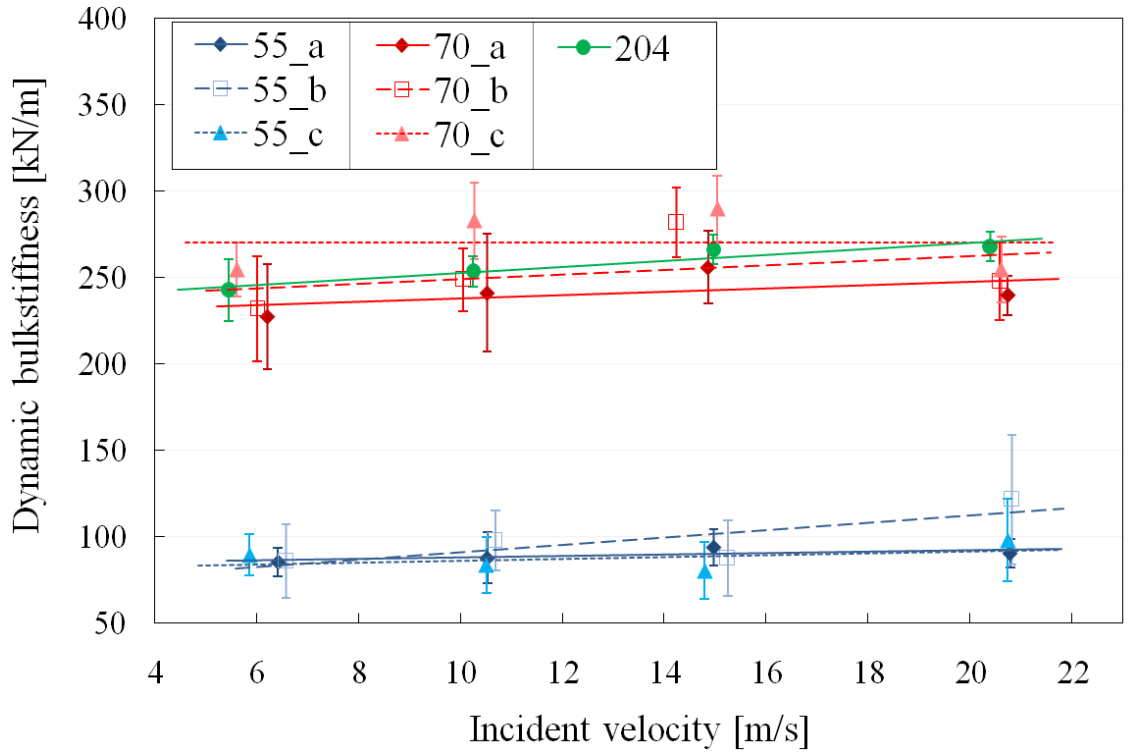

Figure 4.41: Bulk stiffness values for prototypes variants and sliotar core 204

4.3 Modelling results

4.3.1 Model 1

The stiffness and damping coefficients utilised in Model 1 are displayed in Figure 4.42. These values were calculated from Equations 2.13 and 2.14 using experimentally-measured values of contact time and COR (as shown in Figures 4.8 and 4.4, respectively).

Figure 4.43 shows the typical contribution of the stiffness and damping force components, namely kx and $c\dot{x}$ respectively, for a 20 m/s impact for ball types 204 and 206. The high initial value of the damping component resulted in the predicted model force starting at a non-zero value. This was due to the direct proportionality of the damping component on the COM velocity ($\dot{x}$), which starts at the value of the ball incident velocity.

Examples of the comparison between the model force and experimental force are shown for each ball type for a range of impact velocities in Figure 4.44. The closest agreement between the model and experimental data was for ball type 204 (average R-squared value of 0.74). As can be seen in Figure 4.44(a), the model produced reasonable prediction of peak force and contact time, although the actual profile was not replicated. The predictions from Model 1 were less satisfactory for the other ball types, particularly for the traditional ball types 206 and 217, as seen from the discrepancy between the model and experimental peak forces.

Comparison of the force-displacement curves is shown in Figure 4.45. The effect of the initial force discontinuity was more apparent in these graphs. The smaller gradient of the model force-displacement indicated an underestimation of the ball stiffness, with greater discrepancies for the traditional ball types. The near-parallel slopes of modelled force-displacement curves indicated that the model predicted velocity-independent ball stiffness. The model appropriately predicted an increase in hysteresis energy dissipation with increasing velocities, as evident from the closer alignment of the curves in the restitution phase relative to the compression phase. However, the predicted magnitude of hysteresis energy dissipation was undervalued by at least 10%.

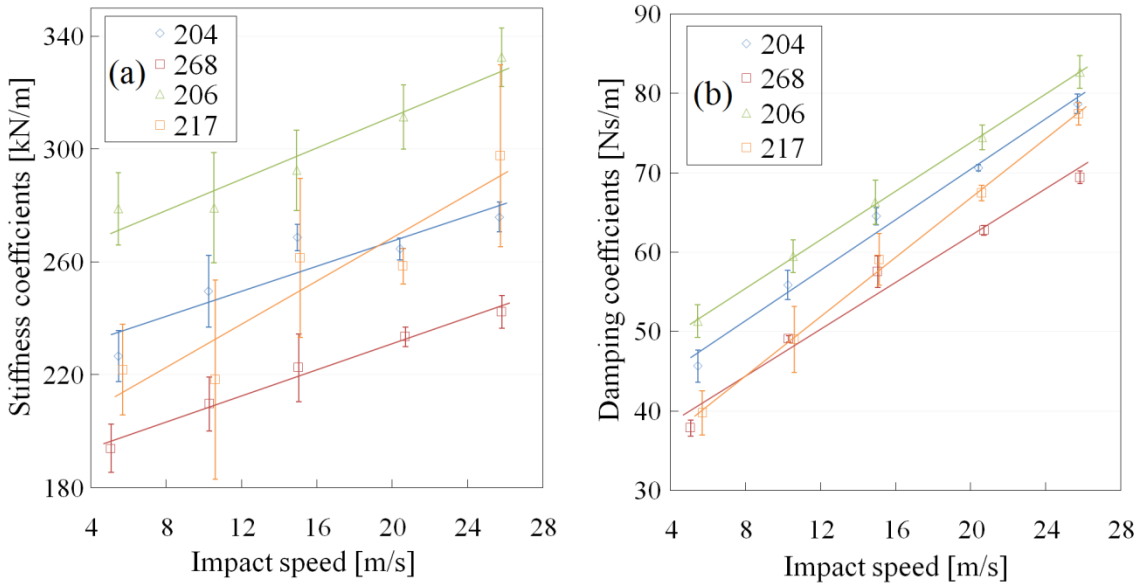

Figure 4.42: Model 1 parameter coefficients for (a) stiffness *k* and (b) damping *c*

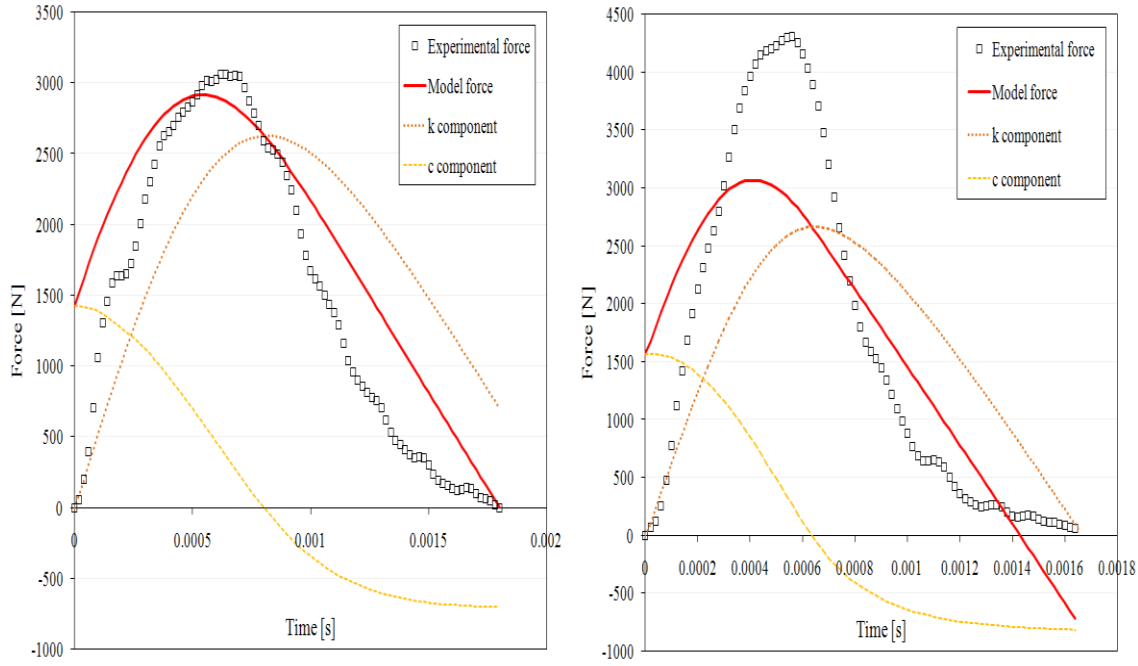

Figure 4.43: Model 1 typical component contribution for 20 m/s impact for (a) 204 and (b) 206

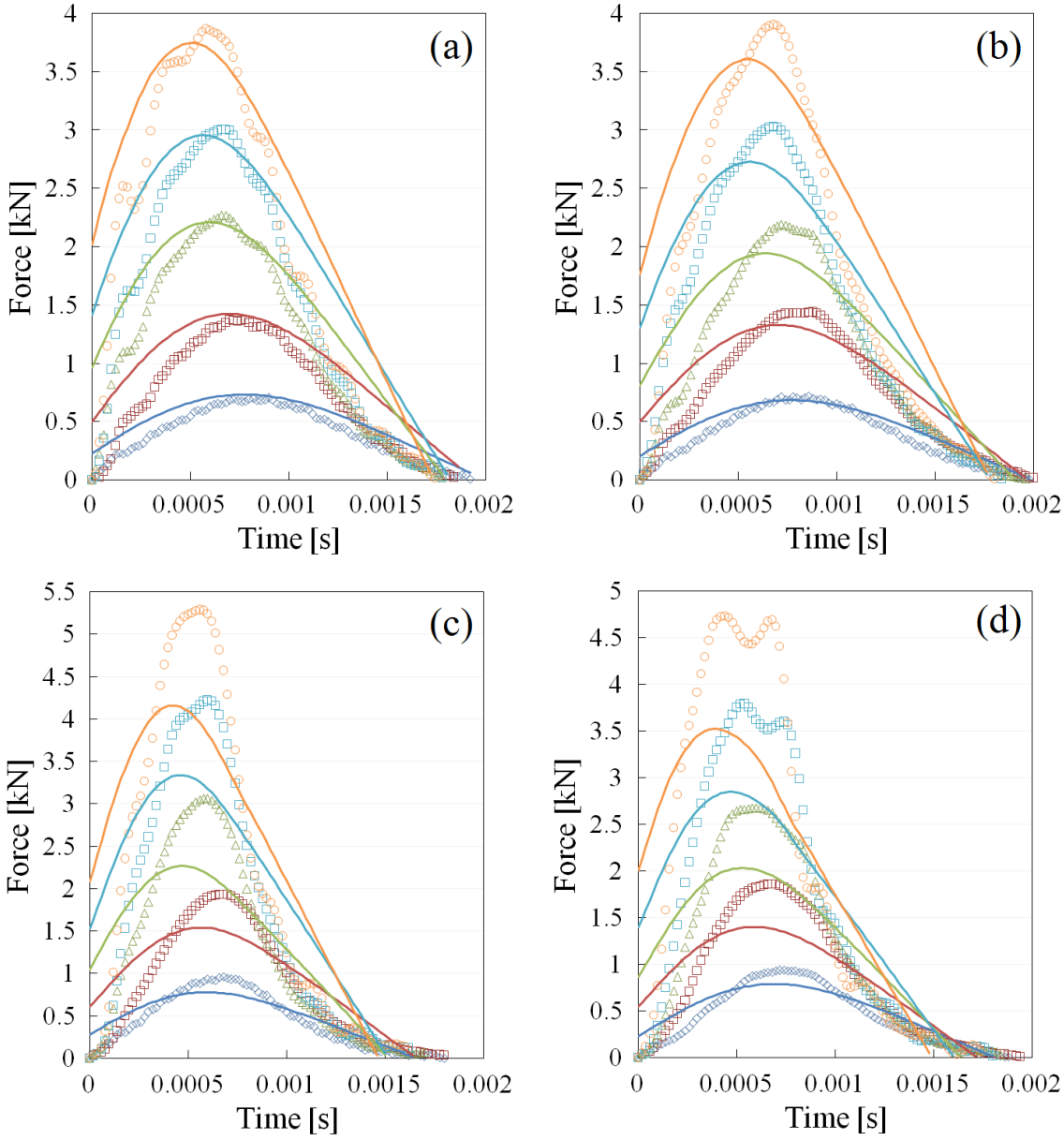

Figure 4.44: Model 1 predicted and experimental force-time data for (a) 204, (b) 268, (c) 206 and (d) 217

	Average percentage difference [%]			
	204	268	206	217
5 m/s: ◇ Experimental — Model	35.7	38.0	42.3	52.9
10 m/s: □ Experimental — Model	48.4	53.1	51.5	52.2
15 m/s: △ Experimental — Model	41.9	56.8	46.4	55.5
20 m/s: □ Experimental — Model	59.9	57.3	62.6	58.3
20 m/s: ○ Experimental — Model	51.1	53.9	56.1	61.8

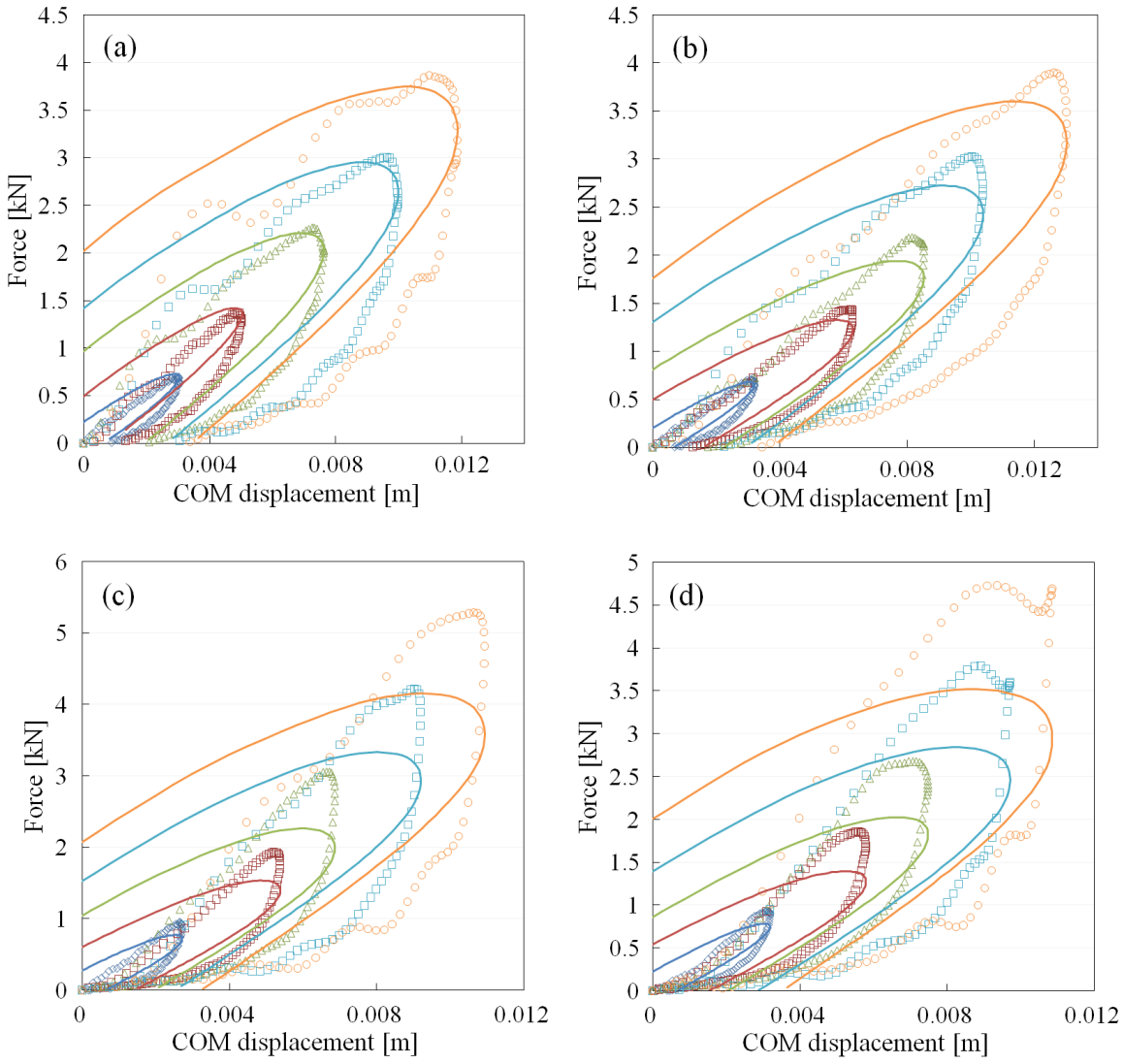

Figure 4.45: Model 1 predicted and experimental force-displacement data for (a) 204, (b) 268, (c) 206 and (d) 217

4.3.2 Model 2

The parametric effect of stiffness coefficient k on the Model 2 force predictions is shown in Figure 4.46. Incrementing the value of k produced a slightly steeper gradient of the compression phase and an offset to the restitution phase gradient. This increased the model force amplitude and delayed the occurrence of predicted peak force.

The influence of the damping parameter q is shown in Figure 4.47 for the same ball types and impact conditions. An increasing value of q resulted in steeper compression and restitution gradients, with the restitution profile becoming increasingly non-linear. This resulted in the predicted peak force occurring slightly earlier in time. All profiles for the variation of q passed through a single point near the start of the restitution phase, corresponding to the COM velocity equalling zero (maximum COM displacement).

The evaluated stiffness coefficients and damping parameters are plotted in Figure 4.48. The stiffness coefficient increases with respect to velocity and the damping parameter decreases with increasing velocity. The stiffness coefficients and damping parameters were described by a power law based trend for each ball type, as specified in Table 4.1.

Table 4.1: Parametric functions for Model 2

Ball type	Stiffness coefficient k [N/m]	Damping parameter q [Ns/m^3]
204	$183557.8u_0^{0.081}$	$474950.7u_0^{-0.251}$
268	$161858.1u_0^{0.116}$	$466663.9u_0^{-0.264}$
206	$215839.6u_0^{0.216}$	$1038637.5u_0^{-0.299}$
217	$161678.4u_0^{0.233}$	$533941.7u_0^{-0.177}$

The contribution of the stiffness and damping components are shown in Figure 4.49 for a 20 m/s impact for ball types 204 and 206. As the damping component was dependent on contact area, the model force began at zero thus avoiding the initial force discontinuity observed in the Model 1.

The model force predictions are compared with experimental data in Figure 4.50. The agreement between Model 2 and experimental data is substantially better than that from Model 1. There were two significant discrepancies between the Model 2 and experimental data. Firstly, the peak force occurrence was predicted too early. Secondly, there was a deviation evident at the end of the restitution phase, particularly pronounced for the polymer ball types, implying an overestimation of the contact time.

The comparison of the model and experimental force-displacement curves is shown in Figure 4.51. Contrary to the first model and in agreement with experimental data, the model predicted an increase in ball stiffness with increasing velocities, as seen from the increasing gradients of the force-displacement curves at higher velocities. However, the rate of this predicted stiffness increase exceeded the rate of increase of experimentally measured stiffness. The model overestimated both the compression energy (area under loading portion of curve) and restitution energy (area under unloading portion of curve). The relative effects of these discrepancies influenced the value of energy loss as calculated from the proportional area enclosed within the hysteresis loop. The magnitudes and trends of the predicted energy loss did not have any significant agreement with experimental data.

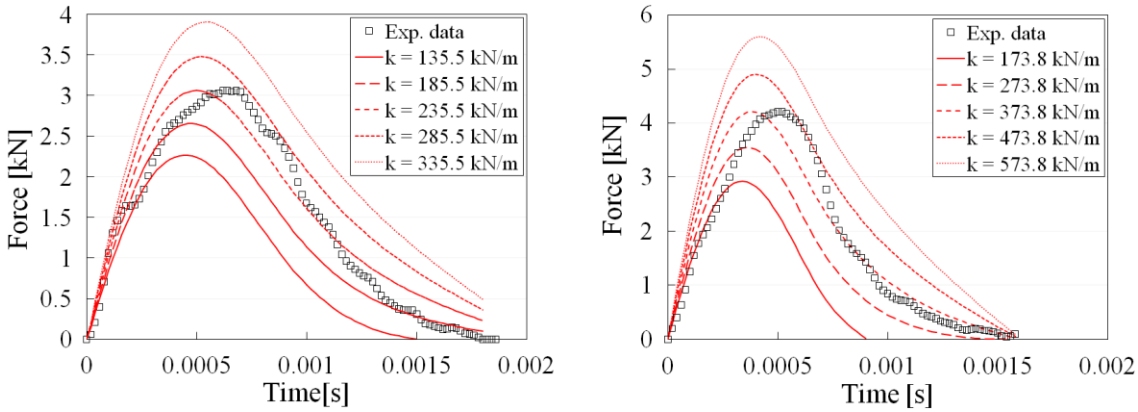

Figure 4.46: Model 2 effect of stiffness coefficient *k* on predicted force for (a) 204 and (b) 206

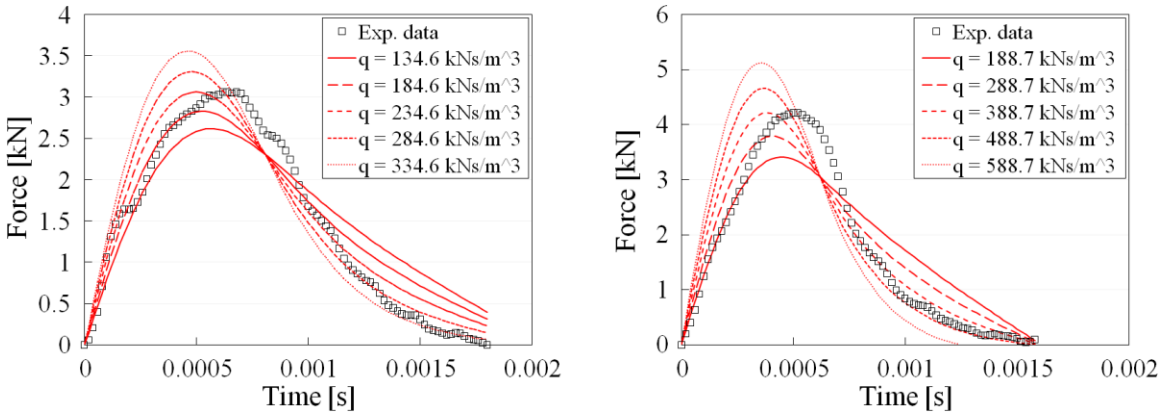

Figure 4.47: Model 2 effect of damping parameter *q* on predicted force for (a) 204 and (b) 206

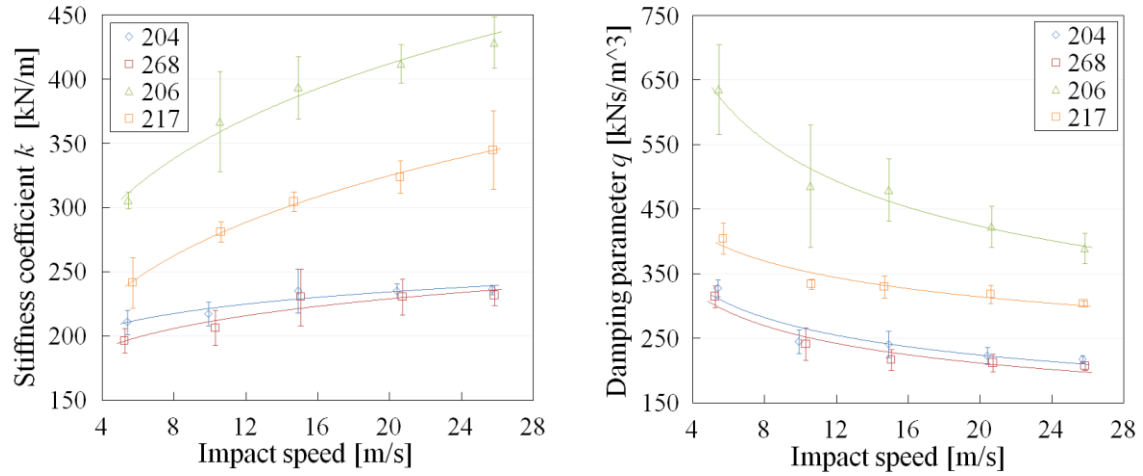

Figure 4.48: Model 2 parameter coefficients for (a) stiffness *k* and (b) damping parameter *q*

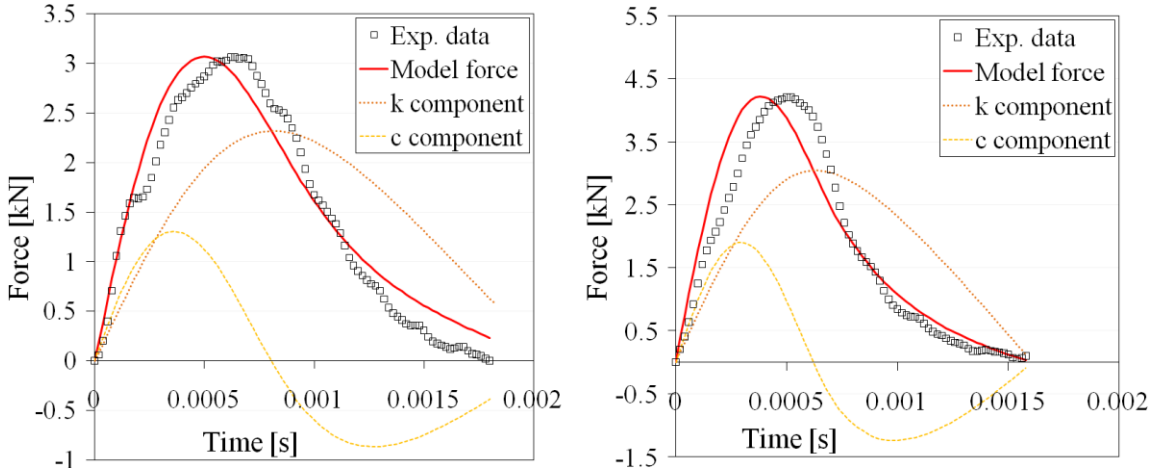

Figure 4.49: Model 2 component contribution for ball types (a) 204 and (b) 206

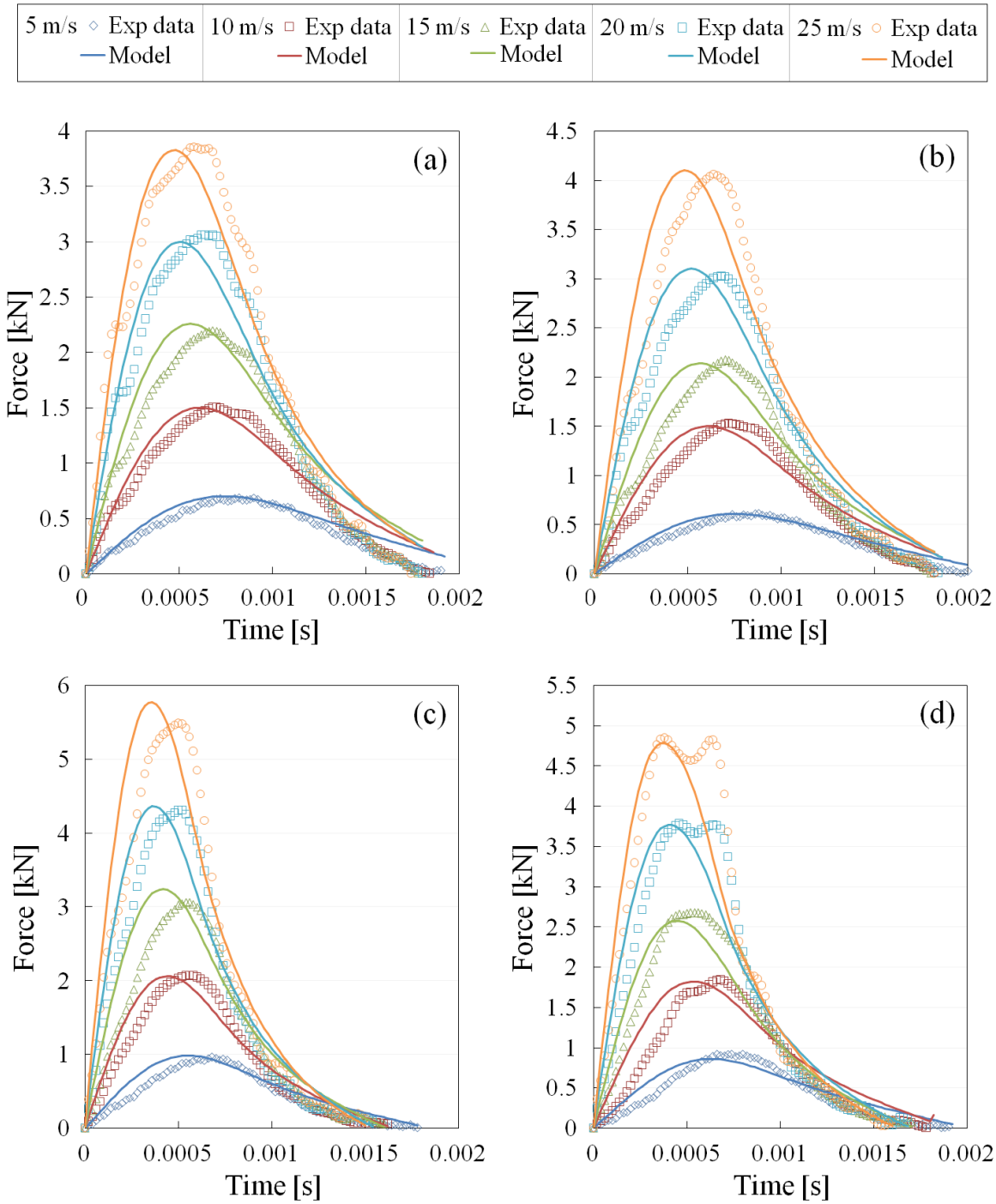

Figure 4.50: Model 2 predicted and experimental force-time data for (a) 204, (b) 268, (c) 206 and (d) 217

	Average percentage difference [%]			
	204	268	206	217
5 m/s: ◇ Experimental — Model	17.5	16.8	29.9	36.8
10 m/s: □ Experimental — Model	16.8	24.5	28.1	46.5
15 m/s: △ Experimental — Model	17.7	28.1	28.7	22.85
20 m/s: □ Experimental — Model	22.3	22.7	26.8	26.9
20 m/s: ○ Experimental — Model	16.8	28.7	22.7	17.8

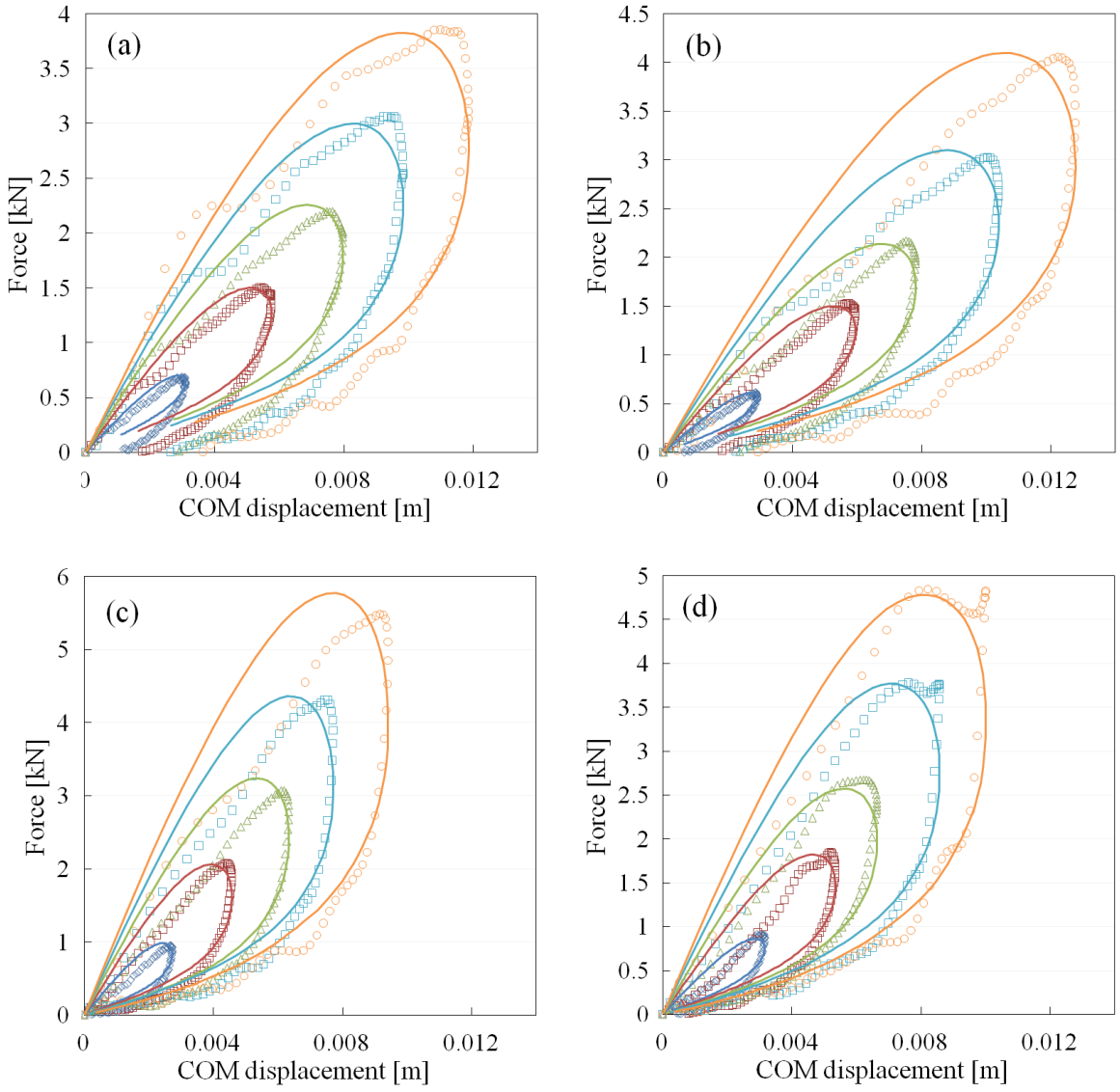

Figure 4.51: Model 2 predicted and experimental force-displacement data for (a) 204, (b) 268, (c) 206 and (d) 217

4.3.3 Model 3

The parametric effect of exponent α on Model 3 predictions is shown in Figure 4.52. The value of α was found to affect the steepness and curvature of force profile. By varying the value of the exponent α, the model predictions could match the time occurrence of the peak force and the gradients of both the compression and restitution phases.

As seen in Figure 4.53, the value of k had a similar effect as it did in Model 2: increasing the magnitude of the predicted force, time-advancing the peak force occurrence, producing a slight increase in the gradients of both the compression and restitution profiles. The variation of the damping parameter q, shown in Figure 4.54, also had a similar effect in Model 3 as in Model 2; providing a greater amplitude and increased profiles' gradient.

The use of the exponent in Model 3 allowed the coincidence of the model predictions with both the compression and restitution phases of the experimental data. This was evident from the single point, through which all q variations passed due to COM velocity equalling zero, coinciding with the experimental data. Singular values of α were found to result in a reasonable agreement with all experimental data for each respective ball type.

The experimentally-fitted values of the stiffness coefficient k and damping parameter q are shown in Figure 4.55. Due to the exponential nature of α, the value of k was highly sensitive to the value a. The disparity of magnitudes and units due to the different exponent values did not permit valid comparison between the stiffness coefficients of each respective ball type. As with Model 2, power trends were fitted to the parameters to express them as a function of impact velocity. The exponent values and parametric power equations are outlined in Table 4.2.

Table 4.2: Parametric functions for Model 3

Ball type	Exponent a	Stiffness coefficient k [N/m^a]	Damping parameter q [Ns/m^3]
204	1.7	$2.457 \times 10^7 \, u_0^{-0.438}$	$6.219 \times 10^5 \, u_0^{-0.333}$
268	2.1	$4.155 \times 10^8 \, u_0^{-0.783}$	$4.952 \times 10^5 \, u_0^{-0.323}$
206	2.9	$1.998 \times 10^{11} \, u_0^{-0.123}$	$1.031 \times 10^6 \, u_0^{-0.319}$
217	2.3	$1.438 \times 10^9 \, u_0^{-0.683}$	$4.170 \times 10^5 \, u_0^{-0.129}$

The contribution of the stiffness and damping components are shown in Figure 4.56 for a 20 m/s impact for ball types 204 and 206. There are two notable differences in the stiffness component introduced by the use of the exponent in this model. Firstly, the stiffness component exhibited a low magnitude for an appreciable duration at the start of impact. This served to reduce the model ball stiffness, an observed discrepancy of the previous model. Secondly, the magnitude of the maximum value of the stiffness component was slightly greater such that it coincided with the experimental force at maximum COM displacement (where COM velocity equalled zero). This ensured that Model 3 exhibited a good agreement with the restitution phase data, contrary to another drawback of the previous model.

The comparison between Model 3 predictions and experimental data is displayed in Figure 4.57. Good agreement was evident between the model and experimental data. However, a deviation was observed at the latter stages of impact, particularly for the traditional ball types 206 and 217. In the experimental data for these ball types, the steep restitution gradient moderated to more gradual force decline. The model predictions did not replicate the change in slope at the latter stages of restitution, instead continuing to decrease at the consistently high rate. This deviation became more apparent in the force-displacement curves shown in Figure 4.58. The rapid descent of the predicted force data produced a larger hysteresis loop area. As the model displayed good agreement for the compression phase for all ball types, the larger area within the hysteresis loop implied an overestimation of the energy loss.

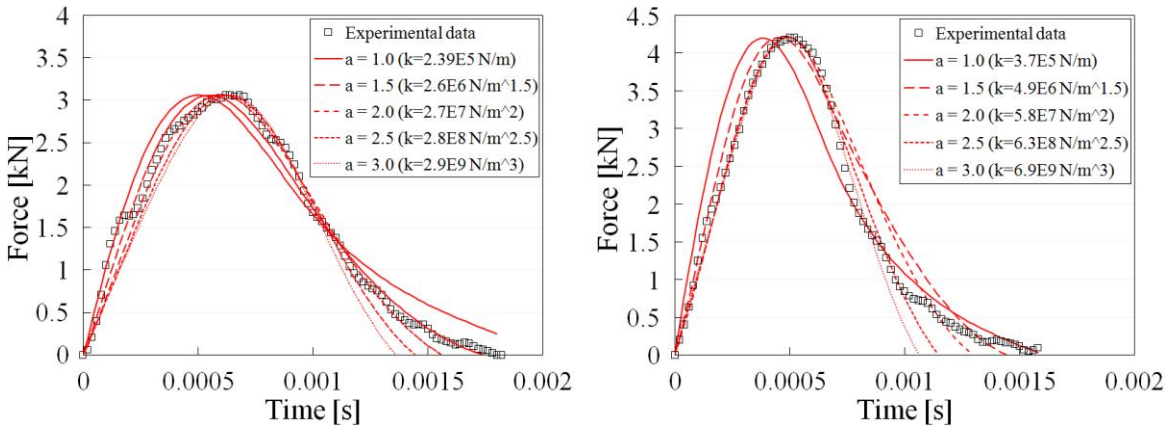

Figure 4.52: Model 3 effect of exponent *a* on predicted force for (a) 204 and (b) 206

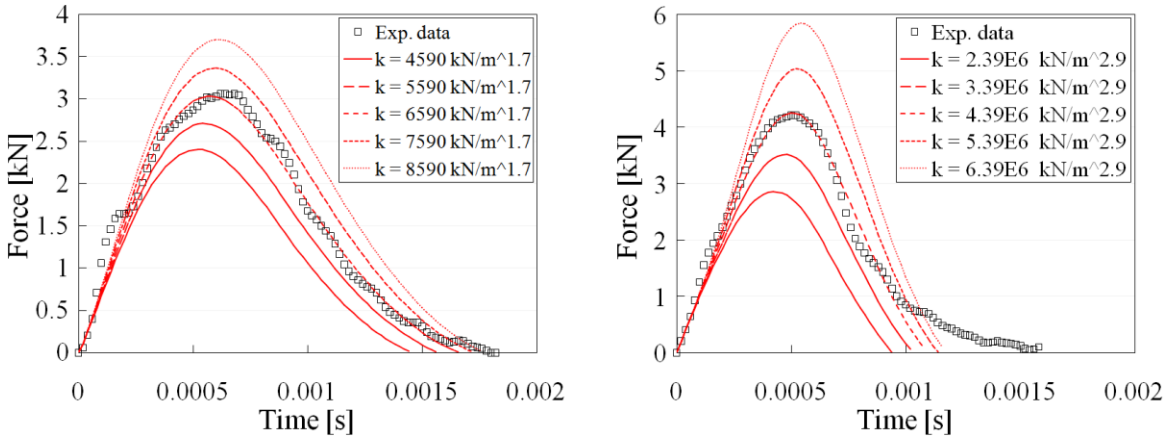

Figure 4.53: Model 3 effect of stiffness *k* on predicted force for (a) 204 and (b) 206

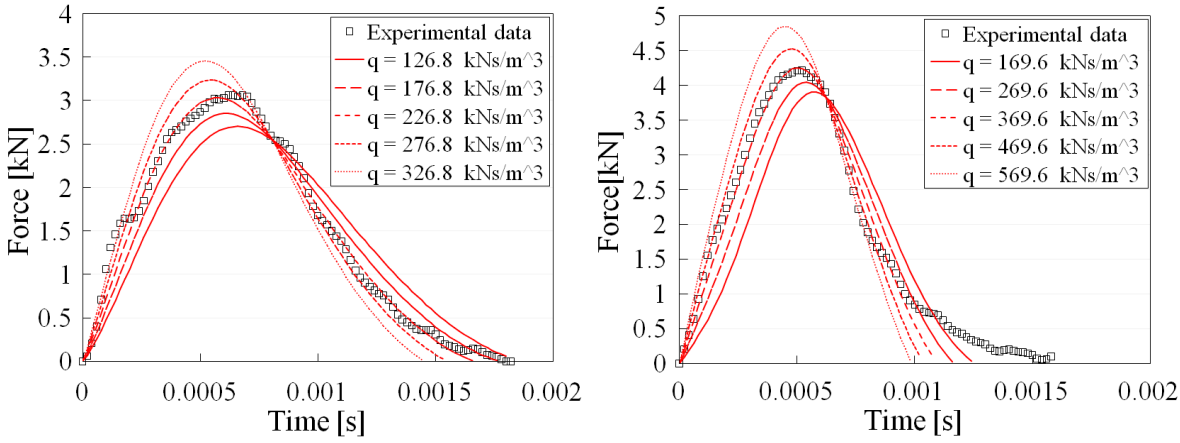

Figure 4.54: Model 3 effect of damping parameter *q* on predicted force for (a) 204 and (b) 206

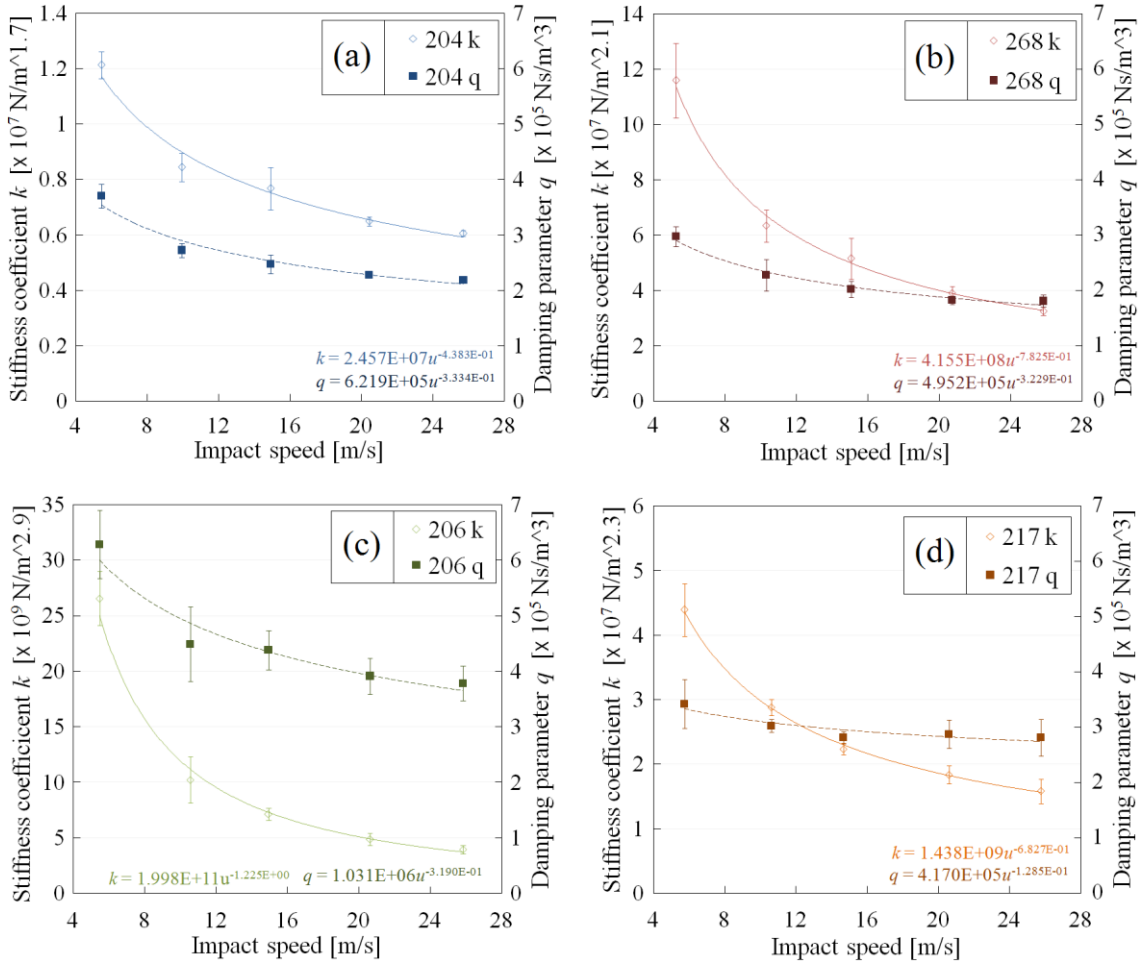

Figure 4.55: Model 3 stiffness coefficients k and damping parameters q for (a) 204, (b) 268, (c) 206 and (d) 217

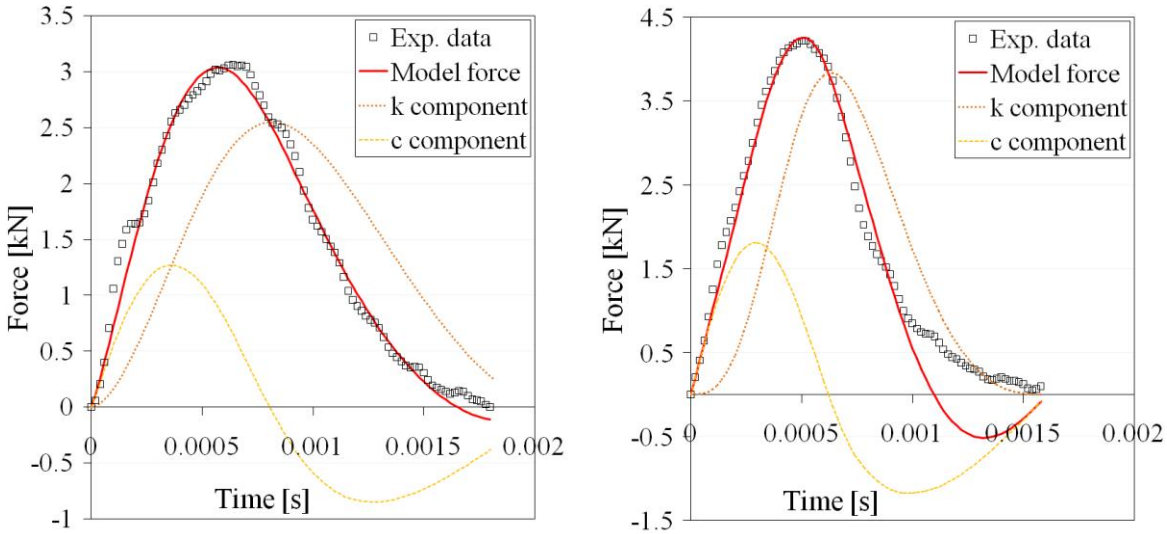

Figure 4.56: Model 3 component contribution for 20 m/s impacts for (a) 204 and (b) 206

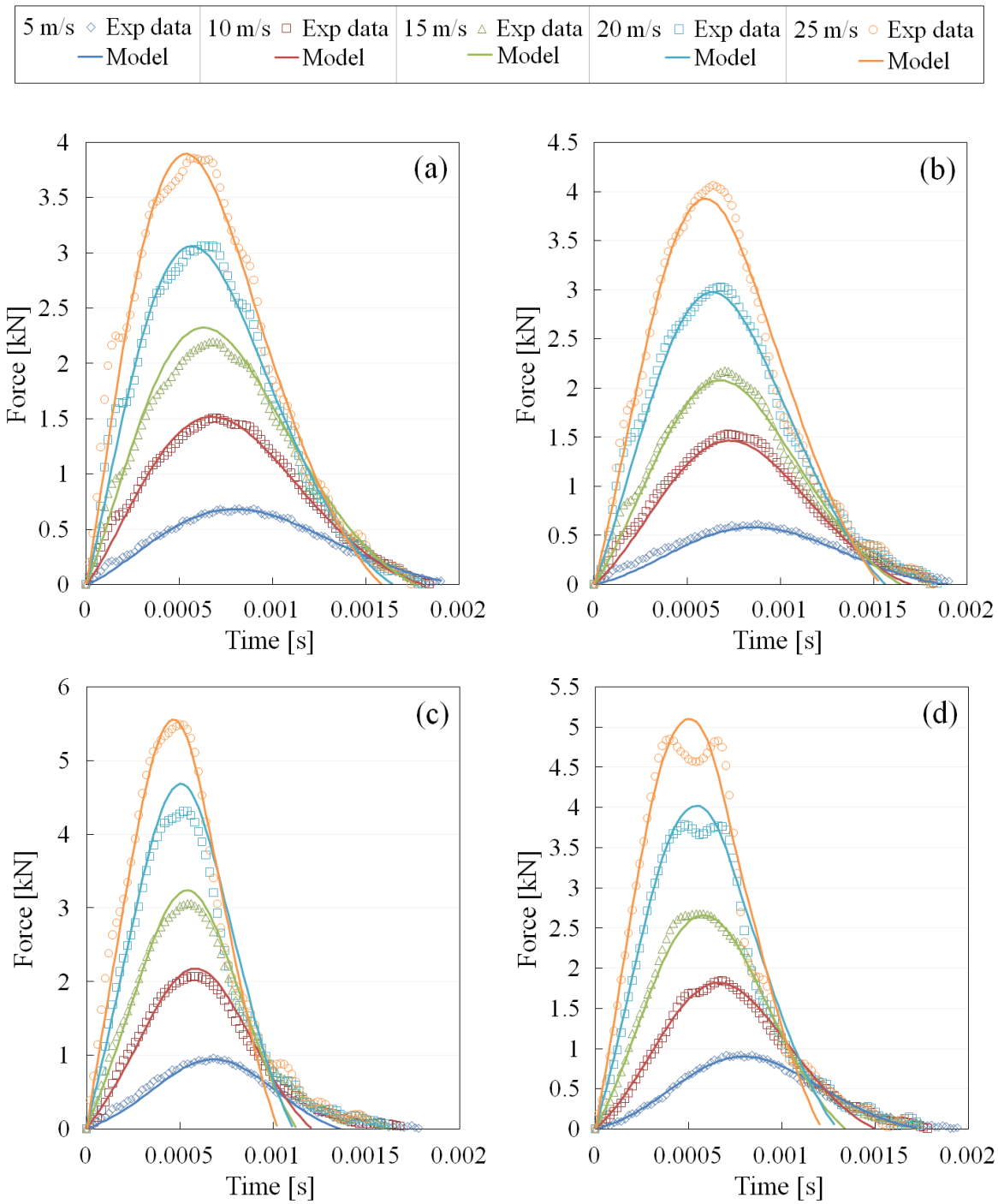

Figure 4.57: Model 3 predicted and experimental force-time data for (a) 204, (b) 268, (c) 206 and (d) 217

	Average percentage difference [%]			
	204	268	206	217
5 m/s: ◇ Experimental — Model	4.4	15.8	19.9	7.9
10 m/s: □ Experimental — Model	8.1	10.1	15.2	12.6
15 m/s: △ Experimental — Model	7.9	8.5	10.6	12.7
20 m/s: □ Experimental — Model	4.7	11.0	13.4	16.1
20 m/s: ○ Experimental — Model	8.4	13.5	11.4	15.7

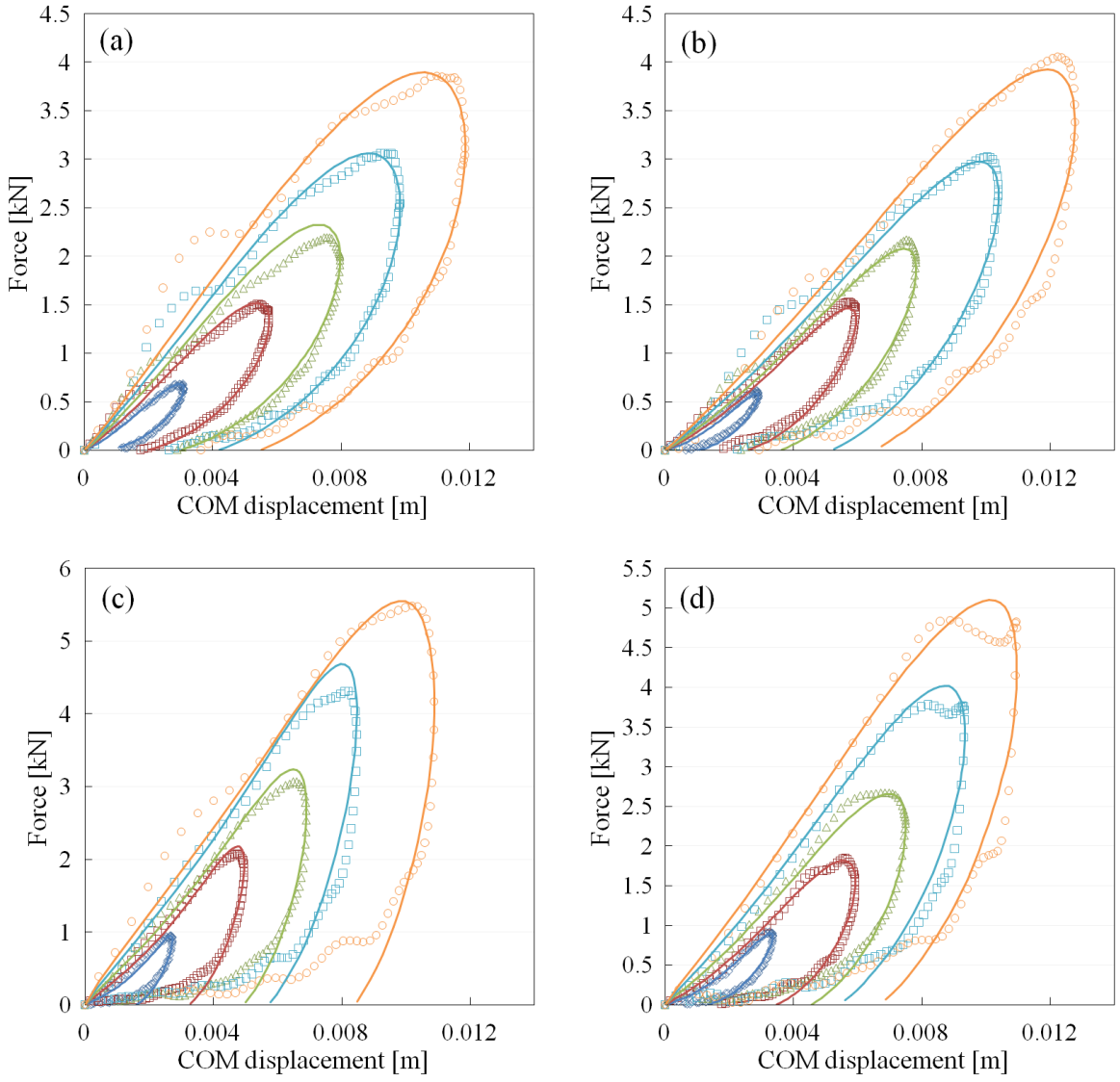

Figure 4.58: Model 3 predicted and experimental force-displacement data for (a) 204, (b) 268, (c) 206 and (d) 217

Chapter 5: Discussion

5.1 Test system development

An automated test system was developed in this present work to enable the collective impact characterisation of a small sports ball. The test system was designed as an advancement of the apparatuses used in equivalent sports [10-15, 21-23], with the advantages of a high range of impact test speeds (5 to 38 m/s) and the capability to measure multiple characteristics from a single impact. The high-speed capability of testing allowed the ball to be subjected to impact conditions representative of those that occur in the sport. The measurement of multiple characteristics from single impacts enabled the determination of the relationship between distinct impact characteristics, as will be discussed later in terms of clarifying deformation measurements and relating ball stiffness to coefficient of restitution performance. This system was designed for intuitive operation, with a user-friendly graphical user interface written in LabVIEW and an entirely automated testing process for each impact. The test system was shown to be repeatable and accurate, as described in Appendix C.

The established test system was used to conduct the first comprehensive characterisation of the sliotar core, the ball used in the Irish sport of hurling. This was the first time that the differences between the two principal categories of ball construction, the modern polymer core and the tradition cork-based core, were defined in engineering terms. In this present work, non-sliotar ball types were also tested to allow objective comparison with the literature. The test system was developed to allow the derivation of viscoelastic characteristics directly from impact data, a capability that does not feature in other regulatory standards [10-15, 21-23]. Moreover, it exhibited none of the limitations reported with other non-impact methods of viscoelastic characterisation [25-28], allowing repeatable measurements of a ball's impact response at strains and strain-rates representative of those occurring in the sport. This allowed for the appropriateness of viscoelastic measurements by quasi-static methods or spring-theory numerical equations, as used by regulatory standards [10, 11, 13, 15], to be analysed.

5.2 Performance characterisation

5.2.1 Coefficient of restitution discussion

The two principal ball categories within the approved range of sliotar cores, those being the modern polymer and traditional cork-based constructions, were observed to have a discernable difference in coefficient of restitution (COR) values, see Figure 4.1 (a). The approved range of sliotar cores consisted of 16 ball types, each from independent branded suppliers. All ball types exhibited a downward trend in COR with respect to incident speed. The larger impact energy associated with higher incident speeds induces a greater extent of deformation, resulting in an increase in energy dissipation corresponding to a decrease in COR. The degree of energy dissipation resulting from the deformation of a larger volume of ball material is dependent on the viscoelastic response of the ball material.

The traditional ball types as a whole exhibited a greater COR than the modern ball types, as evident from the traditional ball types occupying the upper regions of the COR data, see Figure 4.1 (a). Polymeric materials have been reported to demonstrate a greater viscoelastic response then cork materials [107, 114], indicating that polymeric material behaviour is more dependent on strain and strain-rate. Based on this evidence, it seems non-intuitive that the traditional ball types exhibited a COR trend that had a more non-linear relationship with respect to speed than the modern ball types. This indicated that the traditional cork-based ball types had a substantial strain-sensitive viscoelastic response that was not present to the same degree in the modern polymer ball types. Considering the ball constructions, the traditional ball types comprised of layers of distinct material layers with dissimilar viscoelastic properties e.g. yarn, polyester and cork for 217. The progressive engagement of the distinct layers with differing viscoelastic responses at increasing deformation (i.e. increasing incident speed) led to a more non-linear variation in energy dissipation. In contrast, the modern ball types consisted of a more homogeneous construction, with the deformation of the increasing volume of polymeric material producing a more linear increase in energy dissipation. This signified that the traditional ball types were less energy dissipative than modern ball types at low speeds, then converged on modern ball COR at mid-range speeds and diverged from modern ball COR with increasing speed. In contrast, modern ball types

had a more linear reduction in COR with respect to speed. This difference in trend would result in a divergence of performance between the two ball categories

The traditional ball brands exhibited a more consistent COR than the modern ball brands, in terms of both comparison between different traditional ball brands (traditional inter-ball variation) and discrepancy within each individual ball brands (intra-ball-type variation). The small inter-ball variation of the traditional ball types was evident from the relatively close alignment of the dotted-line trends in Figure 4.1. A larger inter-ball variation was apparent for the modern ball types, as observed from span of the modern ball trends (solid lines in Figure 4.1) relative to the traditional ball types. While the wide span of performance between balls from different manufacturers could be attributed to independent manufacturing approaches, the difference between polymer ball types appears to be much larger than the difference between traditional cork-based balls. Given the variation evident between different polymer ball brands, it would further confirm the need to standard the core of sliotar.

The intra-ball-type variation, the discrepancy between the four samples of each approved sliotar core, was gauged from the R-squared values of the COR trends, see Figure 4.1 (a). While testing more than four samples of each approved sliotar core may have defined a performance that was more representative of the full population of each ball brand, the four samples were arbitrarily taken from the 10 sliotars submitted to DCU by each supplier. As each supplier was responsible for the selection of sliotars to be submitted, any scatter and outliers in the experimental data should reflect the market output of each supplier.

The experimental scatter was due to discrepancies between samples within a ball brand, as evident from the clusters of points for each individual ball sample in Figure 4.1 (b). These discrepancies were attributed to poor quality of ball production, with possible factors including variations in construction, manufacturing conditions or constituent materials. One should bear in mind that these balls are covered in identical leather skins and so variations in sliotar cores are visually indistinguishable to the players. The ball samples of the traditional construction, with the exception of ball type 257, exhibited more consistent COR with respect to their individual brands. One conclusion to draw

from this was that traditional ball types had better quality control for construction. This consistency was surprising given the biologically-sourced materials, the multiple material compositions and handcrafted nature of traditional construction. In contrast, the modern ball types with their fully synthetic material composition and automated manufacturing processes exhibited a wide span of performance. Poor quality control was evident in a number of modern ball types, particularly for ball types 259, 268 and 272. These ball types exhibited significant intra-ball-type variation, as shown by the similarly-sloped but offset trends of the individual ball samples in Figure 4.2. While individual ball samples of 259, 268 and 272 exhibited a distinct consistent performance as evident from the clustered data points, there was no collective consistency within each respective brand. By comparison, all samples of ball type 204 exhibited comparable performance, as evident from the closely aligned trends in Figure 4.2.

Likely factors that would result in performance variation would be disparities in ball mass, density/porosity distribution and cellular structure. Samples of different masses could result in different degrees of energy dissipation due to the differing amounts of material involved in the deformation. Samples of similar masses could have differences in density distribution corresponding to the diffusion of porosity through the ball internal structure. Dense material concentrations arising from small foam cells and more prevalent matrix material (solid polymer) could be expected near the surface of the ball due to the initial solidification of the polymer against the tool surface during manufacture. A less dense composition may be present in the ball interior corresponding to larger foam cells and more disconnected struts surrounding the cells. Such a cellular morphology would present a greater compliance, implying a variation in viscoelastic response at such deformation. Other aspects of cellular structure could also affect viscoelastic response would be the morphology of the foam cells (shape, orientation) and their interconnection (open or closed-cell).

The most readily measured intra-ball-type discrepancy was ball mass, of which there was an appreciable variation in a number of ball types as seen in Figure 3.8. Considering that there was consistency in diameters recorded within each ball type, as shown in Figure 3.9, the mass variation corresponded to a variation in density, which has possible implications on the energy dissipative properties of the ball material. The COR values

were mass-normalised to investigate the effect of mass on performance variation, as displayed in Figure 4.3. This mass-normalisation involved dividing the COR value by the ball mass, then multiplying it by the average ball mass, which was rounded to 90 g for simplicity. Mass normalisation of the COR reduced the variation in two of the ball types, 268 and 272, improving the R-squared values by 16% and 5%, respectively. This suggests that ball mass discrepancy was a factor in the intra-ball-type variation of these ball types. However, the intra-ball-type variation of ball types 259 and 257 could not be attributed the ball mass discrepancies, where the mass-normalisation of their COR reduced the R-squared values from 0.902 to 0.862 and from 0.856 to 0.801, respectively. While mass-normalisation indicates that mass discrepancy can be a source of performance variation for some ball types, its inadequacy for other ball types indicates the presence of other factors such as internal density distribution and cell morphology.

Considering the four selected sliotar cores in isolation from the others, as seen in Figure 4.4, the distinction between the performance of modern and traditional ball types becomes clearer. The traditional ball types 206 and 217 exhibited a higher COR and a more non-linear speed-dependence than the modern ball types 204 and 268. The greater energy dissipation in the modern polymer ball types is consistent with reports [26] of greater hysteresis in polymeric materials relative to cork material due to its viscoelastic effects. The non-linearity of the traditional ball types COR trend demonstrated the strain dependence of these ball constructions. For lower amounts of deformation (i.e. at lower incident speeds), the outer layers of the construction had the dominant contribution to energy dissipation. For ball type 217, the outer layers comprised of a comparatively thick sections of yarn and polyester strands, see Figure 3.10. Given the ‘springiness’ of such layers, less energy was dissipated during this deformation corresponding to the significantly greater COR relative to the other three ball types, see left-hand side of Figure 4.4. Traditional ball type 206 had only a relatively thin layer of yarn, resulting in only a marginal difference in COR relative to the polymer ball types. Both traditional ball types exhibited a decreasing reduction in COR with respect to impact speed, demonstrating the strain-dependent stiffening behaviour of the cork material with increasing deformation. The strain-dependent increase in stiffness of the cork material served to reduce the strain on the ball material, inducing less deformation and hence less

energy dissipation. Such strain-dependent stiffening behaviour was not as prevalent in polymeric materials, as will be discussed in Section 5.2.4. Thus the energy dissipation of the modern balls exhibited a more linear COR speed-dependence.

The differences in performance of the modern and traditional ball types in terms of COR magnitude, while discernible, were quite small. This finding contrasted to anecdotal evidence of significant differences in perception of playing performance between the two ball type categories. This discrepancy may be due to the disparity between rigid-body COR, as evaluated thus far, and compliant-body impact that are representative of sports surfaces. As will be discussed further in Section 5.2.4, there was a significant difference in stiffness between the two ball categories, with the traditional ball types tending to be 90% stiffer than the modern types. Such variation in stiffness would result in significant differences in bounce between ball types under sporting conditions.

5.2.2 Force-time discussion

The peak force measurements of the approved sliotar cores were seen to diverge with increasing impact speeds, see Figure 4.5. As all ball types exerted comparable forces at low speeds, high-speed impact regulation was seen to be necessary to distinguish between the behaviour of different ball types. The intra-ball-type variation observed in COR values was not as prominent in the peak force data. The difference between the modern and traditional ball categories was more pronounced for the peak force data than for the COR measurements. This was apparent for the four selected sliotar cores, where the tradition ball types 206 and 217 exhibited peak forces of 5.5 kN and 4.8 kN compared to the 3.9 kN exerted by the modern ball types 204 and 268, for 25 m/s impact, see Figure 4.7.

Distinctive force-time profiles were observed for the four selected sliotar cores, see Figure 4.6. These force-time attributes were associated with the material and construction. For polymer ball types 204 and 268, an initially steep slope with a kink was recorded in the compression phase, particularly evident in the higher speed impacts. This was more pronounced in ball type 204, where the kink levelled out to become a

peak partway through the compression phase. Such behaviour has been observed previously in tennis balls, where an initial peak has been attributed to the abrupt change in stiffness with the buckling of the ball shell [50]. In this case, comparison with high-speed footage suggested that the initial rapid increase in force was attributed with the flattening of the balls' curvature and that the kink represented an abrupt change in ball stiffness during the ball deformation. This abrupt change in polymeric material stiffness at certain deformations has been reported previously [107-110] as a type of viscoelastic strain-dependence, where the buckling of the foam cell walls within the cellular structure results in a reduction in material stiffness. The abrupt change in ball stiffness during deformation will be discussed further in Section 5.2.4.

Slight surface waves were discernible from the high-speed footage of ball type 204, which would explain the extra degree of fluctuation after the kink in the force profile of ball type 204 relative to 268, see Figure 4.6(a) compared to 4.6(b). Traditional ball type 206 had a greater rate of force increase in the compression phase, with little change in the force gradient up until near maximum loading. A double peak with a central trough was observed in traditional ball type 217. This feature was due to the multi-layer construction and has been observed in previous studies on other multi-layer balls such as tennis balls and two-piece golf balls [50, 93]. The double peaks were attributed to the interaction of the central core within the internal structure of the ball. It is more appropriate to discuss the contribution of each ball type's construction in terms of material stiffness, which will be discussed further in Section 5.2.4.

5.2.3 Deformation discussion

The deformation characteristics of the approved sliotar cores, expressed as percentage compression of diameter (Figure 4.9), showed that the ball deformation increased nearly linearly with increasing speed. As observed with coefficient of restitution data, the modern polymer ball types spanned a wider range of deformation values, with the traditional ball types occupying the upper region of this span. This was particularly evident for modern ball types 268 and 272, which exhibited the highest and lowest range of deformations, respectively. The intra-ball-type variations that were observed in the

COR measurements, which were attributed to poor quality control, were also evident in deformation data.

In reviewing the literature there is an obvious ambiguity regarding the method for measuring ball deformation, where many publications [16, 18, 19] have explicitly or implicitly assumed that centre-of-mass (COM) displacement and diameter compression were equivalent measurements. These measures are distinguished according to their measurement methodology, where the COM displacement is measured from the double time integration of the force divided by ball mass and the diameter compression is measured by the reduction of ball diameter perpendicular to the plate. One study stated that the two measures equalled if the diameter compression was significantly less than the ball diameter [19], while another stated the two measures equalled since the impact surface was rigid [16]. Two separate studies on tennis balls had conflicting statements, where one [18] assumed without experimental verification that diameter compression equalled COM displacement, while the other [20] theorised, again without experimental verification, that diameter compression was up to 70% greater than COM displacement. None of these publications appeared to have considered the effect, if any, of the lateral expansion of the ball's diameter parallel to the impact surface. The ambiguity regarding ball deformation was addressed in this present work, with non-sliotar ball types included for objective comparison with the literature. The results showed that there is no universal relationship between COM displacement and diameter compression, as shown in Figure 4.11. A divergence between maximum COM displacement and diameter compression values was observed with increasing incident speeds for ball types 206, 204 and 180 in order of increasing deviation between the values. The cricket ball showed little or no difference between COM displacement and diameter compression for all tested speeds. It was deduced from Figure 4.11 that an increase in lateral expansion resulted in a greater deviation between the COM displacement and diameter compression. This appears to be the first study to report this relationship.

Lateral expansion has been presented in the literature in terms of compression ratios, as described in Section 2.1.4. In accordance with findings in the literature [48, 49], the normal and tangential compression ratios were seen to have an approximately linear relationship, as shown in Figure 4.12. The factor describing this relationship, as derived

from the slope of the linear trends in Figure 4.12, could be considered a useful measure in describing deformation behaviour of a ball: a high value factor (> 10) indicated predominant diameter compression; lower factors signifying the presence of lateral expansion. The factors evaluated in this present work were 3.4, 6.4, 14.5 and 15.3 for ball types 180, 204, 206 and the cricket ball, respectively. Therefore a high factor (> 10) relating the normal and tangential compression ratios indicate that COM displacement and diameter compression yield similar values.

The contribution of lateral expansion to the discrepancy between COM displacement and diameter compression can be more clearly understood by considering high-speed images of the ball's deformation. Examples of the visual analysis for 25 m/s impacts are seen in Figure 4.13. Considering the deformed ball shapes in Figure 4.13, the horizontal distance between the blue outline and the ball edge shows the diameter compression and the horizontal distance between the blue and yellow outlines represents the COM displacement. The coincidence of the yellow outline with the ball edge for ball type 206 and the cricket ball indicates the equivalence of COM displacement and diameter compression for these ball types, see Figure 4.13(b) and (e). These balls are seen to exhibit little or no lateral expansion, i.e. the balls' deformed shapes have not spread in the vertical direction. Conversely, a gap was evident between the yellow outline and the ball surface in increasing magnitude for ball types 204, 180 and PNG respectively, see Figure 4.13(a), (d) and (e). The lateral expansion, as seen from the increment of ball diameter parallel to the impact plate, induced a greater reduction in the diameter perpendicular to the impact plate as the ball material was drawn tangentially towards the lateral poles. The extra reduction in the normal diameter was not accounted for in the force data (from which the COM displacement was derived) as the lateral expansion was perpendicular to the impact plate and hence not sensed by the axial load-cell. This extra reduction in normal diameter due to lateral expansion can therefore be seen to lead to a deviation between COM displacement and diameter compression. This study appears to be the first to experimentally verify the nature of the relationship between COM displacement and diameter compression.

The *contact approach* was an abstract measure of ball deformation that was defined previously as the difference between the ball's non-deformed radius and the distance

between the impact surface and the centre of the circle centred on the deformed ball [97]. This is analogous to the horizontal distance between the impact surface and the left-edge of the yellow outline, see Figure 4.13. This distance is equivalent to the separation between the yellow and green outlines, implying that the COM displacement value equated to the contact approach.

For some ball types, it can be seen that the yellow outline intersected with the edges of contact area between the ball and impact surface, see Figure 4.13(a) and (e). These cases indicated that the COM displacement could be related to the contact area by simple Pythagoras geometry. This observation is consistent with two previous studies that independently reported a geometrical relationship between COM displacement and contact area [97], and between *contact approach* and contact area [50]. However, this geometrical relationship is not applicable for all ball types. The extreme compliance of some ball types, as seen in the impact of ball type PNG (see Figure 4.13(f)) and to a lesser extent ball type 180 (see Figure 4.13(d)), resulted in the diameter of the contact area exceeding the original diameter of the ball. The softer outer layers of the traditional ball types were observed to bunch up outside of the contact area as seen in ball types 206 (see Figure 4.13(b)) and 217 (see Figure 4.13(f)). In both cases, the yellow outlines no longer intersected the edge of the contact area, implying that the COM displacement was not geometrically related to the contact area.

Incidentally, some of the previous statements of equivalence [16, 18, 19] between COM displacement and diameter compression have been appropriate, not for the reasons given in the original papers but rather due to the absence of lateral expansion in the ball impacts examined. In the present study, the experimental verification of the relationship between the COM displacement and diameter compression dispels the ambiguity surrounding the description of ball deformation in the literature. The COM displacement, diameter compression and lateral expansion measures each have their merits in ball characterisation, implying that no one single measure can be used to exclusively describe ball deformation. COM displacement is useful to a certain extent in evaluating contact area, although balls with greater compliance or soft material layers would require consideration of lateral expansion. Diameter expansion and lateral expansion are appropriate in characterising ball loss-of-shape as they describe the

physical change in ball geometry. COM displacement was appropriate for viscoelastic characterisation due to its association with impact force, as will be discussed later in Section 5.2.4. The selection of which quantitative measure to use for model simulation depends upon what the model was attempting to represent. COM displacement values are relevant for mathematical models that represent the ball as a point-centred mass. Diameter compression and lateral expansion values are better suited for finite element models that would attempt to predict the overall change in shape of the ball during deformation.

5.2.4 Viscoelastic discussion

Stiffness is one of the most significant characteristics of a sports ball. Three methods to quantify ball stiffness were employed in this study: quasi-static compression, dynamic impact testing and spring-theory numerical predictions. None of the regulatory standards for different sports' balls involve the measurement of stiffness directly from dynamic impact test data, instead favouring quasi-static compression and equations based on idealised spring theory. While these two methods are relatively easy to conduct, the validity of these techniques has not been satisfactorily defined with respect to their relevance to actual ball impact behaviour.

Quasi-static viscoelastic characterisation

Quasi-static testing has been utilised in several conflicting reports on ball characterisation, with some claiming a general trend between quasi-static data and impact behaviour [32, 58], and others finding no conclusive relationship [20, 25, 51]. There are two principal differences in the loading conditions between quasi-static compression and impact testing. Firstly, quasi-static compression involves bilateral symmetrical compression compared to unilateral asymmetrical deformation during impact. This implies a difference in the strain conditions, where a deformation originates from both sides of the ball and is more distributed throughout the material during quasi-static compression in contrast to the concentrated strain and stress localisation in the

contact region of the ball in impact testing. The viscoelastic effects of the material would tend to differ for either test due to the difference in stress distribution throughout the ball, where a more pronounced stress gradient would exist in impact testing. The second principal difference between the quasi-static and impact test methods is the disparity between deformation rates for the two test methods. This would affect the profile of the stress gradient within the ball, with further discrepancy arising from strain-rate sensitivities of some ball materials. This is particularly significant for some polymeric foams [109, 113], where the strain-rate sensitivity is substantially more influential at strain-rates typical of impact conditions (above 1000 s^{-1}).

In an attempt to resolve the contradicting findings in the literature [20, 25, 32, 51, 58], quasi-static compression was performed on the sliotar cores 204, 268, 206 and 217. The ball types were subjected to cyclic compression of three consecutive cycles to a maximum compression of 15 mm. Compression-rates of 0.5, 1, 2 and 3 mm/s were used, with tests on each sample separated by at least three hours to allow full strain recovery of the ball. The modern ball types exhibited a similar unloading profile for all compression-rates, indicating that the polymeric materials' strain relaxation was constrained by the machine platens retraction. This overlapping of unloading profiles was not as apparent for the traditional ball types, which showed that these ball types recovered at their natural rate thus providing more confidence in the hysteresis measurements for these ball types.

Consideration was given as to which of the cycles were most appropriate for comparison to impact behaviour. The residual strain induced by the first cycle reduced the energy necessary to compress the ball for the subsequent cycles, as seen from the reduction in area underneath the loading portions of the quasi-static force-displacement data curves, see Figure 4.14. The first cycle exhibited more experimental variability than the subsequent cycles, particularly for the traditional ball types, see Figure 4.15. This suggested a greater sensitivity of this cycle to variations in ball types such as imperfect sphericity and inconsistencies in yarn and cork distribution (seen in images of ball cross sections in Figure 3.10). The second and subsequent cycles exhibited more consistent behaviour for all ball types, with hysteresis increasing with compression-rate as would be expected, see Figure 4.18. Previous studies involving quasi-static compression have

used the data arising from the consistent behaviour beyond the first cycle [32, 58]. However, this behaviour consistency is associated with the unrelaxed strain for the initial compression, an occurrence that does not feature in dynamic impact.

Ultimately, the question of which cycle was most appropriate for consideration was not particularly relevant, with no apparent strong relationship between quasi-static and dynamic conditions. The quasi-static and dynamic viscoelastic characteristics are shown in Table 5.1. The stiffness and hysteresis values from the 15 mm quasi-static compression tests were compared to dynamic impacts with a COM displacement of 7.5 mm. This comparison was justified by both test conditions approximating a similar depth of ball material engagement. Both quasi-static compression and dynamic testing were carried out at comparable ambient condition (21 °C at 52 ± 2% RH for quasi-static testing, 22 ± 2 °C at 55 ± 10% RH for dynamic testing). Both tests involved the same ball samples to avoid being misled by intra-ball-type variation.

Table 5.1: Comparison of quasi-static and dynamic viscoelastic measurements

Ball type	Quasi-static stiffness [kN/m] 15 mm	Dynamic stiffness [kN/m] 7.5 mm (full range)	Quasi-static hysteresis 15 mm: 1st cycle 2nd + cycles	Dynamic hysteresis 7.5 mm (full range)
204	43.1 – 47.1	255.0 (242.6 – 267.7)	0.286 – 0.334 0.229 – 0.300	0.725 (0.627 – 0.791)
268	63.0 – 68.4	270.0 (230.0 – 304.5)	0.530 – 0.558 0.446 – 0.499	0.715 (0.602 – 0.782)
206	118.4 – 134.0	535.0 (393.0 – 602.0)	0.585 – 0.589 0.473 – 0.515	0.740 (0.642 – 0.781)
217	155.0 – 189.5	505.0 (381.3 – 608.4)	0.619 – 0.665 0.555 – 0.599	0.710 (0.589 – 0.785)

Comparative analysis of the quasi-static and dynamic stiffness indicated that there was no universal factor to translate between quasi-static to dynamic stiffness for all ball types, with dynamic stiffness generally being four to six times greater than the quasi-

static stiffness. The sequence order of magnitudes of quasi-static testing (204 → 268 → 206 → 217) did not reflect that of impact testing (204 → 268 → 217 → 206). Comparisons of quasi-static stiffness measurements of different ball types were misleading with respect to the balls' dynamic behaviour. Ball type 268 had a quasi-static stiffness apparently 46% higher than ball type 204, despite a difference of only 6 % between their dynamic stiffness values. Similarly, the quasi-static stiffness of ball type 217 was 30 to 40% greater than that of ball types 206 across the range of compression-rates, in contrast to ball type 206 exhibiting a marginally higher dynamic stiffness than ball type 217. The change in quasi-static stiffness with respect to compression-rate also did not reflect the change of dynamic stiffness with respect to speed, compare Figure 4.16 to Figure 4.23. This was evident from the quasi-static stiffness of ball type 217 increasing at twice the rate of ball type 206, despite both sharing a similar increase in dynamic stiffness with respect to speed.

Comparative analysis of the quasi-static hysteresis and impact kinetic energy dissipation yielded even less of a relationship than the stiffness results. Considering the first cycle hysteresis, the dynamic energy dissipation exceeded the quasi-static hysteresis by multiples of 2.5, 1.3, 1.3 and 1.1 for ball types 204, 268, 206 and 217, respectively. These multiplying factors changed to 3, 1.5, 1.5, 1.2 for the subsequent cycles' hysteresis. The disparity between the multiplying factors for different ball types suggested no correlation between impact energy dissipation and quasi-static hysteresis for consideration of either cycle. Moreover, the relative magnitudes of the quasi-static damping did not correspond to the sequence of magnitudes of the impact energy dissipation. This was particularly evident for ball type 204, whose quasi-static damping values were at most half the magnitude of the other ball types, despite all ball types having similar impact damping (within 5 %) at 7.5 mm COM displacement. This would suggest pronounced strain-rate sensitivity in the material of ball type 204.

The lack of any strong relationship between quasi-static and impact data was an indication of the difference in a ball material's long-term and short-term response. To put this in context, quasi-static compression in this present work was conducted in the range of 0.5 to 3 mm/s whereas impact testing in the range of 5 to 25 m/s involved compression rates in the region of 3000 to 13900 mm/s. The long-term behaviour

occurring in quasi-static compression was dominated by effects such as more uniform stress distribution, stress relaxation and delayed strain recovery. In contrast, dynamic impact conditions exhibit short-term behavioural effects such as polymer foam 'spring back', localised stress concentrations and wave propagation. As quasi-static compression cannot replicate these conditions, the quasi-static methodology could not be considered a useful predictor of impact behaviour and its usefulness in both the research and regulation of sports balls is highly questionable.

Dynamic impact conditions

The evaluation of dynamic viscoelastic characteristics required the construction of dynamic force-displacement data curves, where the displacement values represented the distance through which the force acted. Theoretically, the integral of the force with respect to this distance equates to the energy involved in this process. The impact consisted of the ball transitioning from an incident speed to zero speed at maximum compression, and subsequently to a rebound speed. Therefore the energies involved in the loading and unloading processes equalled the incident and rebound kinetic energies, respectively. Given the ambiguity in the literature regarding ball deformation, values of both diameter compression and COM displacement were considered in this study, see Figure 4.19. As seen in Figure 4.20, the COM displacement values were verified as being appropriate for viscoelastic characterisation by exhibiting an excellent agreement (R^2 = 0.98) with incident and rebound kinetic energies, where speeds were measured independently from high-speed footage. Consequently, this implied that the hysteresis area, the proportion of area enclosed within the loop, corresponded to the kinetic energy loss or damping. As mentioned in Section 5.2.3, the diameter compression was influenced by lateral expansion that was not perceptible to the axial load-cell. Therefore the diameter compression did not conform to the force data and was not appropriate for use in force-displacement data curves. From an experimental point of view, the appropriateness of COM displacement for viscoelastic characterisation was a convenient finding; avoiding the complications of limited sample rate (4 kHz) and dimensional accuracy (± 0.46 mm) associated with diameter compression measurement.

Non-linearity was discernible in the leading edge of the each force-displacement data curve, implying a variation of dynamic stiffness throughout the impact, see Figure 4.21. In the polymer ball types, an abrupt change in ball stiffness was observed to occur at 20 to 30% of maximum displacement for each impact, see Figure 4.21(a) and (b). This corresponded to the 'kink' discussed previously with regard to the force-time response. This abrupt change in ball stiffness was been reported previously as an inherent property of polymer foam, where a steep stiffness response at the initial stages of deformation corresponds to linear elastic foam cell wall bending [107-109]. In addition, the flattening of the ball curvature could also contribute to the initially high stiffness response of the polymer balls. The reduction in stiffness beyond the kink corresponded to buckling of the foam cells [104-109]. This effect has been described as "non-linear polymer softening", where similar effects were observed in softball impacts [27, 110]. Additional fluctuations in stiffness were due to wave effects propagating through the homogenous material. These wave effects were more pronounced for the compliant polymer ball 180, as evident from the oscillations in Figure 4.19 (c). The extent of separation of the force-displacement curves for different impact speeds is indicative of the strain-rate sensitivity of the polymeric ball materials: consider the markedly different stiffness values (profile gradient) at COM displacement of 2 mm for each impact speed in Figure 4.21 (a) and (b).

For the multi-compositional traditional ball types, the fluctuation in dynamic stiffness was due to different materials becoming involved in the compression at increased levels of deformation and the interaction between the different materials during this deformation. In ball type 206, the first 3 mm of deformation involved wound yarn with subsequent deformation involving the stiffer cork material. In ball type 217, the first 4 mm involved yarn, the next 3 mm involves a layer of compliant polyester and subsequent deformation impeded on a small stiffer cork core. Where the yarn and polyester layers were the dominant materials involved in the deformation (i.e. at lower speed impacts), a lower stiffness was exhibited due to the ability for the strands to slip over each other. As the ball became compressed beyond the yarn and polyester layers, the cork material presented a higher stiffness to the deformation. In addition to each material's individual contribution, the interaction of each constituent layer resulted in a

variation in stiffness. The high-speed footage showed that the yarn deformed in waves beyond the area of local deformation in ball type 206, see Figure 4.13(b). For ball type 217, the yarn and polyester layers were seen to bunch up and expand beyond the contact region in a more stable manner, see Figure 4.13(c). The fluctuant nature of wave propagation compared to gradual expansion accounted for the greater degree of variation in ball type 206 relative to ball type 217, see Figure 4.21 (c) compared to Figure 4.21 (d). The near-overlapping of the force-displacement data curves for each impact speed indicated little or no strain-rate sensitivity, see Figure 4.21 (C) and (D).

The fluctuation of dynamic stiffness throughout impact was simplified by approximating linear trends in two regions. These regions were divided by the change in gradient of the force-displacement curve that occurred at 20 to 30% of maximum displacement for all ball types. This produced two measures of dynamic stiffness, labelled 'initial stiffness' and 'bulk stiffness' (see Figure 4.22 for the evaluation of these stiffness measures). Such representations of dynamic stiffness do not appear to have been considered before in the literature. The two compound measures of dynamic stiffness is a useful method of encapsulating the viscoelastic material response. The measures of initial stiffness and bulk stiffness are advantageous in identifying a ball's viscoelastic strain and strain-rate dependencies. The two measures of stiffness were seen to increase with increasing speed for all ball types due to the strain dependence of ball stiffness, see Figure 4.23. The strain dependence of a ball's stiffness can be manifested from the flattening of the ball curvature [39], the increased engagement of constituent materials of dissimilar stiffness properties [58, 93, 94] and the material effects such as polymer softening [27, 110]. Strain-rate sensitivity arises from material's response to loading rate and has been reported as being prevalent in polymer foams [105, 107, 109, 113]. For polymer ball types 204 and 268, the bulk stiffness is less than the initial stiffness due the compliance arising from inherent strain-dependent polymer softening, see Figure 4.23(a) and (b). The initial stiffness can be attributed to both the strain-dependent curvature flattening and the strain-rate dependent response of the polymer foam. It is reasoned that the rate of increase of initial stiffness is predominantly due to the strain-rate sensitivities of the material, given that the highest magnitudes of the strain-rates occur during the early stages of impact.

For polymer ball type 204, the bulk stiffness does not change significantly with respect to speed, indicating little strain dependence with regard to the extent of material engagement. This is consistent with a previous theoretical study on polymer softballs that proposed that polymer softening was more dominant than any other form of strain dependence in the ball's stiffness response [110]. The bulk stiffness of polymer ball type 204 appears to reduce at speeds above 20 m/s, see Figure 4.23. This was attributed to the increased contribution of the strain-rate dependent initial stiffness at such speeds. In addition, the presence of surface wave propagation, the fluctuations evident in the high speed force-displacement data curves in Figure 4.21, result in difficulty in recognizing the initiation of bulk stiffness (R-squared value dropped from 0.98 to between 0.94 and 0.96), see Figure 4.22(c). The difference between the initial and bulk stiffnesses is not as pronounced for polymer ball type 268, indicating a smaller effect of polymer softening relative to ball type 204. In addition, the lower rate of increase of initial stiffness and the continuous increase in bulk stiffness suggests lower strain-rate sensitivity in ball type 268 relative to ball type 204, compare Figure 4.23(a) and (b). The greater strain-rate sensitivity of ball type 204 was also evident from the quasi-static testing, where its quasi-static hysteresis was half that of ball type 268 despite both having similar impact energy dissipation.

Differences in strain and strain-rate sensitivities of polymer foams could be attributed to the material cellular structure and properties, such as a variation in pore size and distribution, the morphology of matrix material (solid struts holding the pores open), and the open/closed cells (strain-rate effects due to air flow viscosity). The pore size and distribution of the polymer ball types, which relates to the density distribution of the material, was not adequately defined in the Shore A measurements of the polymer balls' internal structure (see Appendix D). While the internal material exhibited substantially lower Shore A values, no consistent trend in foam structure and hardness was distinguishable across the ball cross section. This was due to the Shore A measurements conducted in this work being motivated by the need to identify the sliotars' polymer grade for specification of prototyping materials, thus the hardness of the matrix material was of greater interest.

For traditional ball type 206, the initial stiffness was less than the bulk stiffness at lower speeds due to the dominant contribution of the softer yarn layer. The inner cork core became more engaged at greater deformations, resulting in the initial stiffness converging with and exceeding the bulk stiffness. For ball type 217, the initial stiffness was less than the bulk stiffness for all tested speeds due to the compaction of the relatively thicker layer of soft yarn and polyester. The stiffness response of the traditional ball types was dominated by the strain-dependence arising from incremental material engagement, as indicated by the greater increase in bulk stiffness with respect to speed and lower deviation between initial and bulk stiffness values, see Figure 4.23(c) and (d). The association of initial and bulk stiffness measures with viscoelastic strain and strain-rate dependencies illustrates the usefulness of the derivation of viscoelastic characteristics directly from impact data. This characterisation is fully representation of ball impact response, thus avoiding the short-comings of non-impact methodologies that have been employed frequently in the literature.

The comparison of the bulk stiffness values for the modern and traditional ball categories allowed the characterisation of two additional differences between the two ball categories that would have a significant effect on ball performance.

Firstly, the difference in stiffness magnitudes of the ball categories gave an insight into compliant-body impact characteristics that are more representative of the sport. The traditional balls were substantially stiffer than the modern types. The polymer ball types occupied a stiffness range from 230 to 300 kN/m; by comparison, the traditional ball types 206 and 217 exhibited bulk stiffnesses in the ranges of 400 to 600 kN/m and 380 to 600 kN/m, respectively. The difference in stiffness would be manifested as a difference in performance between the ball types for sport-representative compliant impact surfaces, where the rebound properties of an impact has been reported as being dependent on the relative stiffnesses of the impacting bodies [19, 79]. This disparity in stiffnesses between the two ball categories would result in a greater difference in performance than indicated by the rigid-body COR values in Figure 4.5.

Secondly, the difference in the rate of increase of stiffness indicates the speed-dependent behaviour of the ball categories. The polymer balls exhibited a lower increase in bulk

stiffness with increasing speed. For ball types 204 and 268, the bulk stiffness increased by approximately 10% and 36% over the range of tested speeds. In contrast, the rate of increase of bulk stiffness of the traditional ball types was significantly greater, with the magnitude increasing by approximately 47% and 65% for ball types 206 and 217, respectively. This corresponded to the difference in linearity of the ball types' COR behaviour. The greater increase in bulk stiffness of the traditional ball types, due to the progressively expanding involvement of distinct material layers, resulted in a greater non-linearity in coefficient of restitution values evident in Figure 4.5. This in turn accounted for the divergence in performance between the two different ball construction types.

Spring-theory numerical predictions

Two equations based on ideal spring theory have had frequent usage in the literature [18, 24, 25, 110]. The validity of these equations were investigated with regards to their relevance to dynamic impact values, see Figure 4.24.

The first equation, Equation 3.2 was a function of mass and contact time. It produced similar values for bulk stiffness for ball type 204, though deviated beyond impact speeds of 20 m/s. Numerical predictions of this equation were found to substantially underestimate the bulk stiffness for ball types 268, 206 and 217 by 10%, up to 46% and up to 54%, respectively.

The dependence of this equation on contact time included the limitations associated with this experimental measurement. As will be discussed in Section 5.2.5, the inertial effects of the impact assembly may have led to the overvaluation of the contact time by up to 25 %, particularly for ball types 217 and 206. Equation 3.2 was used to reverse calculate the contact time by setting the equation to equal the experimentally-measured bulk stiffness. This revealed that the contact times for ball types 268, 206 and 217 were consistently overestimated by 10%, 27% and 30%, respectively, for impacts above 10 m/s. This corresponds to the previous estimate of a 25% experimental error in measuring contact time for ball types 206 and 217 from the width of the force-displacement data

curve. While the equation itself seemed faultless when considering correct values of contact time, it proved difficult to experimentally measure the correct contact time despite rigorous system optimisation efforts. This indicates that this method of evaluating a measure of dynamic stiffness is limited unless using a validated measure of contact time, which proved to be a non-trivial challenge in this work.

The second spring-theory equation, Equation 3.3, was a function of ball mass, peak force and incident speed. The computed stiffness values from Equation 3.3 were found to have a reasonably good agreement with bulk stiffness for the polymer ball types, although underestimating the magnitude by 10%. It replicated the trend for bulk stiffness for ball type 206, although the magnitude discrepancy was less satisfactory at 15%. These underestimates illustrate the shortcoming of the underlying assumption that the ball acts as a linear spring, an assumption that is not applicable given the non-linear stiffness response of these ball types, see Figure 4.21. No satisfactory results were found when Equation 3.3 was applied to data of ball type 217, with significant diverging deviation of 20 to 35% observed between bulk stiffness and the equation result. This divergence highlighted the underlying assumption of this equation that the peak force coincided with maximum compression. Ball type 217 exhibited a double peak in the force-time curve – a characteristic of ball types with dissimilar material layers. Therefore, the peak force occurred a short time before or after maximum compression. This violated the energy balance assumption that was the basis of Equation 3.3, signifying that this equation was not appropriate for use in this ball type. While Equation 3.3 is comprised of more readily measured characteristics compared to Equation 3.2, the simplistic basis of Equation 3.3 on linear spring theory cannot represent the non-linear stiffness response exhibited by the ball types in this present work. While it yields a reasonable prediction of polymer ball stiffness, the unacceptable representation of ball type 217 provided by Equation 3.3 implies that it could not be implemented in sliotar guidelines as has been done for softball and baseball regulations [15].

5.2.5 Test system limitations

The measurement of lateral expansion posed a challenge, particularly for small values, due to the relatively low pixel resolution (210 x 128 pixels) and hence dimensional accuracy (± 0.46 mm) of high-speed footage. In addition to this limitation, the high-speed images had to be analysed carefully to disregard ball surface motion such as dust or yarn strand movement.

A change in gradient the restitution force profile caused difficulty in interpreting the exact time of breaking of contact of the ball against the impact plate. A steep restitution force gradient in both ball types 206 and 217 was seen to change abruptly to a more gradual force decline near the end of impact, see Figure 4.6(c) and 4.6(d). It was considered that the force measurement might have been influenced by the inertial effects of the impact assembly rather than exclusively representing the rebounding ball behaviour. As the ball restored its shape and began to rebound after maximum compression, the load-cell considered the movement of both the ball and the impact assembly (steel plate and M12 bolt). The deflection of the impact assembly, required for the force reading by the load-cell, was miniscule (0.03 mm at 4 kN loading) compared to the ball deformation (12 mm for 4 kN impact). Previous studies have concluded that load-cell compliance had a negligible effect on ball impact characterisation [46, 60]. For impacts that involved higher forces, such as impacts of ball types 206 and 217 above speeds of 20 m/s, the inertial retardation of the impact assembly (350 g relative to 90 g ball) may have resulted in the deflection of impact assembly failing to keep up with the ball rebound in the restitution phase. Therefore, it was reasoned that the rebounding ball behaviour might have been associated with the initially steep restitution gradient before the inertial effects of the load-cell became dominant with the more gradual force decline. This experimental error was encountered in an earlier design of impact assembly, as described in Appendix B. The redesign sought to minimise the mass of the impact plate; however it had to be sufficiently strong and thick to resist deformation in the impact process. The redesigned impact plate was bolted very tightly to the load-cell threads, and additional ceiling support and masses were attached to the test system to maximise rigidity and damp out vibrations. Despite these efforts, the inertial effects of the impact assembly were not completely eliminated. This signified that the contact

times measured from the total width of the force-time profile for ball types 206 and 217, as shown in Figure 4.8, were overestimated by approximately 25% at impact speeds above 15 m/s. There was little apparent effect on the impulse measurement due to the low amplitude of the force discrepancy at the end of impact. This implied that only the contact time and its dependencies, such as stiffness Equation 3.2, were influenced by this insurmountable experimental error, as evident from the 97% agreement between the impulse and differential momentum.

5.3 Prototype production discussion

5.3.1 Screening set of experiments

Arising from the controversial variation in performance of the sliotar in recent years, the Gaelic Athletic Association have considered the possibility of adopting a single standardised core for ball for use in championship matches. Given the divided opinions amongst players regarding preference of difference sliotar brands, it was decided to produce a new ball that exhibited consistent and repeatable playing characteristics. The moulding experiments conducted in this work have been the first steps in this process. The moulding of prototype cores involved an industrial collaboration with a thermoplastic injection moulding company. This collaboration involved the allocation of a moulding machine and the availability of a technician. The cost of the moulding experiments was in the region of €13,000 and took six months to complete. Three grades of polymer were used in this present work, categorised by their Shore A hardnesses of 55A, 70A and 80A. These polymer grades were specified based on the hardness measurements of approved polymer sliotar cores ranging from 60 to 75 Shore A. Two additional additives were also used: a blowing agent to reduce part density by creating porous foam, and a nucleating agent that altered the structure of the foam from coarse (fewer, larger cells) to fine (more, smaller cells).

As encountered with the initiation of manufacturing of any new product, a screening set of experiments was conducted to establish the manufacturing conditions and material compositions that allowed acceptable part production. The relatively large ball volume

(150.53 cm^3) posed a challenge in injection moulding. Such a volume required a substantial cooling time of six minutes, resulting in a cycle time of seven to eight minutes. Due to the semi-automated nature of moulding machines, the machine parameters (temperature, pressures etc.) required moulding of two cycles before a parameter adjustment took effect. This signified that the machine parameter adjustment was limited to at most four per hour until the appropriate value was converged upon.

The screening set of experiments consisted of two steps: the first task being to produce an acceptable ball shape and the second task involving the elimination of the manufacturing defects in these moulded products.

The first task was accomplished by adjustment of the machine parameters and composition. Occurrences of incomplete fill, see Figure 4.25, and surface eruptions, see Figure 4.24, were resolved by adjusting the blowing agent quantity and shot size. The potency of the blowing agent was found to be quite sensitive to the addition quantity. A usage of 1% was found to be most stable.

Once the shot size was defined, the plasticising delay time was increased to 60 seconds to allow the sprue to solidify, thus preventing over-packing from excessive material being forced into the cavity due to the plastising rotation of the screw.

Barrel temperatures were kept as low as possible to prevent material degradation, see Figure 4.27. Material degradation, to which polyurethane is particularly susceptible to, was a consequence of prolonged exposure of the material to high temperatures. Another aspect of material degradation is the hygroscopic nature of the polyurethane. Moisture contamination was found to occur to the material in the barrel and hopper despite sealing the hopper lid from the atmosphere. This resulted in a flaky product that crumbled when removed from the mould, see Figure 4.28. The moisture contamination was minimised by using small batches (0.4 kg) when transferring between the dryer and machine hopper, to limit the exposure time of the material to atmospheric moisture.

The mould temperature was kept at a constant 20 °C due to the observed dominating effect on ball geometry. For cold mould temperatures (< 15 °C), there was an increased likelihood of warpage due to shock cooling of the plastic. Too high a mould temperature

(> 20 °C) resulted in an increased cycling time and a greater probability of distortion of the unconstrained ball as it cooled in air, see Figure 4.26.

Successful production of acceptable ball parts was achieved for the 55A and 70A polymers grades, with inconsistent mouldings occurring for the 80A polymer grade. A large void was evident in the majority of the 80A mouldings, located at the top of the ball near the sprue as it resided in the mould, see Figure 4.34. Venting was increased to determine if a pocket of air was being trapped, but that was found not to be the case. It was theorised that the TPU 80A was too dense (1.13 g/cm^3 as opposed to 1.02 g/cm^3 and 1.04 g/cm^3 for the 55A and 70A grades, respectively) and so it was pooling in the mould. Increasing the blowing agent quantity permitted a more complete fill at the expense of increased cooling time (10 to 15 minutes) and structure stability. The lack of consistency with the increased risk of material degradation and surface rupture indicated that the 80A material grade was not suitable for this process. A rotating mould or a less dense material could be used to resolve this issue.

The nucleating agent was observed to be compatible with the 55A and 70A polymers grades up to addition rates of 5% and 10%, respectively. Quantities of nucleating agent in excess of these values were found to produce distorted ball mouldings, see Figure 4.33. This was attributed to the nucleating agent advancing the rate of material crystallisation to an extent that the expansion caused by the blowing agent was inhibited.

The second task of the screening set of experiments was to resolve the remaining manufacturing defects once the consistent moulding of an acceptable ball part was achieved. These manufacturing defects were typical of the injection moulding process and included cold slugs, flow markings, non-uniform mix distribution and voids.

The presence of a cold slug in the surface of some mouldings was evident in the early stages of production, see Figure 4.30. This was attributed to material seeping into the sprue under the blowing agent pressure in the time between mouldings, with this piece solidifying and becoming embedded in the surface opposite the sprue in the next moulding. A shut-off nozzle was fitted to the barrel to resolve this by preventing material from entering the sprue unless injected.

Flow markings were apparent in all moulded balls, see Figure 4.26. These markings were the boundaries of the extruded stream that entered the cavity via the sprue. As this stream flowed into and filled the cavity, the boundaries did not merge but merely packed together. It was reasoned that this was due to a thin layer of the stream solidifying from contact with the sprue surface as it entered the cavity, resulting in a discontinuous compaction into the spherical shape. On occasional mouldings, the flow lines acted as points of weakness, resulting in cracking propagating along flow lines. This issue was countered by slight adjustments of cooling time and blowing agent quantity, as well as ensuring that material degradation was not occurring. The principal reason for material degradation was the long resident time of the material in the heated barrel. Purging the barrel for cycle times exceeding 10 minutes mitigated this issue.

Non-uniform mix distribution was observed for initial mouldings of new material compositions. This was resolved by setting a high back pressure (30% relative to 2 or 3% for typical moulding applications). This ensured a more thorough mixing during plasticising to provide the uniform mix distribution. Using a pepper grinder type device, the blowing agent pellets were ground to 1.5 mm particles, see Figure 4.35. In addition to promoting a more even material distribution, it eliminated the formation of internal voids that were caused by concentrated pockets of blowing agent, see Figure 4.31.

5.3.2 Variant prototypes discussion

With ball mouldings being produced to an acceptable quality by the machine parameters and material compositions determined from the screening set of experiments, the final task of the moulding experiments was to produce a range of ball types with distinct properties. This resulted in the consistent production of six ball variants. The 55A polymer grade was moulded with 0%, 2.5% and 5% nucleating agent and 70A polymer grades was moulded with 0%, 5% and 10% nucleating agent.

The mass measurements showed that the 70A variants were marginally heavier and the 55A variants were slightly smaller than the target mass of 90 g, see Figure 4.38. Interestingly, these mass values were between 1 and 3 % greater than their respective

values when measured at the time within 10 minutes after time of production. As the TPU material had been dried before production due to its hygroscopic nature, the subsequent moisture absorption of the ball material resulted in an increase in ball mass. This indicates that future production should account for the slight mass increase in the polyurethane material due to its absorption of atmospheric moisture. The introduction of nucleating agent was seen to result in a wider variation of sample masses within each variant type. This could be attributed to the additional material causing increased agitation during mixing of the melt in the barrel, resulting in a slight variation in shot size.

The different polymer grades of 55A and 70A were seen to affect almost exclusively the ball stiffness, with marginal contribution on ball COR. The 70A polymer grades exhibited substantially higher peak forces (see Figure 4.39) and bulk stiffness (see Figure 4.41) than the 55A grades, which was expected given the higher material hardness of 70A. The difference between the two polymer grades was more pronounced for the bulk stiffness measures than to the initial stiffness measures, see Figure 4.41 compared to 4.40. The lower discrepancy between the initial stiffness values of the two polymer grades could be attributed to the ball's having the same radius, thus having a similar surface curvature flattening response. The difference between initial stiffness and bulk stiffness for each prototype variant indicated the presence of non-linear polymer softening, as had been observed for approved sliotar polymer cores.

The 70A polymer grade behaved similarly to the sliotar core 204 in terms of peak forces and stiffness measurements, an unsurprising result given that ball type 204 had been measured at 75A. The 70A polymer grades were seen to have a slightly greater rate of increase in initial stiffness relative to the sliotar core, see Figure 4.40. As discussed in Section 5.2.4, the rate of increase in initial stiffness was indicative of material strain-rate sensitivity. This suggested that the 70A polymer grades exhibited slightly greater strain-rate dependence than the sliotar core. There was little discernible difference between the 55A and 70A grades in terms of the coefficient of restitution magnitudes, see Figure 4.38. The 70A polymer grades were seen to have a more non-linear trend with respect to speed, analogous to the behaviour of the sliotar core 204. This could be attributed to the 70A polymer grade sharing similar stiffness characteristics as the sliotar core 204, both

of which were greater than the stiffness magnitudes of the 55A grades, see Figures 4.40 and 4.41. This COR-speed relationship dependence on ball stiffness is consistent with previous discussion in Section 5.2.4 with regard to comparison of traditional and modern sliotar cores. By this analogy, the 70A polymer grades exhibited a greater stiffening behaviour (strain dependence) than the 55A grades. This would indicate a more heterogeneous variation in material cellular structure in the production of the 70A polymer grade.

While the change in stiffness induced by the different polymer grades resulted in only a marginal difference in COR magnitudes, the different polymer grades would have a significant effect on ball performance by altering the trend of COR with respect to speed. In addition, the adjustment of ball stiffness as achieved from the selection of polymer grades would have affect performance in terms of sports-representative compliant body impacts. As an aside, it is speculated that if the 80A grade were successfully moulded, assuming a linear extrapolation, it would still be excessively livelier than the sliotar. In addition, given that the 70A polymer grade was in the correct range of stiffness relative to the sliotar core, the 80A polymer grade would most likely have provided excessive impact force.

The addition of nucleating agent to the polymer grades was found to decrease the coefficient of restitution slightly, see Figure 4.39, and increase the peak force slightly, see Figure 4.40. These marginal differences could be attributed to either the increased masses of these ball types or to a change in properties of a finer nucleated cell structure. The change in stiffness of the nucleated cell structure was not large compared to the different polymer grades, see Figures 4.40 and 4.41. The nucleating agent seemed to have a more erratic effect with the 55A polymer grade than the 70A polymer grade. The increment addition quantities of the nucleating agent was not reflected in the data, particularly for the 55A grade, where the shift in COR produced by the 5% addition was significantly greater than twice the deviation of the 2.5% addition, see Figure 4.38. This suggested a non-linearity in the quantity/effect characteristics of the nucleating agent. The 2.5% addition of nucleating agent in the 55_b variant produced only a slight decrease in COR (see Figure 4.38) and slight increase in initial stiffness (see Figure 4.40), but exhibited a more pronounced deviation in bulk stiffness (Figure 4.41) which

may account for the slightly higher peak forces. This change in performance did not logically progress with the increased addition of 5% nucleating agent, which exhibited a large deviation in initial stiffness (Figure 4.40) which resulted in a greater magnitude of energy dissipation as evident from the lower COR values, see Figure 4.38. A possible reason for the erratic behaviour of the nucleating agent was that it was reaching critical levels in the polymer grade. Batches of 55A polymer grade with greater than 5% nucleating agent were incapable of being acceptably moulded due to the inhibition of the blowing agent action by the crystallisation induced by the nucleating agent. Therefore, the 5% addition rate used may be near the 'saturation' level of the polymer grade, thus having a more pronounced effect on ball behaviour. The erratic effect of the nucleating agent was not as apparent for the 70A polymer grade, with additional levels of nucleating agent see to produce incrementally smaller COR values (Figure 4.38) and larger peak force, initial stiffness and bulk stiffness values, see Figures 4.39, 4.40 and 4.41.

With regards to the replication of the approved sliotar's behaviour, the selected material grades and additives did not meet the performance targets in terms of COR. This was particularly evident for their measured coefficient of restitution values, where the values of the prototype balls (0.56 to 0.62 at 20 m/s) were greater than provided by the approved sliotar core (0.48 to 0.49 at 20 m/s). The shift in COR induced by material grade or nucleating agent was very small in comparison to the target COR, where prototypes' CORs were approximately 25 % greater than the approved sliotar core 204. The selected material grades and additives satisfied the stiffness criteria, but did not produce sufficient energy dissipative properties. The production of such energy dissipative ball mouldings would require further extensive experimentation with wide range of various materials and additives, a task beyond the time constraints of this project. Development is on-going with prospective manufacturers continuing moulding experiments to produce a ball representative of the sliotar performance.

5.4 Modelling discussion

For their simplicity and differing contributions to representing viscoelastic behaviour, three configurations of mathematical models were implemented in this present work. These mathematical models were featured in a range of publications with reported success [16, 18, 35, 36], although they tended to be based on a single ball type and limited experimental validation. The aim of the present study was to investigate the validity and applicability of these models when applied to more diverse ball types and more extensive impact conditions than those used in the respective publications. These models were applied to the four sliotar cores whose performance and viscoelastic characteristics were reported in this thesis. The phenomenological derivation of the parameters of the models is discussed with regard to their relevance to actual ball properties. The representation of sliotar behaviour by mathematical model with intuitive parametric values would be beneficial in future development of the production of a standardised core. There appears to have been no published research modelling the sliotar core.

5.4.1 Ball model accuracy

The progressive increase in parameter complexity from Model 1 to Model 3 resulted in an improvement in model accuracy in terms of replication of realistic force response. This was evident from the improving alignment of the model simulations and experimental data, see Figures 4.45, 4.51 and 4.58. The accuracy of the three models is expressed in terms of normalised root mean square error (NRMSE) in Table 5.2.

Table 5.2: Mathematical model accuracy (NRMSE) [%]

Ball type	Model 1	Model 2	Model 3
204 (polymer)	18.47 ± 1.74	8.43 ± 1.04	4.38 ± 0.63
268 (polymer)	17.21 ± 1.42	10.04 ± 1.20	5.03 ± 1.42
206 (cork &yarn)	17.84 ± 2.14	11.07 ± 1.51	6.96 ± 0.60
217 (cork, polyester, yarn)	18.60 ± 2.21	11.19 ± 1.69	5.16 ± 1.41

While Model 1 provided reasonable agreement with peak force, contact time and energy loss trends for ball type 204, this replication of experimental data was not evident in the other ball types, see Figure 4.45. The poor accuracy of this model, as from the relatively high NRMSE values in Table 5.2, was attributed to a two important failings. The limitations associated with the stiffness coefficient calculation (Equation 2.13) as a function of contact time, as discussed previously in Section 5.2.5, were present in the model implementation. The undervalued stiffness coefficient produced from the overvaluation of contact time would explain, in part at least, the poorer simulations of the peak forces for ball types 268, 206 and 217. A force-discontinuity, evident from the model force starting at a non-zero value (see Figure 4.43), arose from the direct dependence of damping coefficient on centre-of-mass (COM) speed. This resulted in a poor simulation of the compression and restitution gradients, implying that that the model-generated hysteresis could not be representative of impact energy dissipations, see Figure 4.45. In spite of this, the closer alignment of the predicted restitution profiles relative to the compression profiles indicated that an incremental rate of energy loss was predicted with increasing speeds, reflecting actual ball behaviour. This appropriate prediction of energy loss trend could be attributed to the derivation of the damping coefficient of Model 1, which was based on experimental COR data as per Equation 2.14. The magnitude of predicted energy loss was, however, undervalued by at least 10%. The near-parallel slopes of the predicted force-displacement curves for Model 1 indicated a speed-independent stiffness, a finding that was not reflective of experimental observations. The validity of this model deteriorated for higher speed impacts, as

evident from the average percentage difference increasing from 36% to 51%, 38% to 54%, 42% to 56% and 53% to 62% for ball types 204, 268, 206 and 217, respectively, see Figure 4.45

Model 2 provided a substantial improvement in simulation accuracy as evident from the significant decrease in NRMSE values, see Table 5.2. This model provided similar accuracy in simulating most ball types for full range of speeds, as indicated from the lack of a consistent increase in average percentage difference for the range of impact velocities, see Figure 4.51. The model simulation for ball type 217 was inferior to that of the other ball types, particularly for lower speeds where the average percentage difference was 17%, 25%, 28% and 47% for ball types 204, 268, 206, 217, respectively. One of the principal reasons for the increase in accuracy of Model 2 relative to Model 1 was the consideration of the damping coefficient c as a function of model parameter q and contact area, a method consistent with a number of publications [16, 36, 50]. However, the remaining dependence of the damping component on COM speed ensured that the damping component contributed more during the compression phase relative to the restitution phase given that the absolute magnitude of the COM speed was greater in the compression phase than in the restitution phase. This was evident from comparing the absolute amplitudes of the positive and negative peaks of the damping component in Figures 4.49. This resulted in overestimation of the latter stages of both the compression and restitution force profiles. The early prediction of the occurrence of the peak force resulted in loss of agreement of the model with both compression and restitution gradients, see Figure 4.50. The prioritisation of the model fit to the compression phase, as was implemented in this present work, led to an incorrect prediction of the declination of force at the end of impact and thus the model over-predicted the contact time. An increase in ball stiffness with respect to increasing speed was appropriately simulated, although the magnitude of this rate of increase was substantially overvalued, see Figure 4.51. Considering the model-generated force-displacement curves, this corresponded to an overvaluation of both the incident and rebound energies, see Figure 4.51. The effect of this overvaluation of impact energies varied between ball types, thus

not allowing any consistent correlation between predicted and experimental energy dissipation.

Of the three mathematical models investigated in this work, Model 3 provided the best agreement with regard to matching the experimental force profile for all ball types, see Figure 4.58. The superior accuracy of this model is demonstrated from the reduction in both average percentage agreement (see Figure 4.58) and NRMSE values (Table 5.2) relative to the respective values for the previous two models. It exhibited appropriate predictions for all four sliotar core types at all tested speeds, as indicated from NRME values within 7%. The inclusion of the exponent *a* allowed the model predictions to be skewed such that it achieved a reasonable fit with both the compression and restitution phases. It accounted for the double-peak feature of ball type 217 by simulating a higher pseudo peak force at high speeds (> 20 m/s) such that it provided a reasonable agreement to both compression and restitution phases, see Figure 4.57(d). It accurately predicted the appropriate magnitude and rate of increase of ball stiffness for all ball types with increasing speed, see Figure 4.58. However, the simplicity of the model did not allow the replication of the initial and bulk phases of the stiffness, thus not permitting direct correlation with these experimentally-measured values. The deviation at the end of the restitution phase resulted in an overestimation of the measurement of energy loss from the hysteresis loop, see Figure 4.58. The observed deviation was worth further consideration with regard to the evaluation of contact time. This force decline behaviour was discussed previously with regard to the experimental error attributed to the inertial effects of the impact plate interfering with the force signal at the latter stages of contact. The model predictions produced a substantially smaller contact time, in ascending order, for ball types 268, 217 and 206. The order of the discrepancies' magnitudes matched those of the stiffness measurements' deviations, suggesting that this model could be used to provide an estimation of the contact time.

In summary, Model 1 did not provide sufficiently accurate simulation of impact behaviour despite being used in previous publications with reported success [18, 35]. The diminishing accuracy of this model with increasing impact speed and the poor replication of some ball construction types (arising from its sensitivity to the measurement of contact time) indicate that this model is unsuitable for modelling sliotar

ball impact. Model 2 provided a much better simulation of a ball's viscoelastic behaviour than Model 1 due to the more appropriate values of stiffness coefficient and the dependence of the damping coefficient on contact area, thus allowing the force-time data curve to start at zero. This model could be regarded as the most universal of the three models: while it was inferior to Model 3 in terms of simulation' agreement with experimental data, the lack of parameter exclusivity to a given ball type (the exponent *a* in Model 3) ensured that it tended to be similarly applicable to all tested ball types. Model 3 was found to be superior to the previous two models in terms of simulating ball behaviour. The principal drawback of Model 3 is its dependence on phenomenological parameters, as will be discussed in Section 5.4.2. However, in terms of simulating viscoelastic impact response for a diverse range of ball types for a wide range of impact speeds, Model 3 provided the most accurate simulations of the three tested models. Such a model would be worth further investigation for consideration of a more expansive model, i.e. modelling sliotar impact against a hurley or pitch surface.

5.4.2 Phenomenological basis of model parameters

The most significant limitation to the models in this present work was the phenomenological basis of the model development: that being that the parameters were defined with seemingly arbitrary values such that the model simulations agreed with experimental data. Therefore, given the model's direct dependence on a set of experimental data, the model simulations were difficult to be transferred to impacts or ball types outside of the tested experimental conditions. The phenomenological limitation could be mitigated if the model parameters related to independently measured values from experimental methods such as quasi-static compression or stress relaxation. This present work does not seek to resolve this limitation, as other on-going studies are currently dedicated to this pursuit with more sophisticated modelling methods [26, 32]. However, as discussed in Section 5.2.4, quasi-static compression exhibited little significant relevance to dynamic impact conditions for the sliotar cores tested in this study, demonstrating the challenge of relating the parameters to independent measures of ball properties. In this present work, the phenomenologically-derived model

parameters are discussed with respect to the experimentally-measured viscoelastic characteristics to examine the possibility of any correlations.

Compared to experimental measures of stiffness and hysteresis, the stiffness and damping parameters used for Model 1 possessed appropriate units (N/m and Ns/m respectively) and magnitudes (ranging from 190 to 330 kN/m), see Figure 4.43. These units and general magnitudes compared favourably with actual experimental data, see Figure 4.23. However, the intuitive comparison between model parameters and real-world units is of little use in this model, as the stiffness and damping components implemented in Model 1 were not capable of accurately simulating ball impact behaviour.

Model 2 possessed magnitudes (200 to 450 kN/m) and units of stiffness that reflected ball properties, see Figure 4.49. This intuitive relationship between model parameters and real ball properties would be beneficial in developing a model in relating ball manufacturing conditions to ball performance. The relationship between damping parameter and actual ball energy loss was not immediately evident. The downward trend of the damping parameter conflicted with the trend directions of both the damping coefficient trends in Model 1 and experimentally-measured energy dissipation, see Figure 4.48(b). The magnitudes (in the region of 10^5) and units (Ns/m^3) of the damping parameter did not facilitate intuitive comparison with these other data sets. The sequence order of the damping parameters (268→204→217→206 in ascending order) matched that of the stiffness coefficients', though they did not correspond with the sequence order of experimental data (204/268→206→217 in ascending order of COR).

For Model 3, the damping parameters' magnitudes and trends were similar to those in Model 2. Again, there was no apparent link with actual ball properties, e.g. the damping parameter values of ball type 206 were double those of ball type 268 despite both having similar impact energy dissipation properties, see Figure 4.55(b) and (c) compared to Figure 4.4. The introduction of the exponent to this model, which has been seen to substantially improve the simulation accuracy, served to complicate the association between model parameters and actual ball properties. The exponential effect of *a* produced stiffness coefficient values with extremely large magnitudes, up in the region

of 10^{10}. These stiffness coefficients possessed non-simple units to account for the exponent. The disparity of exponent values did not permit absolute comparison of stiffness coefficients' values between models of different ball types. The stiffness coefficient values decreased with increasing speed, contrary to experimental data. These finding were consistent with the methodology employed by Carré *et al.* [16], although a power law based trend was found to have a better fit with the stiffness coefficients in this present work rather than the exponential fit used by Carré *et al.*. The sequence order matched experimentally measured stiffness (i.e. 206, 217, 268, 204 in descending order of stiffness).

The disparity in magnitudes and trends of the model parameters, particularly for Model 3, do not lend themselves to direct translation between model parameters and experimentally-measured properties. The stiffness values for all models, as measured from the slope of the model-generated force-displacement curves, were influenced by both the stiffness and damping components of the model, see Figure 4.49 and 4.56. Furthermore, the damping parameter seemed to have a greater effect on ball stiffness than the stiffness coefficient, see Figure 4.47 and 4.54. This finding detracted from the elegance of the mass-spring-damper model, where the spring was seen to exclusively represent the stiffness contribution while the damper was exclusively associated with energy dissipation. Indeed, these models may be too simplistic to allow the direct attribution of dynamic stiffness and energy dissipation to the stiffness and damping components, respectively.

Chapter 6: Conclusions

6.1 Developed test system

An automated test system was developed to conduct multi-parametric impact characterisation of the GAA sliotar. This has been the first comprehensive characterisation of the sliotar core. This test system had the ability to derive multiple impact characteristics at a velocity range representative of the sport, advancing on limitations identified in the regulations of other sports balls. In addition, this test system was used to overcome the short-comings reported with other methodologies of ball viscoelastic characterisation. The developed test system will serve as the platform for future official regulatory testing of the sliotar and further development of a standard core for the sliotar.

6.2 Performance characterisation

A divergence in performance characteristics, particularly with force and deformation data, was evident with increasing velocity. This highlighted the need for high-velocity impact characterisation for comprehensive quantification of ball performance properties. Traditional cork-based ball types tended to have marginally higher rigid-body COR values than the modern polymer ball types, with the traditional ball types exhibiting a more non-linear velocity relationship resulting in a divergence in liveliness at higher velocities. Modern ball types were found to exhibit a wider span of liveliness properties, due in part to quality control issues in manufacturing.

The conflicting reports about ball deformation quantification were addressed in this study. The equivalence of diameter compression and COM displacement was found to depend on ball type. The discrepancy observed between these two measures was accounted for by the presence of lateral expansion. Evaluation of both COM displacement and diameter compression values would be necessary for complete ball characterisation in terms of performance, viscoelasticity and model simulations. The use of COM displacement was found to be the appropriate measure of deformation for dynamic force-displacement data curves.

The derivation of dynamic stiffness directly from impact allowed the investigation of the appropriateness of quasi-static compression and spring theory numerical prediction, methods which have been utilised in regulatory standards. Quasi-static compression was found to have limited relevance to dynamic behaviour due to the inability to replicate the material short-duration response. Two equations based on ideal spring theory, that have had frequent use in the literature, evaluated stiffness values that agreed reasonably well with the bulk stiffness properties of modern polymer ball types but were limited in capability of representing the traditional ball types.

The non-linear stiffness response of all ball types was approximated by two measures labelled initial stiffness and bulk stiffness. These measures were found to be useful in interpreting a ball's viscoelastic strain and strain-rate dependencies. Modern polymer balls were shown to exhibit strain-rate sensitivity and traditional multi-compositional balls exhibited strain dependency. The larger increase of bulk stiffness of the traditional ball types over the range of tested velocities produced with the greater non-linearity of COR-velocity relationship of the traditional ball types. In addition to accounting for the liveliness non-linearity, the large difference between bulk stiffnesses of traditional ball types relative to the modern ball types would serve to distinguish the performance characteristics beyond that indicated solely by rigid-body COR characteristics.

6.3 Prototyping production

Ball mouldings were produced by extensive trials of injection moulding, where machine parameters and constituent material quantities were adjusted to produce acceptable quality parts. Six prototype variants were produced using different material grades and nucleating additives. The samples of each prototype variant exhibited reasonably consistent impact behaviour.

The polymer grade had a dominant influence on ball stiffness, where increased polymer hardnesses resulted in an increased ball stiffness that in turn increased the non-linearity of the COR-velocity relationship. The presence of nucleating agent decreased the ball liveliness, although the extent of contribution of the nucleating agent depended upon its

compatibility with the polymer grade. The prototype samples displayed significant viscoelastic strain-rate-behaviour as evident from rapidly increasing initial stiffness values, slightly more than that exhibited by the approved sliotar core. Other than inherent polymer softening, the prototypes had negligible viscoelastic strain-dependencies as seen from the near-constant bulk stiffness with respect to impact velocity.

Ultimately the prototype variants did not replicate the performance of sliotars that passed the current standard, where excessive liveliness was exhibited by the prototypes. Development is on-going with prospective manufacturers investigating of a broader range of materials and additives that would dissipate larger amounts of energy when deformed.

6.4 Mathematical modelling

Phenomenological mathematical models were developed to simulate the impact response of the sliotar core. This analysis employed three mathematical models that are comparable to those established in previous literature. Model 1 was found to be invalid due to the unsatisfactory prediction of three of the ball types due to the limitations associated with the calculation of the stiffness coefficient and the inappropriate evaluation of the damping component. Model 2 simulated the behaviour of all tested ball types with reasonable success, though requiring parameters derived from the experimental data. However, these parameters intuitively reflect realistic ball properties, implying that this model would be useful where consideration of intrinsic material properties is important (i.e. in relating manufacturing conditions to ball performance). In addition, Model 2 was described as the most universal of the investigated models as it did not require ball-specific parameter values.

Model 3 provides the more accurate simulation of the behaviour of all tested ball types, although this simulation required specific values of an exponent for each ball type for greatest accuracy. The dominating influence of the exponent signified that Model 3 was not universally applicable without evaluation of the ball-specific exponent value.

However, the superior accuracy of Model 3 would be useful in developing a more expansive ball model, e.g. modelling ball-surface interaction.

The shortcoming of all three models was phenomenological basis of the input parameters, i.e. the model simulated the data from which it was originally derived. In addition, the intuitive relationship between the model parameters and actual ball properties was not immediately evident. The damping parameters of Models 2 and 3 exhibited a decreasing downward trend comparable to coefficient of restitution data, but the magnitude and units bore no evident resemblance to actual energy loss properties. The stiffness parameters of the second model were appropriately representative of experimental data, although did not correspond to experimentally-measured stiffness given the compound measures of initial and bulk stiffness values. In Model 3, the huge magnitudes and non-standard SI units introduced by the use of the exponent exacerbated the attempt to translate between the stiffness parameters and actual stiffness properties. The issue of the phenomenological basis of these models could be alleviated by establishing the relationship between the stiffness and damping parameters and independently-measured stiffness and energy loss characteristics. As shown earlier in this thesis, quasi-static compression testing was not sufficient to describe impact behaviour. Other independent methods such as stress relaxation and the use of a split Hopkinson pressure bar apparatus have been critiqued in the literature, and so to date the relationship between an independent measurement methodology and dynamic impact conditions and hence model parameters has not been resolved.

6.5 Future work

Future work on characterising impact behaviour would involve further analysis of the material properties.

- Testing sectioned samples of the ball material would yield stiffness moduli characteristics, which could relate to initial and bulk stiffness properties (and hence strain and strain-rate dependence). Such testing could also allow the relationship between Poisson's ratio and ball deformation to be investigated.
- Further investigation of the materials' cellular structure cross sections using hardness testing and optical microscopy image analysis would allow the determination of foam cell size and distribution and morphology of the matrix material (the shape, orientation and alignment of the solid struts between the pores). This is particularly appropriate in the characterisation of prototype balls in developing a standard core.
- Correlation analysis of the relationship between COR and material characteristics such as density distribution, stiffness, pore volume, pore distribution, pore morphology and matrix material morphology.

Further work on characterising ball performance could include:

- Specific orientation testing – further investigation on the effect of ball orientation on the relationship between dynamic and quasi-static test data.
- Compliant-body impact testing – defining the contribution of ball stiffness to compliant body impact such as a hurley or turf section. Such work would involve a mechanical adaption to the existing test system.
- Wet condition impact testing - defining the contribution of water absorption to ball performance. Such work would involve a mechanical adaption to the existing test system.

Further work on prototype production:

- Characterisation (as per first three points) of produced balls as submitted from prospective manufacturers.
- Correlation analysis of these characteristics and manufacturing conditions (machine settings and material composition) to further establish relationship between ball manufacturing and performance.

Further work in ball impact modelling

- Investigation of the phenomenological basis of Models 2 and 3 to relate the model parameters to measureable ball properties, thus allowing implementation of these models without the need for experimental data fitting.
- Development of a mathematical model for improved simulation accuracy. This work could include a hybrid model, where multiple models are linked to represent the impact duration, i.e. using Model 3 to represent the material stiffness response of compression phase and Model 2 to represent stress relaxation response of the restitution phase.

References

[1] Image gallery [homepage on the Internet]. Gaelic Athletic Association. Accessed 14 Sept 2010. Available from: http://www.gaa.ie/gaa-news-and-videos/image-gallery/.

[2] King SJ. A history of hurling. Gill and Macmillan, Dublin. 1996.

[3] O'Maolfabhail A. Camán: 2000 years of hurling in Ireland. Dundalgan Press, Dubdalk. 1973.

[4] Gaelic Athletic Association. Official guide - Part 2 - Playing Rules of Hurling and Football. Dublin: 2007.

[5] Hassett L. Development and analysis of mechanical test standards for sliotars [dissertation]. National University of Ireland, Galway; 1998.

[6] Gaelic Athletic Association. Second draft specification for sliotar tests. 1999.

[7] Rogers R. Development of protective sporting equipment and sliotar test standards for the game of hurling [dissertation]. National University of Ireland, Galway; 1999.

[8] Gaelic Athletic Association. Annual report. 2004.

[9] Gaelic Athletic Association. Official guide - Part 2 - Playing Rules of Hurling and Football. 2008.

[10] BS 5993. Specification for cricket balls. British Standards Institution, London. 1994.

[11] ITF Technical Centre [homepage on the Internet]. International Tennis Federation. Accessed 12 April 2008. Available from: www.itftennis.com/technical.

[12] International Hockey Federation. FIH rules of hockey. Lausanne, Switzerland. 2009

[13] ASTM. F-1888. Standard test method for compression-displacement of baseballs and softballs. West Conshohocken, PA. 2002.

[14] ASTM. F-1887. Standard test method for measuring the coefficient of restitution (COR) of baseballs and softballs. West Conshohocken, PA. 2002.

[15] ASTM. F-2845. Standard test method for measuring the dynamic stiffness (DS) and cylindrical coefficient of restitution (CCOR) of baseballs and softballs. West Conshohocken, PA. 2010.

[16] Carré MJ, James DM, Haake SJ. Impact of a non-homogeneous sphere on a rigid surface. Proc Inst Mech Eng Part C. 2004; 218(3): 273-281.

[17] Cross R. The bounce of a ball. American Journal of Physics. 1999; 67(3): 222-227.

[18] Goodwill SR, Haake SJ. Spring damper model of an impact between a tennis ball and racket. Proc Inst Mech Eng Part C. 2001; 215(11): 1331-1341.

[19] Cross R. The coefficient of restitution for collisions of happy balls, unhappy balls, and tennis balls. American Journal of Physics. 2000; 68(11): 1025-1031.

[20] Cross R. Dynamic properties of tennis balls. Sports Engineering. 1999; 2(1): 23-34.

[21] USGA, R&A Rules Ltd. Initial speed test procedure. 1999.

[22] USGA, R&A Rules Ltd. Overall distance and symmetry test procedure (Phase II). 2004.

[23] NOCSAE. Standard performance specification for newly manufactured lacrosse balls. National Operating Committee on Standards for Athletic Equipment. 2006.

[24] Smith LV, Nathan AM, Duris JG. A determination of the dynamic response of softballs. Sports Engineering. 2010; 12(4): 163-169.

[25] Bryson JA. Impact response of polyurethane. [dissertation] Washington State University. 2009.

[26] Ranga D, Strangwood M. Finite element modelling of the quasi-static and dynamic behaviour of a solid sports ball based on component material properties. Procedia Engineering. 2010; 2(2): 3287-3292.

[27] Smith LV, Duris JG. Progress and challenges in numerically modelling solid sports balls with application to softballs. J Sports Sci. 2009; 27(4): 353-360.

[28] Bryson A, Smith L. Impact response of sports materials. Procedia Engineering. 2010; 2(2): 2961-2966.

[29] Kai M. Science and engineering technology behind Bridgestone tour golf balls. Sports Technology. 2008; 1(1): 57-64.

[30] Fuss FK. Cricket balls: Construction, non-linear visco-elastic properties, quality control and implications for the game. Sports Technology. 2008; 1(1): 41-45.

[31] Roberts J, Jones R, Rothberg S. Measurement of contact time in short duration sports ball impacts: An experimental method and correlation with the perceptions of elite golfers. Sports Engineering. 2001; 4(4): 191-203.

[32] Pugh A, Hamilton R, Nash D, Otto S. Characterization of the materials in golf ball construction for use in finite element analysis. Procedia Engineering. 2010; 2(2): 3231-3236.

[33] Carré M, James D, Haake S. Hybrid method for assessing the performance of sports surfaces during ball impacts. Proceedings of the Institution of Mechanical Engineers, Part L: Journal of Materials: Design and Applications. 2006; 220(1): 31-39.

[34] Iwatsubo T, Kawamura S, Miyamoto K, Yamaguchi T. Numerical analysis of golf club head and ball at various impact points. Sports Engineering. 2000; 3(4): 195-204.

[35] Haake S, Carre M, Goodwill S. The dynamic impact characteristics of tennis balls with tennis rackets. J Sports Sci. 2003; 21(10): 839-850.

[36] Cheng N, Subic A, Takla M. Development of a fast-solving numerical model for the structural analysis of cricket balls. Sports Technology. 2008; 1(2): 132-144.

[37] Daish CB. The physics of ball games. Hodder and Stoughton, London; 1981.

[38] Stronge WJ. Impact mechanics. Cambridge University Press. 2004.

[39] Goldsmith W. Impact: The theory and physical behaviour of colliding solids. Courier Dover Publications; 2001.

[40] Steele C, Jones R, Leaney P. Improved tennis ball design: Incorporating mechanical and psychological influences. J Eng Des. 2008; 19(3): 269-284.

[41] Steele C, Jones R, Leaney P. Human sensory evaluation of tennis balls for quality improvement. Proc Inst Mech Eng Pt B: J Eng Manuf. 2007; 221(5): 799-807.

[42] Cochran AJ. Development and use of one-dimensional models of a golf ball. J Sports Sci. 2002; 20(8): 635-641.

[43] Carré M, Haake S, Baker S, Newell A. The analysis of cricket ball impacts using digital stroboscopic photography. The Engineering of Sport: Design and Development. 1998:295–320.

[44] Dignall R, Haake S, Chadwick S. Modelling of an oblique tennis ball impact on a court surface. The Engineering of Sport: Design and Development (Eds A.Subic and SJ Haake). 2000: 185–192.

[45] Drane PJ, Sherwood JA, Jones JW, Connelly TP. The effect of baseball construction on the game of baseball. The Engineering of Sport 7. 2008; 2: 681-688.

[46] Duris JG. Experimental and numerical characterization of softballs [dissertation]. Washington State University. 2004.

[47] Frequently asked questions: More info on balls [homepage on the Internet]. BATA Baseballs Inc. Accessed 19 March 2008. Available from: http://www.batabaseball.com/faq.html#3.

[48] Arakawa K, Mada T, Komatsu H, Shimizu T, Satou M, Takehara K, et al. Dynamic deformation behavior of a golf ball during normal impact. Exp Mech. 2009; 49(4): 471-477.

[49] Arakawa K, Mada T, Komatsu H, Shimizu T, Satou M, Takehara K, et al. Dynamic contact behavior of a golf ball during an oblique impact. Exp Mech. 2006; 46(6): 691-697.

[50] Goodwill SR, Haake SJ. Modelling of tennis ball impacts on a rigid surface. Proc Inst Mech Eng Part C. 2004; 218(10): 1139-1153.

[51] Hendee SP, Greenwald RM, Crisco JJ. Static and dynamic properties of various baseballs. J Appl. Biomech. 1998;14: 390-400.

[52] Tanaka K, Sato F, Oodaira H, Teranishi Y, Sato F, Ujihashi S. Construction of the finite-element models of golf balls and simulations of their collisions. Proceedings of the Institution of Mechanical Engineers, Part L: Journal of Materials: Design and Applications. 2006; 220(1): 13-22.

[53] USGA, R&A Rules Ltd. Weight and size test procedure. 1999.

[54] Gorham D, Kharaz A. The measurement of particle rebound characteristics. Powder Tech. 2001; 112(3): 193-202.

[55] Wu CY, Li LY, Thornton C. Energy dissipation during normal impact of elastic and elastic-plastic spheres. Int J Impact Eng. 2005; 32(1-4): 593-604.

[56] Bridge NJ. The way balls really bounce. Physics education. 1998; 33(4): 236-241.

[57] Seifried R, Schiehlen W, Eberhard P. Numerical and experimental evaluation of the coefficient of restitution for repeated impacts. Int J Impact Eng. 2005; 32(1-4): 508-524.

[58] Strangwood M, Johnson ADG, Otto SR. Energy losses in viscoelastic golf balls. Proceedings of the Institution of Mechanical Engineers, Part L: Journal of Materials: Design and Applications. 2006; 220(1): 23-30.

[59] Faik S, Witteman H. Modeling of impact dynamics: A literature survey. International ADAMS user conference. 2000; 1-11.

[60] Duris JG, Smith L. Evaluating test methods used to characterize softballs. Proceedings of ISEA2004. 2004; 1-8.

[61] Cross R, Nathan AM. Scattering of a baseball by a bat. American Journal of Physics. 2006; 74(1): 896-904.

[62] Cross R. Grip-slip behavior of a bouncing ball. American Journal of Physics. 2002; 70(11) :1093-1102.

[63] Cross R. Bounce of a spinning ball near normal incidence. American journal of physics. 2005; 73(1): 914-920.

[64] Cross R. Measurements of the horizontal coefficient of restitution for a superball and a tennis ball. American Journal of Physics. 2002; 70(5): 482-489.

[65] Monk S, Davis C, Otto S, Strangwood M. Material and surface effects on the spin and launch angle generated from a wedge/ball interaction in golf. Sports Engineering. 2005; 8(1): 3-11.

[66] Carré B, Newell H. The dynamic behaviour of cricket balls during impact and variations due to grass and soil type. Sports Engineering. 1999; 2(3): 145-160.

[67] El Hor H, Linz SJ. Bounce of a particle: Oblique impact on structured surfaces. Chaos Solitons and Fractals. 2008; 36(1): 73-81.

[68] Arakawa K, Mada T, Komatsu H, Shimizu T, Satou M, Takehara K, et al. Dynamic contact behavior of a golf ball during oblique impact: Effect of friction between the ball and target. Exp Mech. 2007; 47(2): 277-282.

[69] Haake SJ. Impact problems of balls in tennis and golf. Transactions of the Japan Society of Mechanical Engineers. C. 1998; 64(623): 2318-2327.

[70] Doménech A. A classical experiment revisited: The bounce of balls and superballs in three dimensions. American journal of physics. 2005; 73(1): 28-36.

[71] Le Maitre R. Effect of temperature on bounce. 1989. Accessed on 20 Oct 2009. Available from www.oxfordcroquet.com/tech/rim/3/index.asp.

[72] Knowles K, Cooke A, Lennox T, Mastropietro S. Design of real tennis balls. The engineering of sport, research, development and innovation: Proceedings of the 3rd international conference on the engineering of sport. 2000. 43-50.

[73] Zhang J, Kikuchi N, Li V, Yee A, Nusholtz G. Constitutive modeling of polymeric foam material subjected to dynamic crash loading. Int J Impact Eng. 1998 5; 21(5): 369-386.

[74] Drane PJ, Sherwood JA. In: Characterization of the effect of temperature on baseball COR performance. Proceedings of the 5th conference of engineering of sport, M. hubbard, RD mehta, and JM pallis (eds.), international sports engineering association (ISEA); 2004. p. 59–65.

[75] Smith LV. Bat and ball test methods and performance characteristics. Amateur Softball Association; 2007.

[76] Liu TH, Chen YC, Hsieh CH, Smith RW. Analyses of polyurethane softballs on variable humidity conditions. Journal of Medical and Biological Engineering. 2009; 29(4).

[77] Kagan D, Atkinson D. The coefficient of restitution of baseballs as a function of relative humidity. The Physics Teacher. 2004; 42: 330.

[78] Kantak AA, Davis RH. Oblique collisions and rebound of spheres from a wetted surface. J Fluid Mech. 2004; 509: 63-81.

[79] Dong H, Moys MH. Measurement of impact behaviour between balls and walls in grinding mills. Minerals Eng. 2003; 16(6): 543-550.

[80] Gugan D. Experiments on the game of croquet: Bouncing and rolling balls. 2002. Available from: www.oxfordcroquet.com/tech/gugan1/index.asp.

[81] Smith L, Ison A. Rigid wall effects on softball coefficient of restitution measurements. The Engineering of Sport 6. 2006: 29-34.

[82] Carré M, Haake S, Baker S, Newell A. In: Predicting the dynamic behaviour of cricket balls after impact with a deformable pitch. The engineering of sport, research, development and innovation: Proceedings of the 3rd international conference on the engineering of sport. 2000. 177–184.

[83] Brody H. Bounce of a tennis ball. Journal of Science and Medicine in Sport. 2003; 6(1): 113-119.

[84] Haake S, Chadwick S, Dignall R, Goodwill S, Rose P. Engineering tennis-slowing the game down. Sports Engineering. 2000; 3(2): 131-143.

[85] Nathan AM. Characterising the performance of baseball bats. American Journal of Physics. 2003; 71: 134.

[86] Cross R. Impact of a ball with a bat or racket. American Journal of Physics. 1999; 67: 692.

[87] Jones JW, Sherwood JA, Drane PJ. Experimental investigation of youth baseball bat performance. The Engineering of Sport 7. 2008: 663-671.

[88] Sherwood JA, Drane PJ. An experimental investigation of the effect of use on the performance of composite bats. The Engineering of Sport 7. 2008: 673-680.

[89] Nathan A. Effect of ball properties on ball-bat coefficient of restitution. 2009. Accessed on 20 Apr 2010. Available from: http://webusers.npl.illinois.edu/~a-nathan/pob/.

[90] Fallon LP, Sherwood JA. In: A study of the barrel constructions of baseball bats. Proc 4th international conference on the engineering of sport; 2002.

[91] Kharaz A, Gorham D, Salman A. Accurate measurement of particle impact parameters. Measurement Science and Technology. 1999; 10: 31.

[92] Mikrotron GmbH. MC13xx Users Manual Rev 1.06. 2003.

[93] Penner AR. The physics of golf. Reports on Progress in Physics. 2003; 66: 131.

[94] Ranga D, Cornish J, Strangwood M. The role of materials and construction on hockey ball performance. The Engineering of Sport 7. 2008: 457-464.

[95] Nathan AM. Dynamics of the baseball–bat collision. American Journal of Physics. 2000; 68: 979.

[96] Dalton J. In: Compression by any other name. Proceedings of world scientific congress of golf, science and golf IV, St Andrews, Scotland; 2002. 22–26.

[97] Hocknell A, Jones R, Rothberg S. Experimental analysis of impacts with large elastic deformation: I. linear motion. Measurement Science and Technology. 1996; 7: 1247.

[98] Cordingley L, Mitchell S, Jones R. Measurement and modelling of hollow rubber spheres: Surface-normal impacts. Plastics, Rubber and Composites, 33. 2004; 2(3): 99-106.

[99] Fuss FK. Logarithmic visco-elastic impact modelling of golf balls. The engineering of sport. 2008: 45-51.

[100] Vikram B, Fuss FK. Non-linear viscoelastic impact modelling of cricket balls. The Impact of Technology on Sport II. 2007: 303-309.

[101] Singh H, Smith L. In: Describing the performance of cricket bats and balls. Proc IMAC-XXVI, Orlando, FL. 2008.

[102] Gugan D. Inelastic collision and the hertz theory of impact. American Journal of Physics. 2000; 68: 920.

[103] Falcon E, Laroche C, Fauve S, Coste C. Behavior of one inelastic ball bouncing repeatedly off the ground. The European Physical Journal B. 1998; 3(1): 45-57.

[104] Saha M, Mahfuz H, Chakravarty U, Uddin M, Kabir ME, Jeelani S. Effect of density, microstructure, and strain rate on compression behavior of polymeric foams. Materials Science and Engineering: A. 2005; 406(1-2): 328-336.

[105] Avalle M, Belingardi G, Montanini R. Characterization of polymeric structural foams under compressive impact loading by means of energy-absorption diagram. Int J Impact Eng. 2001; 25(5): 455-472.

[106] Chen W, Lu F, Winfree N. High-strain-rate compressive behavior of a rigid polyurethane foam with various densities. Exp Mech. 2002; 42(1): 65-73.

[107] Qi H, Boyce M. Stress-strain behavior of thermoplastic polyurethanes. Mech Mater. 2005; 37(8): 817-839.

[108] Viot P, Beani F, Lataillade JL. Polymeric foam behavior under dynamic compressive loading. J Mater Sci. 2005; 40(22): 5829-5837.

[109] Song B, Chen WW, Dou S, Winfree NA, Kang JH. Strain-rate effects on elastic and early cell-collapse responses of a polystyrene foam. Int J Impact Eng. 2005; 31(5): 509-521.

[110] Smith LV. Measuring the hardness of softballs. Proc IMAC-XXVI, Orlando, FL. 2008.

[111] Cochran AJ. In: Club face flexibility and coefficient of restitution. Proc. World Science Congress of Golf; 1998. 486–492.

[112] Fuss FK. Non-linear viscoelastic properties of golf balls. The Impact of Technology on Sport II. 2007: 207-221.

[113] Ouellet S, Cronin D, Worswick M. Compressive response of polymeric foams under quasi-static, medium and high strain rate conditions. Polym Test. 2006; 25(6): 731-743.

[114] Gibson LJ, Ashby MF. Cellular solids: Structure and properties. Cambridge University Press; 1999.

[115] Lakes R. Viscoelastic measurement techniques. Rev Sci Instrum. 2004; 75: 797.

[116] Price D, Jones R, Harland A, Silberschmidt V. Viscoelasticity of multi-layer textile reinforced polymer composites used in soccer balls. J Mater Sci. 2008; 43(8): 2833-2843.

[117] Menard KP. Dynamic Mechanical Analysis: A practical introduction. CRC; 2008.

[118] Chen W, Lu F, Frew D, Forrestal M. Dynamic compression testing of soft materials. Journal of applied mechanics. 2002; 69(3): 214-223.

[119] Chen W, Lu F, Cheng M. Tension and compression tests of two polymers under quasi-static and dynamic loading. Polym Test. 2002; 21(2): 113-121.

[120] Nicholls RL, Miller K, Elliott BC. Modelling deformation behaviour of the baseball. Journal of Applied Biomechanics. 2005; 21(1): 18-30.

[121] Subhash G, Liu Q, Gao X. Quasistatic and high strain rate uniaxial compressive response of polymeric structural foams. Int J Impact Eng. 2006 7; 32(7): 1113-1126.

[122] Bergström J, Boyce M. Constitutive modeling of the large strain time-dependent behavior of elastomers. J Mech Phys Solids. 1998; 46(5): 931-954.

[123] Strangwood M. Materials in golf. Materials in Sports Equipment, Woodhead Publishing Ltd. 2003:129-152.

[124] Adair R. In: The physics of baseball; the standardisation of balls and bats for recreational soft-ball. International symposium on safety in baseball and softball; 1997: 21-28.

[125] Miah A. New balls please: Tennis, technology, and the changing game. Tennis, Science and Technology. Blackwell Science: London. 2000: 285–292.

[126] Davis C. The role of technology in sporting performance. 2004. Accessed on 20 May 2009. Available from: http://core.materials.ac.uk/search/detail.php?id=2651.

[127] Blackwell J, Knudson D. Effect of type 3 (oversize) tennis ball on serve performance and upper extremity muscle activity. Sports Biomech. 2002; 1(2): 187-192.

[128] Cooke K, Davey PR. Tennis ball diameter: The effect on performance and the concurrent physiological responses. J Sports Sci. 2005; 23(1): 31-39.

[129] Chauvin DJ, Carlson LE. In: A comparative test method for dynamic response of baseballs and softballs. International symposium on safety in Baseball/Softball; 1997: 38.

[130] Adler P, Monticone R. Injuries and deaths related to baseball. Youth baseball protective equipment project final report.Washington, DC: Consumer Product Safety Commission. 1996: 1-43.

[131] Flynn T, Fennessy K, Horgan N, Walsh B, O'Connell E, Cleary P, et al. Ocular injury in hurling. Br J Sports Med. 2005; 39(8): 493.

[132] Saeed A, Khan I, Dunne O, Stack J, Beatty S. Ocular injury requiring hospitalisation in the south east of ireland: 2001-2007. Injury. 2010; 41(1): 86-91.

[133] Khan M, Flynn T, O'Connell E, Stack J, Beatty S. The impact of new regulations on the incidence and severity of ocular injury sustained in hurling. Eye. 2006; 22(4): 475-478.

[134] Crowley P, Condon K. Analysis of hurling and camogie injuries. Br Med J. 1989; 23(3): 183.

[135] Shewchenko N, Withnall C, Keown M, Gittens R, Dvorak J. Heading in football. part 3: Effect of ball properties on head response. Br J Sports Med. 2005; 39(supplement 1): 33-39.

[136] Proctor SK. In: The golf equipment market 1984 - 1994. Science and golf II: Proceedings of the 1994 world scientific conference of golf; 1994. 369.

[137] Subic A, Cooke A. Materials in cricket. Materials in Sports Equipment. Woodhead Publishing Ltd. 2003: 342–372.

[138] Rawlings Inc [homepage on the Internet]. Accessed 29 October 2010. Available from: www.rawlings.com.

[139] Yang CC, Lin YY, Chen CW, Lin CC, College TPE. The influence of softball COR for changing ball material. J Biomech. 2007; 40(2): 614.

[140] USITC. Certain cosftballs and PU cores therefor investigation no. 337-ta-190. United States International Trade Commission; 1985.

[141] Bois PA, Kolling S, Koesters M, Frank T. Material behaviour of polymers under impact loading. Int J Impact Eng. 2006; 32(5): 725-740.

[142] Kipp ME, Chhabildas LC, Reinhart WD, Wong MK. In: Polyurethane foam impact experiments and simulations. AIP conference proceedings; 2000. 313.

[143] Mills NJ. Finite element models for the viscoelasticity of open-cell polyurethane foam. Cellular polymers. 2006; 25(5): 293-316.

[144] Dixon S, Stiles V. Impact absorption of tennis shoe-surface combinations. Sports Engineering. 2003; 6(1): 1-9.

[145] Rosato DV, Rosato DV, Rosato MG. Injection molding handbook. Springer Netherlands; 2000.

[146] Bryce DM. Plastic injection molding: Manufacturing process fundamentals. Sme; 1996.

[147] Kamal MR. Injection molding: Technology and fundamentals. Hanser Verlag; 2009.

[148] Drobny JG. Handbook of thermoplastic elastomers. Plastics Design Library; 2007.

[149] Murphy J. Additives for plastics handbook. Elsevier; 2001.

[150] Banik K, Mennig G. Effect of mold temperature on the long-term viscoelastic behavior of polybutylene terepthalate. Polym Eng Sci. 2008; 48(5): 957-965.

[151] Private communication. John O'Connell, TCL Plastics Ltd, Dublin. April 2009.

[152] Private communication. Ronan Kennedy, Total Polymer Solutions Ltd, Dublin. April 2009.

[153] McKay SE, Robbins T, Cole RS. Modern sport and chemistry: What a golf fanatic should know. J Chem Educ. 2008; 85(10): 1319.

[154] Vikram B, Fuss FK. Non-linear viscoelastic properties and construction of cricket balls. The Impact of Technology on Sport II. 2007: 297-302.

[155] Singh R, Davies P, Bajaj A. Estimation of the dynamical properties of polyurethane foam through use of prony series. J Sound Vibrat. 2003; 264(5): 1005-1043.

Appendices

APPENDIX A: Test system development

A.1 System design considerations

An automated projection system has been designed to determine the characteristics of currently approved cores. The system had five main requirements:

1. To project at velocities of up to 38ms^{-1} – maximum velocity encountered in the sport.
2. To project without imparting spin – spin will cause an undesirable variation in rebound angles and velocities.
3. To project balls of slightly varying diameters – to allow for the small variation of diameters of currently approved cores.
4. Precise aim – necessary as the impact area is small due to the location of the load-cell and the small field of view of the high speed camera.
5. Fully automated – can be left running with minimal human supervision to allow for batch and repeatability testing.

There are many types of commercially available projection methods such as rotating discs or air cannons that did not fulfil the above criteria.

The rotating wheel pitching machine, shown in Figure A.1(a), was dismissed for two major reasons. Firstly, the friction of the wheels against the sliotar core would cause wear and potentially unravel the yarn-wound cores. Secondly, due to the imperfect sphericity of the cores, this method of propulsion would have poor aim, with manufacturers of these machines typically supplying their own make of ball for best accuracy.

The pneumatic cannon, as used by the ITF for testing racket strings as shown in Figure A.1(b), was rejected because the approved sliotar cores had slightly varying diameters, requiring barrels of various diameters for high velocity propulsion. In addition, the air pressure acting directly on the imperfect sphericity of the cores would cause them to rotate and spin. The pneumatic cannon with a sabot had the advantage of propelling a range of diameters of balls without spin, but this process was difficult to automate as the sabot exited the barrel after the ball. It also added complications having multiple projectiles, and so this method was also rejected.

The use of a rotational striker was also considered, such as a motor driving a reciprocating linear drive, See Figure A.1 (c). This mechanical system consisted of a rod had one end connected to the edge of a flywheel rotating at 2100 RPM, and the other end connected to a slider that slid up and down a linear rail that was connected to a piston, which was locked in a stationary position. When it was time to fire, the brake would release on the piston, the slider would lock onto the one end of the rail by an electromagnet or actuated gate, thus pushing the entire piston forward and propelling the ball. This design had the advantage that the velocity was easily achievable and that the piston was brought to a halt by its own accord at the start and end of the stroke. However this design was discarded due to it being relatively cumbersome, the difficulty in timing and achieving retention force for the mechanism that locks the slider to the rail, and the problem of overheating that would arise from the slider moving within the rail when the system was not being fired, as the flywheel would be constantly running to maintain its velocity.

The selected projection method was a pneumatic actuator (SMC C95SDB63-500), as shown in Figure A.1 (d). The core rested within a conical indent on the output of the actuator. This design allowed for a small variation in the diameters of the cores that it could project, and no spin was induced as the ball was propelled with unidirectional motion.

(a)

(b)

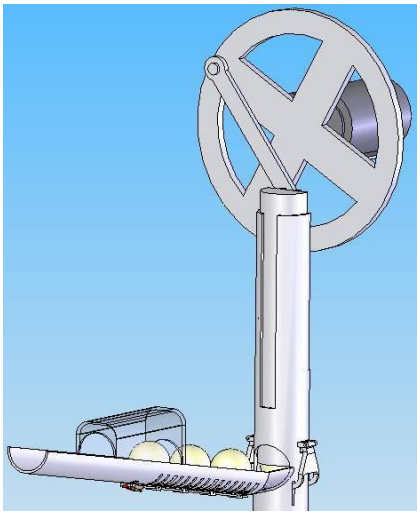

(c)

(d)

Figure A.1: Methods of ball projection: (a) rotating wheel pitching machine (b) air cannon, and (c) rotational reciprocating linear drive, and (d) pneumatic actuator

With the projection methodology decided, attention was turned to the design of the overall test system. An early design concept (December 2007) is shown in Figure A.2. For the purposes of clarity, this view shows only essential components and does not show parts such as casings, brackets or the enclosure sheeting. The overall enclosure frame is as large as reasonably possible, for maximum stability and rigidity yet considering the size of the room in which it will be placed. It may be fabricated in two or three sections and welded in situ if necessary for transportation reasons. The ball is to be fired vertically upwards to impact against the steel impact plate overhead. This orientation is considered most advantageous as it is travelling in the direction of gravity

before impact, thus eliminating variables by considering single dimensional motion. The ball will fall down on its own accord under gravity through the feeder channel system, where it will join the queue to re-enter the projectile mechanism.

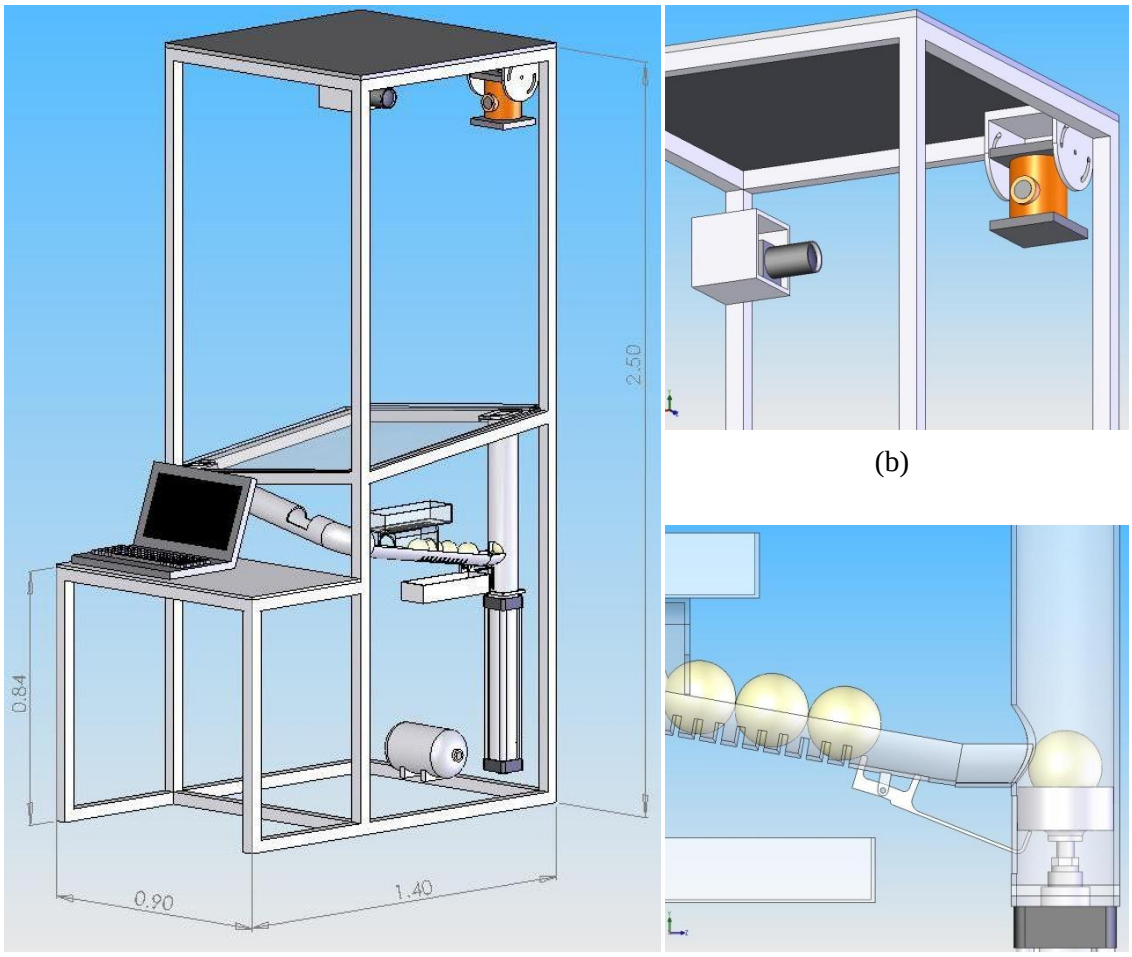

(a) (b) (c)

Figure A.2: Early design concept (a) system overview, (b) impact area, (c) firing area

The impact plate is to be fitted with a load cell to measure the impulse of the impact. The enclosure frame is sufficiently rigid and localised masses may be placed above the impact plate to ensure that it does not deflect under impact. The high speed camera will be mounted directly across from the impact plate, see Figure A.2 (b). The mounting of the pneumatic actuator will be dampened to minimize vibration of the overall rig, as vibration would have a drastic adverse effect on the accuracy of the high speed camera.

A sprung lever mechanism will allow one core at a time to enter the breech of the projection barrel, see Figure A.2 (c).

This design was further refined following specification of the pneumatic components (described in Section A.2) and consultation with workshop technicians with regard to feasible fabrication methods. The design as of April 2008 is shown in Figure A.3. This design modified slightly over the course of fabrication from July 2008 to February 2009, the most notable modification being the replacement of a large external frame with an internal frame suspended by vibration suppression bolts. The finalised design (as of August 2008) is shown in rendered images in Figure A.4.

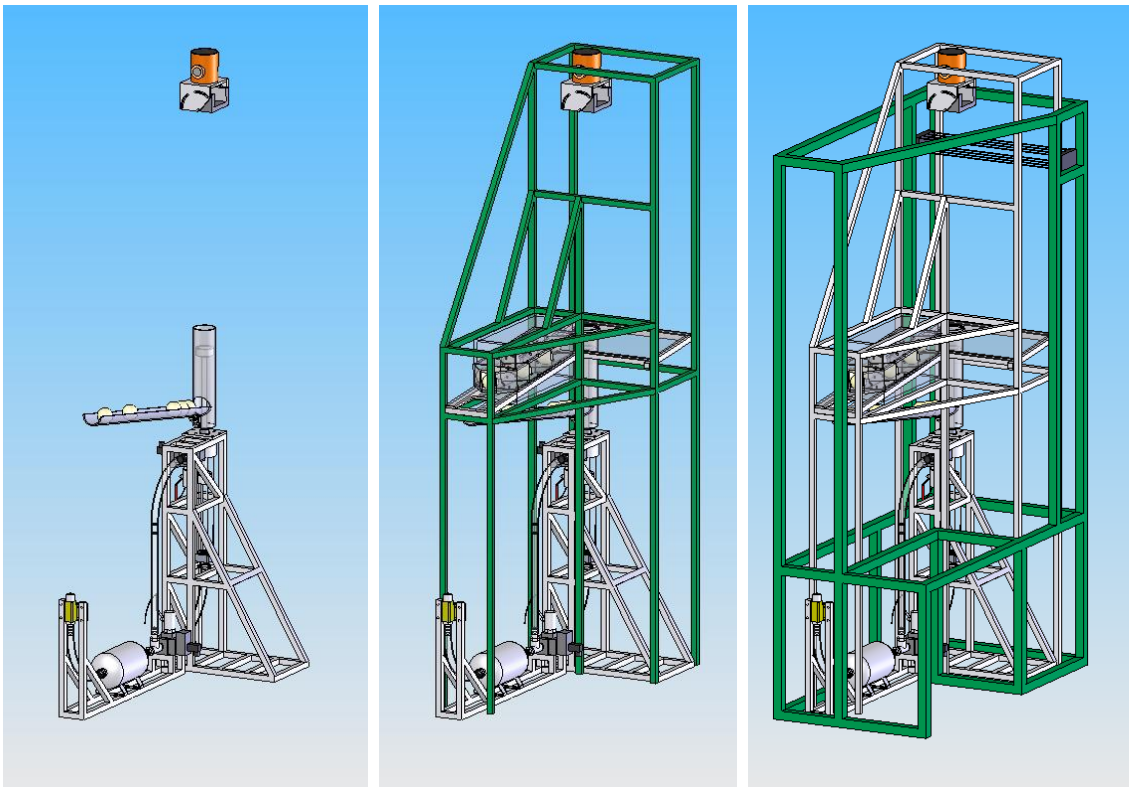

(a) (b) (c)

Figure A.3: Refined system design (a) pneumatic assembly, (b) system with impact frame, (c) system with external frame

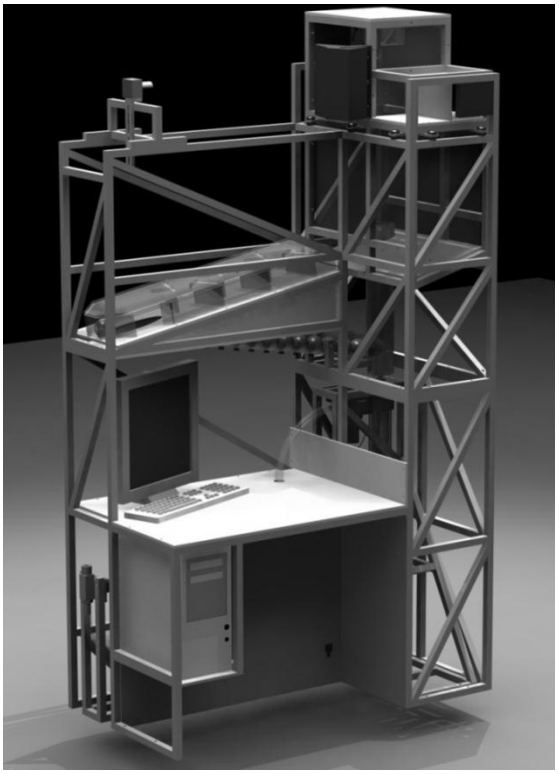

(a)

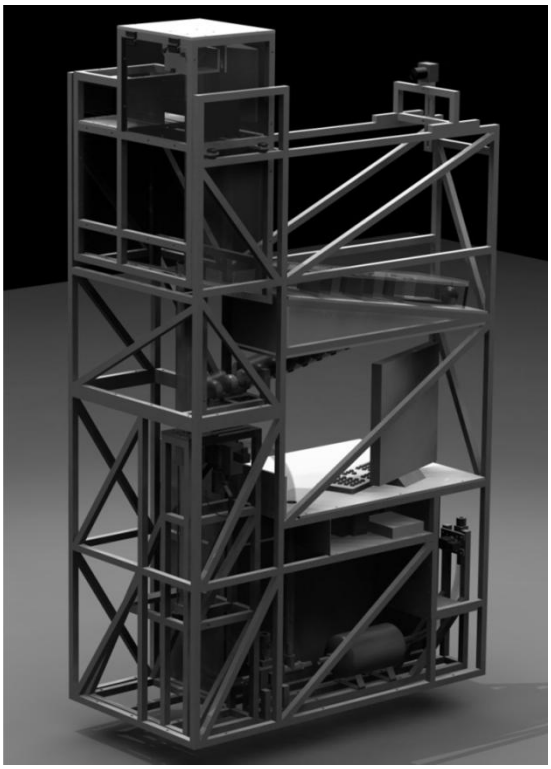

(b)

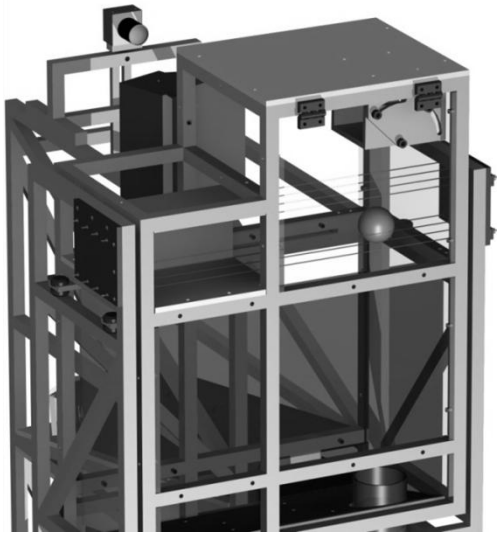

(c)

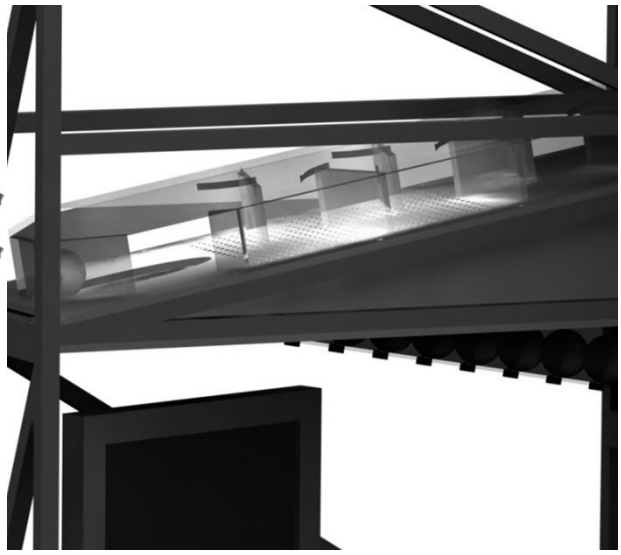

(d)

Figure A.4: Final system design (a) front view, (b) rear view, (c) impact area, (d) water conditioning unit

A.2 Pneumatic components selection and modification

Pneumatic actuators were specified in two ways: the bore (the internal diameter of the cylinder) and the stroke (the length of the cylinder through which the piston travels). It was necessary for the actuator to be reasonably compact, in order to be easily incorporated into the overall system, yet have a sufficiently large bore and stroke so that it could achieve the necessary velocities. Theoretically, larger bore actuators could accelerate more quickly due to the air pressure acting on the larger surface area of the piston. However, the maintenance of this accelerating pressure necessitated a sufficient flow rate into the actuator. The flow rate of gas through an aperture was dictated by a condition called choked flow, where the flow rate converged to a limit that was a function of the cross sectional area through which it was flowing, even if the back pressure was further increased [1, 2]. This was because the flow has reached sonic conditions (i.e. moving at the speed of sound) and a divergent nozzle would be required to accelerate the flow to supersonic velocities. The choked mass flow rate can be calculated from the following generalized equation [2]:

$$\dot{m} = C\,A\sqrt{k\,\rho\,P\left(\frac{2}{k+1}\right)^{(k+1)/(k-1)}} \qquad \text{[kg/s]} \qquad \text{(A.1)}$$

The discharge coefficient C related to flow through an orifice and was a function of the ratio of the pipe and orifice diameters. This geometry was not present in the pneumatic system, but typical values for the discharge coefficient were in the range of 0.6 – 0.7 [3]. To anticipate the worst possible scenario, C was taken to be 0.6 for these calculations. The cross sectional area A was the minimum cross sectional area that the flow passed through. The specific heat ratio k was 1.4 for dry air at 20 ˚C. The density ρ was 1.2 kg m^{-3} at 20˚C. The pressure P had a maximum of 0.8 MPa (8 bar), the maximum pressure rating on the valves.

[1] Emercon Process Control, "Control valve handbook," 2005.
[2] A. C. Walshaw and D. A. Jobson. (1979), *Mechanics of Fluids,*
[3] H. Robert, D. W. Green and J. O. Maloney. (1997), *Perry's Chemical Engineers' Handbook.*

The theoretical velocities for each of the standard dimensions of actuators were calculated, assuming that a 0.65kg piston accelerated with no inefficiencies under 8 bar pressure, with the flow choking at the aperture of the G1 sized (diameter 25.4 mm) ports. As can be seen in Fig A.5, larger bore actuators had a higher initial acceleration but were more susceptible to limitation by choked flow.

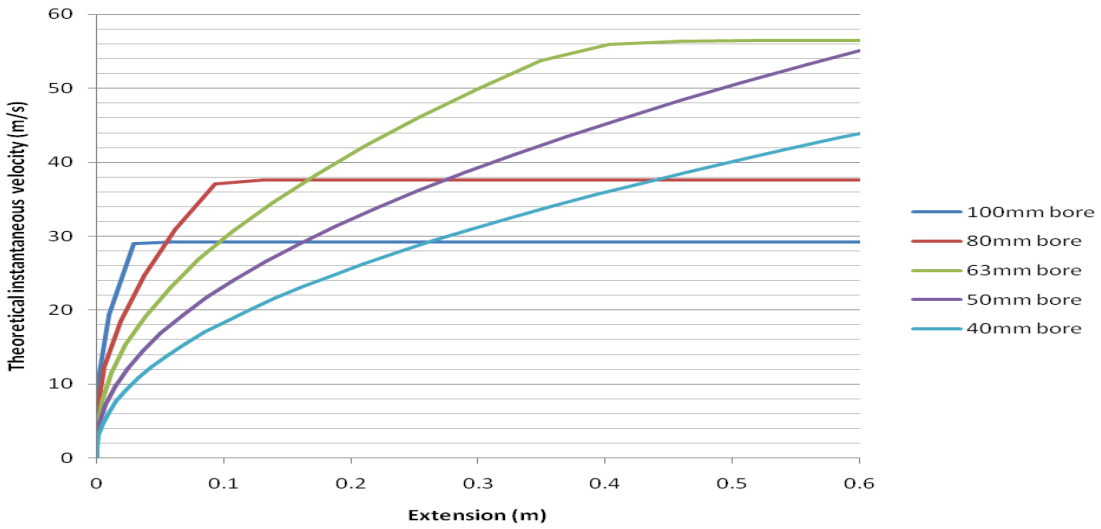

Figure A.5: Theoretical extension velocities of standard dimensioned pneumatic actuators

A bore of 63mm allowed acceleration to the highest velocity without choked flow restricting its extension. A sufficient velocity was theoretically achievable at 0.25m extension, so an overall stroke of 0.5m was deemed suitable. The chosen actuator was a C95SDB63-500 purchased from SMC Pneumatics. The maximum extension velocity of the actuator as bought was specified as 4 m/s. Due to the low load requirement for this project (mass of core is 90 g), a higher extension velocity could be achieved if two significant modifications were carried out to the actuator: to increase the port sizes of the actuator and to reduce the mass of the piston.

The first modification was to increase the inlet and exhaust ports of the actuator. This ensured that velocity of the piston was not restricted by choked flow developing at the entrance and exit apertures of the actuator. . The theoretical velocities for a 63mm bore actuator with standard dimension of ports were computed, assuming that a 0.65kg piston accelerated with no inefficiencies under 8 bar pressure.

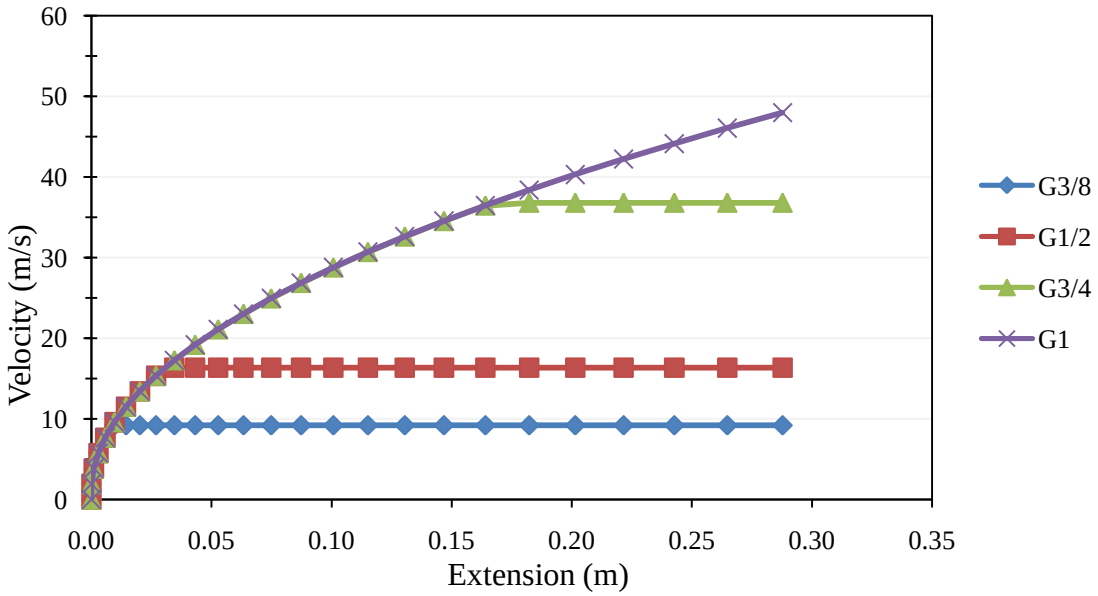

Figure A.6: Theoretical extension velocities for 63 mm actuator with standard dimensioned ports

Figure A.6 indicated that the extension velocity of the actuator with G1 ports would not be restricted by choked flow. The G3/8 ports on the purchased actuator were plugged, and the bottom endplate was bored and tapped for the G1 inlet port and a collar section was fitted for providing the G1 exhaust port.

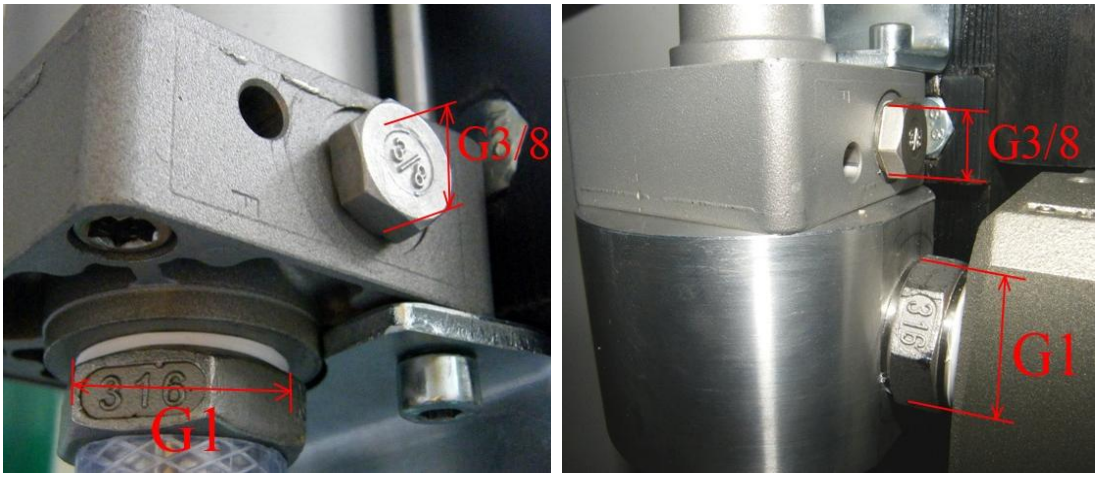

Figure A.7: Actuator port modifications

The second modification is to replace the piston by a lighter one. The original piston consisted of an aluminium alloy head with a steel rod, with a total mass of 2.08kg. In order to facilitate the desired acceleration, the mass of the new piston had to be in the region of 0.5 kg. This required the piston material to have a density of less than 1600 kg/m^3, signifying polymeric materials. There are several stages in prototyping polymer materials, with parts failing partly due to the trial-and-error nature of the control program development and partly due to the piston design. The first prototype piston assembly was constructed with a polyetheretherketone (PEEK) piston head and polyphenylene sulphide (PPS) rod. This piston assembly disintegrated under sustained impacts due to two major design flaws. Firstly, the pin joint used for joining the rod to the head was perpendicular to the axis of the rod, thus increasing the stress concentration in the rod. Secondly the recess for the rubber sealing O-ring caused cracking and eventually catastrophic failure. The second prototype piston assembly consisted of a Nylon6 and Nylon 66 piston head and rod respectively. This material was significantly cheaper and lighter, but marginally weaker than previous materials. The piston head was connected to the rod by an axial bolt, and the new design had no recesses or notches, instead using two solid precisely machined ridges for sealing within the actuator. Subsequent prototype iterations investigated different geometries to reduce the mass, with the final piston assembly consisting of a machined out Nylon 66 piston head, a hollow Nylon 66 piston rod, a lightweight Nylon output and a 6 mm aluminium threaded bar for holding the whole assembly in compression. Bump stops were fitted near both extremities of the piston rod to prevent the piston head impacting against the inside of the actuator end surfaces.

Figure A.8: Piston design iterations, from left to right: Original piston (too heavy), first prototype (disintegrated), second prototype, third prototype (optimized)

A.3 Pneumatic system control

The most significant challenge in the modification was the control of the piston. A control system with millisecond precision was developed to manage two 3/2 directional control solenoid valves that allowed air into either end of the actuator, this accelerating and decelerating the piston within the length of the stroke. The timings of these valves were critical, ensuring that the piston accelerated for as much as possible of the stroke, yet stopped before impacting against the top of the actuator. This was to avoid damage to the piston, as the plastic piston would break in high velocity impacts with the top of the metal actuator. It was not feasible to used shock absorbers due to their unsuitability to high velocities, and springs would cause minimal deceleration with additional complexities such as unpredictable piston retraction.

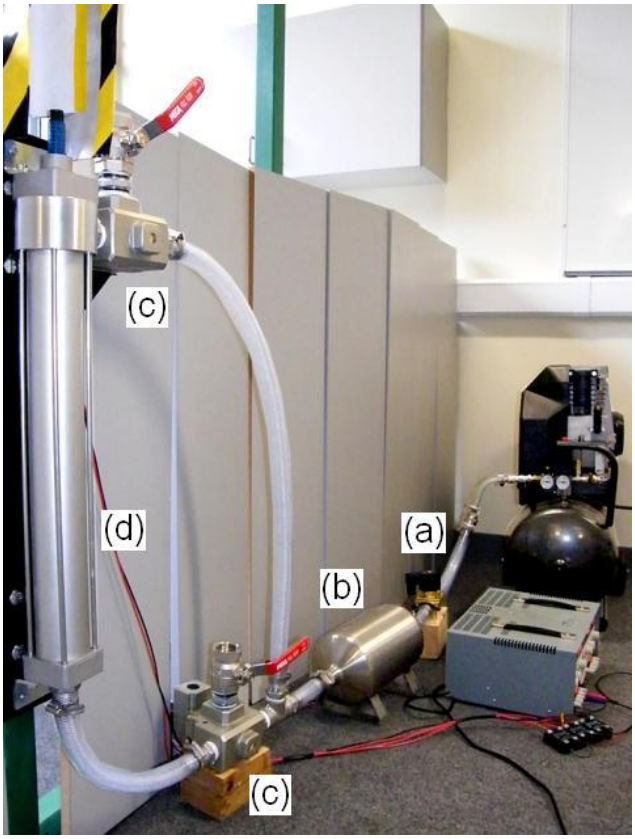

Figure A.9: Projection system under trial: (a) 2 way solenoid valve, (b) air reservoir, (c) 3/2 solenoid valve, (d) actuator

As shown in Fig. A.9, a two-way solenoid valve (SMC VP3165-105DA-Q) allowed air to enter the air reservoir from the high pressure air source. The air reservoir (Festo CRVZS-5) acted as a buffer, ensuring a quick supply of air to the actuator. Two large 3/2 solenoid valves controlled the flow into either end of the actuator, thus controlling the acceleration and deceleration of the piston. These large valves had G1 sized ports to avoid choked flow developing within them. With the same reasoning, large diameter PVC tubing was used between the air reservoir and the actuator, with the tubing bent at its minimum curve radius (25 cm) to keep the system was compact as possible.

The acceleration and subsequent deceleration of the piston was provided by controlling the valves that allow the high pressure air into the both ends of the actuator. As explained in Section 3.1.2, the valves were controlled by a LabVIEW program via digital outputs and relays. The high-speed camera was used to measure the extension

velocity and displacement of the piston in order to establish the optimal valve timings. A sample extension is shown Fig. A.10, the bottom valve was open for the duration between the green lines (31 milliseconds) accelerating the piston. The top valve was open for the duration between the red lines, 12 milliseconds after the bottom valve first opens, staying open for 32 milliseconds. Ideally the bottom valve would close before the top valve opens, but due to the response time of the valves, the bottom valve must be open for that duration in order to allow sufficient air through to provide the acceleration, hence the overlap when both valves were open.

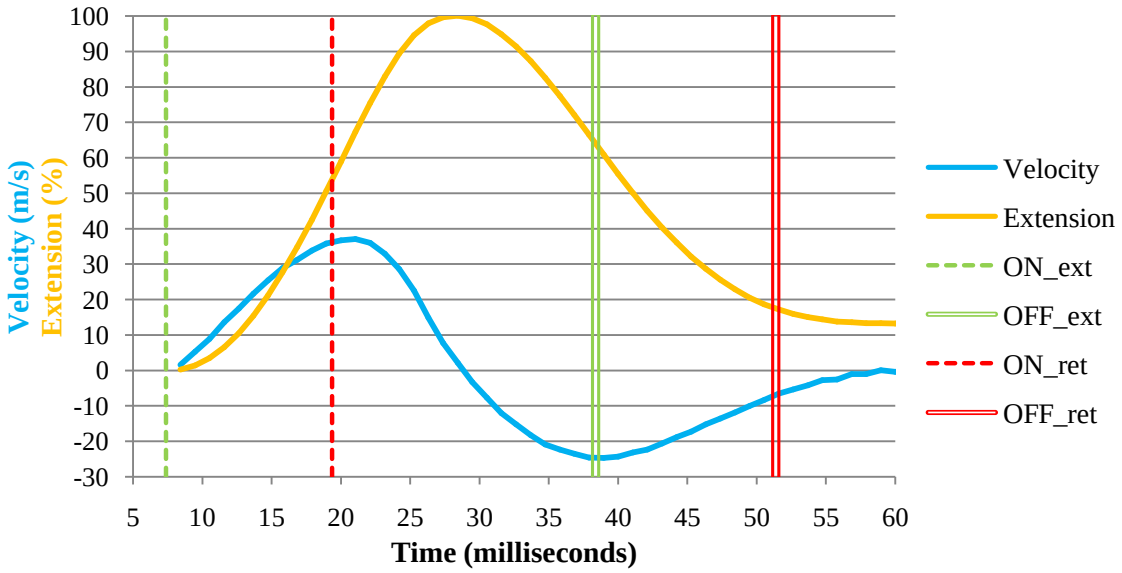

Figure A.10: Velocity and extension profile for Piston Prototype 2 at 8 bar pressure

Appendix B: Data acquisition equipment setup and calibration

B.1 High-speed camera setup and calibration

The calibration the high speed camera entailed three aspects: the dimensional precision, the camera frame-rate accuracy and the image processing accuracy. The high-speed camera in this present work was used at a setting of 230 x 160 pixels at 4000 frames-per-second (fps). The height of the camera was adjusted to the level of the impact plate such that it was perpendicular to the ball in contact with the plate. The camera was positioned on the rails level at a distance from the impact plate to give a field-of-view of 217 x 74 mm.

Using a calibrated chart in the camera's field-of-view, the dimensional precision was determined to be 0.46 mm per pixel. This implied a dimensional accuracy of ±0.46 mm/pix. Using another calibration chart with an orthogonal array of dots, lens distortion was found to be negligible. Due to the high frame-rate, only a small area in the centre of the sensor was used, thus avoiding the warping that could be present in the edges of the lens.

The camera frame-rate of 4000 fps provided a data resolution of ±0.25 milliseconds. The accuracy of camera frame-rate was verified experimentally to be 0.04% for a range of frame-rate setting by observing a motor of known RPM.

An image processing algorithm was written in LabVIEW to extract velocity and deformation from the high-speed footage. The velocity was measured from tracking the centre-point of the motion of the ball. The accuracy of the computation of this centre point was verified by manually going through several sequences of high-speed images. The deformation was measured from the algorithm computing the edge of the ball. The curvature of the ball implied a gradual transition in the image between the ball and the background. A matt black background was used and the lighting (two halogen floodlights, one halogen spotlight) was adjusted provide a high contrast between the ball and background. Furthermore, the image processing algorithm increased the image brightness/contrast/gamma settings to obtain a cleaner image. As before, the accuracy of the deformation measurement was confirmed from manual frame-by-frame analysis of the high-speed footage.

The cumulative accuracy of the camera and software was verified by recording a ball falling under gravity. The ball's velocity was calculated based on the height from which it dropped ($v = \sqrt{(2gh)}$). This yielded an experimental error of ± 0.8 %. The velocity measurement of the camera

was also verified by differential momentum and impulse measurement agreeing within 3%, as shown in Figure B.3. This will be discussed further in Section B.2.

B.2 Load-cell setup and calibration

There was an iteration of design of the impact assembly. The initial design consisted of a hard steel surface mounted on a securable aluminium pivot assembly, shown in Figure B.1. The impact plate was inclined at an angle of 4° to ensure that the ball did not re-enter the projection barrel from the rebound. A button compression load-cell, a Sensotec Model 53, was integrated within the impact plate for measuring impact force. The load-cell was placed in pre-compression of 30N between the impact assembly and the rebound chamber ceiling that was directly supported from the ceiling of the room. This strain-gauge type load-cell had a maximum rating of 4.4 kN with a maximum deflection of 76μm at maximum load. This impact plate assembly was used for the performance characterisation of the approved sliotar cores, including results in Figures 4.2, 4.2, 4.3, 4.5, 4.9.

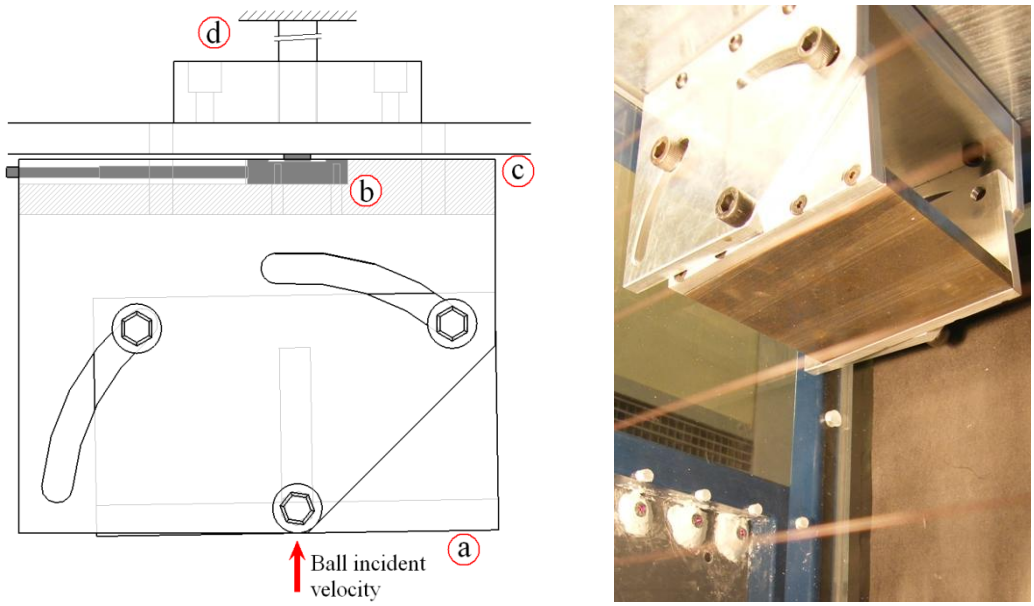

Figure B.1: Initial impact assembly (a) impact surface, (b) load-cell, (c) test system ceiling and (d) support to room's concrete ceiling

The impact assembly was later redesigned for two reasons to allow better measurement of force-time data. Firstly, the overloading of the original load-cell's capacity at high velocity impacts was resolved with a new load-cell with a maximum capacity of 24.5 kN. Secondly, the relatively large mass of the impact assembly (1.8 kg) between the ball and load-cell and issues caused discrepancies in the force measurement in the restitution phase of impact. This was resolved in the redesign, shown in Figure 3.4 and Figure B.2, where a lighter steel plate (350 g) was connected directly to the threaded load-cell. This impact assembly was used for the majority of experimental work reported in this thesis.

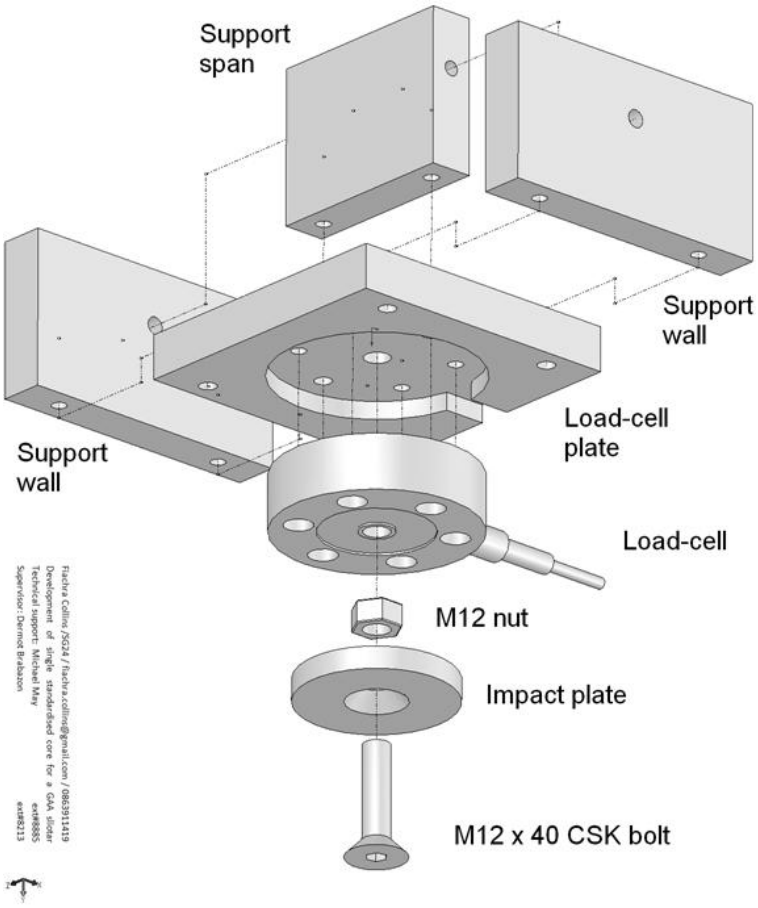

Figure B.2: Exploded view of redesigned impact assembly

The load-cell (RLU02500, RDP Electronics Ltd, UK) was calibrated using a compression testing machine (FB050TM, Zwick/Roell, Germany). The transducer amplifier (DR7DC, RDP

Electronics, UK) was adjusted to output a voltage of 10 V at 12 kN. The maximum of 12 kN rather than 24.5 kN was selected to allow greater data resolution as LabVIEW acquired data in the range of 0 to 10 volts. The calibration data, shown in Figure B.3, showed that the load-cell exhibited a linear voltage response with zero hysteresis.

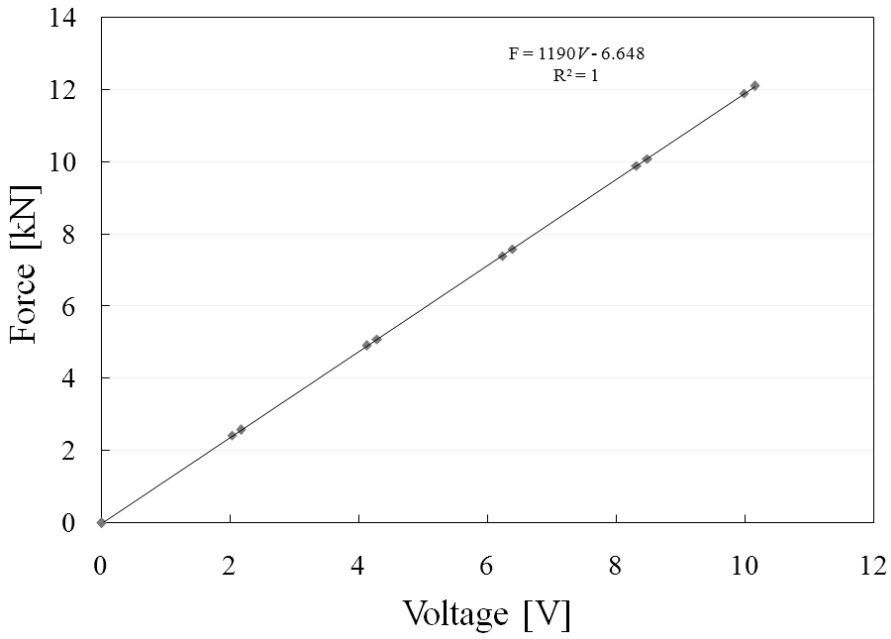

Figure B.3: Calibration data for load-cell

Verification of the calibration of both the load-cell and high-speed camera was provided by comparison of impulse with differential momentum, as shown in Figure B.4. Impulse was measured from the area underneath the force-time data profile for each impact. The differential momentum from calculated from the velocity measurements from high-speed footage. The variance of scatter relative to the linear trend was found to be within 3 %.

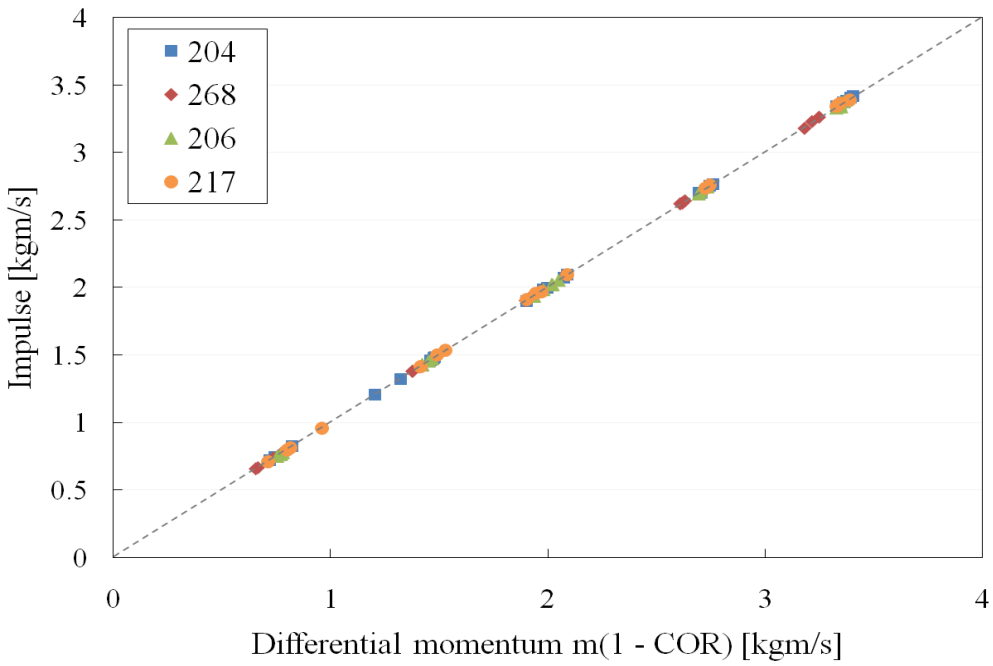

Figure B.4: Impact data verification: impulse Vs differential momentum

The verification of the calibration of the load-cell data indicated that the force-time signal appropriately represented the acceleration force of the ball's centre of mass. This was further demonstrated by the ratio of the initial and final COM velocity (first time integral of the force divided by mass) having a 98% agreement with the coefficient of restitution as independently measured from high-speed footage. This agreement is shown for three impact speeds (ball type 204) in Figure B.5.

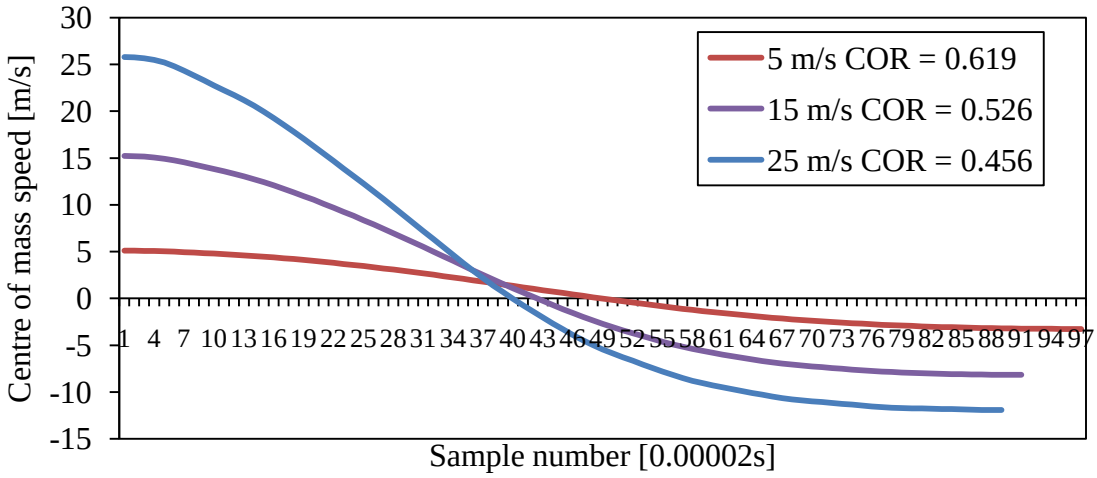

Figure B.5: Agreement between COM velocity extremity values and COR

B.3 Test system repeatability

The repeatability of system measurements was determined for two ball types (polymer ball type 207, cork-based ball type 217) for 10 impacts at both 10m/s and 20 m/s. These ball types were positioned at a constant specific orientation to avoid variations due to discrepancies in ball construction. The coefficients of variation for coefficient of restitution, peak force and diameter compression are shown in Table B.1.

Table B.1: Specific orientation coefficients of variation (10 impacts at 10 and 20 m/s)

Ball type	COR	Peak force	Diameter compression
207 (polymer)	0.47%	0.43%	3.2%
217 (cork, polyester, yarn)	0.57%	1.1%	4.3%

Further evidence of the repeatability of system measurements is shown by the relatively small error bars on all data graphs, where each marker represents 5 impacts separated by at least two minutes, indicating 95% confidence intervals (*t*-distribution). This is expressed in terms of coefficients of variation in Table B.2.

Table B.2: Test data coefficients of variation (5 impacts at 5, 10, 15, 20 and 25 m/s)

Ball type	COR	Peak force	COM displacement	Initial stiffness	Bulk stiffness
204 (polymer)	0.8 – 1.8%	1 – 3%	2 – 4%	6 – 11%	2 – 4%
268 (polymer)	1.4 – 2.3%	3 – 4%	2 – 6%	3 – 11%	3 – 8%
206 (cork &yarn)	1.0 – 1.9%	1 – 3%	3 – 5%	4 – 13%	2 – 6%
217 (cork, polyester, yarn)	1.4 – 2.0%	2 – 4%	4 – 6%	8 – 14%	4 – 8%

The relatively small coefficients of variation of the test data indicate excellent repeatability of system measurements. The slightly larger variation in the stiffness

measurements, particularly the initial stiffness measurement, was attributed to the subjective judgement of the fit of the linear trend to the force-displacement gradient. This relatively larger variation is not significant compared to the difference between ball types as discussed in this work.

B.4 Test system safety features

The system was designed with consideration to the user ergonomics. The workstation that contained the operating computer was placed at typical desk height. The data acquisition electronics and the pneumatic system components were easily accessible for adjustment and maintenance. Hazardous areas were shielded from the user: 3 mm aluminium sheeting surrounded the pneumatic components; the actuator output was shielded by a 5 mm transparent perspex tube; and the rebound chamber was clad with 10 mm perspex sheeting. Electrical safety was another important aspect in this system, considering that the system was connected to 220 V electricity and contained expensive electronic equipment, water and interaction with people. The electrical safety system, as shown in Fig B.6, was installed by a qualified electrician and conformed to the standards of the ETCI (Electro Technical Council of Ireland). Six sockets were fitted to the test system: two for the PC, two for lights, one for the camera power supply and one for 5V transformer. Each double socket was controlled by an independent 20 amp miniature circuit breaker (MCB). A key-release emergency stop button could cut power to two of the double sockets in the case of an emergency or maintenance. Since the abrupt shut down of the PC was undesirable due to risk of data loss, the first socket was independent from the emergency stop button. Another 10 amp MCB was located at the 24 volt output of the transformer. The entire steel frame of the system was earthed to prevent live leakage or static build-up.

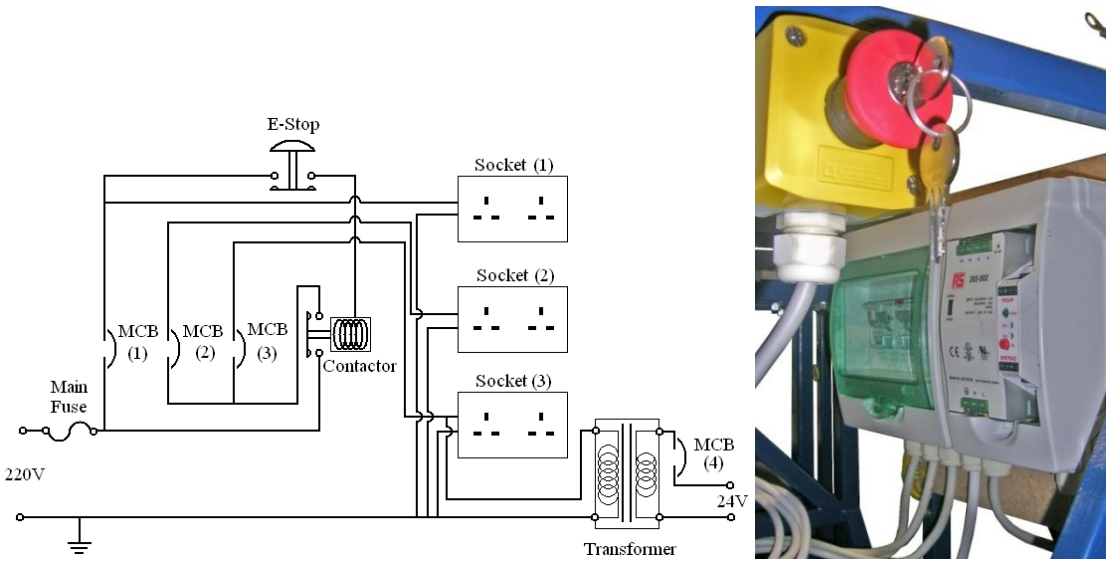

Figure B.6: Electrical safety system

A laser photodiode timing array, adapted from the design from a previous final year project[4], was part of the original design of the test system. This device was positioned beneath the impact plate and consisted of two parallel rows of eight lasers (Maplin LE07H) pointing horizontally at eight selective wavelength photodiodes (Epigap EPD-660-5/0.5). The output voltage from the photodiodes depended upon the presence or absence of the laser light on the sensor. The photodiodes were found to be highly sensitive to alignmentAn electronics circuit board amplified and converted the eight voltage outputs from the photodiodes to two digital signals corresponding to each row. However, experimental trials of this device found it to be unsuitable for this type of system, principally due to vibrations of impact affecting the alignment of the laser-beams. This timing array was mounted to the test system that was subject to impact vibrations that, despite the shock-suppression bolts and rigid fixture to the floor, disrupted the alignment of the laser beams. This issue, coupled with indeterminate software interference between programs for the timing array and the pneumatic system, led to the cessation of use of the timing array.

[4] Carty-Mole, A., "Development of a projectile measurement device", School of Mechanical and Manufacturing, Dublin City University, 2007.

Appendix C: LabVIEW Control programs

As discussed in Section 3.1, the entire automated test system was controlled by a series of LabVIEW virtual instruments (VIs). LabVIEW is a graphical data-flow programming language that has popular usage in science and engineering disciplines. A VI consists of the front panel, the interface that the user sees and interacts with, and the block diagram, where the algorithms and subVIs are implemented. Execution of data on the block diagram occurred from left to right of the screen. The overall control of the test system is comprised of a number of individual VIs, which will be presented in the following text in the order in which they execute.

C.1 Top_level VI

SubVIs: *Channel_switches.vi, Fill_reservoir.vi, Camera_acq.vi, Loadcell_acq.vi, Actuator.vi, Valve_timings_verification.vi, Image_processing.vi, Read_prev_graphs.vi*

The user interface for the test system was the *Top_level* VI, which managed the synchronised execution of nine subVI programs required for the running of the test system. The block diagram for this program is shown in Figure C.1.

Upon starting the *Top_level* VI, it created a folder, if one did not already exist, with a file-name corresponding to the day's date. This helped maintain order for the data being saved in the day's testing. The ball identification number and sample number was inputted by the user to ensure that data for a particular ball type is saved under the correct label. The user used a drop-down menu on the front panel to select the desired projection velocity. This selection triggered a case-structure to assign the appropriate pressure value to the air reservoir sensor, the time value to synchronise the camera acquisition and the impact and the time values to the directional control solenoid valves. The user also selected the desired frame-rate and resolution for the high speed camera.

When the user pressed fire, the program first queried the feeder channel sensors using the *Channel_switches* VI, with a YES/NO dialog appearing on screen requiring the user to confirm the number of balls in the feeder channel. This ensured that the sensors were operating correctly, and gave the user a last chance to look over the system to see if anything was amiss before proceeding. Once this is confirmed, the *Fill_reservoir* subVI was executed to fill the air reservoir to the correct pressure. When this is achieved, the solenoid valves, the camera and the loadcell are all run by their individual subVIs in the appropriate order to complete the ball

propulsion and impact data acquisition. Also present, but disabled, in this portion of the code is the *Valve_timings_verificiation* subVI, which uses analog inputs to verify that the digital outputs used for the triggering of the directional control valves are responding with the correct timing. As will be explained in great detail in Section C.x, the valve timings are software-based and thus dependent on processes running on the computer, either in LabVIEW program or other Windows operations. The *Valve_timings_verificiation* subVI is disabled due to a limit of the data acquisition card, which only allows multiple analog inputs if they are at the same sampling frequency. Higher spec DAQ cards have multiplexers that allow multiple analog input sampling rates. The *Valve_timings_verificiation* subVI can be enabled if the, which used a high-rate analog input, is disabled. It is for this reason also that the *Fill_reservoir* subVI, which uses an analog input for the pressure sensor, is in a separate structure to the *Loadcell_acquisition* subVI. The fact that the *Valve_timings_verificiation* subVI cannot be used in tandem with the *Loadcell_acquisition* subVI was not an important issue, as it was only required for debugging problems.

Once the impact is complete, the AVI file path is passed to the *Image_processing* program, which analysed the data to obtain impact characteristics. Real time display of the processed footage is passed via global variables to be shown to the user on the *Top_level* VI. This assured the user that the processing parameters were optimised to accurately derive the impact characteristics from the footage, and informed the user of the progress of the image processing. The *Image_processing* VI outputs the impact characteristics to be displayed graphically under *Current results* and *Accuracy analysis* tabs in the front panel of the *Top_level* VI. This data, along with the load-cell data, is then written to spreadsheet format for further analysis in programs such as MS Excel. The data from these complied spreadsheets was displayed using the *Read_previous_graphs* subVI in the *Previous results* tab on the front panel to allow the user to compare the current results with previous results for that or a different type of ball. This subVI was disabled at the time of writing due to it not being fully implemented in the *Top_level* program.

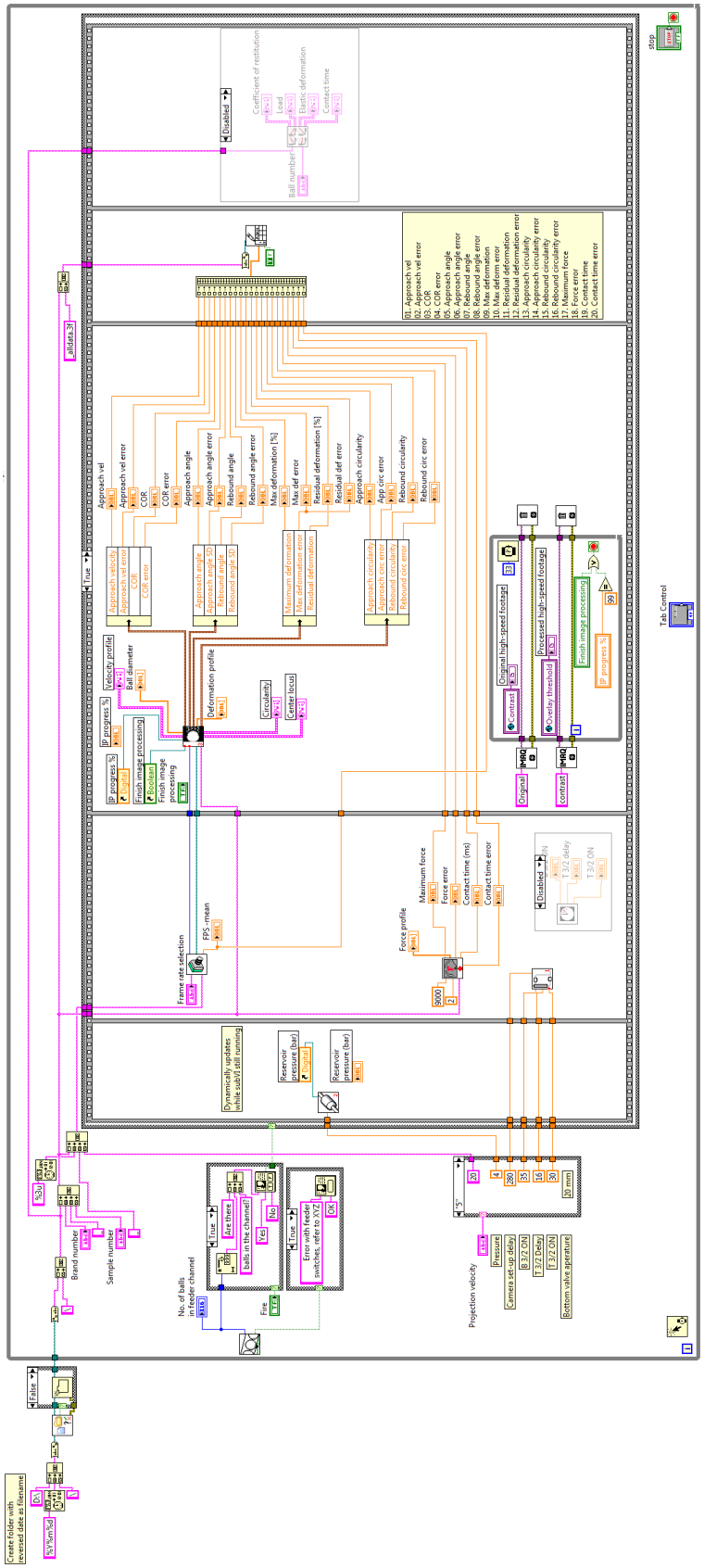

Figure C.1: Top-level VI block diagram

C.2 Channel_switches VI

SubVIs: *Feeder_sensor* VI

The feeder channel was the tube that accommodated up to 14 balls, passing them one by one into the firing area. The sensors aligned along the length of this channel had two purposes: firstly, to inform the system of the number of times to fire in order to produce the desired number of impacts for each ball; and secondly, to ensure that the previously fired ball has returned to the channel before the next is fired. Problems that would prevent the ball from returning, such as fouling or the ball disintegrating or getting stuck, would require the system to shut down and the user to rectify the issue.

The channel sensors are lever microswitches with 5V(dc) applied to one of the terminals. The *Feeder_sensor* VI, shown in Figure C.2, uses an analog input to read the voltage on the other terminal, which was 0V if the switch was depressed (ball present) and 5V otherwise. The *Channel_switches* VI, shown in Figure C.3, compiles the readings from all 13 sensors to count the number of balls in the channel. It checked also that readings were in the correct sequence, ensuring that none of the switches were behaving incorrectly.

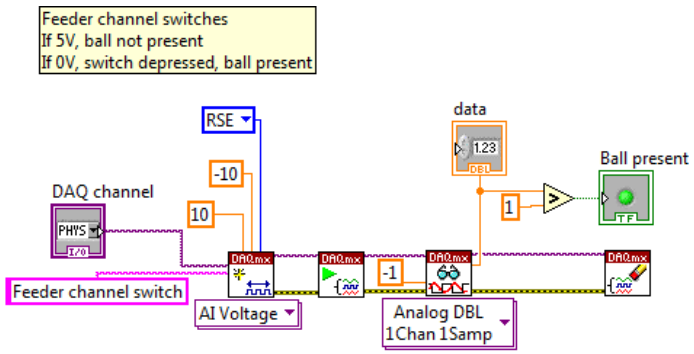

Figure C.2: Feeder sensor program block diagram

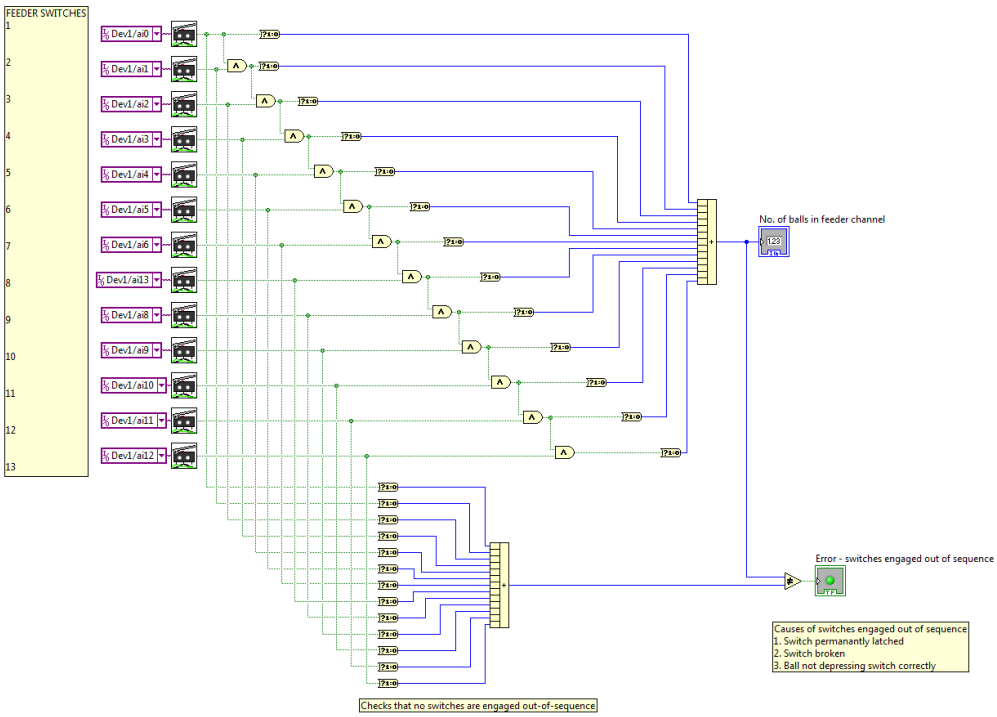

Figure C.3: Channel switches program block diagram

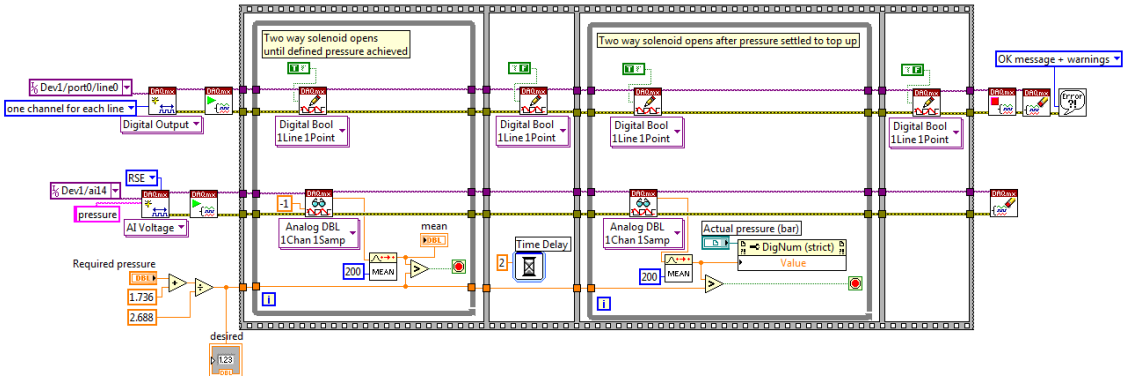

Figure C.4: Channel switches program block diagram

C.3 Fill_reservoir VI

The air reservoir is a 5 litre vessel with three apertures: one connected to the compressed air supply via a 2-way solenoid valve, the second connected to the pneumatic actuator via the directional control valves, and the third connected to a pressure sensor. Using a digital output via a relay, the 2-way solenoid valve is opened until the correct pressure is reached according to the pressure sensor, which is read by an analog input.

C.4 Camera_acq VI

LabVIEW communicates with the high speed camera via a base CameraLink cable connected to the NI PCIe 1429 frame-grabber card. The camera was supplied with propriety software that allowed the saving of different settings into user presets. These presets could be controlled by LabVIEW software using serial commands. It was not possible to acquire and process the high speed footage simultaneously, as the time required for processing each frame exceeded the desired frame-rate of the camera. To this end, the high speed footage was saved in an uncompressed AVI codec for subsequent image processing. A time stamp was recorded periodically to ensure that the correct frame-rate was achieved, and it was found that even the process of writing the frames to AVI was time-intensive and resulted in diminished frame-rates. To achieve the high-speed image acquisition, an LL ring buffer algorithm was used, which created a predefined number of memory slots in which the each acquired frame is stored temporarily during acquisition. These frames were then extracted post-acquisition and written to AVI, and the ring buffer was cleared for the next acquisition. To prevent excessive use of CPU and disk space, and to reduce the time taken for the image processing, the buffer magnitude was set to 400 (approximately 90 milliseconds at 4500 fps). This required the synchronisation of the camera with the pneumatic system such that the small acquisition window coincided with the impact. This synchronisation was realised by delaying the pneumatic propulsion for a period in the region of 0.2 – 0.3 seconds, depending on the projection velocity. This time duration allowed for the ring buffer to be set up for the camera and for the transit of the ball up to the impact plate.

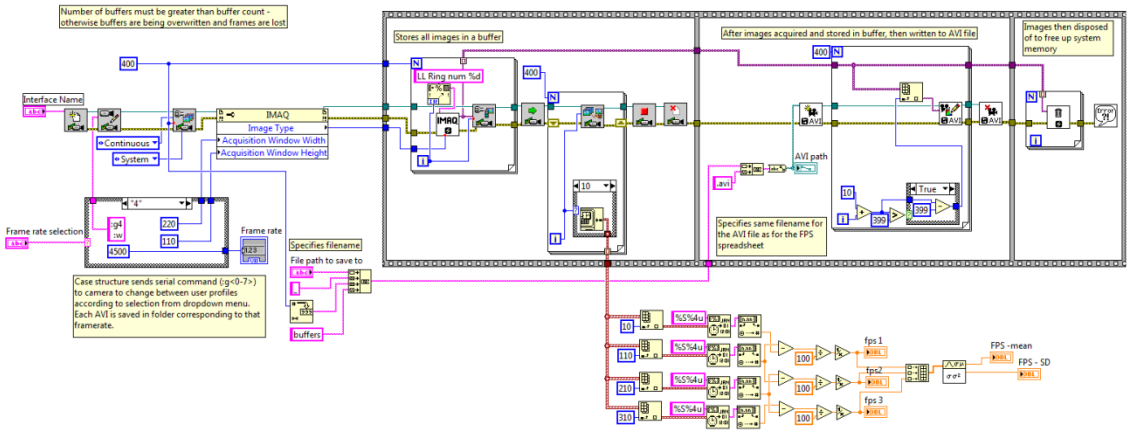

Figure C.5: High-speed camera acquisition program block diagram

C.5 Loadcell_acq VI

The acquisition program from the load-cell, shown in Figure C.6, obtained data at 50 kHz via analog input. This duration was far in excess of the impact duration, but it avoided the extra complication of synchronising the load-cell. The data was converted from a voltage to a force reading using the calibration equation. The force reading was then thresholded at a value above the precompression load to isolate the initial peak that corresponded to the ball impact, saved in spreadsheet format and analysed to obtain the impact force characteristics. The pre-compression of the load-cell was monitored to ensure repeatability with the system.

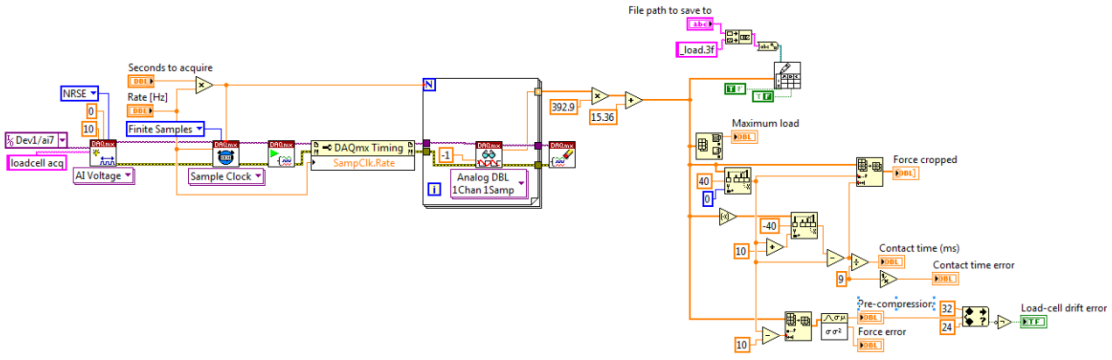

Figure C.6: Load-cell acquisition program block diagram

C.6 Actuator VI

In order to control the extension of the pneumatic actuator, the *Actuator* program, shown in Figure C.7 has two tasks: to trigger the bottom directional control solenoid valve that accelerates the piston and to trigger the top directional control solenoid valve that decelerates the piston, preventing it from hitting the end of the actuator. This is achieved by the synchronised use of two digital outputs that uses software timing to trigger the valves. Software timing has an accuracy of ± 1 ms but is dependent on the CPU capacity. RAM-intensive processes occurring in the CPU, whether from LabVIEW or other Windows-based programs such as anti-virus, affect the accuracy of the software timing capabilities, which had catastrophic effects on the pneumatic system, resulting in several piston breakages. Refinement of *Actuator* program, iterative redesigns of the piston, and debugging and elimination of interfering programs. The final version of the *Actuator* VI is shown in Fig C.6(a), with separate tasks controlling the two digital outputs. An alternative program for the actuator, shown in Fig C.6(b), was more elegant using a single task and a 2D boolean array controlling the digital outputs, but proved to be less accurate at maintain the correct timings. It was found that the program for acquisition from the laser photodiode timing array interfered with the *Actuator* VI, which was the secondary reason for discarding the laser photodiode system from the system. Windows-based operations, particularly the anti-virus scanner, were shut down during testing.

C.7 Valve_timings_verification VI

The *valve_timings_verification* program was not used in the regular running of the system, but rather when debugging was necessary when the actuator was not behaving predictably. The digital outputs for the directional control valves were wired up to two analog inputs and this program verified that the software timing signals were acceptable for the correct running of the pneumatic actuator.

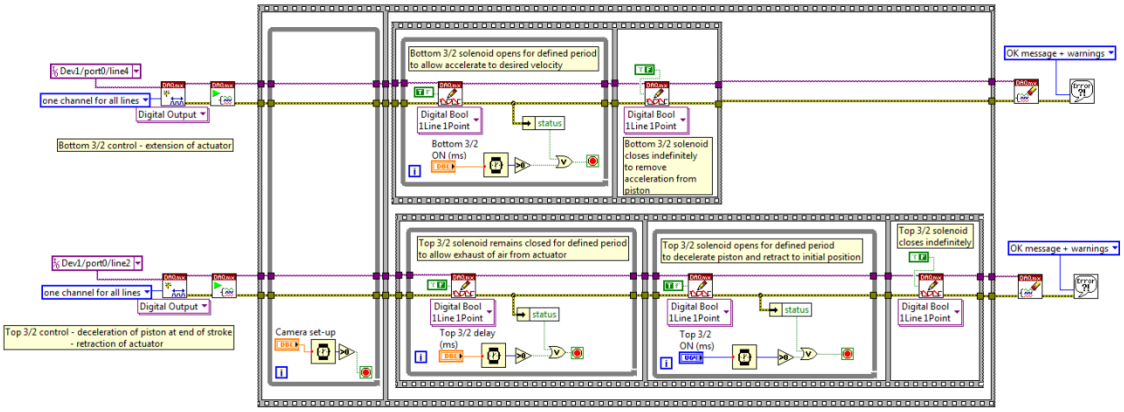

Figure C.7: Actuator control program block diagram

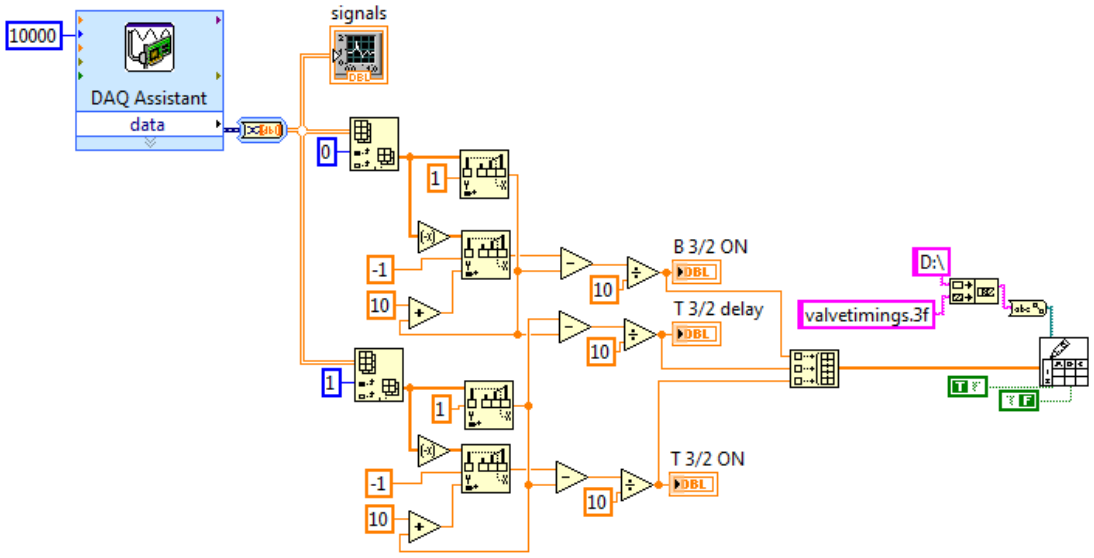

Figure C.8: Valve timings program block diagram

C.8 Image_processing VI

The image processing algorithm, shown in Figure C.9, used NI IMAQ Vision software to open the AVI file frame by frame and apply a series of image processing steps to each frame:

a) Image cropped such that the left side of the image is level with the plane of the impact plate

b) Brightness and contrast adjusted to improve the clarity of the image;

c) Threshold performed to produce a 1-bit image (pure black and white) from 8-bit image (256 shades of grey)

d) Image filtered to remove unwanted objects.

Global variables were used to pass information between the *Image_processing* VI and the *Top_level* VI. Two stages of the image processing algorithm and the percentage progress were exported to the *Top_level* VI to inform the user of the accuracy and progress of the subVI, with the user having the ability to remotely stop the *Image_process* VI from the *Top_level* VI.

In order to evaluate the accuracy of the image processing, the pixel values of original image were divided by the pixel values of the processed image. This produced a 1-bit image with the white values corresponding to the areas of the original image that were below the threshold value of the processed image. An image processing algorithm was deemed accurate if a circle with a uniformly thin ouline was visible, tracing the outline of the ball. This implied that the threshold encapsulated the shape of the ball without including any background objects.

Thus validated, the area and perimeter of the ball was calculated using standard NI IMAQ VIs for measuring the ball circularity. The centre coordinates of the ball were passed into a shift register, and compared to the previous iteration to calculate the ball velocity. This calculation was only performed between limited coordinates, i.e. when the ball was fully visible on the screen and not truncated off the edge of the frame, and just prior to impact when the ball will deform. The velocity vector was displayed as a red line projecting from the ball centre for user feedback. The diameter of the ball under impact was measured for the average of the four horizontal pixel rows in the centre of the ball. Once the image processing is completed, either by the user stopping it or all frames being processed, the data was passed out of the loop as 1D arrays to be manipulated into the relevant motion and deformation characteristics.

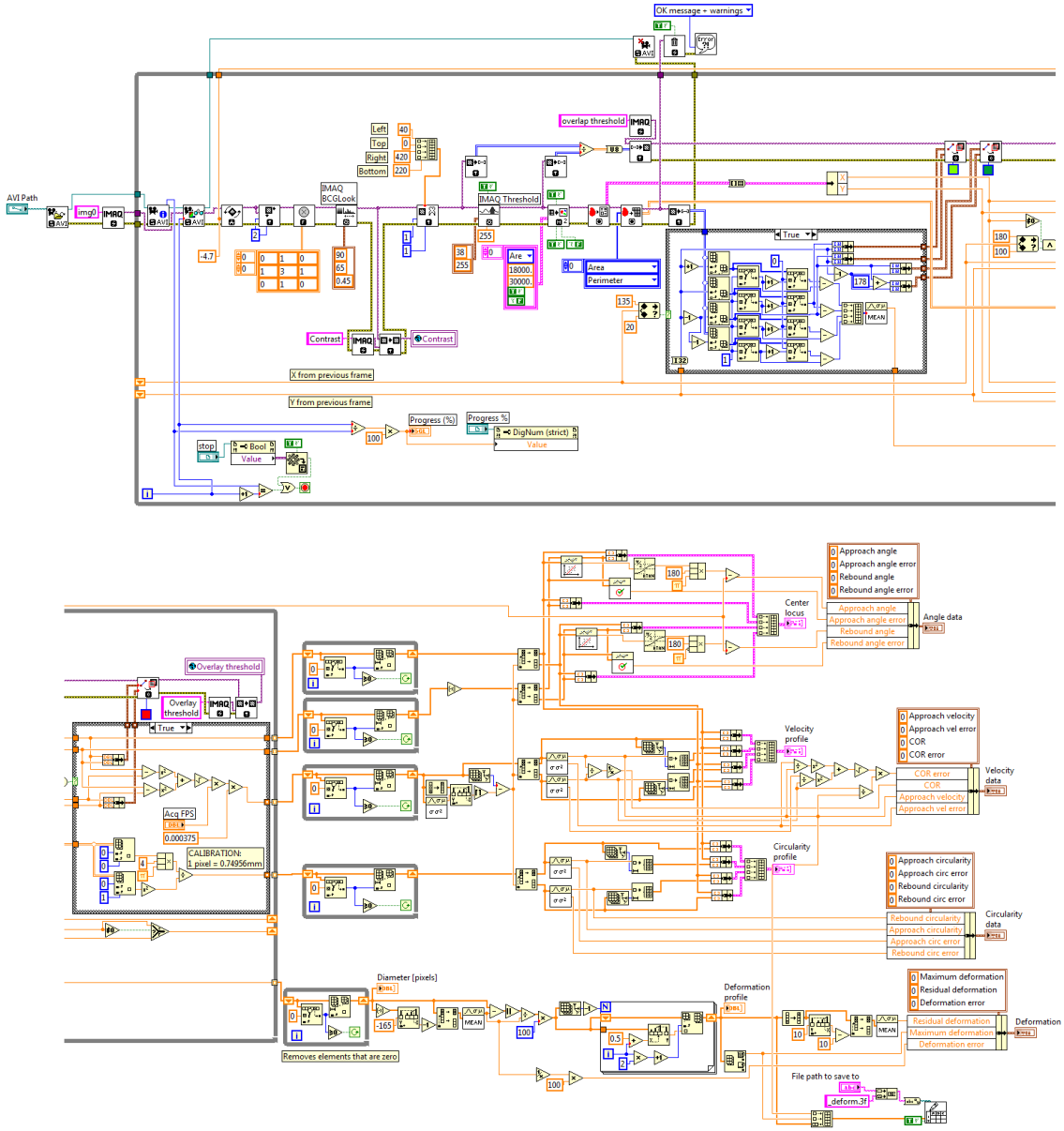

Figure C.9: Image processing algorithm block diagram

C.9 Read_prev_graphs VI

The *Read_prev_graphs* program read and displayed spreadsheet data that had been written for previous impacts, with the purpose of providing extra feedback and information to the user. This VI separated the characteristics accorded to the column under which they had been saved and created XY plots of the variation of coefficient of restitution, force, deformation and contact time with respect to incident velocity.

C.10 Laser_photodiodes VI

As discussed in Sections 3.x and C.6, a laser photodiode timing array was discarded from the test system. To summarise, the timing array was unfeasible for two reasons: firstly, the degradation of the alignment of the laser beams with the recipient photodiodes due to the shock vibrations of impact; and secondly, the interference of the *Laser_photodiodes* VI with the timing signals in the *Actuator* VI. The *Laser_photodiodes* VI used the two hardware counters to time the duration between the ball breaking one set of beams and breaking the next set. This timing was achieved using the NI DAQmx *Two edge separation* algorithm, with a *start arm trigger* used to measure the rebound of the ball back through the same sets of beams but in the opposite direction. This program enabled accurate velocity measurement, but was found to interfere with the program controlling the pneumatic actuator. The 2 counter inputs running in parallel with the camera (PCIe 1429), load-cell and actuator (analog input, 2 digital outputs) upset the timings for the valves, although it was unclear whether it was a software or hardware issue. As this timing system was concluded to be unsuitable for this application, the *Laser_photodiode* VI was removed from the *Top_level* program.

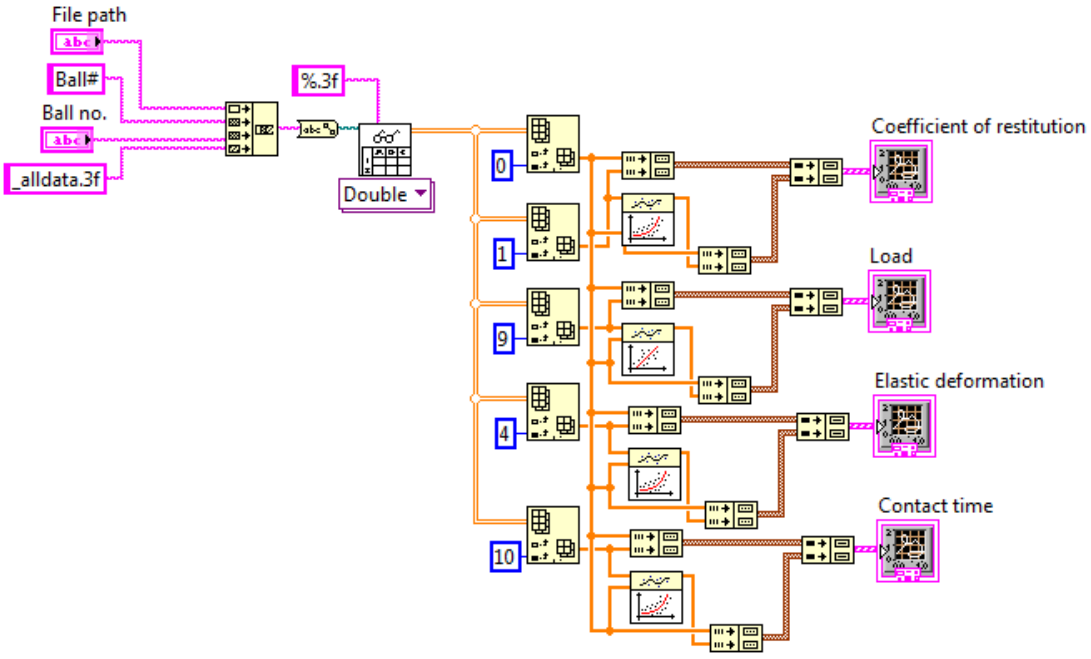

Figure C.10: Read previous graphs program block diagram

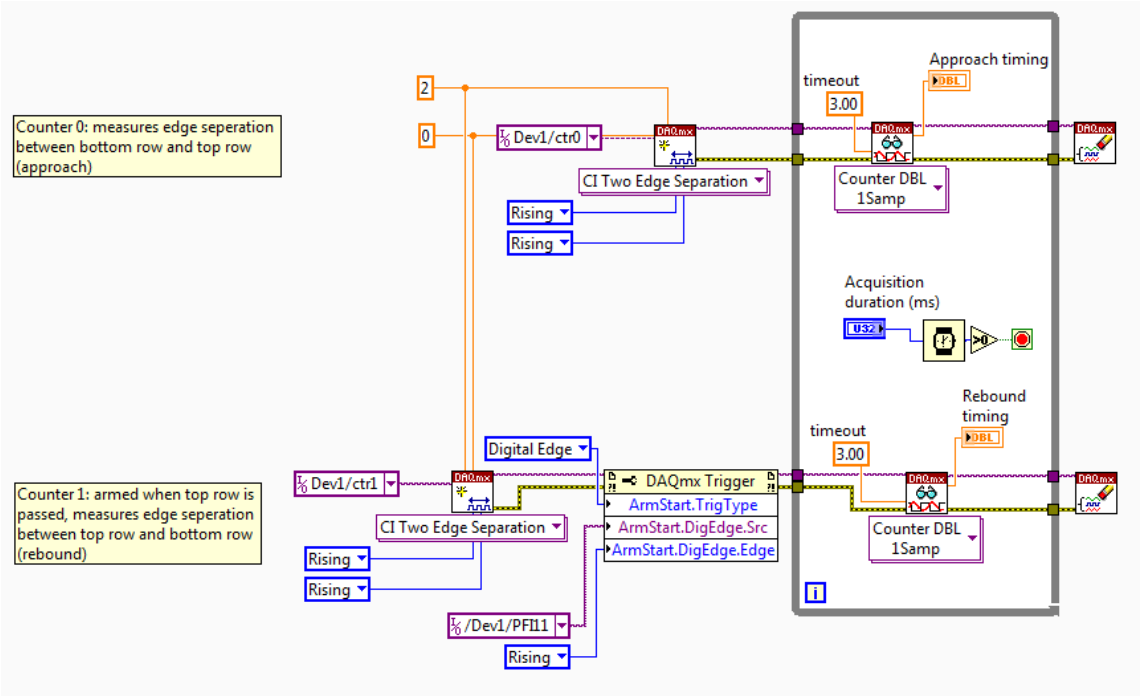

Figure C.11: Laser-photodiode timing array acquisition program block diagram

Appendix D: Polymer hardness characterisation

The Shore hardness of the polymer cores were measured using a handheld Shore A durometer. The purpose of this characterisation was to aid in selecting the polymer grades for prototype production, where commercially available polymer grades are specified according to Shore hardness values.

This device has a slender pin that indented the surface of the ball, with a gauge indicating the hardness. Only the polymer cores were tested for Shore hardness, as the pin of the durometer slipped between the strands of the yarn-wound surfaces of tradition balls, thus being an unsuitable device for accurately measuring the hardness of these ball types. With the ball resting against a rigid surface, the exterior surface of the ball was measured at four points, and the ball is sawn in half using a hacksaw to measure the interior hardness (six points equally separated across ball diameter). The mean surface and internal hardness values (with 95% confidence intervals) are shown in Figure D.1.

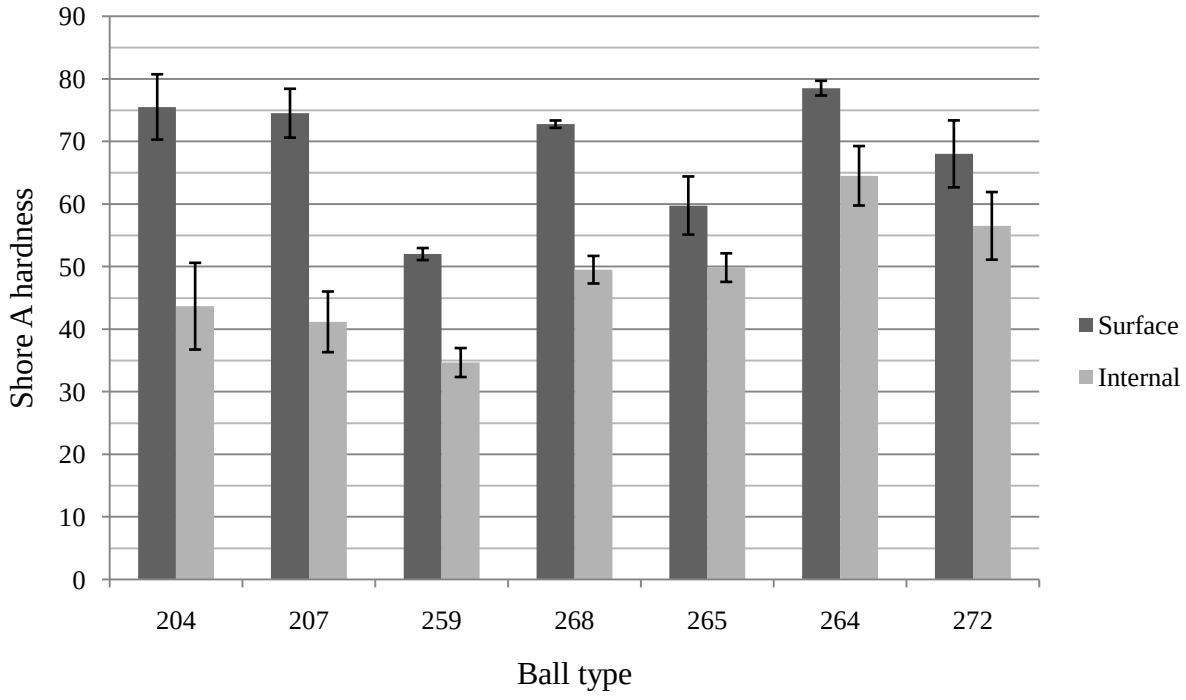

Figure D.1: Hardness values of approved polymer cores

There was no defined profile of hardness across the internal diameter, with the variation randomly distributed as seen in Figure D.2. The accuracy of the hardness values of the ball interior were questionable, with the durometer possibly giving erroneous readings if the pin slipped into the porosities of the foamed structure. A more detailed analysis of the hardness distribution throughout the ball internal structure would require careful use of the durometer, such that the pore size does not interfere with the reading, and preparation of a fine surface finish to avoid erroneous measurements from surface fluctuations.

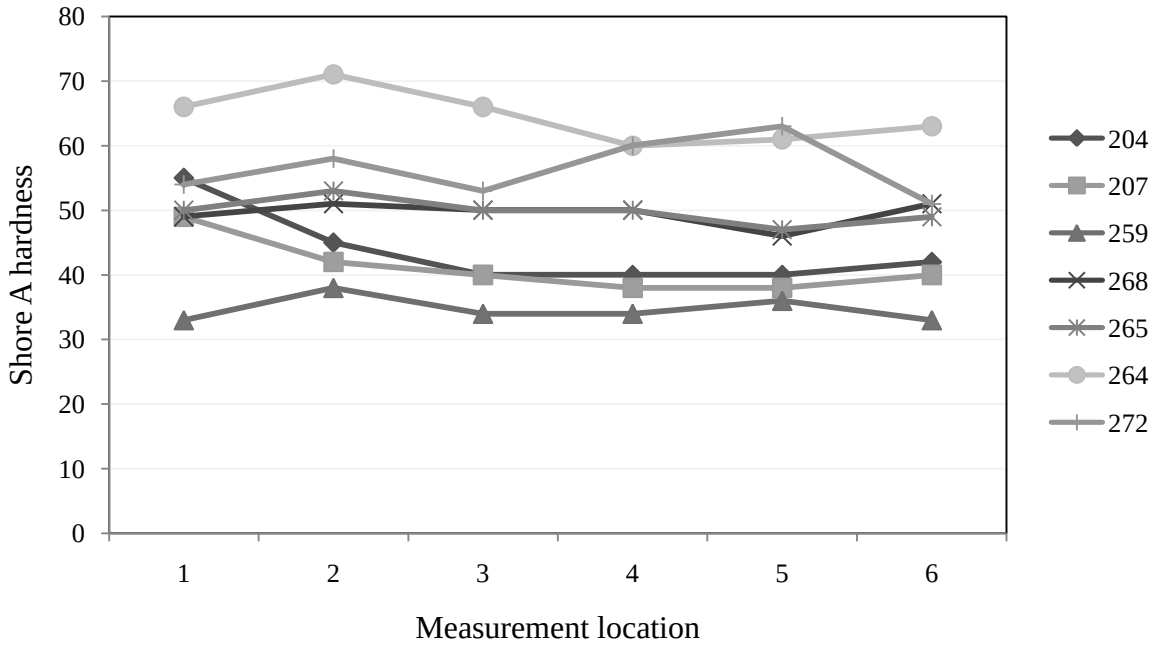

Figure D.2: Distribution of hardness measurements across ball internal cross sections

Appendix E: Ideal spring-theory equations derivation (Model 1)

General equation of motion:

$$m\ddot{x} + c\dot{x} + kx = -mg \tag{D.1}$$

Integrating, with initial conditions of $\dot{x}(0) = u$ and $x(0) = 0$, where u is ball incident velocity

$$x(t) = \left[\frac{cg-2ku}{2k\omega_d}\sin\omega_d t + \frac{mg}{k}\cos\omega_d t\right]\left[\exp\left(-\frac{c}{2m}t\right) - \frac{mg}{k}\right] \tag{D.2}$$

where $\omega_d = \frac{1}{m}\sqrt{2km - c^2}$ (D.3)

Rearranging Equation D.2 yields:

$$x(t) = -\frac{u}{\omega_d}\exp\left(-\frac{c}{2m}t\right)\sin\omega_d t - \frac{mg}{k}\left[1 - \exp\left(-\frac{c}{2m}t\right)\left(\cos\omega_d t + \frac{c}{2m\omega_d}\sin\omega_d t\right)\right] \tag{D.4}$$

The maximum magnitude of the first term on the right-hand side, $\frac{u}{\omega_d}$, is the dynamic deformation arising from impact at velocity *u*; the maximum magnitude of the second term, $\frac{mg}{k}$, is the static deformation due to its weight. The assumption at $\frac{mg}{k} \ll \frac{u}{\omega_d}$ is reasonable for a reasonably compliant ball, so the second term on the right-hand side of Equation D.4 can be neglected, leaving

$$x(t) = -\frac{u}{\omega_d}exp\left(-\frac{c}{2m}t\right)\sin\omega_d t \tag{D.5}$$

The contact time ΔT is the first finite solution of $x(\Delta T) = 0$

$$-\frac{u}{\omega_d}\exp\left(-\frac{c}{2m}\Delta T\right)\sin\omega_d \Delta T = 0 \tag{D.6}$$

$$\rightarrow \Delta T = \frac{\pi}{\omega_d} \tag{D.7}$$

Differentiating Equation D.5 gives

$$\dot{x}(t) = -\frac{cu}{2m\omega_d}\exp\left(-\frac{c}{2m}t\right)\sin\omega_d t - u\exp\left(-\frac{c}{2m}t\right)\cos\omega_d t \tag{D.8}$$

Rebound speed *v* is found by substituting in $t = \Delta T$

$$v = \dot{x}(\Delta T) = u\exp\left(-\frac{c}{2m}\Delta T\right) \tag{D.9}$$

Coefficient of restitution can be written as

$$\mathrm{COR} = \frac{\dot{x}(\Delta T)}{\dot{x}(0)} = \exp\left(-\frac{c\Delta T}{2m}\right) \tag{D.10}$$

Rearranging Equation D.10 gives the viscous damping, *c*:

$$\rightarrow c = -\frac{2m}{\Delta T}\ln \mathrm{COR} \tag{D.11}$$

By manipulating Equations D.3, D.7, D.10, the stiffness, *k*, can be expressed as

$$k = m\left(\frac{\pi}{\Delta T}\right)^2\left[1 + \left(\frac{\ln \mathrm{COR}}{\pi}\right)^2\right] \tag{D.12}$$

For a ball with significant bounce (i.e. COR > 0.5), $\frac{\ln \mathrm{COR}}{\pi} \ll 1$

$$\rightarrow k = m\left(\frac{\pi}{\Delta T}\right)^2 \tag{D.13}$$